

UNIVERSITÉ PIERRE ET MARIE CURIE

N° attribué par la bibliothèque  
████████████████████████████

## THÈSE

pour obtenir le grade de

**DOCTEUR de Université Pierre et Marie Curie**

Spécialité : **Physique Théorique**

préparée au **Laboratoire de Physique Nucléaire et Hautes Énergies**

dans le cadre de l'École Doctorale **ED389**

présentée et soutenue publiquement  
par

**François SICARD**

le 20 Décembre 2010

Titre:  
**Out-of-equilibrium dynamics in infinite  
one-dimensional self-gravitating systems**

Directeur de thèse: **Michael JOYCE**

### Jury

|                      |                    |
|----------------------|--------------------|
| M. ,                 | Président du jury  |
| M. Thierry DAUXOIS,  | Examinateur        |
| M. Duccio FANELLI,   | Rapporteur         |
| M. Michael JOYCE,    | Directeur de thèse |
| M. Alexander KNEBE,  | Rapporteur         |
| M. Gilles TARJUS,    | Examinateur        |
| M. Patrick VALAGEAS, | Examinateur        |



# Résumé

La formation des structures dans l'univers demeure une des interrogations majeures en cosmologie. La croissance des structures dans le régime linéaire, où l'amplitude des fluctuations est faible, est bien comprise analytiquement, mais les simulations numériques à  $N$ -corps restent l'outil principal pour sonder le régime “non-linéaire” où ces fluctuations sont grandes. Nous abordons cette question d'un point de vue différent de ceux utilisés couramment en cosmologie, celui de la physique statistique et plus particulièrement celui de la dynamique hors-équilibre des systèmes avec *interaction à longue portée*. Nous étudions une classe particulière de modèles  $1-d$  qui présentent une évolution similaire à celle rencontrée dans les modèles  $3-d$ . Nous montrons que le clustering spatial qui se développe présente des propriétés (fractales) d'invariance d'échelles, et que des propriétés d'auto-similarité apparaissent lors de l'évolution temporelle. D'autre part, les exposants caractérisant cette invariance d'échelle peuvent être expliqués par l'hypothèse du “stable-clustering”. En suivant une analyse de type halos sélectionnés par un algorithme “friend-of-friend”, nous montrons que le clustering non-linéaire de ces modèles  $1-d$  correspond au développement d'une “hiérarchie fractale statistiquement virielisée”. Nous terminons par une étude formalisant une classification des interactions basée sur des propriétés de convergence de la force agissant sur une particule en fonction de la taille du système, plutôt que sur les propriétés de convergence de l'énergie potentielle, habituellement considérée en physique statistique des systèmes avec interaction à longue portée.

# Abstract

The formation of structures in the universe is one of the major questions in cosmology. The growth of structure in the linear regime of low amplitude fluctuations is well understood analytically, but  $N$ -body simulations remain the main tool to probe the “non-linear” regime where fluctuations are large. We study this question approaching the problem from the more general perspective to the usual one in cosmology, that of statistical physics. Indeed, this question can be seen as a well posed problem of out-of-equilibrium dynamics of systems with *long-range interaction*. In this context, it is natural to develop simplified models to improve our understanding of this system, reducing the question to fundamental aspects. We define a class of infinite  $1 - d$  self-gravitating systems relevant to cosmology, and we observe strong qualitative similarities with the evolution of the analogous  $3 - d$  systems. We highlight that the spatial clustering which develops may have scale invariant (fractal) properties, and that they display “self-similar” properties in their temporal evolution. We show that the measured exponents characterizing the scale-invariant clustering can be very well accounted for using an appropriately generalized “stable-clustering” hypothesis. Further by means of an analysis in terms of halo selected using a friend-of-friend algorithm we show that, in the corresponding spatial range, structures are, statistically virialized. Thus the non-linear clustering in these  $1 - d$  models corresponds to the development of a “virialized fractal hierarchy”. We conclude with a separate study which formalizes a classification of pair-interactions based on the convergence properties of the forces acting on particles as a function of system size, rather than the convergence of the potential energy, as it is usual in statistical physics of long-range-interacting systems.

# Contents

|                                                                                              |           |
|----------------------------------------------------------------------------------------------|-----------|
| Résumé . . . . .                                                                             | iii       |
| Abstract . . . . .                                                                           | iv        |
| Contents . . . . .                                                                           | v         |
| <b>Introduction en Français</b>                                                              | <b>1</b>  |
| <b>Introduction</b>                                                                          | <b>5</b>  |
| <b>1 Dynamics and thermodynamics of systems with long-range interaction: an introduction</b> | <b>9</b>  |
| 1 Definition of long-range interactions . . . . .                                            | 10        |
| 2 Equilibrium statistical mechanics of long-range interacting systems . . . . .              | 12        |
| 2.1 The mean-field Ising model . . . . .                                                     | 12        |
| 2.2 Inequivalence of ensembles: the BEG mean-field model . . . . .                           | 14        |
| 2.3 Mean-field and large deviation theory . . . . .                                          | 17        |
| 3 Out-of-equilibrium dynamics of long-range interacting systems . . . . .                    | 19        |
| 3.1 Introduction . . . . .                                                                   | 19        |
| 3.2 Slow relaxation to equilibrium: the ferromagnetic Hamiltonian-Mean-Field model . . . . . | 21        |
| 3.3 Convergence towards a stationary state of the Vlasov equation                            | 24        |
| 4 Conclusion . . . . .                                                                       | 27        |
| <b>2 Basic results on self-gravitating systems</b>                                           | <b>29</b> |
| 1 Finite self-gravitating systems: statistical equilibrium and dynamical evolution . . . . . | 29        |
| 1.1 Statistical equilibrium of self-gravitating systems . . . . .                            | 30        |
| 1.2 Virial equilibrium . . . . .                                                             | 35        |
| 2 Introduction to Cosmology . . . . .                                                        | 37        |
| 2.1 the Friedmann-Robertson-Walker universe . . . . .                                        | 38        |
| 2.2 Cosmic Expansion . . . . .                                                               | 39        |
| 2.3 Cosmic Constituents . . . . .                                                            | 40        |
| 2.4 The $\Lambda$ CDM model . . . . .                                                        | 42        |
| 2.5 The Newtonian approximation . . . . .                                                    | 42        |
| 3 Infinite self-gravitating systems in cosmology: analytical results . . . . .               | 43        |
| 3.1 Non-equilibrium evolution of a self-gravitating system . . . . .                         | 43        |
| 3.2 Perturbation theory . . . . .                                                            | 49        |
| 3.3 Limit of linear theory: a non-continuous approach . . . . .                              | 55        |
| 4 Background on Stochastic point processes . . . . .                                         | 59        |
| 4.1 Stochastic distributions . . . . .                                                       | 59        |

|          |                                                                                                      |            |
|----------|------------------------------------------------------------------------------------------------------|------------|
| 4.2      | Classification of stochastic processes . . . . .                                                     | 66         |
| 4.3      | Causal bounds on the Power spectrum . . . . .                                                        | 67         |
| 5        | The non-linear regime: numerical simulation . . . . .                                                | 68         |
| 5.1      | $N$ -body simulations . . . . .                                                                      | 68         |
| 5.2      | Initial conditions . . . . .                                                                         | 70         |
| 5.3      | Self-similarity . . . . .                                                                            | 71         |
| 5.4      | From linear theory to stable clustering . . . . .                                                    | 73         |
| 5.5      | Halo models . . . . .                                                                                | 73         |
| <b>3</b> | <b>1 – <math>d</math> gravity in infinite point distributions</b>                                    | <b>79</b>  |
| 1        | From finite to infinite systems . . . . .                                                            | 80         |
| 1.1      | Definitions . . . . .                                                                                | 80         |
| 1.2      | Finite system . . . . .                                                                              | 80         |
| 1.3      | Infinite system limit . . . . .                                                                      | 81         |
| 2        | Forces in infinite perturbed lattices . . . . .                                                      | 86         |
| 2.1      | Stochastic perturbed lattices . . . . .                                                              | 86         |
| 2.2      | Mean value and variance of the total force . . . . .                                                 | 87         |
| 2.3      | Lattice with uncorrelated displacements . . . . .                                                    | 89         |
| 2.4      | Lattice with correlated displacements . . . . .                                                      | 90         |
| 3        | Dynamics of 1d gravitational systems . . . . .                                                       | 93         |
| 3.1      | Toy models: static . . . . .                                                                         | 93         |
| 3.2      | Toy models: expanding . . . . .                                                                      | 94         |
| 3.3      | Discussion of previous literature . . . . .                                                          | 97         |
| 4        | Conclusion . . . . .                                                                                 | 101        |
| <b>4</b> | <b>Dynamics of infinite one dimensional self-gravitating systems: self-similarity and its limits</b> | <b>103</b> |
| 1        | Numerical simulation . . . . .                                                                       | 104        |
| 1.1      | Integration of dynamics . . . . .                                                                    | 104        |
| 1.2      | Initial conditions . . . . .                                                                         | 108        |
| 1.3      | Choice of units . . . . .                                                                            | 112        |
| 1.4      | Statistical measures . . . . .                                                                       | 114        |
| 2        | Basic results: comparison with $3 - d$ . . . . .                                                     | 115        |
| 2.1      | Visual inspection . . . . .                                                                          | 115        |
| 2.2      | Development of fluctuations in real space: hierarchical clustering                                   | 122        |
| 2.3      | Development of correlation in real space: self-similarity . . . . .                                  | 128        |
| 2.4      | Development of correlations in reciprocal space . . . . .                                            | 134        |
| 3        | Evolution from causal density seeds . . . . .                                                        | 141        |
| 3.1      | Visual inspection . . . . .                                                                          | 141        |
| 3.2      | The power spectrum . . . . .                                                                         | 144        |
| 3.3      | Correlation function . . . . .                                                                       | 148        |
| 3.4      | Normalized mass variance . . . . .                                                                   | 151        |
| 4        | Development of the range of self-similarity and characteristic exponents                             | 154        |
| 4.1      | Evolution of the spatial extent of non-linear SS clustering . . . . .                                | 154        |
| 4.2      | Stable clustering in one dimension . . . . .                                                         | 156        |
| 4.3      | Prediction of exponents of power-law clustering (expanding case) . . . . .                           | 161        |
| 4.4      | Exponent of the power-law clustering in the static limit . . . . .                                   | 161        |

---

|                                                        |                                                                                                                         |            |
|--------------------------------------------------------|-------------------------------------------------------------------------------------------------------------------------|------------|
| 5                                                      | Conclusion . . . . .                                                                                                    | 162        |
| <b>5</b>                                               | <b>Dynamics of infinite one dimensional self-gravitating systems: scale invariance, halos and virialization</b>         | <b>165</b> |
| 1                                                      | Tools for fractal analysis . . . . .                                                                                    | 165        |
| 1.1                                                    | The Hausdorff Dimension . . . . .                                                                                       | 166        |
| 1.2                                                    | Box Counting Dimension . . . . .                                                                                        | 167        |
| 1.3                                                    | Generalized dimension . . . . .                                                                                         | 168        |
| 1.4                                                    | Relation to 2-point analysis . . . . .                                                                                  | 169        |
| 2                                                      | Fractal analysis of evolved self-gravitating distributions . . . . .                                                    | 169        |
| 2.1                                                    | Algorithm . . . . .                                                                                                     | 170        |
| 2.2                                                    | Temporal evolution of the generalized dimensions . . . . .                                                              | 170        |
| 2.3                                                    | Dependence of exponents on initial conditions and model . . . . .                                                       | 172        |
| 3                                                      | Halos and virialization . . . . .                                                                                       | 176        |
| 3.1                                                    | Halo selection: The Friend-of-Friend algorithm . . . . .                                                                | 176        |
| 3.2                                                    | Testing for virialization of halos . . . . .                                                                            | 182        |
| 3.3                                                    | Statistical tests for stability of the probability distribution of the virial ratio in scale-invariant regime . . . . . | 193        |
| 4                                                      | Conclusion . . . . .                                                                                                    | 195        |
| <b>6</b>                                               | <b>A dynamical classification of the range of pair interactions</b>                                                     | <b>197</b> |
| 1                                                      | The force PDF in uniform stochastic point processes: general results .                                                  | 198        |
| 1.1                                                    | Stochastic point processes . . . . .                                                                                    | 198        |
| 1.2                                                    | General expression for the force PDF . . . . .                                                                          | 200        |
| 1.3                                                    | Analyticity properties of the force PDF . . . . .                                                                       | 201        |
| 2                                                      | Large distance behavior of pair interactions and the force PDF . . .                                                    | 202        |
| 2.1                                                    | Variance of the force in infinite system limit . . . . .                                                                | 203        |
| 2.2                                                    | Force PDF for an integrable pair force . . . . .                                                                        | 203        |
| 2.3                                                    | Force PDF for a non-integrable pair forces . . . . .                                                                    | 204        |
| 3                                                      | Definedness of dynamics in an infinite uniform system . . . . .                                                         | 205        |
| 3.1                                                    | Evolution of fluctuations and definedness of PDF . . . . .                                                              | 205        |
| 3.2                                                    | PDF of force differences . . . . .                                                                                      | 207        |
| 3.3                                                    | Conditions for definedness of dynamics in an infinite system .                                                          | 208        |
| 4                                                      | Discussion and conclusions . . . . .                                                                                    | 209        |
| <b>Conclusion and perspectives</b>                     |                                                                                                                         | <b>213</b> |
| <b>A One and two point properties of uniform SPP</b>   |                                                                                                                         | <b>219</b> |
| <b>B Small k behavior of <math>\tilde{f}(k)</math></b> |                                                                                                                         | <b>221</b> |
| <b>Bibliography</b>                                    |                                                                                                                         | <b>223</b> |

## CONTENTS

---

# Introduction en Français

La compréhension de la formation des structures dans l'univers demeure l'une des interrogations majeures en cosmologie. La distribution de matière observée aujourd'hui à grande échelle dans l'univers apparaît en effet très inhomogène et présente une distribution très structurée de galaxies : amas de galaxies, superamas, vide et filaments. D'autre part, les observations du fond diffus cosmologique (CMB) suggèrent que l'univers présentait par le passé une distribution de matière représentée par de faibles fluctuations de densité autour d'une distribution homogène. Selon l'approche théorique du modèle “standard” de la cosmologie, la matière présente dans l'univers est principalement constituée de *Matière Noire* (“*Dark Matter*”) n'intéragissant essentiellement que par l'interaction gravitationnelle. Sur les échelles spatiales pertinentes pour l'étude de la formation des structures dans l'univers, l'approximation Newtonienne de l'interaction gravitationnelle s'applique et la question se réduit alors à la formation des structures dans un système de particules auto-gravitantes partant d'une condition initiale correspondant à une répartition de matière presque uniformément distribuée.

La compréhension analytique de ce problème reste essentiellement limitée aux approches perturbatives linéaires des solutions des équations de type fluide (*i.e.* le régime linéaire de formation des structures). L'étude du régime non-linéaire est ainsi principalement abordée par des simulations numériques. Le degré de sophistication et de parallélisation de ces simulations cosmologiques s'est amélioré de façon impressionante ces dernières années avec notamment l'utilisation de simulations hautement parallélisées. En dépit de ces progrès, les simulations numériques en cosmologie restent limitées par une résolution modeste (au maximum 2 ou 3 ordres de grandeur en ce qui concerne les échelles spatiales du régime non-linéaire). L'absence de support analytique laisse également ouvert la question de la pertinence des résultats dérivés de ces simulations.

Dans cette thèse, nous approchons cette question d'un point de vue différent de ceux utilisés couramment en cosmologie : celui de la physique statistique. En effet, la formation de structures dans l'univers via l'approximation Newtonienne de l'interaction gravitationnelle peut être simplement vue comme un problème de dynamique hors-équilibre des interactions à longue portée. Dans le contexte de la physique statistique, il est alors naturel de développer des modèles simplifiés (*modèles jouets*) afin d'améliorer notre compréhension de ce système, en le réduisant autant que possible à ses aspects fondamentaux. Les versions unidimensionnelles de ce problème cosmologique présentent l'opportunité de pouvoir sonder des échelles spatiales beaucoup plus étendues (même pour un nombre limité de particules). De

plus, ces approches sont extrêmement précises, étant uniquement limitées par la précision numérique de la machine. Cette thèse présente une étude détaillée d'une classe particulière de modèles, ainsi que des résultats généraux sur la dynamique hors-équilibre des systèmes avec interaction à longue portée.

Les deux premiers chapitres introductifs sont consacrés à la présentation des bases nécessaires afin de comprendre le contexte et les résultats de cette thèse. Le premier chapitre introductif présente un aperçu des méthodes de la physique statistique des interactions à longue portée, tandis que le second présente une introduction à la formation des structures en cosmologie.

Dans le Chapitre 1, nous introduisons la dynamique et la thermodynamique des systèmes avec interaction à longue portée, dont la gravitation Newtonienne est un cas particulier, en mettant en valeur les résultats importants qui ont émergés ces dernières années. Ces résultats ne présentent cependant pas un intérêt fondamental pour l'étude des systèmes auto-gravitants en cosmologie, ces derniers faisant partie des systèmes d'extension infinie plutôt que finie. Ils sont néanmoins pertinents pour l'étude faite dans le Chapitre 6.

Le Chapitre 2 élargit les considérations faites dans le premier chapitre au cas spécifique des systèmes finis auto-gravitants, et passe en revue les bases du modèle cosmologique “standard”, en s’intéressant plus particulièrement à la formation des structures à grande échelle. En considérant que les systèmes particulaires en cosmologie sont d’extension spatiale infinie, une attention toute particulière doit être attachée à la définition de la force gravitationnelle dans ces systèmes. Nous introduisons la théorie cinétique utilisée pour étudier la dynamique hors-équilibre des systèmes infinis auto-gravitants en cosmologie nécessaire à la dérivation de l’approche hydrodynamique standard de ces systèmes. Nous présentons ensuite l’approche perturbative de ces équations de type fluide, ainsi que l’analyse numérique du régime non-linéaire de formation des structures dans l’univers, en discutant les notions centrales utilisées dans ce contexte : auto-similarité, “stable-clustering” et les modèles des “halos”.

Dans le Chapitre 3, nous introduisons et définissons la classe des modèles jouets unidimensionnels que nous étudions dans cette thèse. Nous abordons cette question d'un point de vue de la théorie des processus stochastiques de points, et traitons en particulier la question de la définition de la force totale agissant sur une particule appartenant à un système d'extension spatiale infinie. Nous montrons que cette question réside en fait dans une subtilité de l'application de “l’arnaque de Jeans” en une dimension. Nous insistons sur le fait que la force devient bien définie en une dimension pour une classe particulière de condition initiale, la classe des réseaux infinis perturbés, qui représente les processus de points pertinents dans les simulations numériques à  $N$ -corps en cosmologie. Le texte de ce chapitre est tiré d'un article publié dans Phys. Rev. E [70].

Dans le Chapitre 4, nous présentons les résultats de notre analyse numérique de l'évolution dynamique de ces modèles jouets. Nous montrons qu'ils présentent

de forte similarités *qualitatives* avec les systèmes tridimensionnels analogues, notamment le comportement auto-similaire (*i.e.* un *scaling dynamique*) en partant de conditions initiales pour le spectre de puissance (*i.e.* la transformée de Fourier de la fonction de corrélation) en loi de puissance. Nous explorons également les aspects particuliers de ces comportements que nous ne pouvons pas étudier aussi simplement dans les simulations numériques tridimensionnelles à cause des difficultés numériques rencontrées. Nous étudions en particulier la formation des structures pour une classe particulière de condition initiale, celle correspondant à des fluctuations de densité dites “causales”. Nous explorons le régime fortement non-linéaire et dérivons les exposants qui le caractérisent. Dans le cadre d’un univers en expansion, nous montrons que nos résultats sont bien expliqués par un modèle basé sur l’hypothèse du “*stable clustering*”, analogue à celui parfois proposé en trois dimensions.

Dans le Chapitre 5, nous explorons plus en détail les propriétés des distributions de particules produites dans les modèles définis précédemment. Nous effectuons une analyse multifractale de ces distributions et la complétons par une approche analogue à celle utilisée actuellement dans les simulations numériques tridimensionnelles en cosmologie, dans lesquelles la distribution est décrite par une collection de “halos” de taille finie. Nous concluons qu’une description en terme de structures statistiquement virialisées est valide, précisément dans le régime fractal non-linéaire de formation des structures. L’interprétation de nos résultats amène à penser que dans le régime non-linéaire invariant d’échelle, la distribution peut être vue comme correspondant à une sorte de hiérarchie virialisée.

Le Chapitre 6 présente des résultats qui généralisent aux interactions décroissantes à grande distance en loi de puissance l’approche introduite dans le Chapitre 3 pour étudier la définition de la force gravitationnelle en une dimension dans un système d’extension spatiale infinie. Nous donnons ainsi une classification “dynamique” de la portée des interactions s’appuyant sur les propriétés de convergence de la force à grande distance. Nous expliquons également qu’une condition de convergence plus faible est en fait suffisante pour définir la dynamique dans la limite des systèmes d’extension spatiale infinie. Notre conclusion centrale est que l’interaction gravitationnelle (quelque soit la dimension spatiale) est le cas limite pour lequel la dynamique dans la limite des systèmes infinis est bien défini. Le texte de ce chapitre est tiré d’un article publié dans J. Stat. Phys. [68].

Nous terminons cette thèse par une discussion sur les perspectives de recherche envisagées.



# Introduction

The formation of structure in the universe is one of the major open questions in cosmology. Indeed the distribution of visible matter at large scales in the universe appears to be very inhomogeneous today, and presents a highly structured distribution of galaxies: cluster of galaxies, superclusters, voids and filaments. On the other hand, it is inferred from observations of the Cosmic Microwave Background radiation that the universe was in the past very close to homogeneous with tiny density fluctuations. In the theoretical framework of the “standard” cosmological model, it is postulated that the matter in the universe is constituted mainly by so-called *Dark Matter* interacting essentially through gravity. On the spatial scales, relevant to the formation of large structures in the universe, the Newtonian approximation to gravity applies, and thus the problem reduces to the evolution of clustering in an infinite self-gravitating system with close to uniform initial conditions.

Analytical understanding of this problem is limited essentially to linear perturbative approaches to the solution of the fluid equations (*i.e.* the “linear regime” of structure formation), and the study of the “non-linear” regime is mainly probed through numerical investigation. The degrees of sophistication and parallelization of the algorithms used in cosmological simulations has increased impressively in the last decades, with the use notably of highly multithreaded clusters on both CPU and GPU. Despite this progress, cosmological numerical simulations remain limited by a modest resolution (at very most two or three orders of magnitude in scale for non-linear clustering). The absence of analytical “benchmarks” also leaves open to doubt the reliability of the results drawn from them. In this thesis, we approach this problem from a different perspective to the usual one in cosmology, that of statistical physics. Indeed, the formation of structures in the universe through the usual Newtonian gravitational interaction can be seen as a well posed problem of out-of-equilibrium dynamics of systems with *long-range interaction*. In the context of statistical physics, it is natural to develop simplified models (“toy-models”) to try to improve our understanding of this system, reducing as much as possible the question to fundamental aspects. One dimensional versions of the cosmological problem of gravity present the particular interest that they give the opportunity to probe a very large range of scales (even for a number of particles which can be simulated on a single processor). Furthermore, as we will explain, they are extremely precise, being limited only by machine precision. In this thesis we report a detailed study of a class of such models, as well as some more general results on out-of-equilibrium dynamics of long-range interacting systems.

## Organization of the thesis

The first two introductory chapters of this thesis are devoted to giving some standard background which is useful for understanding the context and the results of this thesis. The manuscript is addressed to the two communities, whose methods and problems are relevant, cosmological and statistical physics one. The first introductory chapter gives a review of some relevant methods in statistical physics, while the second one introduces the basics of structure formation in cosmology.

In Chapter 1 we thus give an introduction to the dynamics and thermodynamics of systems with long-range interaction, of which the Newtonian gravitational interaction is an example, outlining important results which have emerged in statistical physics in recent years. These results turn out not to be so directly relevant for our study of self-gravitating systems, because the latter are *infinite* rather than *finite*. They are, however, relevant background to the study we report in Chapter 6.

The second chapter extends the considerations of the previous chapter to the specific case of self-gravitating systems, and then reviews the basics of the standard cosmological model, focusing on the formation of large scale structures. Considering that the systems of particles in cosmology are infinite rather than finite, particular attention must be said to the definition of the gravitational force in these systems. We give an introduction to the kinetic theory used to study the out-of-equilibrium dynamics of infinite self-gravitating systems in cosmology which allows the derivation of the usual hydrodynamic description of these systems. We then present the perturbative treatment of these fluid equations, and then the numerical investigations of the non-linear regime of the formation of structures in the Universe, discussing central notions which are used in this context: self-similarity, stable clustering and “halo models”.

In Chapter 3 we introduce and define the class of  $1 - d$  toy models we study in this thesis. We address the problem of their general formulation in the context of stochastic point process theory, in particular the question of the definition of the total force acting on a particle belonging to an infinite system. We show that this problem arises from a subtlety about how the so-called “Jeans’ swindle” is applied in  $1 - d$ . We underline that the force turns out to be well-defined in  $1 - d$  for a broad class of distributions, a class of perturbed infinite lattice, which are the point processes relevant to cosmological  $N$ -body simulations. The text of this chapter is taken from an article published in Phys. Rev. E. [70]

In Chapter 4 we present results of a numerical investigation of the dynamical evolution of these toy models. We show that they are physically interesting as they present very strong qualitative similarities with the evolution of the analogous  $3 - d$  systems, notably “self-similar” behavior (*i.e.* dynamical scaling) starting from power-law initial conditions. We also explore aspects of these behaviors which one cannot easily probe with  $3 - d$  numerical simulations due to numerical difficulties. We study in particular structure formation for the particular class of initial condition corresponding to “causal fluctuations”. We explore further the strongly clustered regime and derive the exponents which characterize it. We show that our results, for the expanding models, are well accounted for by a model based on a “stable-clustering” hypothesis, analogous to that sometimes proposed in  $3 - d$ .

In Chapter 5 we explore further the properties of the particle distributions produced in models we have studied in the previous chapter. We perform a multifractal

analysis and complete it with an approach analogous to that now used canonically in  $3 - d$   $N$ -body simulations in cosmology in which the distribution is described as a collection of finite “halos”. We reach the conclusion that a description in terms of statistically virialized structures is valid, precisely in the regime where there is fractal clustering. We interpret our results to mean that in the regime of non-linear fractal clustering the distribution can be said to correspond to a kind of “virialized hierarchy”.

Chapter 6 reports results which generalize *to any pair interaction* decaying as a power-law at large separation the approach used in Chapter 3 to determine whether the  $1 - d$  gravitational force is defined in an infinite system. In so doing it gives a “dynamical” classification of the range of pair interactions based on the convergence properties of the force at large distances. It also explains that a weaker convergence condition is in fact a sufficient one for dynamics to be defined in the infinite system limit. Our central conclusion in this respect is that the gravitational interaction (in any dimension) is the limiting case for which an infinite system limit for dynamics can be meaningfully defined. The text of this chapter is taken from an article published in J. Stat. Phys. [68].

We conclude this thesis with a brief discussion of some perspectives for further work.

## INTRODUCTION

# Chapter 1

## Dynamics and thermodynamics of systems with long-range interaction: an introduction

In this first introductory chapter we give a synthetic introduction to the dynamics and thermodynamics of systems with long-range interaction (LRI), and outline the differences with short-range interacting (SRI) systems. It does not contain original material and is based principally on [15,31,43]. Systems with long-range interactions are characterized by a pair potential which decays at large distances as a power law, with an exponent smaller than the space dimension: examples are gravitational and Coulomb interactions (see e.g. [31, 43]). The thermodynamic and dynamical properties of such systems were poorly understood until a few years ago. Substantial progress has been made only recently, when it was realized that the lack of additivity induced by long-range interactions does not hinder the development of a fully consistent thermodynamics formalism. This has, as we will see in more detail in this introductory chapter, however, important consequences: entropy is no more a convex function of macroscopic extensive parameters (energy, magnetization, etc.), and the set of accessible macroscopic states does not form a convex region in the space of thermodynamic parameters. This is at the origin of ensemble inequivalence, which in turn determines curious thermodynamic properties such as negative specific heat in the microcanonical ensemble, first discussed in the context of astrophysics [81]. On the other hand, it has been recognized that systems with long-range interactions display universal non-equilibrium features. In particular, long-lived metastable states, also called quasi-stationary states (QSS) may develop, in which the system remains trapped for a long time before relaxing towards thermodynamic equilibrium.

Historically, it was with the work of Emden and Chandrasekhar [32,54], and later Antonov, Lynden-Bell and Thirring [6,81,103], in the context of astrophysics, that it was realized that for systems with long-range interactions the thermodynamic entropy might not have a global maximum, and therefore thermodynamic equilibrium itself could not exist. The appearance and meaning of negative temperature was first discussed in a seminal paper by Onsager on point vortices interacting via a long-range logarithmic potential in two-dimensions [122].

We formalize this presentation in the following with the study of the equilibrium

statistical mechanics and the out-of-equilibrium dynamics of systems with LRI. We simply search to illustrate in each case, with the use of toy models, a unifying concept: the *mean-field theory* for statistical equilibrium study and the *Vlasov equation* for out-of-equilibrium dynamics.

## 1 Definition of long-range interactions

In this section, we give a pedagogical introduction to the theory of LRI systems. We outline the crucial differences with SRI systems, and present the general idea with a simple toy model: the *Ising model* [30]. Let us consider in Fig. 1.1 a macroscopic

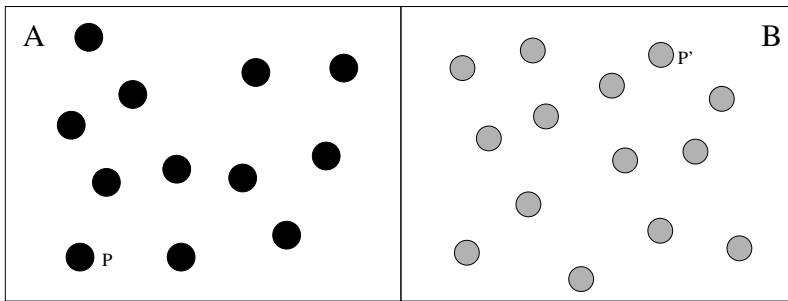


Figure 1.1: Schematic representation of a system made of two sub-systems  $A$  and  $B$ . Particles  $P$  and  $P'$  do not belong to the same sub-system.

system divided into two sub-systems  $A$  and  $B$ . The total energy  $E$  of the macroscopic system is then equal to the sum of the energies of each sub-systems ( $E_A$  or  $E_B$ ), plus the interaction energy  $E_{AB}$  between these two sub-systems, *i.e.*  $E = E_A + E_B + E_{AB}$ . When one considers a short-range interaction between the constituents of this system, this interface energy  $E_{AB}$  is proportional to the surface between these two sub-systems. For a macroscopic system, this is negligible in comparison with the volume energy. The energy of the particle  $P$  in  $A$  is thus insensitive to whether the particle  $P'$  in  $B$  is present. However, this argument is not valid if the interaction is sufficiently long-range as the interface energy is no longer negligible in comparison with the volume energy. To illustrate this difference, we consider the *Ising model*:  $N$  spins  $S_i = \pm 1$ , with  $i \in [1, N]$ , are fixed on a regular lattice and interact with an interaction of infinite range and independent of the distance between the spins. We then can write the Hamiltonian

$$H = -J \sum_{i \neq j} S_i S_j. \quad (1.1)$$

If the parameter  $J > 0$ , the interaction is called *ferromagnetic*, if  $J < 0$  the interaction is called *anti-ferromagnetic* and if  $J = 0$  the spins are non-interacting. When all the spins are ordered in the same positive way, the total energy is simply  $E = -JN(N-1)$ . If we divide the system into two different subsystems made identically of  $N' = N/2$  spins, each subsystem, independently of the other, has a total energy  $E' = -J \frac{N(N-2)}{4}$ . We then obtain  $E \neq 2E'$ . Let us note that the use of a coupling constant  $J' = J/N$  renormalized by the number of spins, as common use for

this mean-field model, gives energies of order  $N$ , *i.e.* the system is called *extensive*, but does not solve the lack of *additivity* of this model.

In the following, we will consider this non-additivity criterion as the definition of long-range interacting system: **a macroscopic system would be considered as “long-range” if we cannot write its total energy as the sum of the energies of independant macroscopic subsystems.** Following this definition, a pair-interaction decaying as a power-law with the distance as  $1/r^\alpha$ , is long-range, when the exponent  $\alpha < d$ , where  $d$  is the spatial dimension.

To illustrate this proposition, we consider a “modified” Ising model which is now not independant of the distance between the spins (the spins are nevertheless still fixed on the lattice sites), and without short-range divergence

$$H = -J \sum_{i \neq j} \frac{S_i S_j}{d_{ij}^\alpha} \quad (1.2)$$

where  $d_{ij}$  represents the distance between two sites  $i$  and  $j$ . This system will be “long-range”, or non-additive, if the spins far away from the site  $i$  contribute in a non-negligible way to the energy of the spin  $S_i$ . This contribution is then negligible as soon as the sum

$$\sum_{j \neq i, N \rightarrow \infty} \frac{1}{d_{ij}^\alpha} \quad (1.3)$$

converges, for a system size going to infinity. Comparing this sum with an integral, one clearly sees that it converges as soon as  $\alpha > d$  where  $d$  is the space dimension. This demonstration can be generalized to the cases where the two-body interaction potential in  $1/r^\alpha$ .<sup>1</sup>

This analysis include the gravitational newtonian interaction but not the Van der Waals interaction. Let us note that this criterion does not correspond to the terminology of critical phenomena, in which long range potential is defined as  $\alpha < D + 2 - \eta$ , where  $\eta$  is a critical exponent which depends on the system, but usually small [20]. Then the designation “long-range” used in the critical phenomena community has a larger meaning than the one refered to in this thesis. Our long-range interactions are also called *non-integrable interactions*.

The non-additivity can generate, as we will see, unusual behaviours as the thermodynamics at equilibrium or out-of-equilibrium dynamical relaxation properties are concerned. Indeed, phase separation in the usual meaning is impossible. This calls into question the equivalence of ensembles between the canonical and the micro-canonical ensembles. Furthermore, the dynamics is now coherent at the scale of the whole system, and this changes the usual understanding of the relaxation towards equilibrium. These different aspects have already been studied in detail in each specific domain: self-gravitating system [124], bidimensional turbulence [34], and plasma physics [53]. As far as equilibrium statistical mechanics and its anomalies are concerned, we can refer to the work of Hertel and Thirring [81]; the similarity of the methods to solve these different models has been developped in the studies

---

<sup>1</sup>We do not consider the limit case where  $\alpha = d$ , as in this case the presence of semi-convergent integrals can yield particular behaviours.

of Spohn et al. [63, 109] and Kiessling et al. [93, 94, 144]. As far as the dynamics is concerned, Chavanis, Sommeria and Robert [34, 36] have developed the analogies between bidimensional turbulence and self-gravitating systems, considering the formal proximity between the Euler and Vlasov equations.

## 2 Equilibrium statistical mechanics of long-range interacting systems

Following the definition of LRI systems introduced previously, the thermodynamics of these systems presents unusual behaviours in comparison with the thermodynamics of SRI systems: the energy is not additive, and then many standard results of the usual thermodynamics and statistical mechanics become inaccurate.

### 2.1 The mean-field Ising model

Let us consider the example of the mean-field Ising model. Its Hamiltonian is

$$H = -\frac{J}{N} \sum_{i,j=1}^N S_i S_j, \quad (1.4)$$

where  $S_i$  represents the spin with value  $\pm 1$ . The coupling constant is renormalized by a factor depending on the number of spins in the system,  $N$ , in order to preserve the extensivity of the system. Without this trick, the thermodynamic limit would not exist in the *usual sense*, *i.e.* the total energy of the system would not be proportional to the system size in the limit where  $N \rightarrow \infty$ . However, even if the interaction is renormalized to keep the system extensive, it is still non-additive; a consequence is that it cannot separate itself into two different phases. Let us imagine a system where the entropy  $S(e)$  is not concave (see Fig. 1.2), and let us consider an energy  $e_0$  below the tangent. For a system with short-range interaction, this curve cannot

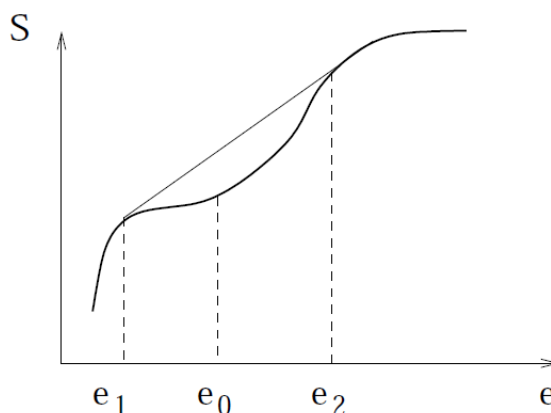


Figure 1.2: Schematic representation of a non-concave entropy in the case of an additive system: for the energy  $e_0$  a phase separation occurs.

represent the entropy  $S(e)$ . The reason is that, owing to additivity, the system represented by this curve is unstable in the energy interval  $e_1 < e_0 < e_2$ . Entropy can

be gained by phase separating the system into two subsystems corresponding to  $e_1$  and  $e_2$ , keeping the total energy fixed. The average energy and entropy densities in the coexistence region are given by the weighted average of the corresponding densities of the two coexisting systems. Thus the correct entropy curve in this region is given by the common tangent line, resulting in an overall concave curve.

However, in systems with long-range interactions, the average energy density of two coexisting subsystems is not given by the weighted average of the energy density of the two subsystems. Therefore, the nonconcave curve in Fig. 1.2 could, in principle, represent an entropy curve of a stable system, and phase separation need not take place. This results in a negative specific heat (see e.g. [31]). Since within the canonical ensemble specific heat is non-negative, the microcanonical and canonical ensembles are not equivalent. The above considerations suggest that the inequivalence of the two ensembles is particularly manifested whenever a coexistence of two phases is found within the canonical ensemble. This inequivalence between the microcanonical and canonical ensembles is known for years in astrophysics, but took time to grow on the statistical physics community where people get used to the canonical ensemble: M. Lax shed light on the inequivalence of ensemble in the spherical model of Berlin and Kac [100], and Hertel and Thirring studied in [81] a simple model inspired from gravity, exactly solvable in both the canonical and microcanonical ensembles, bringing into light the negative specific heat.

The importance of the microcanonical ensemble, as well as its differences with the canonical ensemble, has also been studied these last ten years by D. Gross, even without any long-range interaction, in the domain of systems with few degrees of liberty [78], as in nuclear physics for example.

Let us note that a new definition of the entropy has emerged to solve the physical questions of the long-range interacting systems, intrinsically non-additive [147]: the usual entropy of Gibbs,  $S_G = -\sum_i p_i \ln p_i$ , for a set of probability  $p_i$ , is replaced by the *Tsallis entropy* that depends on a parameter  $q$

$$S_q = \frac{1 - \sum_i p_i^q}{q - 1}, \quad (1.5)$$

and a new thermodynamical formalism is developed, depending on this new parameter  $q$ .  $S_q$  is said non-additive, as the  $q$ -entropy of the union of two independent subsystems (in probability) is not equal to the sum of the two entropies of these subsystems taken independently.  $S_q$  becomes  $S_G$  when  $q \rightarrow 1$ . It seems that this entropy works to describe systems out-of-equilibrium instead of a description of systems at equilibrium (see e.g. [31]).

In the following, we will explain the results of the mean-field approach. Indeed, as often in statistical mechanics, the usual approach is to perform a mean-field approximation. We will use a pedagogical approach based on the use of toy models: we start studying simple models where an analytical approach can be performed.

We must note that we only restrict the analysis to the class of lattice systems. As far as continuous systems are concerned, *i.e.* systems made of particles with translational degrees of freedom, the additivity property is still satisfied in all cases

for which the system does not collapse if the pair-interaction  $V(\mathbf{r}) \propto |\mathbf{r}|^{-\alpha}$  decays at large distances faster than the power law  $r^{-d}$  where  $d$  is the dimension space. Moreover, following Ruelle [136], two conditions must also be considered in the case of continuous systems: the *stability* condition and the *temperedness* condition.

The *stability* condition assures that there will not be situations of collapse of the system. The potential is said to be stable if there exists  $A \geq 0$  such that

$$\sum_{1 \leq i < j \leq N} V(\mathbf{r}_i - \mathbf{r}_j) \geq -NA \quad (1.6)$$

for each configuration  $(\mathbf{r}_1, \dots, \mathbf{r}_N)$ . We note that for this it is necessary that  $V(\mathbf{r})$  to be bounded below for  $r \rightarrow 0$ . Therefore, for the occurrence of normal thermodynamic behavior it is possible to adopt, following Ruelle [136], the following conditions on the two-body potential: the first is the *stability* condition, while the second is

$$V(\mathbf{r}) \leq C|\mathbf{r}|^{-\alpha} \quad (1.7)$$

whenever  $|\mathbf{r}| \geq R_0 > 0$ ; this condition, for  $C > 0$  and  $\alpha > d$ , is called *temperedness*. When *stability* and *temperedness* are satisfied there are theorems that assure the equivalence of ensembles [31].

If we consider LRI systems for which the potential decays at large distance according to  $|\mathbf{r}|^{-\alpha}$  with  $\alpha < d$ , depending on whether it will do so considering repulsion at large distance, or attraction at large distance, the *temperedness* condition or the *stability* condition will be violated, respectively. In both cases, it can be shown that, increasing the size of the systems, the total energy will increase faster than  $N$ , violating the extensivity property, and also the additivity property will not hold [136].

## 2.2 Inequivalence of ensembles: the BEG mean-field model

In the following, we focus our attention on a solvable model introduced originally to study the binary mixing of  $He^3 - He^4$ , and which illustrates the particularities of the thermodynamics of non-additive systems: the *Blume-Emery-Griffiths* (BEG) model [26]. The canonical phase diagram of this model is well known [30], and presents an interesting phenomenology: a line of second order phase transition and a line of first order transition disjoined by a tricritical point. The microcanonical approach has been studied in [30]. Here we present a brief analysis of the BEG model in both the canonical and microcanonical ensembles (see e.g. [15] for more details).

One defines the BEG model as a lattice where each site is occupied by a spin  $S_i = 0, \pm 1$ . one can write the Hamiltonian

$$H = \Delta \sum_{i=1}^N S_i^2 - \frac{J}{N} \left( \sum_{i=1}^N S_i \right)^2, \quad (1.8)$$

where  $J > 0$  is a ferromagnetic coupling constant, and  $\Delta$  controls the energy difference between the magnetic states ( $S_i = \pm 1$ ) and the non-magnetic state ( $S_i = 0$ ). In this Hamiltonian the interaction is renormalized by  $1/N$  to keep the system extensive. However, it does not prevent it from the non-additivity.

### The canonical solution

For small value of  $\Delta/J$ , the system becomes closer to the mean-field Ising model, and undergoes a second order phase transition when  $\beta$  changes. Conversely, when  $T = 0$ , and  $2\Delta/J = 1$ , the paramagnetic phases  $S_i = 0$  for all  $i$ , and ferromagnetic phases  $S_i = 1$  for all  $i$ , are degenerated: a first order phase transition takes place between these two fundamental states. The canonical solution is known for years [26]; the usual method defined the partition function

$$Z(\beta, N) = \sum_{S_i} \exp \left( -\beta \Delta \sum_i S_i^2 + \frac{\beta J}{2N} \left( \sum_i S_i \right)^2 \right). \quad (1.9)$$

One uses the gaussian transformation

$$\exp \left( \frac{\beta N J m^2}{2} \right) = \sqrt{\frac{N}{\pi \beta J}} \int_{-\infty}^{+\infty} dv \exp \left( \frac{-Nv^2}{2\beta J} + Nmv \right), \quad (1.10)$$

to perform the sum over all the accessible configurations:

$$Z(\beta, N) = \sqrt{\frac{N}{\pi \beta J}} \int_{-\infty}^{+\infty} dv \exp \left( \frac{-Nv^2}{2\beta J} \right) \left[ 1 + 2e^{-\beta \Delta} \cosh v \right]^N. \quad (1.11)$$

This last integral can be evaluated by the saddle point method in the limit where  $N \rightarrow \infty$ . The free energy per particles is then

$$F(\beta) = -\frac{1}{\beta} \min_v \left( \frac{v^2}{2\beta J} - \ln[1 + 2e^{-\beta \Delta} \cosh v] \right). \quad (1.12)$$

The line of second order transition is then given by the expression

$$\beta J = \frac{1}{2} e^{\beta \Delta} + 1. \quad (1.13)$$

The tricritical point which separates this line from the first order transition line is at  $\Delta/J = \ln(4)/3$ ,  $\beta J = 3$ . The first order line transition must be obtained numerically. We give in Fig. 1.3 the schematic representation of the canonical phase transition diagram.

### The microcanonical solution

We are now interesting in the microcanonical solution of the BEG model. We then determine the entropy of the system for a given energy. Let us note by  $N_+$ ,  $N_-$ , and  $N_0$  the number of spin  $+1$ ,  $-1$ , and  $0$  of a given microscopic configuration. We note  $q$  the quadrupole moment, and  $m$  the magnetisation per spin,

$$q = \frac{1}{N} \sum_i S_i^2 = \frac{N_+ + N_-}{N}, \quad (1.14)$$

$$m = \frac{1}{N} \sum_i S_i = \frac{N_+ - N_-}{N}. \quad (1.15)$$

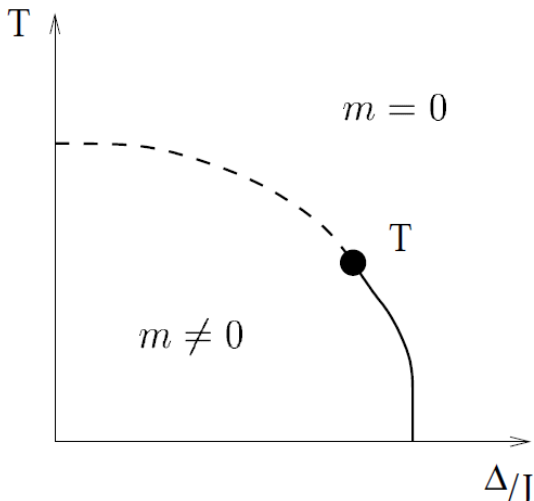


Figure 1.3: Schematic representation of the canonical phase diagram of the mean-field BEG model. For small values of  $\Delta/J$  there is a second order transition (dashed line). When  $\Delta/J$  increases a first order transition appears. This two regimes are separated by a tricritical point ( $T$ ). For  $\Delta/J > 1/2$ , there is no more transition.

The energy per particle, renormalized by  $\Delta$  for convenience, can simply be written

$$e = \frac{H}{\Delta N} \left( q - \frac{J}{2\Delta} m^2 \right). \quad (1.16)$$

As  $N_0 + N_+ + N_- = N$ , the parameters  $q$  and  $m$  are enough to obtain  $N_0$ ,  $N_+$ , and  $N_-$ . By simple combinatory, one obtains the number of microscopic configurations for given  $q$  and  $m$ :

$$\Omega(q, m) = \frac{N!}{N_+! N_-! N_0!}. \quad (1.17)$$

Using the Stirling formula and the standard definition of the entropy, one obtains

$$s(q, m) = -\frac{q+m}{2} \ln \frac{q+m}{2} - \frac{q-m}{2} \ln \frac{q-m}{2} - (1-q) \ln(1-q) - \ln 3. \quad (1.18)$$

The microcanonical entropy is then obtained by maximizing  $s$  for a constant  $e$ . Giving the constraint  $q = e + km^2$ , with  $k = J/2\Delta$ , we obtain a variational problem with a single variable:

$$S(e) = \sup_m (s(e + km^2, m)). \quad (1.19)$$

The microcanonical temperature is then given by  $\Delta\beta = \partial S/\partial e$ .

As in the canonical ensemble, the equation of the second order transition line can be obtained analytically. This critical line stops in a tricritical point given by  $k \approx 1.0813$  and  $\beta\Delta \approx 1.3998$ . These values are close to the canonical values but different as  $k \approx 1.0820$  and  $\beta\Delta \approx 1.3995$ . The second order line stretches off the microcanonical one. In the region between these two different tricritical points, the transition is first order in canonical ensemble, but stays continuous in the microcanonical ensemble (see Figs. 1.4). Beyond the microcanonical tricritical point, the temperature undergoes a discontinuity at the transition of the microcanonical

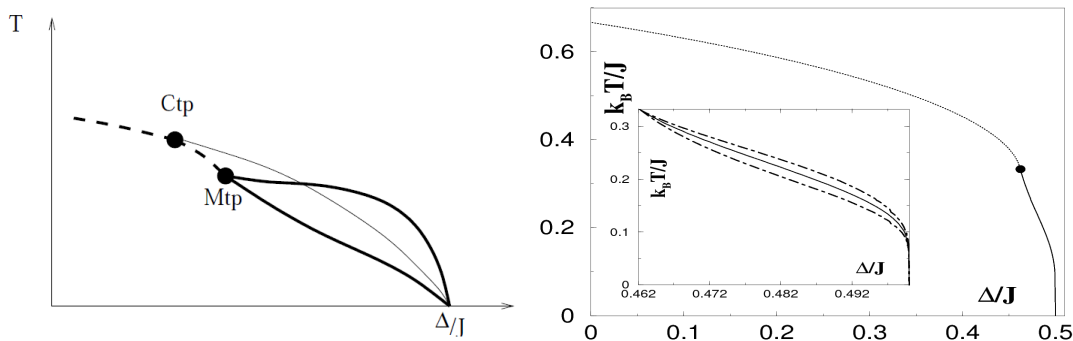


Figure 1.4: Schematic representation of the  $(\Delta/J, T)$  phase diagrams of the BEG model within the canonical and microcanonical ensembles (from [18]). We represent the tricritical canonical point (Ctp) and the tricritical microcanonical point (Mtp). The bold dashed line (on the left of Ctp) illustrates that in the microcanonical ensemble the continuous transition coincides with the canonical one. The line represents the first order canonical phase transition. The bold line represents the microcanonical first order phase transition. The area between delimited by the bold line is not accessible.

critical energy; the two lines in Fig. 1.4 represent the temperature at each side of the jump. All the transitions disappear at  $T = 0, \Delta/J = 1/2$ .

The BEG mean-field model is solvable analytically in both the canonical and microcanonical ensembles. The phenomenology around the tricritical point is interesting as it brings to light the inequivalence of ensembles, with area with negative specific heat and temperature discontinuities.

In the next section, we briefly present a general method to study the equilibrium properties of systems with long-range interaction, which is necessary to solve more complicated models.

## 2.3 Mean-field and large deviation theory

The mean-field approximation consists in evaluate the field on a particle, assuming that all the particles are in a mean state. For LRI systems, a large number of particles contribute to this mean-field, and the fluctuations around this mean-field should be small with the large number theory. It is then conceivable that we can obtain a very good approximation of the real behaviour with this mean-field approach. Furthermore, one can show that the mean-field approximation becomes exact in numerous models, for a large number of particles.

In this subsection we introduce, following [15] without any mathematical rigor, the *large-deviation theory*, a mathematical tool essential to show the accuracy of the mean-field approximation in many instances. It is above all a powerful tool to obtain the equilibrium states in the microcanonical and canonical ensembles.

A rigorous approach of the large-deviation theory is given in [44]; reference [52] gives an application of this theory to statistical physics, with a mathematical point of view.

### How does large-deviation theory work?

Let us consider a sum of  $N$  random variables identically distributed  $X_k$ . Assuming they follow the same probability distribution, with a null average, the empirical average  $S_N$  is then

$$S_N = \frac{1}{N} \sum_{k=1}^N X_k. \quad (1.20)$$

The large number law states that  $S_N$  tends to the average value of  $X_k$ , *i.e.* zero in our case, when  $N$  goes to infinity. If the assumptions of the central limit theorem are valid, one can consider that the function  $P(\sqrt{N}S_N = x)$  goes to a gaussian distribution in  $x$  if we consider random variables with null mean. The fluctuations of  $S_N$  are of order  $1/\sqrt{N}$ . It is also interesting to study the behavior of the tail of the distribution: what is the probability for a fluctuation of order 1? *i.e.* what is the value of  $P(S_N = x)$ ? The large deviation theory is essential to answer this question.

Let us consider an example to illustrate large deviation theory. We consider a coin, and the random variable  $X_k$ , following  $X_k = 1$  for the reverse side,  $X_k = 0$  for the head side. Combinatory simply gives

$$P(S_N = x) = \frac{N!}{\left(\frac{1+x}{2}N\right)!\left(\frac{1-x}{2}N\right)!2^N} \quad (1.21)$$

which gives with the Stirling formula

$$\ln P(x) \sim -N\left(\frac{1+x}{2}\ln\frac{1+x}{2} + \frac{1-x}{2}\ln\frac{1-x}{2} + \ln 2\right) \quad (1.22)$$

$$\sim -NI(x). \quad (1.23)$$

One says that  $S_N$  follows a large deviation principle, with rate function  $I$ .  $I(x)$  is the opposite of the entropy attached to a configuration with a mean value  $x$ . One sees that the values of  $x$  such that  $I(x) > 0$  are exponentially suppressed with  $N$ . Moreover, to satisfy the normalization condition of the probability, one needs  $I(x) \geq 0$ , and  $\inf I(x) = 0$ .

### the Cramer theorem

The Cramer theorem [52] is the mathematical basis to answer to this question for random variables  $X_k$  following the same rapidly decreasing probability distribution. Let us once more consider

$$S_N = \frac{1}{N} \sum_{k=1}^N X_k, \quad (1.24)$$

where  $P(S_N = x)$  follows the large deviation principle

$$\ln P(S_N = x) \sim -NI(x). \quad (1.25)$$

The cramer theorem allows us to compute the rate function  $I(x)$ . To do this, one defines the function

$$\Psi(\lambda) = \langle e^{\lambda \cdot X_1} \rangle, \quad (1.26)$$

where  $\lambda$  is a real value and  $\langle \dots \rangle$  denotes the average value of the probability distribution of  $X_1$  (or of any  $X_k$  as they are identically distributed). The rate function  $I(x)$  is then given by the Legendre transformation of  $\ln \Psi$ :

$$I(x) = \sup_{\lambda} \left( \lambda \cdot x - \ln \Psi(\lambda) \right). \quad (1.27)$$

This theorem is valid if the probability distribution of  $X_k$  is rapidly decreasing at infinity in order to  $\Psi$  to be definite. This gives a general method to evaluate the rate function, when the combinatory methods are not possible, as in the case of a continuous probability density function.

One must note that the large deviation approach does not work for all the systems with long-range interaction. This method consists in introducing coarse-grained variables, and this description is useful to describe structures at the scale of the system. This method is thus useless when interesting phenomena take place at microscopic scales. This can be the case when one considers repulsive force at long range; the mean-field approach predicts the absence of structures at large scales, and the interesting physics at small scale must be studied with a different approach.

In this first introductory section, we have presented the theory of equilibrium statistical mechanics of LRI systems. We have illustrated an interesting result of LRI with the BEG model: the inequivalence of ensemble. We have also introduced the main tool to study these systems, the mean-field approach and have given comments on the large deviation theory .

We have seen in the previous subsection that the equilibrium statistical mechanics provides powerful tools which give information about the microscopic states of LRI systems. However, it is essential to understand the relaxation properties of these systems. It appears that the relaxation time of these systems is very long, and increases with the number of constituents in the system as we will discuss below.

### 3 Out-of-equilibrium dynamics of long-range interacting systems

In the introductory section on the equilibrium properties of LRI systems, we used solvable toy models to shed light on general concepts. We will follow the same approach in this section to introduce the out-of-equilibrium dynamics of LRI systems.

#### 3.1 Introduction

The kinetic theory proposes to study the evolution of macroscopic observables, starting with microscopic equations. However, this evolution is not easy to obtain. It is usually impossible to consider the correlations between particles coming from the dynamics. The kinetic theory describes a system through the use of probability distribution in the  $N$ -particles phase space,  $f_N(\mathbf{r}_1, \mathbf{p}_1, \dots, \mathbf{r}_N, \mathbf{p}_N, t)$ . All the essential information about the correlation are contained in this function. The easiest approximation consists in neglecting these correlations, and in describing the system

with a one-particle probability distribution,  $f(\mathbf{r}, \mathbf{p}, t)$ ; The  $N$ -particles probability distribution is then linked to the one-particle distribution function through the relation

$$f_N(\mathbf{r}_1, \mathbf{p}_1, \dots, \mathbf{r}_N, \mathbf{p}_N, t) = f(\mathbf{r}_1, \mathbf{p}_1, t) \dots f(\mathbf{r}_N, \mathbf{p}_N, t). \quad (1.28)$$

This one-particle function evolves under the mean-field potential, and under the collisions between the particles

$$\frac{\partial f}{\partial t} + \mathbf{p} \cdot \nabla_{\mathbf{r}} f - \nabla_{\mathbf{r}} V \cdot \nabla_{\mathbf{p}} f = C(f), \quad (1.29)$$

where  $V$  is the potential, and  $C(f)$  represents the collisional evolution. If we neglect the collision term, we obtain the *Vlasov equation* that could be seen as the dynamical equivalent of the mean field approximation in the equilibrium analysis.

General results exist allowing to show the convergence of the particular dynamics through the dynamics of the Vlasov equation, for a number of particles which goes to infinity. The Braun and Hepp theorem [28] gives mathematical rigour to state this. Let us consider a classical system of  $N$  particles, interacting through the potential,

$$E_p = \frac{1}{N} \sum_{1 \leq i < j \leq N} \Phi(\mathbf{x}_i - \mathbf{x}_j), \quad (1.30)$$

where the potential  $\Phi$  is even and regular enough. Then for all time  $t$ , and for any given acceptable error  $\epsilon$ , there exists a number  $N$  of particles for which the particular and Vlasov dynamics coincide until the time  $t$ , with a maximal error  $\epsilon$ . As for any equilibrium study, the renormalization factor  $1/N$  of the interaction corresponds to the limit where the number of particles goes to infinity, keeping constant the microscopic time scale of the system. This could be the physical interesting limit. Moreover, let us note that the regularity assumption of the  $\Phi$  potential is not valid for self-gravitating systems. This difficulty comes from the short distance singularity of this interaction.

The Vlasov equation acquires from the particular dynamics the same conserved quantities (total energy, momentum, ...). Furthermore, the consideration of a continuous description generates also an infinite number of conserved quantities, called the *Casimirs*. Indeed, the Vlasov equation is a non-linear equation of advection of the density  $f$ , which means that the quantities

$$I[\phi] = \int d\mathbf{r} d\mathbf{p} \phi(f(\mathbf{r}, \mathbf{p}, t)), \quad (1.31)$$

where  $\phi$  is some function, are conserved. These new conserved quantities play an important role in the particular dynamics. Furthermore, it is known that this equation has many stationary solutions. These two points then give intuition why the relaxation toward equilibrium of systems with LRI are very slow.

### collisional relaxation and violent relaxation

If one neglects collisions between particles, *i.e.* the right hand side of Eq. (1.29)  $C(f) = 0$ , creating an infinite number of new conserved quantities, one could think that the Vlasov dynamics would not relax towards a statistical equilibrium. In

reality, the Vlasov dynamics creates rapidly a finer and finer filamentation of the density  $f$ . Then an equilibrium distribution can appear for the density  $\bar{f}$ , coarse-grained density of the real density  $f$ . This is the idea of *violent relaxation* introduced by Lynden-Bell in 1968 in astrophysics [103]. This violent relaxation plays its role on shorter time scale than the collisional relaxation, and then gives a statistical equilibrium different from the standars collisional equilibrium, as it contains new conserved quantities. We will come back again to the Vlasov equation with its illustration in the ferromagnetic Hamiltonian-Mean-Field toy model.

The result of Braun and Hepp can lead to the idea that the Vlasov equation can play the same role as the mean-field approximation at equilibrium. In reality, the theorem shows the convergence towards the Vlavov dynamics when  $N \rightarrow \infty$ , for any bounded temporal interval. In other words, the discrete dynamics and the Vlasov dynamics coincide over a time scale which scales with the number of particles  $N$ .

### 3.2 Slow relaxation to equilibrium: the ferromagnetic Hamiltonian-Mean-Field model

To illustrate the particular behaviour of relaxation towards equilibrium in LRI systems, we consider the well known toy model: the ferromagnetic Hamiltonian-Mean-Field (HMF) model [30]. It describes the interaction of  $N$  identical particles which move on a circle of radius unity. We can write its hamiltonian

$$H = \sum_j \frac{p_j^2}{2} - \frac{1}{N} \sum_{i,j} \cos(\theta_i - \theta_j), \quad (1.32)$$

where the particle position  $\theta_i$  is between 0 and  $2\pi$ . The coupling constant is negative and the system tends naturally to a magnetized state, *i.e.*  $\mathbf{M}_1 = (\sum e^{i\theta_j})/N \neq 0$ . In that case, it has been shown in [5] that the canonical and microcanonical ensembles were equivalent. However, for some particular initial conditions, the system does not relax to equilibrium (see e.g. Fig. 1.5). In fact, the system relaxes towards equilibrium, but relaxes slower as the number of particles increases. For sufficiently large  $N$ , however, it is difficult to observe this relaxation in numerical simulations. Fig. 1.6 illustrates this behaviour: the magnetisation stays initially close to 0, and relaxes to its equilibrium value  $M_1 = |\mathbf{M}_1| \neq 0$  for times that increase with the number of particles in the system. Let us consider this evolution through the eyes of the Vlasov equation:

- the system quickly evolves following the Vlavov dynamics, in a time scale independant of the number of particles;
- the system stays trapped near one of the numerous stationary states of the Vlasov equation. If the violent relaxation theory is valid, this state is the statisical equilibrium of the Vlasov equation. In reality, it does not correspond however exactly to this statistical equilibrium;
- the system evolves slowly under the effects of collisions. The time scale depends now on the number of particles in the system. One can assume that the system evolves among the numerous stationary states of the Vlasov equation;

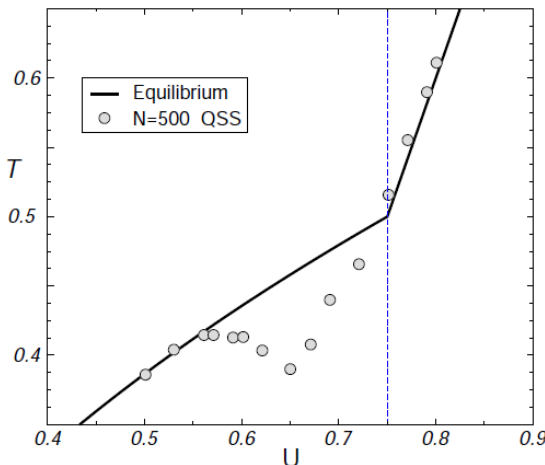


Figure 1.5: Representation of the  $(T, U)$  diagram (from [15]) for the ferromagnetic HMF model. The straight line represents the canonical equilibrium state. The vertical dashed line marks where the second order phase transition takes place. The circular points stand for the result of the molecular numerical simulation, starting with out-of-equilibrium initial condition and for long integration time.

- finally, the system reaches a stable stationary state of the Vlasov equation: the collisional statistical equilibrium. This is different from the statistical equilibrium of the Vlasov equation, as the Casimirs are not conserved through the collisional relaxation.

The system could of course stay trapped in these stable stationary states for different reasons (as it is the case for the antiferromagnetic HMF model [16, 17]). However, these states are the most natural hypothesis.

The ferromagnetic HMF model is a popular toy model to study the Vlasov dynamics. The idea of this section is not to perform a complete analytical analysis of the HMF model, although the simplicity of this model gives this opportunity. In the following the approach of the Vlasov stable stationary states, and the slow evolution towards equilibrium, amongst the stable stationary states of the vlasov dynamics are illustrated with the results of numerical analysis (see e.g. [156] for more details).

### The Vlasov equation

The first step of the evolution presented above corresponds to a rapid evolution, under the effect of the Vlasov dynamics, on a time scale independant of the number of particles in the system. To determine the stationary states of this equation for the HMF model one considers the equation of motion

$$\frac{d\theta_j}{dt} = p_j, \quad \frac{dp_j}{dt} = -M_x \sin \theta_j + M_j \cos \theta_j, \quad (1.33)$$

where  $M_x$  and  $M_y$  represent the real and imaginary parts of the complex magnetisation  $\mathbf{M}_1$ . To follow the Vlasov approach, one must consider the approximation of

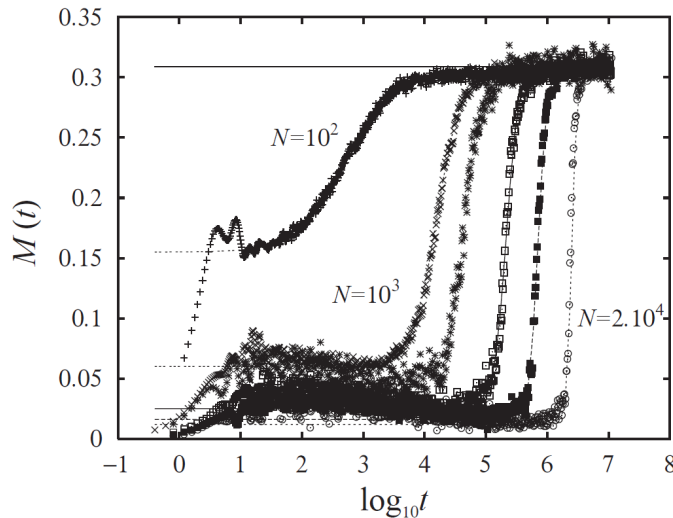


Figure 1.6: Temporal evolution of the magnetisation  $M(t)$  for a number of particles  $N = 100(1000)$ ,  $1000(100)$ ,  $2000(8)$ ,  $5000(8)$ ,  $10000(8)$  and  $20000(4)$  from left to right (from [156]). We give in bracket the number of realisations used to perform the ensemble average. The horizontal line represents the equilibrium value of the magnetization.

the discrete distribution

$$\frac{1}{N} \sum_{j=1}^N \delta(\theta - \theta_j, p - p_j) \quad (1.34)$$

with a continuous density in the one-particle phase space  $f(\theta, p, t)$ . One can write

$$M_x[f] \equiv \int \cos(\theta) f(\theta, p, t) d\theta dp, \quad M_y[f] \equiv \int \sin(\theta) f(\theta, p, t) d\theta dp. \quad (1.35)$$

In this approximation (which becomes exact in the limit  $N \rightarrow \infty$ ) all the particles feel the same potential

$$V(\theta)[f] = 1 - M_x[f] \cos \theta - M_y[f] \sin \theta. \quad (1.36)$$

The Vlasov equation can be written [31]

$$\frac{\partial f}{\partial t} + p \frac{\partial f}{\partial \theta} - \frac{dV}{d\theta}[f] \frac{\partial f}{\partial p} = 0. \quad (1.37)$$

As explained previously, the Vlasov equation conserves the energy and the momentum of the system, *i.e.*

$$H[f] = \int \frac{p^2}{2} f(\theta, p, t) d\theta dp - \frac{M_x^2 + M_y^2}{2} \quad (1.38)$$

and

$$P = \int p f(\theta, p, t) d\theta dp, \quad (1.39)$$

and conserves an infinite number of new quantities, the so called *Casimirs*

$$C_\phi[f] = \int \phi(f(\theta, p, t)) d\theta dp, \quad (1.40)$$

where  $\phi$  is a continuous function. The stationary states of the Vlasov equation, obtained with the method of characteristics [41], are given by the density  $f$  constant along the characteristics of the equation *i.e.* the level line of the energy  $\epsilon$

$$\epsilon(\theta, p) = \frac{p^2}{2} + V(\theta) = \frac{p^2}{2} + 1 - M_x[f] \cos \theta - M_y[f] \sin \theta. \quad (1.41)$$

The stationary solutions of the Vlasov equation are then given by  $f(\theta, p) = \psi(\epsilon(\theta, p))$ , where  $\psi$  is any function. The particular case  $\psi = \exp(-\beta\epsilon)$  corresponds to statistical equilibrium.

One could expect that a large number of stationary states would prevent the Vlasov equation to reach its statistical equilibrium, and on the other hand would spark off the slow relaxation or the QSS observed with the particular dynamics. It is then interesting to study the stability of these stationary states to give an explanation of the slow relaxation towards equilibrium for a particular class of initial conditions.

The main idea of this method for a dynamical system can be introduced as follow (see e.g. [15] for more details): considering a conserved quantity  $F[f]$  using conserved quantities as energy and casimirs, any extemum  $f_0$  of  $F$  is a stationary point of the dynamics. Moreover, if  $f_0$  is a strict maximum or minimum of  $F$ ,  $f_0$  is said to be *formaly stable*. The different kind of stabilities can be studied in [83]. This is a standard method in plasma physics which gives the opportunity to obtain results of non-linear stability. This was used, for example, by Kandrup for self-gravitating systems [91]. The formal functional quantity considered in [15] is

$$F[f] = C_s[f] - \beta H[f] - \mu \int f(\theta, p, t) d\theta dp \quad (1.42)$$

where  $\beta$  and  $\mu$  are two free parameters. The energy  $H$ , the Casimir  $C_s$  and  $\int f = 1$  are quantities conserved by the dynamics. The critical points of this functional gives the stationary states of the Vlasov equation. The stability of these stationary states is then studied considering the second variations of this functional. Yamaguchi et al. studied in [156] a simple criterion for stability for all the homogeneous stationary states of the Vlasov equation and showed that the presence of these stable stationary states would give an explanation to the slow relaxation toward equilibrium for a certain class of initial conditions.

### 3.3 Convergence towards a stationary state of the Vlasov equation

If the initial condition does not correspond to a stable stationary solution of the Vlasov equation, it is natural to assume that the system will evolve, under the effect of the Vlasov dynamics, towards a stable stationary solution after a rapid evolution. This hypothesis can however only be tested with numerical simulations (see e.g. [156, 159]).

These numerical simulations show that, after a rapid relaxation, the evolution can be parametrized with an evolution among the stable stationary states of the Vlasov equation; the system reaches finally the statistical equilibrium. Two main points remain however unsolved: one the one hand, the Vlasov stationary state chosen by the violent relaxation is not explained, and on the other hand, the dynamics which governs the slow evolution among the stationary states.

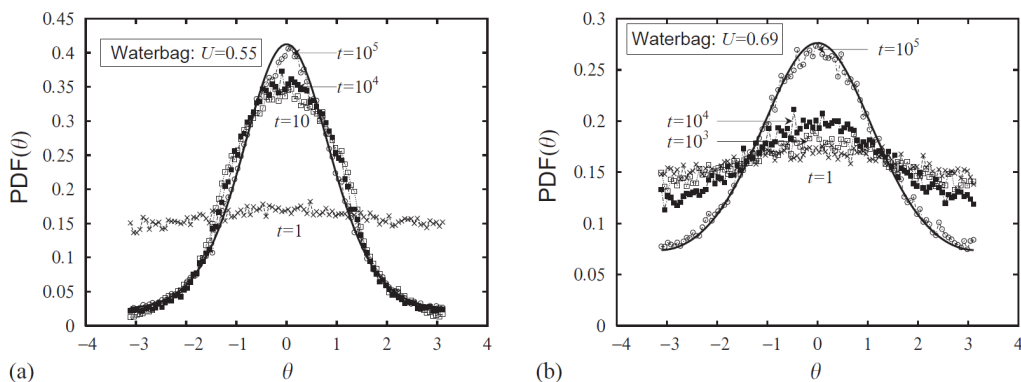


Figure 1.7: Temporal evolution of the distribution  $f(\theta, t)$  obtained for a “water-bag” initial condition for the velocities (from [156]). The number of particles is  $N = 1000$  and an ensemble average over 100 realisations is performed. For  $U = 0.55$  and  $U = 0.69$ , we represent the distribution at time  $t = 1$  (cross),  $t = 10$  (white square),  $t = 10^4$  (black square) and  $t = 10^5$  (white circle). The straight line represents the equilibrium distribution.

The numerical study of the slow evolution has been studied in [156] for the HMF model. We consider the results presented in Fig. 1.7 to illustrate briefly the slow convergence of the angular and velocity distributions towards the statistical equilibrium state. The initial condition of this simulation is a *water-bag* velocity distribution and an homogeneous angle distribution. For  $U = 0.55$  (left hand panel in Fig. 1.7), the initial condition is unstable and the system undergoes a rapid evolution between  $t = 1$  and  $t = 10$ . The system evolves then slowly towards the equilibrium state reached for  $t \sim 10^5$ . For  $U = 0.69$  (right hand panel in Fig. 1.7), the initial condition is stable. The dynamics is then very slow right from the begining and the equilibrium state is reached at  $t \sim 10^5$ . One must notice that, although the dynamics evolves slowly, it seems that the evolution of the system is continuous. It is then difficult to define a QSS (see e.g. [156, 159]).

We conclude this introductory section with the study of the time scales of the HMF model. We have already said that the relaxation time, *i.e.* the lifetime of the out-of-equilibrium states, increases with the number of particles in the system. It is thus interesting to understand this temporal dependence to identify the different regimes of the dynamical evolution. Astrophysics provides a very nice example to illustrate this question: It is believed that the structure of galaxies arises from violent relaxation while the collisional relaxation could play a role in the dynamics of the globular clusters [34].

As far as the HMF model is concerned, the theorem of Braun and Hepp [28] states that the Vlasov dynamics and the particular dynamics coincide on a timescale of order  $\ln N$ . One could then expect a first relaxation time  $t_{rel} \sim \ln N$ . Using the HMF model with  $U = 0.69$  and water-bag velocity distribution and homogeneous angular distribution, Yamaguchi et al. studied in [156] the temporal evolution of  $M_1(t)$  for a number of particle  $N = 10^2, 10^3, 2.10^3, 5.10^3, 10^4$  and  $2.10^4$  (see Fig. 1.8). To study the timescale relaxation represented in Fig. 1.8,  $M_1(t)$  is approximated by

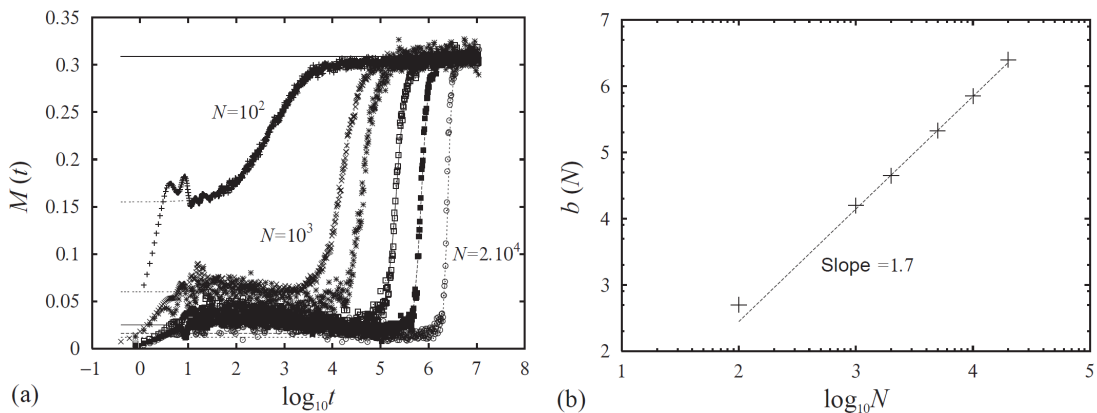


Figure 1.8: Panel (a) presents the temporal evolution of the magnetization  $M(t)$  for different particles numbers  $N = 100(1000), 1000(100), 2000(8), 5000(8), 10000(8)$  and  $20000(4)$  from left to right. The number between brackets corresponds to the number of samples. The horizontal line represents the equilibrium value of  $M$ . Panel (b) shows the logarithmic timescale  $b(N)$  as a function of  $N$ . The dashed line corresponds to  $b(N) \sim N^{1.7}$ . (from [156])

hyperbolic tangent [156], *i.e.*

$$M_1(t) = \left[ 1 + \tanh \left( a(N)(\log_{10} t - b(N)) \right) \right] c(N) + d(N), \quad (1.43)$$

where the parameters  $a(N)$ ,  $b(N)$ ,  $c(N)$  and  $d(N)$  represent respectively the slope at time  $\log_{10}(t) = b(N)$ , the time scale, the semi-difference between the initial level and the equilibrium level of  $M_1(t)$  and the initial level of  $M_1(t)$ . The equilibrium level is given by the statistical mechanics and the initial level by the fluctuation proportional to  $1/\sqrt{N}$ . Fig. 1.8 shows that, for  $U = 0.69$ ,  $b(N) \propto N^{1.7}$  which is the same dependance found by Zanette et al in [159] for different initial conditions. This exponent stays unexplained, but analytical approaches try to explain it (see e.g. [90]).

Let us recall briefly the results presented above. We have characterized the stationary states of the Vlasov equation and presented a method to study their stability. It has been shown in [156] that it was possible to analyse them as maxima of a functional constructed with conserved quantities as energy and Casimirs. For a class of initial conditions which are not stable stationary states of the Vlasov equation, the system rapidly relaxes towards a stable stationary state, *i.e.* the so

called *violent relaxation*. The system then evolves slowly among the stable stationary states towards the statistical equilibrium state, the so called *collisional relaxation*.

This introductory chapter was limited to the study of different toy models. It is however expected that it could be generalized to any long-range interacting systems even if the analysis of each system must be adapted to each model.

## 4 Conclusion

In this first introductory chapter we have given a brief overview of the physics of long-range interacting systems: the statistical mechanics at equilibrium and the out-of-equilibrium dynamics. We have illustrated the particular behaviours which emerge from these systems using simple toy models: the *Blume-Emery-Griffiths* model, the *Ising* model and the *Hamiltonian-Mean-Field* model which have been used as tools in the statistical physics community to probe the physics of the LRI systems.

In the first section of this chapter, we have underlined the inequivalence of ensembles between the microcanonical and the canonical ensemble in the BEG model. We have also introduced the mean-field approach and the large-deviation theory which is the mathematical basis to justify the relevance of this approach.

However, the knowledge of the equilibrium properties remains incomplete if we cannot probe the physics of the relaxation towards this equilibrium. This was the subject of the second section of this chapter. Following a kinetic theory approach, we have introduced the Vlasov equation which can be seen as the *dynamical equivalent* of the mean field approximation. We have seen that the Vlasov equation has an infinite number of conserved quantities, the so-called Casimirs, which underlie the slow relaxation towards equilibrium. We have briefly presented a method extracted from [156] which gives the opportunity to obtain the stationary states of the Vlasov equation as well as to analyse their stability. Indeed, for a class of initial conditions which are not stable stationary states of the Vlasov equation, the system rapidly relaxes towards a stable stationary state, and then evolves slowly among these stationary states until it reaches the statistical equilibrium through the collisional relaxation.



# Chapter 2

## Basic results on self-gravitating systems

We first extend the considerations of the previous chapter to the specific case of self-gravitating systems discussing the statistical equilibrium of self-gravitating systems: we use the mean field approximation introduced in Chapter 1 for an LRI system, which leads to the well known *isothermal sphere* solution. The rest of the chapter concerns self-gravitating systems in the context of cosmology, which are intrinsically different to those considered in Chapter 1 because they are *infinite* rather than *finite*. To give some background, we review the basics of the standard cosmological model, focusing on the formation of large scale structure. The understanding of the origin of large scale structure in the universe (cluster of galaxies, superclusters) is indeed one of the major unsolved questions in cosmology. In the next section we give an introduction to the kinetic theory used to study the out-of-equilibrium dynamics of infinite self-gravitating systems in cosmology, and which allow the derivation of the equation of an (infinite) self-gravitating fluid (*i.e.* a hydrodynamic description of the system). We present the perturbation theory of these fluid equations, where the density field is described with smooth functions, and consider non-continuous approach in terms of discrete particles. Following [126], this latter analysis leads to a condition on the initial fluctuation for the applicability of fluid linear theory. We then introduce the concept of stochastic distributions and the most important quantities that characterize them, as density fields in cosmology are usually treated as a mean background positive density with small positive and negative stochastic fluctuations. We conclude this introductory chapter with a section which presents the numerical investigations of the non-linear regime of the formation of structures in the Universe, and a discussion of central notions which are used in this context (self-similarity, stable clustering and halo models).

### 1 Finite self-gravitating systems: statistical equilibrium and dynamical evolution

In this section we first present some aspects of the statistical mechanics of finite self-gravitating systems. We discuss the mean-field approach, already introduced in Chapter 1, in this particular case and discuss the resulting isothermal spheres solution. We also introduce an important result for self-gravitating systems, the

virial theorem.

## 1.1 Statistical equilibrium of self-gravitating systems

In the case that a self-gravitating system is sufficiently far from other matter in the universe so that tidal forces due to the latter are sufficiently weak (*i.e.* play a role only on a timescale much longer than the characteristic timescale for the evolution of the system itself), one would expect to be able to treat this system as isolated and apply a statistical mechanics treatment like that discussed for a generic LRI in Chapter 1. One such case are astrophysical systems such as globular clusters and galaxies, which are made of stars which, except when they are close enough to be in contact physically, interact via the  $1/r$  potential. Another case where such an approach may be useful are dark matter “halos” around astrophysical object, postulated to be constituted of (perhaps elementary) particles which interact essentially through gravity alone.

Realistic astrophysical systems of this kind are open in the sense that particles in these systems can escape to infinity. It is easy to see, however, that in the microcanonical ensemble the integral defining the density of state  $g(E)$ , *i.e.*

$$g(E) = \frac{1}{N!} \int dq \, dp \, \delta(E - H(q, p)), \quad (2.1)$$

will diverge if the range of spatial integrations is extended to infinity [124]. This divergence is in addition to any divergence we may encounter due to the short distance behaviour of the potential. A similar divergence of  $g(E)$  will occur even for an ideal gas if it were not confined in a box. We are, therefore, forced to introduce the first artificiality: one must confine the system inside a spherical box of radius  $R$ . This assumption can be justified if one can demonstrate that the fractional rate of evaporation of particles from the system is small.

Given such a confining volume and a suitable short distance behaviour of the potential, one can, in principle, compute the phase volume  $g(E, V)$  and the entropy  $S(E, V)$ . However, these quantities behave in an unfamiliar manner for gravitating systems. The central difficulty arises from the non-extensive nature of the energy already introduced in Chapter 1.

There is also another well known property of gravitating systems [124]: gravitating systems in virial equilibrium have negative specific heat. However, systems described by the canonical distribution cannot have negative specific heat. No such constraint exists for the microcanonical distribution. Therefore it is often claimed that the microcanonical distribution is the proper distribution to use in the study of gravitating systems [124].

Let us note that even though the canonical distribution cannot be derived from the microcanonical distribution in the presence of long-range forces one can, purely as a formal mathematical concept, define the partition function for such systems. Comparing the function  $E(\beta)$  obtained from the microcanonical distribution with the corresponding function obtained from the partition function one can prove that the negative specific heat region of the microcanonical distribution is replaced by a phase transition in the canonical distribution [124].

In the following, we shall assume that the potential effects due to the short distance singularity is regularized by a *soft* or *hard* core radius. This assumption

allows us to concentrate on the statistical aspects of the gravitating system, without worrying about the complicating details of close encounters. Let us note that, as far as numerical simulation are concerned, it is principally the soft core regularization which is used as its numerical implementation is less *numerically costly*.

### Mean field equilibrium of gravitating systems

In the following, we study the physics of the gravitating systems in the mean field limit introduced in Chapter 1, which ignores the granularity and correlations present in the  $N$ -particle system.

Consider a system of  $N$  particles interacting with each other through the two-body potential  $U$ . The entropy  $S$  of this system, in the microcanonical description, is defined through the relation

$$e^S = g(E) = \frac{1}{N!} \int d^{3N}x \, d^{3N}p \, \delta(E - H) = \frac{A}{N!} \int d^{3N}x \left( E - \frac{1}{2} \sum_{i \neq j} U(x_i, x_j) \right)^{3N/2}, \quad (2.2)$$

wherein one has performed the momentum integrations and replaced  $(3N/2 - 1)$  by  $3N/2$ . We shall approximate this expression in the following manner. Let the spatial volume  $V$  be divided into  $M$  (with  $M \ll N$ ) cells of equal size, large enough to contain many particles but small enough for the potential to be treated as a constant inside each cell. Instead of integrating over the particle coordinates  $(x_1, x_2, \dots, x_N)$ , we shall sum over the number of particles  $n_a$  in the cell centred at  $x_a$ , where  $a = 1, 2, \dots, M$ . Using the standard result that the integration over  $\frac{d^{3N}x}{N!}$  can be replaced by

$$\sum_{n_1=1}^{\infty} \frac{1}{n_1!} \cdots \sum_{n_M=1}^{\infty} \frac{1}{n_M!} \delta\left(N - \sum_a n_a\right) \left(\frac{V}{M}\right)^N, \quad (2.3)$$

one can rewrite Eq. (2.2) as

$$\begin{aligned} e^S &= \sum_{n_1=1}^{\infty} \frac{1}{n_1!} \cdots \sum_{n_M=1}^{\infty} \frac{1}{n_M!} \delta\left(N - \sum_a n_a\right) \left(\frac{V}{M}\right)^N \left(E - \frac{1}{2} \sum_{a \neq b}^M n_a U_{ab} n_b\right)^{3N/2} \\ &\approx \sum_{n_1=1}^{\infty} \cdots \sum_{n_M=1}^{\infty} \delta\left(N - \sum_a n_a\right) \exp S[n_a], \end{aligned} \quad (2.4)$$

where

$$S[n_a] = \frac{3}{2} N \ln \left( E - \frac{1}{2} \sum_{a \neq b}^M n_a U(x_a, x_b) n_b \right) - \sum_{a=1}^M n_a \ln(n_a M/V). \quad (2.5)$$

In arriving at the last expression, the Stirling approximation for the factorials is used and the unimportant constant  $A$  is ignored. The mean field limit is now obtained by retaining in the sum in Eq. (2.4) only the term for which the summand reaches the maximum value, subject to the constraint on the total number. That is, one assumes

$$\sum_{n_a} e^{S[n_a]} \approx e^{S[n_{a,max}]}, \quad (2.6)$$

where  $n_{a,max}$  is the solution to the variational problem

$$\left( \frac{\partial S}{\partial n_a} \right)_{n_a=n_{a,max}} = 0 \quad (2.7)$$

with  $\sum_{a=1}^M n_a = N$ . Imposing this constraint with a lagrange multiplier and using expression Eq. (2.5) for  $S$ , one obtains the equation satisfied by  $n_{a,max}$ ,

$$\frac{1}{T} \sum_{b=1}^M U(x_a, x_b) n_{b,max} + \ln(n_{a,max} M/V) = \text{constant}, \quad (2.8)$$

where we have defined the temperature  $T$  as

$$\frac{1}{T} = \frac{3}{2} N \left( E - \frac{1}{2} \sum_{a \neq b}^M n_a U(x_a, x_b) n_b \right)^{-1} = \beta. \quad (2.9)$$

We see from Eq. (2.5) that this expression is also equal to  $\partial S / \partial E$ ; therefore,  $T$  is indeed the correct thermodynamic temperature. We can now return back to the continuum limit with the replacements

$$n_{a,max} M/V = \rho(x_a) \quad \text{and} \quad \sum_{a=1}^M \rightarrow \frac{M}{V}. \quad (2.10)$$

In this limit the extremum solution Eq. (2.8) is given by

$$\rho(x) = A \exp[-\beta \phi(x)] \quad \text{and} \quad \phi(x) = \int d^3y U(x, y) \rho(y), \quad (2.11)$$

which, in the case of gravitational interactions, becomes

$$\phi(x) = -G \int \frac{\rho(y) d^3y}{|x - y|}. \quad (2.12)$$

This equation represents the equilibrium configuration for a gravitating system in the mean field limit. The constant  $\beta$  is already determined through Eq. (2.9) in terms of the total energy of the system. The constant  $A$  has to be fixed in terms of the total number (or mass) of the particles in the system. A more formal derivation of the above result can be given using the functional integral representation of the partition function. It turns out that the saddle point approximation of the functional integral leads to the mean field description (see e.g. [124]).

An important point needs to be noted about the mean field result we have obtained: the various manipulations tacitly assume that the expressions we are dealing with are finite. Unfortunately, for gravitational interactions without a short distance cutoff, the quantity  $e^S$ , and hence all the terms we have been handling, are divergent. One should therefore remember that a short distance cutoff is needed to justify the entire procedure. One shall continue to work with Eq. (2.12) because of its mathematical convenience. The effects due to the short distance cutoff are described in [124].

### Isothermal spheres

It can easily be shown that among all the solutions to Eq. (2.8) the spherically symmetric configuration maximises the entropy (see e.g. [6]). This solution represents what is known as the *gravitational isothermal sphere*. The extemum condition for the entropy is equivalent to the following differential equation for the gravitational potential:

$$\nabla^2 \phi = 4\pi G \rho_c e^{-\beta[\phi(x)-\phi(0)]}. \quad (2.13)$$

Given the solution to this equation, all other quantities can be determined. As we shall see, this system shows several peculiarities. It is convenient to introduce length, mass, and energy scales by the definitions

$$L_0 = (4\pi G \rho_c \beta)^{1/2}, \quad M_0 = 4\pi \rho_c L_0^3, \quad \phi_0 \equiv \beta^{-1} = \frac{GM_0}{L_0}, \quad (2.14)$$

where  $\rho_c = \rho(0)$ . All other physical variables can be expressed in terms of the dimensionless quantities

$$x \equiv \frac{r}{L_0}, \quad n = \frac{\rho}{\rho_c}, \quad m = \frac{M(r)}{M_0}, \quad y \equiv \beta[\phi - \phi(0)]. \quad (2.15)$$

In terms of  $y(x)$ , the isothermal equation Eq. (2.13) becomes

$$\frac{1}{x^2} \frac{d}{dx} \left( x^2 \frac{dy}{dx} \right) = e^{-y}, \quad (2.16)$$

with the boundary condition  $y(0) = y'(0) = 0$ . Let us consider the nature of the solutions to this equation.

By direct substitution, one sees that  $n = 2/x^2$ ,  $m = 2x$ ,  $y = 2 \ln(x)$  satisfies these equations. This solution, however, is singular at the origin and hence is not physically admissible. The importance of this solution lies in the fact that other (physically admissible) solutions tend to this solution for large values of  $x$  [124]. This asymptotic behavior of all solutions shows that the density decreases as  $1/r^2$  for large  $r$ , implying that the mass contained inside a sphere of radius  $r$  increases as  $M(r) \propto r$  at large  $r$ . To find physically useful solutions, it is necessary to assume that the system is enclosed in a spherical box of radius  $R$ . In what follows, it will be assumed that the system has some cutoff radius  $R$ .

Eq. (2.16) is invariant under the transformation  $y \rightarrow y+a$ ,  $x \rightarrow kx$  with  $k^2 = e^a$ . This invariance implies that, given a solution with some value of  $y(0)$ , we can obtain a solution with any other value of  $y(0)$  by simple rescaling. Therefore, only one of the two integration constants in Eq. (2.16) is really nontrivial. Hence it must be possible to reduce the degree of the equation from two to one by a judicious choice of variables [124]. One such of set variables is

$$v \equiv \frac{m}{x}, \quad u \equiv \frac{nx^3}{m} = \frac{nx^2}{v}. \quad (2.17)$$

In terms of  $v$  and  $u$ , Eq. (2.13) becomes

$$\frac{u}{v} \frac{dv}{du} = -\frac{u-1}{u+v-3}. \quad (2.18)$$

The boundary conditions  $y(0) = y'(0) = 0$  translate into the following:  $v$  is zero at  $u = 3$ , and  $\frac{dv}{du} = -5/3$  at  $(3, 0)$ . The solution  $v(u)$  has to be obtained numerically: it is plotted in Fig. 2.1 as the spiraling curve. The singular points of this differential equation are given by the intersection of the straight lines  $u = 1$  and  $u + v = 3$ , on which the numerator and denominator of the right-hand side of Eq. (2.18) vanish; that is, the singular point is at  $u_s = 1$ ,  $v_s = 2$ , corresponding to the solution  $n = 2/x^2$ ,  $m = 2x$ . It is obvious from the nature of the equation that the solutions will spiral around the singular point.

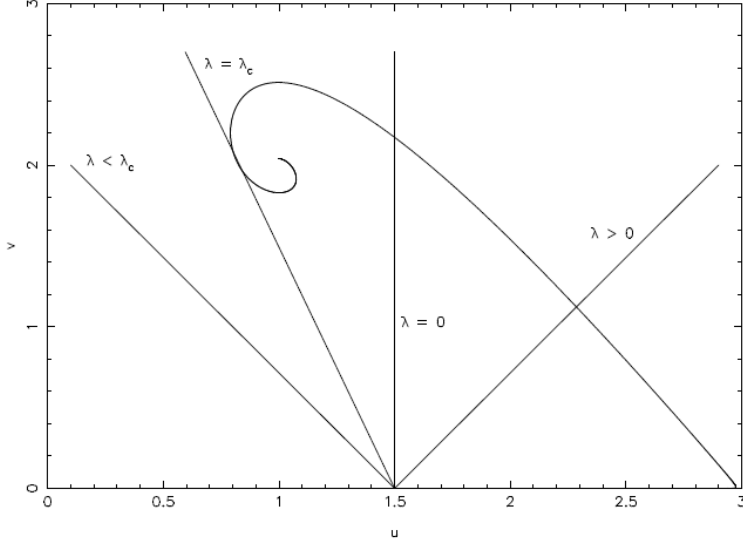


Figure 2.1: Bound on  $RE/GM^2$  for the isothermal sphere (from [124]).

The nature of the solution shown in Fig. 2.1 allow one to put interesting bounds on some physical quantities, including the energy. To see this, one shall compute the total energy  $E$  of the isothermal sphere. The potential and kinetic energies are

$$U = - \int_0^R \frac{GM(r)}{r} \frac{dM}{dr} dr = - \frac{GM_0^2}{L_0} \int_0^{x_0} mn x dx \quad (2.19)$$

$$K = \frac{3M}{2\beta} = \frac{3GM_0^2}{2L_0} m(x_0) = \frac{3GM_0^2}{2L_0} \int_0^{x_0} nx^2 dx, \quad (2.20)$$

where  $x_0 = R/L_0$ . The total energy is therefore,

$$E = K + U = \frac{GM_0^2}{2L_0} \int_0^{x_0} dx (3nx^2 - 2mn x) \quad (2.21)$$

$$= \frac{GM_0^2}{2L_0} \int_0^{x_0} dx \frac{d}{dx} (2nx^2 - 3m) = \frac{GM_0^2}{L_0} \left( n_0 x_0^3 - \frac{3}{2} m_0 \right), \quad (2.22)$$

where  $n_0 = n(x_0)$  and  $m_0 = m(x_0)$ . The dimensionless quantity  $RE/GM^2$  is given by

$$\lambda = \frac{RE}{GM^2} = \frac{1}{v_0} \left( u_0 - \frac{3}{2} \right). \quad (2.23)$$

Note that the combination  $RE/GM^2$  is a function of  $(u, v)$  alone. One now considers the constraints on  $\lambda$ . Suppose one specifies some value for  $\lambda$  by specifying  $R$ ,  $E$ , and  $M$ . Then such an isothermal sphere must lie on the curve

$$v = \frac{1}{\lambda} \left( u - \frac{3}{2} \right), \quad \lambda \equiv \frac{RE}{GM^2}, \quad (2.24)$$

which is a straight line through the point  $(1.5, 0)$  with a slope  $\lambda^{-1}$ . On the other hand, since all isothermal spheres must lie on the  $u - v$  curve, an isothermal sphere can exist only if the line in Eq. (2.24) intersects the  $(u - v)$  curve.

For large positive  $\lambda$  (positive  $E$ ), there is just one intersection. When  $\lambda = 0$  (zero energy), one still has a unique isothermal sphere. When  $\lambda$  is negative (negative  $E$ ), the line can cut the  $(u - v)$  curve at more than one point; thus more than one isothermal sphere can exist with a given value of  $\lambda$ . But as one decreases  $\lambda$  (more and more negative  $E$ ), the line in Eq. (2.24) will slope more and more to the left; and when  $\lambda$  is smaller than a critical value  $\lambda_c$ , the intersection will cease to exist. Thus no isothermal sphere can exist if  $RE/GM^2$  is below a critical value  $\lambda_c$  [124]. This fact follows immediately from the nature of the  $(u - v)$  curve and Eq. (2.24). The value of  $\lambda_c$  can be found from the numerical solution shown in the figure. It turns out to be about  $-0.335$ .

The isothermal sphere has a special status as a solution to the mean-field equations. Isothermal spheres, however, cannot exist if  $RE/GM^2 < -0.335$ . Even when  $RE/GM^2 > -0.335$ , the isothermal solution need not be stable. The stability of this solution can be investigated by studying the second variation of the entropy. Such a detailed analysis shows that the following results are true [124]. Systems with  $RE/GM^2 < -0.335$  cannot evolve into isothermal spheres. The entropy has no extremum for such systems. Systems with  $RE/GM^2 > -0.335$  and  $\rho(0) > 709 \rho(R)$  can exist in a metastable (saddle point state) isothermal-sphere configuration. Here  $\rho(0)$  and  $\rho(R)$  denote the densities at the center and edge, respectively. The entropy extrema exist but they are not local extrema. Systems with  $RE/GM^2 > -0.335$  and  $\rho(0) < 709 \rho(R)$  can form isothermal spheres which are a local maximum of the entropy.

## 1.2 Virial equilibrium

As we explained in Chapter 1, a system with an initial condition which is not a stable equilibrium solution of the Vlasov equation knows a rapid evolution on a timescale independent of the number of particles  $N$  in the system, the so called violent relaxation. The system then evolves for a long time, which behaves as a power of  $N$ , among the numerous stable stationary states of the Vlasov equation. It is then interesting to link this evolution with the main general tool of particles dynamics: the virial theorem. Let us note that this theorem applies to any, smooth and non-smooth distribution of particles.

We derive below the virial relation which provides a powerful constraint on self-gravitating systems in a macroscopically stationary state. Let us consider a perfect self-gravitating system of  $N$  particles, that is without a surrounding box and with

a perfect  $1/r$  potential. The Hamiltonian is therefore

$$H(q_\mu, p_\mu) = \sum_{i=1}^N \frac{\mathbf{p}_i^2}{2m} - \sum_{i=1}^{N-1} \frac{Gm^2}{|\mathbf{q}_i - \mathbf{q}_j|}, \quad (2.25)$$

where  $q_i$  and  $p_i$  represent the position and the momentum of the  $i^{th}$  particle respectively. Introducing the *moment of inertia tensor* [25]:

$$I_{\mu\nu} = \sum_{i=1}^N m q_{i,\mu} q_{i,\nu} \quad (2.26)$$

where  $q_{i,\mu}$  is the  $\mu^{th}$  position component of the  $i^{th}$  particle, the second time derivative of this expression is

$$\ddot{I}_{\mu\nu} = \sum_{i=1}^N m \left( \ddot{q}_{i,\mu} q_{i,\nu} + q_{i,\mu} \ddot{q}_{i,\nu} + 2 \dot{q}_{i,\mu} \dot{q}_{i,\nu} \right). \quad (2.27)$$

Using that the acceleration of a particle is given by

$$\ddot{q}_{i,\mu} = Gm \sum_{j \neq i=1}^N \frac{q_{j,\mu} q_{i,\mu}}{|\mathbf{q}_j - \mathbf{q}_i|^3}, \quad (2.28)$$

one obtains

$$\begin{aligned} \ddot{I}_{\mu\nu} &= 2m \sum_{i=1}^N \dot{q}_{i,\mu} \dot{q}_{i,\nu} + Gm^2 \sum_{i \neq j=1}^N \frac{1}{|\mathbf{q}_j - \mathbf{q}_i|^3} \left[ (q_{j,\mu} - q_{i,\mu}) q_{i,\nu} + q_{i,\mu} (q_{j,\nu} - q_{i,\nu}) \right] \\ &= 2m \sum_{i=1}^N \dot{q}_{i,\mu} \dot{q}_{i,\nu} - Gm^2 \sum_{i \neq j=1}^N \frac{(q_{j,\mu} - q_{i,\mu})(q_{j,\nu} - q_{i,\nu})}{|\mathbf{q}_j - \mathbf{q}_i|^3}. \end{aligned} \quad (2.29)$$

The trace of  $\ddot{I}_{\mu\nu}$  is

$$\ddot{I} = \sum_{\mu=1}^3 \ddot{I}_{\mu\mu} = 2m \sum_{i=1}^N \dot{\mathbf{q}}_i^2 - Gm^2 \sum_{i \neq j=1}^N \frac{1}{|\mathbf{q}_j - \mathbf{q}_i|}. \quad (2.30)$$

The first term is actually four times the total kinetic energy of the system while the second is twice its total potential energy:

$$\frac{1}{2} \ddot{I} = 2K + U. \quad (2.31)$$

Assuming that the system is in a state such that  $\ddot{I} = 0$ , we have the famous relation

$$2K + U = 0, \quad (2.32)$$

which in all textbooks on astrophysics is called the *virial theorem*. Since the total energy is  $E = K + U$ , we obtain the following relation

$$E = -K = \frac{U}{2}. \quad (2.33)$$

Let us note that the crucial assumption involved in deriving the scalar virial theorem is that the moment of inertia  $I$  is *time-independent*. However, in a system with a small number of particles, there are necessarily statistical fluctuations in  $I$  simply due to the finite-size, and Eq. (2.32) could be expected to hold only for the time-averaged values of  $K$  and  $U$ .

## 2 Introduction to Cosmology

The basic hypothesis used to construct the standard cosmological model is given by the *Cosmological Principle*. One way to state it is : “*Viewed on sufficiently large distance scales, the universe is homogeneous and isotropic*”.

Homogeneity means that the universe is translationally invariant, *i.e.* it looks the same from all points, and isotropy means that the universe is rotationally invariant, *i.e.* it looks the same in all directions. For a long time, there was no clear observational evidences for this statement. It had the status of a postulate, in the same manner as, for example, Einstein’s Principle of Relativity. In fact, given only 2 points from which the universe appears isotropic, one can prove homogeneity considering that our position in the universe is not special.

The Cosmological Principle, stated as above, is a strong hypothesis. There is another version of it, called the *conditional cosmological principle*, which hypothesises only *statistical isotropy* and *statistical homogeneity*. This is a much weaker assumption, which allows one to admit notably the possibility of a fractal distribution of matter, in which the density averaged in an infinite volume is zero.

An indication to support the hypothesis of strict homogeneity and isotropy at large scales is the fact that the model based on it describes remarkably well the large scale dynamics of the observed universe, given by the Hubble law. Direct evidence of the isotropy of the universe is given by that of the temperature of the *Cosmic Microwave background* (CMB) radiation, which pervades the universe [127]. Indeed it took more than two decades after its discovery to detect the fluctuations of the temperature as a function of the angle of observation, which are at a level of about one in ten thousand [55]. However, all these observations do not constitute, of course, a direct test of the hypothesis.

The only direct current observation which directly probes the homogeneity of the universe is that provided by  $3-d$  surveys constraining the distribution of visible matter, notably galaxy and cluster surveys. Given that current cosmological model describes a universe in which 80% of the matter is non visible “dark matter”, this is an incomplete test of homogeneity. However, it is plausible to suppose that the visible matter trace the dark matter one, and therefore these kind of observations are a good probe of homogeneity.

In Fig. 2.2 we show a slice of the largest galaxy survey to date. It is apparent that at small scales the distributions of galaxies is very inhomogeneous, with complex structures as cluster of galaxies and voids. However, at large scale, there is an evidence that the distribution of galaxies reaches a definitive (non-zero) density. This is shown in Fig. 2.3, in which the density in function of the scale is shown. For large scales, the density presents a crossover to a constant density, *i.e.* to homogeneity.

Assuming that the universe is homogeneous and isotropic at sufficiently large scales, the large scale dynamics of the universe is described with an exactly homogeneous (equal density everywhere) and isotropic model: the *Friedmann-Robertson-Walker* model, based on the framework of the General Theory of Relativity, proposed by Albert Einstein, and which explains and describes gravity.

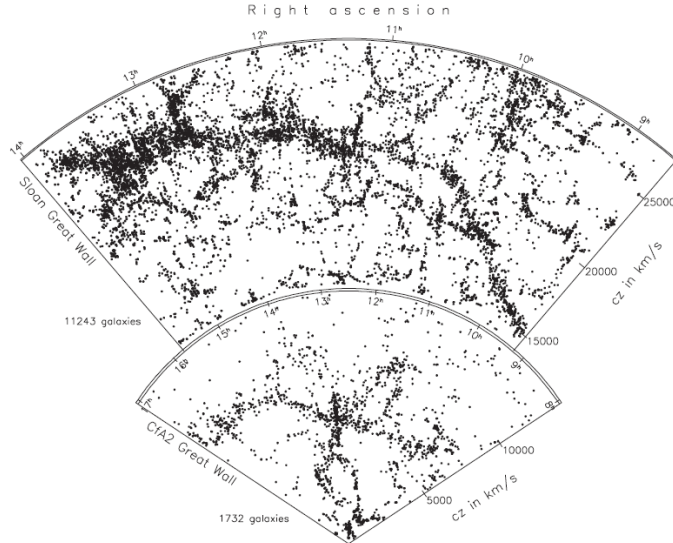


Figure 2.2: Slices of the 2dF and SDSS surveys. Observe how at small scales (small redshift) the galaxies are highly clustered, forming walls and filaments.

## 2.1 the Friedmann-Robertson-Walker universe

General relativity is a metric theory that describes gravity as the manifestation of the curvature of spacetime. This theory, coupled to cosmological principle, implies that the universe should either be expanding or contracting, with a geometry which may be flat, hyperbolic or spherical. Usually the associated spatial curvature is denoted by means of the curvature coefficient  $k$ . It has the value  $k = 0$  for a flat space,  $k = +1$  for a spherical space, and  $k = -1$  for a negatively curved hyperbolic space. The spacetime metric of these universes is the *Robertson-Walker metric*

$$ds^2 = c^2 dt^2 - a^2(t) \left( dr^2 + R_c^2 S_k^2(r/R_c) (d\theta^2 + \sin^2 \theta d\phi^2) \right), \quad (2.34)$$

where  $R_c$  is the radius of curvature, and  $S_k(r)$  is the function given by

$$S_k(x) = \begin{cases} \sin(x) & \text{if } k = +1, \\ x & \text{if } k = 0, \\ \sinh(x) & \text{if } k = -1. \end{cases} \quad (2.35)$$

The variable  $t$  is the so-called cosmic time. The dimensionless scale factor  $a(t)$  describes the expansion (or contraction) of the universe, and may be normalized with respect to the present-day value, *i.e.*  $a(t_0) = 1$ . The constant  $c$  is the velocity of light and  $r, \theta, \phi$  are the spherical coordinates. Friedmann solved Einstein's equations for general homogeneous and isotropic universe models, and derived the time dependence of the expansion factor. The resulting equations are known as the *Friedmann-Robertson-Walker-Lemaître* (FRW) equations:

$$\frac{\ddot{a}}{a} = -\frac{4\pi G}{3} \left( \rho + \frac{3p}{c^2} \right) + \frac{\Lambda}{3}, \quad (2.36)$$

and

$$\left( \frac{\dot{a}}{a} \right)^2 = \frac{8\pi G\rho}{3} - \frac{kc^2}{a^2 R_0^2} + \frac{\Lambda}{3}. \quad (2.37)$$

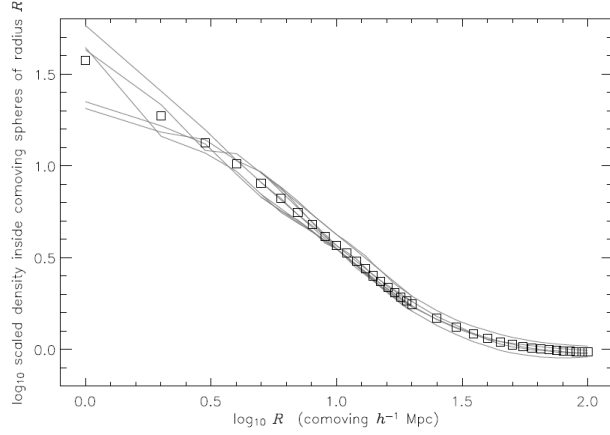


Figure 2.3: Representation of the average comoving density (*i.e.* number counted divided by expected from an homogeneous distribution) as function of a comoving sphere of radius  $R$ . Observe how at  $\log_{10} R \approx 1.5$  the density stabilizes, which means that observed at scales larger than this one the universe is homogeneous (from [56]).

In the FRW equations,  $G$  is Newton's gravitational constant,  $\rho$  is the energy density of the universe,  $p$  is the pressure of the various cosmic exponents,  $\Lambda$  is the cosmological constant, and  $R_0$  is the present-day value of the curvature radius. The evolution of the energy density  $\rho$  of the universe can be inferred from the energy equation obtained by combining the FRW equations Eqs. (2.36) and (2.37). This is given by

$$\dot{\rho} + 3\left(\rho + \frac{p}{c^2}\right)\frac{\dot{a}}{a} = 0. \quad (2.38)$$

The macroscopic nature of the medium is expressed by the equation of state,  $p = p(\rho)$ , which for most cosmologically relevant components may be expressed as

$$p = w\rho c^2. \quad (2.39)$$

Here  $w$  is called the equation of state parameter. Eqs. (2.38) and (2.39) can be combined to give the evolution of energy density with the expansion of the universe:

$$\rho(t) \propto a(t)^{-3(1+w)}. \quad (2.40)$$

## 2.2 Cosmic Expansion

The expansion rate of the universe is expressed in terms of the Hubble parameter,

$$H(t) = \frac{\dot{a}}{a}. \quad (2.41)$$

The present-day value of  $H(t)$ , sometimes called the *Hubble constant*, is often parametrized in terms of a dimensionless factor  $h$ , ( $h = H_0/100 \text{ km}^{-1}\text{s} \text{ Mpc}$ ), where  $H_0$  is the Hubble constant express in units of  $\text{km s}^{-1}\text{Mpc}^{-1}$ . The expansion of the universe does not only express itself in continuously growing distances between any two objects, it also leads to the increase of the wavelengths of photons. This resulting

cosmological redshift  $z$  of a presently observed object is given by the relation

$$1 + z = \frac{a(t_0)}{a(t)} = \frac{1}{a(t)}, \quad (2.42)$$

where  $a(t)$  is the expansion factor of the universe at the time the observed light was emitted.

### 2.3 Cosmic Constituents

The evolution of the universe is fully dictated by its energy density  $\rho$  and its curvature  $k$ . The energy density of the universe is conveniently expressed in terms of the density needed to produce a geometrically flat universe, the critical density:

$$\rho_c(t) = \frac{3H^2}{8\pi G}. \quad (2.43)$$

The contribution of any component towards the energy density of the universe may be expressed in terms of the ratio of its energy density to the critical density. This ratio is denoted by  $\Omega(t)$ , the *density parameter*, and is expressed as:

$$\Omega(t) = \frac{\rho(t)}{\rho_c(t)} = \frac{8\pi G\rho}{3H^2}. \quad (2.44)$$

The value of  $\Omega(t)$  at  $t = t_0$ , denoted by  $\Omega$  is given by

$$\Omega = \frac{8\pi G\rho_0}{3H_0^2}. \quad (2.45)$$

According to the “standard model” the universe contains a variety of components. While the contributions of magnetic fields and gravitational waves may be taken to be negligible, the most important ingredients of the universe are radiation, baryonic matter, nonbaryonic dark matter and dark energy. The equation of state parameter  $w$  for radiation and matter (baryonic as well as nonbaryonic) is  $1/3$  and  $0$  respectively, whereas for dark energy its value is less than  $-1/3$ . If the dark energy is in the form of a cosmological constant, then  $w = -1$ . Thus Eq. (2.40) suggests that radiation ( $\rho_r \propto a^{-4}$ ), matter ( $\rho_m \propto a^{-3}$ ), and dark energy ( $\rho_\Lambda = \text{constant}$ ) have evolved differently with the expansion of the universe.

As the radiation cools off as a result of the expansion of the universe, its spectrum peaks at microwave wavelengths and is observed today in the form of the CMB with a temperature of  $T_0 = 2,725 K^\circ$ . Since the temperature of radiation scales in inverse proportion to the scale factor ( $T \propto a^{-1}(t)$ ), it must have been very high in the early universe. The almost perfect blackbody spectrum of CMB defines the strongest evidence for the existence of a very hot and dense phase in the early universe (see Fig. 2.4). At very early times radiation was dynamically dominant component of the universe. Its current density constituted only a fraction of  $10^{-5}$  of the total density. Baryonic matter  $\Omega_b$  is composed mostly of composite particles made of three quarks which participate in the strong interaction. However, it only represents a minor cosmological component and accounts for a mere 4,4% of the energy content

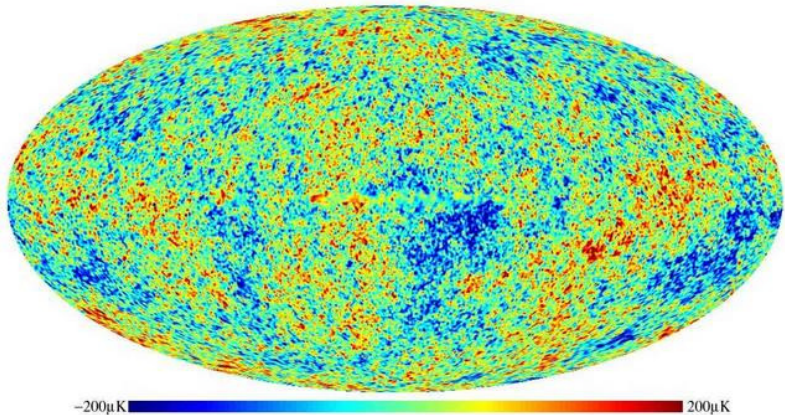


Figure 2.4: Sky projection of the Cosmic Microwave Background measured with the Wilkinson Microwave Anisotropy Probe (WMAP) experiment.

of the universe. Nonbaryonic dark matter  $\Omega_{dm}$  is a very important component for the formation of structures in the universe. The combined contribution of matter to the energy density is usually expressed as  $\Omega_m$ .

One of the most pressing problems in astrophysics is the identity of this dark matter. While its presence is unmistakably felt through its gravitational attraction, it has yet escaped direct observation or detection in the laboratory. Dark matter is pressureless and insensitive to the electromagnetic influence of radiation.

Fluctuations in the dark matter could have started growing as soon as matter began to dominate the dynamics of the universe at around the epoch of *matter-radiation equality* ( $\rho_r = \rho_m$ ). This occurs at a scale of  $a(t) \approx 10^{-4}$ . The growth of these fluctuations in the dark matter created the gravitational potential wells. After the baryonic matter and radiation decoupled at the epoch of recombination, the baryonic matter started falling into these gravitational potential wells. This process is believed to have led to the formation of galaxies and stars. Dark matter plays a central role in the modelling of structure formation. Indeed, without dark matter, the epoch of galaxy formation would occur substantially later in the universe than is observed.

The cosmological framework of the Hot Big Bang in a spatially homogeneous and isotropic universe is so widely accepted that it is called the *standard Hot Big Bang Model*. This model is supported by many observations, notably

- the relation between distance and recession velocity (Hubble law) as a consequence of its metric implies that the universe has a finite age;
- the almost perfect black-body spectrum of the Cosmic Microwave Background is evidence for an extremely hot initial phase of the universe;
- the excellent match in the observed abundances of light elements and predictions from primordial nucleosynthesis;
- the evident evolution of the appearance of objects as function of their distance from us.

| Parameter        | Value                                             | Description                  |
|------------------|---------------------------------------------------|------------------------------|
| $H_0$            | $70.4 \pm 2.4 \text{ km s}^{-1}\text{Mpc}^{-1}$   | Hubble parameter             |
| $\Omega_m$       | $0.277 \pm 0.029$                                 | Matter Density               |
| $\Omega_b$       | $0.0459 \pm 0.0028$                               | Baryon Density               |
| $\Omega_\Lambda$ | $0.723 \pm 0.029$                                 | Dark Energy Density          |
| $\rho_c$         | $0.94 \pm 0.07 \times 10^{-26} \text{ kg m}^{-3}$ | Critical Density             |
| $t_0$            | $13.72 \pm 0.14 \text{ Gyr}$                      | Age of the Universe          |
| $\sigma_8$       | $0.811 \pm 0.032$                                 | Galaxy fluctuation amplitude |
| $n$              | $0.960 \pm 0.014$                                 | Spectral Index               |

Table 2.1: Values of cosmological parameters (from WMAP5 + SDSS [57]).

We now have evidence (see e.g. [60, 61]) to suggest that universe at the present epoch is undergoing an accelerated expansion, *i.e.*  $\ddot{a} > 0$ . This could be due to the presence of an elusive medium called dark energy. Dark energy ( $\Omega_\Lambda$ ) is the most dominant component of our universe at the present epoch. It accounts for approximatively 73% of cosmic energy density. The nature of Dark Energy is even more mysterious than dark matter. All that can be said about dark energy is that it has a negative pressure. This is apparent from Eq. (2.36) which suggests that for  $\ddot{a} > 0$ , we need  $p < -\rho/3$ . Most observational studies agree with the Dark Energy being equivalent to a cosmological constant although other options are still viable.

## 2.4 The $\Lambda$ CDM model

The current understanding of the components of the universe is encoded in the *Lambda Cold Dark Matter* ( $\Lambda$ CDM) model. In this model one attempts to explain supernova observations in terms of the accelerated expansion of the universe. Indeed, supernovae are useful in cosmology as they represent excellent standard candles across cosmological distances [60, 61]. They allow the expansion history of the universe to be measured by looking at the relationship between the distance to an object and its redshift, which gives how fast it is receding from us. This model is accounted remarkably well notably for the spectrum of fluctuations in temperature observed in the Cosmic Microwave Background. In the acronym  $\Lambda$ CDM, the term  $\Lambda$  refers to the dark energy ( $\Omega_\Lambda$ ) which is believed to be the driving force behind the accelerated expansion of the universe at the present epoch.  $\Lambda$  is assumed to have the form of a cosmological constant ( $w = -1$ ). Cold Dark Matter refers to a model where the dark matter is explained as being cold, *i.e.* its velocity was non-relativistic at an epoch when it decoupled from other constituents of the universe. This type of dark matter is assumed to be non-baryonic, dissipationless and collisionless. The  $\Lambda$ CDM model has several parameters from which the most important are shown in Tab. 2.4.

## 2.5 The Newtonian approximation

In practice in cosmology the study of how irregularities in the matter distribution in the universe develop is treated almost exclusively in the Newtonian limit. This

approximation is justified by the fact that in the formation of large scale structures one considers a regime in which

- particle velocities are typically non-relativistic (e.g. in “cold” dark matter cosmology);
- the gravitational fields generated are “sufficiently weak”;
- the physical scale considered where “non-linear” structures form are small compared to the horizon size (characterizing the scale at which constraints associated to the finiteness of the speed of light are expected to become important).

In this thesis we will consider solely the Newtonian limit.

### 3 Infinite self-gravitating systems in cosmology: analytical results

We now review some standard methods to describe the non-equilibrium dynamical evolution of particular self-gravitating systems in cosmology. This is a key subject because it will permit us to justify the fluid formalism used in cosmology. We review the basics of kinetic theory, *i.e.* the non-equilibrium evolution of a system of interacting particles. To do so, we study the well known BBGKY hierarchy. We then explain the approximations made in the derivation of a fluid theory from the kinetic one, and introduce the perturbative methods used in both the Eulerian and Lagrangian approach. We conclude this section with a discrete approach which helps to classify the limits of the application of linear theory.

#### 3.1 Non-equilibrium evolution of a self-gravitating system

It is important to underline here the crucial difference between finite (Newtonian) systems, as discussed in the previous section, and the *infinite* (Newtonian) systems we consider here, and which are those principally of relevance in the context of the structure formation in cosmology. We consider in cosmology systems — distributions of particles — which are of *infinite extent and have a non-zero mean density*. The Newtonian force on particle  $i$ ,  $\mathbf{F}_i$ , due to all the others (in a system of particles of equal mass  $m$ ), *i.e.*

$$\mathbf{F}_i = -Gm \sum_{j \neq i} \frac{(\mathbf{r}_i - \mathbf{r}_j)}{|\mathbf{r}_i - \mathbf{r}_j|^3}, \quad (2.46)$$

in such a system is badly defined due to the contribution of the mean density. The force used in the Newtonian limit of cosmology is that obtained *when the contribution of the mean density is removed*. This can be written formally in different ways: most often this is done by writing  $\mathbf{F}_i = -\nabla \phi_i$ , and specify that the potential  $\phi_i$  is calculated from the *modified* Poisson equation

$$\nabla^2 \phi_i = 4\pi G (\rho - \rho_0), \quad (2.47)$$

where  $\rho(\mathbf{r})$  is the mass density field and  $\rho_0$  is its mean value. Alternatively, it can be written using a prescription of symmetric summation (which sets the contribution

of the mean density to zero)

$$\mathbf{F}'_i = -Gm \lim_{R \rightarrow \infty} \sum_{j \in V_i(R)} \frac{(\mathbf{r}_i - \mathbf{r}_j)}{|\mathbf{r}_i - \mathbf{r}_j|^3}, \quad (2.48)$$

where  $V_i(R)$  is the sphere of radius  $R$  centered on the particle  $i$ . As pointed out by Kiessling [95] a more physically appealing version is

$$\mathbf{F}'_i = -Gm \lim_{\mu \rightarrow 0} \sum \frac{(\mathbf{r}_i - \mathbf{r}_j)}{|\mathbf{r}_i - \mathbf{r}_j|^3} e^{-\mu |\mathbf{r}_i - \mathbf{r}_j|} \quad (2.49)$$

In the cosmological context, this ‘‘subtraction’’ of the mean density is properly justified by the fact that the mean density sources the Hubble expansion, and the force  $\mathbf{F}'_i$  appears in the equation of motion in ‘‘comoving coordinates’’, *i.e.* in which particles remain fixed when they follow the Hubble expansion. Indeed the equation of motion in these coordinates for a particle is

$$\frac{d^2 \mathbf{x}_i}{dt^2} + 2 H(t) \frac{d\mathbf{x}_i}{dt} = \frac{\mathbf{F}'_i}{a^3}, \quad (2.50)$$

where  $\mathbf{F}'_i$  is given by one of the expressions above,  $a(t)$  is the scale factor of the model considered and  $H(t) = \dot{a}/a$  is the Hubble ‘‘constant’’. Formally we can define a non-expanding (*i.e.* static universe) limit to these equations by setting  $H = 0$ . As, however, there is no such static solution in a universe with non-zero mean density, such a model does not have the physical motivation of the expanding model. The adoption of the modified force in this case is known as the ‘‘Jeans swindle’’ as it was first introduced by Jeans to treat the growth of perturbation in a static (but infinite) universe. As discussed by Kiessling (and in Chapters 3 and 6 of this thesis) the use of the term ‘‘swindle’’ is inappropriate as in fact the prescription is a mathematically well defined regularization of the Newtonian problem.

We will consider in the rest of this section mostly this limit  $H = 0$ , as the presence of this term is not essential to understanding the approaches presented and essential results. In treating the force term we will assume that the system is an infinite periodic system, and take the appropriate expression for the force to be defined. Issues concerning the well definedness of these forces (and indeed the assumed equivalence of the different expressions above) will be ignored here, but they will be treated in detail in Chapters 3 and 6 of this thesis.

### The BBGKY hierarchy

If we have a system for which we can write a Hamiltonian, we know, by using the Liouville theorem [73], how an ensemble of such systems evolves: if the function  $f(q_\mu, p_\nu, t)$  is the density function of these systems in phase space, it satisfies

$$\partial_t f + \sum_{\mu=1}^{3N} \dot{q}_\mu \partial_{q_\mu} f + \sum_{\nu=1}^{3N} \dot{p}_\nu \partial_{p_\nu} f = 0, \quad (2.51)$$

where we have assumed that the system contains  $N$  particles in  $3N$  dimensions. It is important to note that this equation is very similar to the Vlasov equation, but

it is crucial to understand that they describe two different quantities. Eq. (2.51) describes exactly the evolution of an ensemble  $f(q_\mu, p_\nu, t)$  of identical systems on phase space ( $6N$  dimensions), while the Vlasov equation describes approximately the evolution of the particle density  $f(x, v, t)$  in the 6 dimensional  $(x, v)$ -space for one of these systems. What we are going to see now is that we can obtain the Vlasov equation from Eq. (2.51). We will illustrate this for a periodic gravitating system.

Let us denote by  $f^{(N)}$  the density in the  $N$ -particle phase space used with the Liouville theorem, and which depends on the coordinates of the  $N$  particles. We make also a change of variables to replace the momenta with the velocities:  $p_\mu \rightarrow mv_\mu$  and write  $x_\mu$  instead  $q_\mu$  for the positions so that Eq. (2.51) becomes

$$\partial_t f^{(N)} + \sum_{\mu=1}^{3N} \dot{x}_\mu \partial_{x_\mu} f^{(N)} + \sum_{\nu=1}^{3N} \dot{v}_\nu \partial_{v_\nu} f^{(N)} = 0, \quad (2.52)$$

or equivalently

$$\partial_t f^{(N)} + \sum_{i=1}^N v_i \nabla_{x_i} f^{(N)} + \sum_{i=1}^N \frac{1}{m} F_i \nabla_{v_i} f^{(N)} = 0, \quad (2.53)$$

with

$$F_i = Gm^2 \sum_{n \in Z^3} \sum_{i \neq j} \frac{x_i - x_j + Ln}{|x_i - x_j + Ln|^3}, \quad (2.54)$$

where  $L$  is the period of the system. The subscript are such that  $x_1 = (x_1, x_2, x_3)$ ,  $\dots$ ,  $x_N = (x_{3N-2}, x_{3N-1}, x_{3N})$ . A similar notation is used for the velocities.

We define now the function  $f^{(1)}$  by

$$f^{(1)}(x_1, v_1, t) = \int f^{(N)}(x_\mu, v_\nu, t) d^3x_2 d^3v_2 \dots d^3x_N d^3v_N, \quad (2.55)$$

that is by integrating  $f^{(N)}$  over all the particle positions and velocities except those of the first particle. The integrals for the positions are done over the box size while those for the velocities are done over the whole real axis. The next step is to integrate in the same way Eq. (2.52) or Eq. (2.53). The first term becomes  $\partial_t f^{(1)}$ . For the other terms, we note that

$$\int_0^L \dot{x}_\mu \partial_{x_\mu} f^{(N)} dx_\nu = v_\mu \partial_{x_\mu} \int_0^L f^{(N)} dx_\nu \quad (2.56)$$

if  $\mu \neq \nu$ .

$$\int_0^L \dot{x}_\mu \partial_{x_\mu} f^{(N)} dx_\mu = v_\mu \int_0^L \partial_{x_\mu} f^{(N)} dx_\mu = 0, \quad (2.57)$$

because of the periodicity of the box.

$$\int_{-\infty}^{+\infty} \dot{v}_\mu \partial_{v_\mu} f^{(N)} dv_\nu = \frac{F_\mu}{m} \partial_{v_\mu} \int_{-\infty}^{+\infty} f^{(N)} dv_\nu \quad (2.58)$$

if  $\mu \neq \nu$ , and finally

$$\int_{-\infty}^{+\infty} \dot{v}_\mu \partial_{v_\mu} f^{(N)} dv_\mu = 0, \quad (2.59)$$

by assuming that  $\lim_{v_\mu \rightarrow \pm\infty} f^{(N)} = 0$ , which is a reasonable hypothesis even if we consider a perfect  $1/r$  potential, without modification at small scale. By putting all this together, we get

$$\partial_t f^{(1)} + v_1 \cdot \nabla_{x_1} f^{(1)} + \int \frac{1}{m} F_1 \cdot \nabla_{v_1} f^{(N)} d^3 x_2 d^3 v_2 \dots d^3 x_N d^3 v_N = 0. \quad (2.60)$$

Let us suppose now that the function  $f^{(N)}$  is a symmetric function of the particles numbers:

$$f^{(N)}(x_1, v_1, \dots, x_N, v_N, t) = f^{(N)}(x_{\sigma(1)}, v_{\sigma(1)}, \dots, x_{\sigma(N)}, v_{\sigma(N)}, t) \quad (2.61)$$

for any permutation  $\sigma$  of the first  $N$  integers. Note that this has no effect on the dynamics of a system. We are free to choose any phase space functions in the Liouville equation, and our choice is only motivated by the fact that it puts all the particles on the same level. By noting that

$$\frac{1}{m} F_1 = \sum_{i=2}^N Gm \sum_{n \in Z^3} \frac{x_i - x_1 + Ln}{|x_i - x_1 + Ln|^3} \equiv \frac{1}{m} \sum_{i=2}^N F_{1,i}, \quad (2.62)$$

where  $F_{1,i}$  is the force on particle 1 due to particle  $i$ , the symmetry of  $f^{(N)}$  allows us to write the third term of Eq. (2.60) as

$$\frac{(N-1)}{m} \int F_{1,2} \cdot \nabla_{v_1} f^{(N)} d^3 x_2 d^3 v_2 \dots d^3 x_N d^3 v_N. \quad (2.63)$$

By defining the following function

$$f^{(2)}(x_1, v_1, x_2, v_2, t) = \int f^{(N)} d^3 x_3 d^3 v_3 \dots d^3 x_N d^3 v_N, \quad (2.64)$$

Eq. (2.60) becomes

$$\partial_t f^{(1)} + v_1 \cdot \nabla_{x_1} f^{(1)} + \frac{(N-1)}{m} \int F_{1,2} \cdot \nabla_{v_1} f^{(2)} d^3 x_2 d^3 v_2 = 0. \quad (2.65)$$

This gives the evolution of the one particle function  $f^{(1)}$  in function of the two particles function  $f^{(2)}$ . If we had started by integrating over  $x_3, v_3, \dots, x_N, v_N$ , we would have obtained an equation of  $f^{(2)}$  in function of the three particles function

$$f^{(3)}(x_1, \dots, v_3) = \int f^{(N)} d^3 x_4 d^3 v_4 \dots d^3 x_N d^3 v_N. \quad (2.66)$$

We can continue in a similar way for higher order functions and obtain a sequence of equations of the type

$$\partial_t f^{(n)} = F(f^{(n+1)}), \quad (2.67)$$

known as the *Bogoliubov-Born-Green-Kirwood-Yvon* (BBGKY) hierarchy. Without any approximations these equations are not easier to solve than Liouville equation. The advantage is that by choosing a judicious approximative function for one of the  $f^{(i)}$ , we can reduce the number of equations and have a chance to solve them or at

least obtain interesting informations concerning the evolution of the system studied. Let us assume that

$$f^{(2)}(x_1, v_1, x_2, v_2) = f^{(1)}(x_1, v_1)f^{(1)}(x_2, v_2) + g(x_1, v_1, x_2, v_2) \quad (2.68)$$

and consider the last function  $g$  to be negligible. We can assume without loss of generality that

$$\int f^{(n)} d^3x_1 d^3v_1 \dots d^3x_N d^3v_N = 1. \quad (2.69)$$

This allows us to see  $f^{(1)}(x, v)$  as the probability density of finding a particle at  $(x, v)$  in the ensemble of systems represented by  $f^{(N)}$ . The function  $f^{(2)}(x_1, v_1, x_2, v_2)$  is then simply the density probability to have one particle at  $(x_1, v_1)$  and one at  $(x_2, v_2)$ . Therefore  $g(x_1, v_1, x_2, v_2)$  is the two-particle correlation function as it gives the change in the probability to find a particle at  $(x_1, v_1)$  when it is known that there is another one at  $(x_2, v_2)$ . By replacing  $f^{(2)}$  by Eq. (2.68) in Eq. (2.65), we obtain

$$\begin{aligned} \partial_t f^{(1)} + v_1 \cdot \nabla_{x_1} f^{(1)} &+ \frac{(N-1)}{m} \nabla_{v_1} f^{(1)} \cdot \int F_{1,2} \cdot f^{(1)}(x_2, v_2, t) d^3x_2 d^3v_2 \\ &+ \frac{(N-1)}{m} \int F_{1,2} \cdot \nabla_{v_1} g d^3x_2 d^3v_2 = 0. \end{aligned} \quad (2.70)$$

In the Vlasov equation, the function  $f$  satisfies

$$\int f(x, v, t) d^3x d^3v = N. \quad (2.71)$$

Multiplying Eq. (2.70) by  $N$  and writing  $f \equiv Nf^{(1)}$ , we get

$$\begin{aligned} \partial_t f + v_1 \cdot \nabla_{x_1} f &+ \frac{(N-1)}{Nm} \nabla_{v_1} f \cdot \int F_{1,2} \cdot f(x_2, v_2, t) d^3x_2 d^3v_2 \\ &+ \frac{N(N-1)}{m} \int F_{1,2} \cdot \nabla_{v_1} g d^3x_2 d^3v_2 = 0. \end{aligned} \quad (2.72)$$

By assuming that  $g(x_1, v_1, x_2, v_2) = 0$ , we find

$$\partial_t f + v_1 \cdot \nabla_{x_1} f + \frac{(N-1)}{Nm^2} \nabla_v f \cdot \int F_{1,2} \rho(x_2, t) d^3x_2 = 0, \quad (2.73)$$

where we have used the fact that the integral of  $f$  over the velocity is the mass density  $\rho(x, t)$  divided by the mass of a particle. By approximating  $(N-1)/N \approx 1$ , we have

$$\partial_t f + v \cdot \nabla_x f + \frac{1}{m} F \cdot \nabla_v f = 0. \quad (2.74)$$

This is the Vlasov equation for our periodic system.

Two important points have to be noted concerning this demonstration to obtain the Vlasov equation from the Liouville equation. The first one is that the function  $f$  does not describe a particular system, but is an average over an ensemble of systems and it gives only a probability to find a particle at a certain point. According to [47],

Boltzmann's point of view was that the evolution of  $f$  has to be understood as *the most probable behaviour of a member of an ensemble of systems*. By choosing an ensemble of systems with equal functions  $f(x, v, t)$ , one can therefore expect that the Vlasov equation describes relatively well the evolution of one particular system of the ensemble as they should all behave similarly concerning macroscopic quantities. The second point is that we have neglected the two-particle correlation function  $g$  and approximated  $(N - 1)/N$  by 1.

### From Vlasov equation to fluid equations

We have just seen that the Vlasov equation can be derived from the Liouville equation by making certain approximations. In this section we show that with further approximations, the Vlasov equation yields the fluid equations. The method is based on a moment integration technique of the Vlasov equation. One multiplies this equation successively by rising powers of the velocity and integrates the resulting equation over the entire velocity space. The system of hydrodynamic equations obtained consists of an infinite set for the infinitely many possible moments of the one-particle distribution function (see e.g. [146]). In the following, we only consider the derivation of the first two moment equations, *i.e.* the continuity equation and the momentum conservation equation.

Using that  $m \int f dv = \rho(x, t)$ , we obtain after having integrated the Vlasov equation with respect to  $v$ ,

$$\partial_t \rho + m \int_{R^3} v \cdot \nabla_x f dv = 0. \quad (2.75)$$

We have assumed that  $\lim_{v_i \rightarrow \pm\infty} f = 0$ . We can find the average of one of the components of the velocity at a point  $x$  by calculating

$$\bar{v}_i \equiv \frac{\int_{Z^3} f v_i d^3 v}{\int_{Z^3} f d^3 v} = \frac{m}{\rho(x, t)} \int_{Z^3} f v_i d^3 v. \quad (2.76)$$

This allows us to write Eq. (2.75) as

$$\partial_t \rho + \nabla_x \cdot (\rho \bar{v}) = 0, \quad (2.77)$$

with  $\bar{v} \equiv (\bar{v}_1, \bar{v}_2, \bar{v}_3)$ . This is the so called continuity equation of fluid dynamics. Now we multiply the Vlasov equation by  $v_i$  and integrate over  $v$ :

$$\partial_t \int f v_i d^3 v + \int v_i v \cdot \nabla_x f d^3 v + \frac{1}{m} F_i \int (v_i \nabla_v f) d^3 v = 0. \quad (2.78)$$

The last term can be evaluated by noting that

$$\int v_i \partial_{v_j} f dv_j = - \int \delta_{ij} f dv_j. \quad (2.79)$$

Using Eq. (2.76), we get

$$\partial_t (\rho \bar{v}_i) + \sum_{j=1}^3 \partial_{x_j} (v_i \bar{v}_j \rho) - \frac{1}{m} F_i \rho = 0. \quad (2.80)$$

With Eq. (2.77), the first term can be written as

$$\partial_t(\rho\bar{v}_i) = \rho\partial_t\bar{v}_i - \bar{v}_i\partial_{x_j}(\rho\bar{v}_j) \quad (2.81)$$

and defining

$$\sigma_{ij}^2 \equiv \overline{v_i v_j} - \bar{v}_i \bar{v}_j, \quad (2.82)$$

we obtain

$$\partial_t\bar{v}_i + \bar{v} \cdot \nabla_x \bar{v}_i = \frac{F_i}{m} - \frac{1}{\rho} \partial_{x_j}(\rho\sigma_{ij}^2). \quad (2.83)$$

Setting the term containing  $\sigma_{ij}^2$  on the rhs to zero, one obtains the (pressureless) Euler equation. In the Euler equation, this term is related to the pressure as it is given by  $-(\partial_{x_i} p)/\rho$ . This shows that  $\rho\sigma_{ij}^2$  can be considered as a “pressure” due to the particle velocities.

## 3.2 Perturbation theory

As general solutions to the equations - Vlasov equation, fluid equation - which we have discussed and which are supposed to approximate the evolution of gravitating systems are not known, their study is mainly restricted to a perturbative analysis.

### Jeans instability

Let us consider the Vlasov equation for a periodic system. We assume that  $f(\mathbf{x}, \mathbf{v}, t) = f_0(\mathbf{v})$ . This is actually a solution of the Vlasov equation (the resulting density function is constant so that  $\mathbf{F} = \mathbf{0}$ ). We suppose now small perturbations:

$$f(\mathbf{x}, \mathbf{v}, t) = f_0(\mathbf{v}) + f_1(\mathbf{x}, \mathbf{v}, t) \quad (2.84)$$

with  $|f_1(\mathbf{x}, \mathbf{v}, t)| \ll f_0(\mathbf{v})$ . We assume that these fluctuations do not change the number of particles, that is

$$N = \int_{C_L} d^3x \int_{R^3} f(\mathbf{x}, \mathbf{v}, t) d^3v = \int_{C_L} d^3x \int_{R^3} f_0(\mathbf{v}) d^3v = \frac{L^3 \rho_0}{m}. \quad (2.85)$$

According to the modified Poisson equation

$$\nabla^2 \Phi_1 = 4\pi G m \int_{R^3} f_1(\mathbf{x}, \mathbf{v}, t) d^3v. \quad (2.86)$$

We have denoted the potential by  $\Phi_1$  in order to remember that this is a perturbation around  $\Phi_0 = 0$ . The Vlasov equation is, at linear order in the perturbations,

$$\partial_t f_1 + \mathbf{v} \cdot \nabla_{\mathbf{x}} f_1 - \nabla_{\mathbf{x}} \Phi_1 \cdot \nabla_{\mathbf{v}} f_0 = 0. \quad (2.87)$$

Because of the periodicity of the system we can expand  $f_1$  and  $\Phi_1$  in Fourier series and because of the linearity of the “linear” Vlasov equation, we look for solutions of the type ([25])

$$f_1(\mathbf{x}, \mathbf{v}, t) = f_{\mathbf{k}}(\mathbf{v}) \exp[i(\mathbf{k} \cdot \mathbf{x} - \omega t)], \quad (2.88)$$

$$\Phi_1(\mathbf{x}, t) = \Phi_{\mathbf{k}} \exp[i(\mathbf{k} \cdot \mathbf{x} - \omega t)], \quad (2.89)$$

with usual  $\mathbf{k} = 2\pi\mathbf{n}/L$ . Inserting this in Eq. (2.86) and Eq. (2.87), we obtain that the following equations must be satisfied

$$-k^2 \Phi_{\mathbf{k}} = 4\pi Gm \int_{R^3} f_{\mathbf{k}}(\mathbf{v}) d^3v, \quad (2.90)$$

$$\Phi_{\mathbf{k}} \cdot \mathbf{k} \cdot \nabla_{\mathbf{v}} f_0 = f_{\mathbf{k}}(\mathbf{v})(\mathbf{v} \cdot \mathbf{k} - \omega). \quad (2.91)$$

Integrating the second with respect to  $\mathbf{v}$ , and combining the two together we obtain a dispersion relation

$$1 + \frac{4\pi Gm}{k^2} \int_{R^3} \frac{\mathbf{k} \cdot \nabla_{\mathbf{v}} f_0}{\mathbf{v} \cdot \mathbf{k} - \omega} d^3v = 0. \quad (2.92)$$

Considering a Maxwellian distribution for  $f_0$

$$f_0(\mathbf{v}) = \frac{\rho_0}{m} \frac{1}{(2\pi\sigma^2)^{3/2}} \exp\left(-\frac{v^2}{2\sigma^2}\right), \quad (2.93)$$

where  $\rho_0$  is the average density. The dispersion relation becomes

$$1 - \frac{2\sqrt{2\pi}G\rho_0}{k\sigma^3} \int_{-\infty}^{+\infty} \frac{v \exp(-v^2/2\sigma^2)}{kv - \omega} dv = 0. \quad (2.94)$$

If  $\omega = 0$ , one finds

$$k^2(\omega = 0) \equiv k_J^2 = \frac{4\pi G\rho_0}{\sigma^2}. \quad (2.95)$$

A calculation (see e.g. [25]) shows that if  $k^2 < k_J^2$ ,  $\omega$  has to be complex in order to satisfy the dispersion relation, and therefore the perturbations becomes unstable as they can grow exponentially. This implies that if there are fluctuations of a size larger than  $\lambda_J \equiv 2\pi/k_J$ , they will start to develop. The length  $\lambda_J$  is called the Jeans length and the instability related to this length is the Jeans instability. Qualitatively this instability is due to the fact that if a density fluctuation is large enough, it contains enough matter to collapse as the velocity dispersion - or temperature - of the particles, which acts as a pressure, is not sufficiently large to counter the gravitational force.

### Linear fluid equations

We consider the set of fluid equations

$$\partial_t \rho + \nabla(\rho \mathbf{v}) = 0, \quad (2.96)$$

$$\partial_t \mathbf{v} + (\mathbf{v} \cdot \nabla) \mathbf{v} = -\nabla \Phi \quad (2.97)$$

$$\nabla^2 \Phi = 4\pi G(\rho - \rho_0) \quad (2.98)$$

which gives in terms of the density contrast  $\delta(\mathbf{x}, t) = (\rho(\mathbf{x}, t) - \rho_0)/\rho_0$

$$\begin{aligned} \partial_t \delta + \nabla \cdot [(1 + \delta) \mathbf{v}] &= 0, \\ \partial_t \mathbf{v} + (\mathbf{v} \cdot \nabla) \mathbf{v} &= -\nabla \Phi, \\ \nabla^2 \Phi &= 4\pi G \rho_0 \delta. \end{aligned} \quad (2.99)$$

We assume that the system is originally at rest  $\mathbf{v}(\mathbf{x}, t) = \mathbf{0}$  and that  $\delta(\mathbf{x}, t) = 0$ . This satisfies the fluid equations. We suppose now that there are small density

fluctuations such that  $|\delta(\mathbf{x}, t)| \ll 1$ . They give rise to small fluctuations in the potential  $\Phi$  and in the velocity field  $\mathbf{v}$ . At first order in these quantities, the set of Eqs. (2.99) becomes

$$\partial_t \delta + \nabla \cdot \mathbf{v} = 0, \quad (2.100)$$

$$\partial_t \mathbf{v} = -\nabla \Phi, \quad (2.101)$$

$$\nabla^2 \Phi = 4\pi G \rho_0 \delta. \quad (2.102)$$

Differentiating Eq. (2.100) with respect to  $t$ , one gets

$$\ddot{\delta} + \nabla \cdot \partial_t \mathbf{v} = 0. \quad (2.103)$$

Taking the divergence of Eq. (2.101); one can use Eq. (2.102) to get

$$\nabla \cdot \partial_t \mathbf{v} = -4\pi G \rho \delta. \quad (2.104)$$

Putting these last two equations together, one finds

$$\ddot{\delta} = 4\pi G \rho_0 \delta, \quad (2.105)$$

whose general solution is  $a_+ \exp(\sqrt{4\pi G \rho_0} t) + a_- \exp(-\sqrt{4\pi G \rho_0} t)$ , i.e. the sum of the so called *growing* and *decaying* modes of perturbations. One finds in the growing mode

$$\delta(\mathbf{x}, t) = \delta_0(\mathbf{x}) \exp(\sqrt{4\pi G \rho_0} t). \quad (2.106)$$

It is also important to note that if we expand the density contrast in Fourier series, Eq. (2.106) becomes

$$\delta_{\mathbf{k}}(t) = \delta_{\mathbf{k}}(0) \exp(\sqrt{4\pi G \rho_0} t). \quad (2.107)$$

Each mode evolves independently from all the others. Let us note that in the expanding case, Eq. (2.105) is simply modified to

$$\ddot{\delta} + 2 H \dot{\delta} = \frac{4\pi G \rho_0}{a^3} \delta, \quad (2.108)$$

whose general solution can also be written as the a sum of a growing mode  $\delta_+ \propto a(t)$  and a decaying mode  $\delta_- \propto a^{-3/2}$  for the case that  $a(t) \propto t^{2/3}$  in the EdS universe. However, as we have already underlined above, the presence of the expansion is not essential to understanding essential results.

### Linear Lagrangian theory & Zeldovich approximation

In the previous section, we have considered the evolution of small perturbations of density on a uniform distribution of matter. With the Lagrangian approach, the function which describes the evolution of the matter is the displacement field  $\mathbf{f}(\mathbf{x}, t)$  of the fluid element. In this section we are going to look at a perturbation theory for this displacement field. This can be particularly interesting as it can describe situations in which the density fluctuations can become very large, and which can therefore not be described with the linear approach we have considered in the previous section.

As we have a vector field  $\mathbf{v}(\mathbf{x}, t)$  which describes the velocity of the fluid at  $(\mathbf{x}, t)$ , we can look for integral curves of this vector field, that is the function  $\mathbf{f}(\mathbf{x}, t)$  such that for any  $\mathbf{x}_0$  in the fixed space,  $\mathbf{f}(\mathbf{x}_0, 0) = \mathbf{x}_0$  and

$$\frac{d\mathbf{f}}{dt}\Big|_{(\mathbf{x}_0, t)} = \frac{\partial \mathbf{f}}{\partial t}\Big|_{(\mathbf{x}_0, t)} = \mathbf{v}\left(\mathbf{f}(\mathbf{x}_0, t), t\right). \quad (2.109)$$

This means that for a given  $\mathbf{x}_0$ , by varying  $t$ ,  $\mathbf{f}(\mathbf{x}_0, t)$  traces the trajectory of a point in the fluid which follows the flow and which is at  $\mathbf{x}_0$  when  $t = t_0$ . Let us consider the set of Eqs. (2.99)

The left hand side of Eq. (2.97) contains two terms: the first,  $\partial_t \mathbf{v}$ , is related to the variation of  $\mathbf{v}$  at a fixed  $\mathbf{x}$  while the second is related to the variation of  $\mathbf{v}$  in the direction of the flow at a fixed time. The sum of the two is therefore the acceleration of a point following the flow. Indeed, if such a point is at  $\mathbf{x}$  at time  $t$ , it goes to  $\mathbf{x} + \mathbf{v} dt$  at time  $t + dt$  and its velocity is given by

$$\mathbf{v}(\mathbf{x} + \mathbf{v} dt, t + dt) = \mathbf{v}(\mathbf{x}, t) + \partial_t \mathbf{v}|_{(\mathbf{x}, t)} dt + (\mathbf{v} \cdot \nabla_{\mathbf{x}}) \mathbf{v}|_{(\mathbf{x}, t)} dt + O(dt^2), \quad (2.110)$$

so that its acceleration is  $\partial_t \mathbf{v} + (\mathbf{v} \cdot \nabla_{\mathbf{x}}) \mathbf{v}$ . According to Eq. (2.97), this acceleration is equal to  $\mathbf{g}(\mathbf{x}, t) = -\nabla \Phi$ , with

$$\nabla_{\mathbf{x}} \times \mathbf{g} = \mathbf{0}, \quad (2.111)$$

and using  $\mathbf{f}$ , we can rewrite this equation as

$$\frac{d^2 \mathbf{f}}{dt^2}\Big|_{(\mathbf{x}_0, t)} = \mathbf{g}\left(\mathbf{f}(\mathbf{x}_0, t), t\right), \quad (2.112)$$

since, for a fixed  $\mathbf{x}_0$ ,  $\mathbf{f}(\mathbf{x}_0, t)$  follows the flow. Eq. (2.96) describes mass conservation: if we consider an infinite volume  $d^3 \mathbf{x}$ , the variation of  $\rho d^3 \mathbf{x}$  (the mass in an infinitesimal volume around  $\mathbf{x}$ ) is equal to the difference between what comes in and what goes out. If we follow the fluid, the infinitesimal volume  $d^3 \mathbf{x}$  is deformed. For instance, if it is contracted, this means that locally the density increases. This can be expressed by the following formula

$$\rho(\mathbf{x}_0, 0) d^3 \mathbf{x} = \rho\left(\mathbf{f}(\mathbf{x}_0, t), t\right) J_{\mathbf{f}}(\mathbf{x}_0, t) d^3 \mathbf{x}, \quad (2.113)$$

where  $J_{\mathbf{f}}(\mathbf{x}, t)$  is the determinant, evaluated at  $(\mathbf{x}, t)$ , of the Jacobian matrix  $J_{\mathbf{f}} \equiv (\partial \mathbf{f} / \partial \mathbf{x})$  related to the transformation  $\mathbf{x} \rightarrow \mathbf{f}(\mathbf{x}, t)$ . If we know the function  $\mathbf{f}(\mathbf{x}, t)$  and its inverse, that is the function  $\mathbf{h}(\mathbf{x}, t)$  such that  $\mathbf{h}(\mathbf{f}(\mathbf{x}, t)) = \mathbf{x}$ , we can find the density at any point from the density at  $t = 0$ :

$$\rho(\mathbf{x}, t) = \frac{1}{J_{\mathbf{f}}(\mathbf{h}(\mathbf{x}, t), t)} \rho\left(\mathbf{h}(\mathbf{x}, t), 0\right). \quad (2.114)$$

This is Eq. (2.96) expressed in terms of  $\mathbf{f}(\mathbf{x}, t)$ . What remains to do now is to obtain Eqs. (2.98) and (2.111) in terms of function. From now on we assume that  $\mathbf{f}$  has an inverse  $\mathbf{h}$ . Eq. (2.112) tells us that

$$\mathbf{g}(\mathbf{x}, t) = \frac{d^2 \mathbf{f}}{dt^2}\Big|_{(\mathbf{h}(\mathbf{x}, t), t)} \equiv \ddot{\mathbf{f}}(\mathbf{h}(\mathbf{x}, t), t). \quad (2.115)$$

Since we are interested in  $\nabla \cdot \mathbf{g}$  and  $\nabla \times \mathbf{g}$ , the first quantity to calculate is  $\partial g_i / \partial x_j \equiv g_{i,j}$ . By using the last equation, we find

$$g_{i,j} = \frac{\partial \ddot{f}_i}{\partial x_k} \frac{\partial h_k}{\partial x_j} \equiv \ddot{f}_{i,k} h_{k,j} \quad (2.116)$$

where summation over repeated indices is implicit. Note that as  $\mathbf{h}$  is the inverse of  $\mathbf{f}$ , the Jacobian matrix of  $\mathbf{h}$  is related to the one of  $\mathbf{f}$  by

$$J_{\mathbf{h}}(\mathbf{x}, t) \equiv \left( \frac{\partial \mathbf{h}}{\partial \mathbf{x}} \right) = \frac{1}{J_{\mathbf{f}}(\mathbf{h}(\mathbf{x}, t), t)} \text{adj} \left[ J_{\mathbf{f}}(\mathbf{h}(\mathbf{x}, t), t) \right]. \quad (2.117)$$

Here  $\text{adj}$  means the *adjoint*:

$$\left( \text{adj } J_{\mathbf{f}} \right)_{ij} = \frac{1}{2} \epsilon_{imn} \epsilon_{jkl} f_{k,m} f_{l,n}, \quad (2.118)$$

where  $\epsilon_{ijk}$  is the permutation of Levi-Civita tensor. The divergence of  $\mathbf{g}$  can then be written

$$(\nabla \cdot \mathbf{g})(\mathbf{x}, t) = \ddot{f}_{i,k} \frac{1}{2} \frac{1}{J_{\mathbf{f}}} \epsilon_{kmn} \epsilon_{irs} f_{r,m} f_{s,n} = \left[ \frac{\epsilon_{irs}}{2} \frac{\partial(\ddot{\mathbf{f}}_i, f_r, f_s)}{\partial(x_1, x_2, x_3)} \right]_{\mathbf{h}(\mathbf{x}, t), t} \quad (2.119)$$

with

$$\frac{\partial(\ddot{\mathbf{f}}_i, f_r, f_s)}{\partial(x_1, x_2, x_3)} \equiv \epsilon_{jkl} \ddot{f}_{i,j} f_{r,k} f_{s,l}. \quad (2.120)$$

The Eq. (2.97) becomes by using Eq. (2.114)

$$\left[ \epsilon_{irs} \frac{\partial(\ddot{\mathbf{f}}_i, f_r, f_s)}{\partial(x_1, x_2, x_3)} \right]_{\mathbf{x}, t} = -4 \pi G \left[ \rho(\mathbf{x}, 0) - \rho_0 J_{\mathbf{f}}(\mathbf{x}, t) \right]. \quad (2.121)$$

For the rotational of  $\mathbf{g}$  we have

$$(\nabla \times \mathbf{g})_i = \epsilon_{ijk} g_{k,j} \quad (2.122)$$

so that, after some calculations, Eq. (2.111) becomes

$$\frac{\partial(\ddot{f}_k, f_k, f_i)}{\partial(x_1, x_2, x_3)} = 0 \quad (2.123)$$

for  $i = 1, 2, 3$ . By definition we have  $\mathbf{f}(\mathbf{x}, 0) = \mathbf{x}$ . This implies that  $J_{\mathbf{f}}(\mathbf{x}, 0) = 1$ . If  $\mathbf{v}(\mathbf{x}, 0)$  and  $\rho(\mathbf{x}, 0)$  are known, the second equation gives us  $\dot{\mathbf{f}}(\mathbf{x}, 0)$  and what remains to do is to solve the last two equations.

In the following we are going to look a perturbation theory for the displacement field  $\mathbf{f}(\mathbf{x}, t)$  of the fluid element. If we write the displacement field  $\mathbf{f}(\mathbf{x}, t) = \mathbf{x} + \mathbf{p}(\mathbf{x}, t)$ , we obtain at first order in  $\mathbf{p}$

$$\nabla \cdot (\ddot{\mathbf{p}} - 4\pi G \rho_0 \mathbf{p}) = -4\pi G \rho_0 \delta(\mathbf{x}, 0), \quad (2.124)$$

$$\nabla \times \ddot{\mathbf{p}} = \mathbf{0}. \quad (2.125)$$

where  $\delta(\mathbf{x})$  is the density contrast. The first equation can be solved by assuming that  $\mathbf{p} = \nabla\chi$ . The second equation can be rewritten as

$$\nabla^2(\ddot{\chi} - 4\pi G\rho_0\chi) = -4\pi G\rho_0\delta(\mathbf{x}, 0). \quad (2.126)$$

If we consider a periodic system, one can write

$$\delta(\mathbf{x}, 0) = \sum_{\mathbf{k} \neq 0} \delta_{\mathbf{k}} \exp(i\mathbf{k} \cdot \mathbf{x}), \quad (2.127)$$

$$\chi(\mathbf{x}, t) = \sum_{\mathbf{k} \neq 0} \chi_{\mathbf{k}}(t) \exp(i\mathbf{k} \cdot \mathbf{x}). \quad (2.128)$$

Eq. (2.126) becomes

$$\ddot{\chi}_{\mathbf{k}} - 4\pi G\rho_0\chi_{\mathbf{k}} = \frac{4\pi G\rho_0}{k^2}\delta_{\mathbf{k}}. \quad (2.129)$$

The general solution is

$$\chi_{\mathbf{k}} = A_+ \exp\left(\sqrt{4\pi G\rho_0}t\right) + A_- \exp\left(-\sqrt{4\pi G\rho_0}t\right) - \frac{\delta_{\mathbf{k}}}{k^2}. \quad (2.130)$$

With the initial conditions for  $\mathbf{p}$ , we find that

$$\mathbf{p}(\mathbf{x}, t) = \left[ \cosh\left(\sqrt{4\pi G\rho_0}t\right) - 1 \right] \sum_{\mathbf{k} \neq 0} \frac{i\mathbf{k}\delta_{\mathbf{k}}}{k^2} \exp(i\mathbf{k} \cdot \mathbf{x}). \quad (2.131)$$

We can rewrite this expression as

$$\mathbf{p}(\mathbf{x}, t) = \left[ \frac{\cosh\left(\sqrt{4\pi G\rho_0}t\right) - 1}{4\pi G\rho_0} \right] \mathbf{g}(\mathbf{x}, 0), \quad (2.132)$$

where  $\mathbf{g}$  is the force field. This means that a fluid element, initially at  $\mathbf{x}$ , is accelerated according to

$$\ddot{\mathbf{p}} = \cosh\left(\sqrt{4\pi G\rho_0}t\right) \mathbf{g}(\mathbf{x}, 0). \quad (2.133)$$

It is interesting to compare these result with Eq. (2.107)

$$\delta_{\mathbf{k}}(t) = \delta_{\mathbf{k}}(0) \cosh\left(\sqrt{4\pi G\rho_0}t\right). \quad (2.134)$$

This implies that

$$\mathbf{g}(\mathbf{x}, t) = \cosh\left(\sqrt{4\pi G\rho_0}t\right) \mathbf{g}(\mathbf{x}, 0), \quad (2.135)$$

since  $\mathbf{g}(\mathbf{x}, t)$  can be expressed in terms of the  $\delta_{\mathbf{k}}$ . We would then expect that a fluid element is accelerated according to

$$\ddot{\mathbf{p}}(\mathbf{x}, t) = \mathbf{g}\left(\mathbf{x} + \mathbf{p}(\mathbf{x}, t), t\right) = \cosh\left(\sqrt{4\pi G\rho_0}t\right) \mathbf{g}\left(\mathbf{x} + \mathbf{p}(\mathbf{x}, t), 0\right) \quad (2.136)$$

and for small displacement this gives Eq. (2.133).

Writing the vector field  $\mathbf{p}$  as the sum of a curl-free part  $\mathbf{p}_D$  and a divergence-less part  $\mathbf{p}_R$  (*i.e.*  $\mathbf{p}_D$  can be written as the gradient of a scalar function, and  $\mathbf{p}_R$  as the curl of a vector field), one finds that

$$\mathbf{p}(\mathbf{x}, t) = \ddot{\mathbf{p}}(\mathbf{x}, 0) \frac{\cosh(\sqrt{4\pi G\rho_0}t) - 1}{4\pi G\rho_0} + \dot{\mathbf{p}}_D(\mathbf{x}, 0) \frac{\sinh(\sqrt{4\pi G\rho_0}t)}{\sqrt{4\pi G\rho_0}} + \dot{\mathbf{p}}_R(\mathbf{x}, 0)t, \quad (2.137)$$

with the initial condition  $\mathbf{p}(\mathbf{x}, 0) = \mathbf{0}$ . Since the gravitational force is conservative  $\ddot{\mathbf{p}}(\mathbf{x}, 0) = \ddot{\mathbf{p}}_D(\mathbf{x}, 0)$ . The asymptotic behavior of the solution Eq. (2.137) is

$$\mathbf{p}(\mathbf{x}, t) \xrightarrow{t \rightarrow \infty} \frac{1}{2} \left[ \frac{\ddot{\mathbf{p}}(\mathbf{x}, 0)}{4\pi G\rho_0} + \frac{\ddot{\mathbf{p}}_D(\mathbf{x}, 0)}{\sqrt{4\pi G\rho_0}} \right] \exp\left(\sqrt{4\pi G\rho_0}t\right). \quad (2.138)$$

By choosing  $\dot{\mathbf{p}}_R(\mathbf{x}, 0) = \mathbf{0}$  and  $\sqrt{4\pi G\rho_0} \ddot{\mathbf{p}}(\mathbf{x}, 0) = \dot{\mathbf{p}}(\mathbf{x}, 0)$ , the solution is then directly in its asymptotic regime. This is the static space version of the *Zeldovich approximation*, more usually given in an expanding background.

### 3.3 Limit of linear theory: a non-continuous approach

For the moment, we have only considered a continuous approach to study the evolution of self-gravitating systems, *i.e.* we have described the density field using a smooth function. This has allowed us to obtain different result concerning this evolution by using a perturbative approach. However, to understand the limit of linear theory and the validity of the fluid approximation, it is interesting to follow a non-continuous approach in terms of discrete particles. We consider in the following the derivation of Peebles in [126].

Let us consider again  $N$  particles of mass  $m$  in a periodic box of volume  $V = L^3$ . The density function at time  $t$  is given by

$$\rho(\mathbf{x}, t) = m \sum_{i=1}^N \delta_D(\mathbf{x} - \mathbf{x}_i(t)), \quad (2.139)$$

where  $\mathbf{x}_i(t)$  is the position of particle  $i$  at time  $t$ . The Fourier coefficients of the density contrast are given by

$$\delta_{\mathbf{k}}(t) = \begin{cases} \frac{1}{N} \sum_{i=1}^N \exp(-i\mathbf{k} \cdot \mathbf{x}_i(t)) & \text{if } k \neq 0 \\ 0 & \text{otherwise} \end{cases} \quad (2.140)$$

We obtain the derivatives

$$\dot{\delta}_{\mathbf{k}} = \frac{1}{N} \sum_{i=1}^N (-i\mathbf{k} \cdot \dot{\mathbf{x}}_i) e^{-i\mathbf{k} \cdot \mathbf{x}_i}, \quad (2.141)$$

$$\ddot{\delta}_{\mathbf{k}} = \frac{1}{N} \sum_{i=1}^N (-i\mathbf{k} \cdot \ddot{\mathbf{x}}_i - (\mathbf{k} \cdot \dot{\mathbf{x}}_i)^2) e^{-i\mathbf{k} \cdot \mathbf{x}_i}. \quad (2.142)$$

Melding the equation of evolution Eq. (2.50) with  $H = 0$  and the Laplace-Poisson equation on obtains

$$\ddot{\mathbf{x}}_i = 4\pi G\rho_0 \sum_{k \neq 0} \frac{i\mathbf{k}}{k^2} \delta_{\mathbf{k}} e^{i\mathbf{k} \cdot \mathbf{x}_i} \quad (2.143)$$

Inserting this in Eq. (2.50) one obtains

$$\ddot{\delta}_{\mathbf{k}} = 4\pi G\rho_0 + A - C, \quad (2.144)$$

where  $A$  and  $C$  represent the nonlinear part of the equation,

$$A = 4\pi G\rho_0 \sum_{\mathbf{q} \neq 0, \mathbf{k}} \frac{\mathbf{k} \cdot \mathbf{q}}{q^2} \delta_{\mathbf{k}} \delta_{\mathbf{k}-\mathbf{q}} \quad \text{and} \quad C = \frac{1}{N} \sum_{i=1}^N (\mathbf{k} \cdot \dot{\mathbf{x}}_i)^2 e^{-i\mathbf{k} \cdot \mathbf{x}_i}. \quad (2.145)$$

If we can neglect during some time the last two terms on the rhs in the last line, we are left with a linear equation identical to what we have obtained in Eq. (2.105). This shows that the last two terms of the last line of Eq. (2.144) are due to non-linear effects and the discrete nature of the particles. A careful analysis of these two terms should therefore provide us interesting information on the applicability of the linear theory.

The problem with Eq. (2.144) is that it is not closed for the  $\delta_{\mathbf{k}}$  as it still contains the particle velocities  $\dot{\mathbf{x}}_i$ . Despite this and following [126], one can show that *even if at small scales the dynamics are non-linear, linear theory can be used at large scales*.

Once gravity starts to act, some clusters can be created, where ‘‘clusters’’ means virialised structures. The velocities of the particles in such objects can be very high. This implies that the term  $C$  in Eq. (2.145) can be very large and this could have an important effect on the evolution of every  $\delta_k$ . This is in fact not true. Using Eq. (2.142), we have

$$\ddot{\delta}_{\mathbf{k}} = \frac{1}{N} \sum_{i=1}^N [-i\mathbf{k} \cdot \mathbf{g}(\mathbf{x}_i) - (\mathbf{k} \cdot \dot{\mathbf{x}}_i)^2] \exp(-i\mathbf{k} \cdot \mathbf{x}_i), \quad (2.146)$$

where  $\mathbf{g}(\mathbf{x}_i)$  is the gravitational field at  $\mathbf{x}_i$ . If  $N_c$  clusters are created, we can rewrite this expression as

$$\ddot{\delta}_{\mathbf{k}} = \frac{1}{N} \left\{ \sum_{\alpha=1}^{N_c} \sum_{i \in I_{\alpha}} [-i\mathbf{k} \cdot \mathbf{g}(\mathbf{x}_i) - (\mathbf{k} \cdot \dot{\mathbf{x}}_i)^2] \exp(-i\mathbf{k} \cdot \mathbf{x}_i) + \sum_{i \notin \text{cluster}} [-i\mathbf{k} \cdot \mathbf{g}(\mathbf{x}_i) - (\mathbf{k} \cdot \dot{\mathbf{x}}_i)^2] \exp(-i\mathbf{k} \cdot \mathbf{x}_i) \right\}, \quad (2.147)$$

where ‘‘ $i \in I_{\alpha}$ ’’ means all the particles in the cluster  $\alpha$  which contains  $N_{\alpha}$  particles, and ‘‘ $i \notin \text{clusters}$ ’’ means all the particles which are not in a cluster. For particles which are in a cluster we can decompose the field  $\mathbf{g}(\mathbf{x})$  into two parts:  $\mathbf{g}_1(\mathbf{x}) + \mathbf{g}_2(\mathbf{x})$  where the first term is due to force of all the other particles in the same cluster while the second is the force from the rest. If we consider one cluster, we can write its contribution to the right hand side of Eq. (2.147) as

$$\sum_{i \in I_{\alpha}} [-i\mathbf{k} \cdot \mathbf{g}_1(\mathbf{x}_i) - i\mathbf{k} \cdot \mathbf{g}_2(\mathbf{x}_i) - (\mathbf{k} \cdot \dot{\mathbf{x}}_i)^2] \cdot \exp(-i\mathbf{k} \cdot \mathbf{x}_i) \quad (2.148)$$

The part containing  $\mathbf{g}_1(\mathbf{x}_i)$  can be written as

$$\sum_{i \in I_{\alpha}} [-i\mathbf{k} \cdot \mathbf{g}_1(\mathbf{x}_i)] \exp(-i\mathbf{k} \cdot \mathbf{x}_i) = \sum_{i \in I_{\alpha}} \left[ -i\mathbf{k} \cdot Gm \sum_{j \neq i \in I_{\alpha}} \frac{\mathbf{x}_j - \mathbf{x}_i}{|\mathbf{x}_j - \mathbf{x}_i|^3} \right] \exp(-i\mathbf{k} \cdot \mathbf{x}_i). \quad (2.149)$$

Defining  $\mathbf{X}_\alpha$  as the centre of mass of the cluster

$$\mathbf{X}_\alpha = \frac{1}{N_\alpha} \sum_{i \in I_\alpha} \mathbf{x}_i, \quad (2.150)$$

the last expression becomes

$$\exp(-i\mathbf{k} \cdot \mathbf{X}_\alpha) \sum_{i \in I_\alpha} \left[ -i\mathbf{k} \cdot Gm \sum_{j \neq i \in I_\alpha} \frac{\mathbf{y}_j - \mathbf{y}_i}{|\mathbf{y}_j - \mathbf{y}_i|^3} \right] \exp(-i\mathbf{k} \cdot \mathbf{y}_i) \quad (2.151)$$

where  $\mathbf{y}_i = \mathbf{x}_i - \mathbf{X}_\alpha$ . These vectors do not have a length longer than the cluster size which we will denote by  $R$ . This means that for  $\mathbf{k}$  such that  $|\mathbf{k}| \ll 1/R$  we can make the following approximation

$$\sum_{i \in I_\alpha} [-i\mathbf{k} \cdot \mathbf{g}_1(\mathbf{x}_i)] \exp(-i\mathbf{k} \cdot \mathbf{x}_i) \approx \exp(-i\mathbf{k} \cdot \mathbf{X}_\alpha) \sum_{i \in I_\alpha} \left[ -i\mathbf{k} \cdot Gm \sum_{j \neq i \in I_\alpha} \frac{\mathbf{y}_j - \mathbf{y}_i}{|\mathbf{y}_j - \mathbf{y}_i|^3} \right] (1 - i\mathbf{k} \cdot \mathbf{y}_i), \quad (2.152)$$

which can be written as

$$\frac{Gm}{2} \exp(-i\mathbf{k} \cdot \mathbf{X}_\alpha) k_\mu k_\nu \sum_{j \neq i \in I_\alpha} \frac{(y_{i,\mu} - y_{j,\mu})(y_{i,\nu} - y_{j,\nu})}{|\mathbf{y}_i - \mathbf{y}_j|^3} \quad (2.153)$$

with an implicit summation over  $\mu$  and  $\nu$ . Using the results derived in section ??, this becomes simply

$$\sum_{i \in I_\alpha} [-i\mathbf{k} \cdot \mathbf{g}_1(\mathbf{x}_i)] \exp(-i\mathbf{k} \cdot \mathbf{x}_i) = \exp(-i\mathbf{k} \cdot \mathbf{X}_\alpha) \sum_{i \in I_\alpha} (\mathbf{k} \cdot \dot{\mathbf{y}}_i)^2. \quad (2.154)$$

Inserting this expression in Eq. (2.148) and neglecting terms of order  $(kR)^2$ , it comes

$$\begin{aligned} \exp(-i\mathbf{k} \cdot \mathbf{X}_\alpha) & \sum_{i \in I_\alpha} \{ (\mathbf{k} \cdot \dot{\mathbf{y}}_i)^2 - [i\mathbf{k} \cdot \mathbf{g}_2(\mathbf{x}_i) + (\mathbf{k} \cdot \dot{\mathbf{x}}_i)^2] \exp(-i\mathbf{k} \cdot \mathbf{y}_i) \} \\ & \approx N_\alpha \exp(-i\mathbf{k} \cdot \mathbf{X}_\alpha) \left[ -i\mathbf{k} \cdot \mathbf{g}_2(\mathbf{X}_\alpha) + (\mathbf{k} \cdot \dot{\mathbf{X}}_\alpha)^2 \right]. \end{aligned} \quad (2.155)$$

Then Eq. (2.147) becomes

$$\ddot{\delta}_{\mathbf{k}} = \frac{1}{N} \left\{ \sum_{\alpha=1}^{N_e} N_\alpha [-i\mathbf{k} \cdot \mathbf{g}_2(\mathbf{X}_\alpha) - (\mathbf{k} \cdot \dot{\mathbf{X}}_\alpha)^2] \exp(-i\mathbf{k} \cdot \mathbf{X}_\alpha) + \sum_{i \notin \text{cluster}} [-i\mathbf{k} \cdot \mathbf{g}(\mathbf{x}_i) - (\mathbf{k} \cdot \dot{\mathbf{x}}_i)^2] \exp(-i\mathbf{k} \cdot \mathbf{x}_i) \right\} \quad (2.156)$$

This shows that clusters can be considered as “macro-particles” for what concerns the evolution of  $\delta_{\mathbf{k}}$  for  $\mathbf{k}$  much smaller than the inverse of the cluster size. Indeed this evolution depends to a good approximation only on the motion of the centre of mass of the clusters and not on what happens inside them. This is actually quite in agreement with the intuition that once a cluster is created, it is seen as a big particle when it is looked from far away. Note that this is valid if we can neglect terms of order  $(kR)^2$  in Eq. (2.156).

Let us now study the term  $\delta_{\mathbf{k}}$  for  $\mathbf{k} \neq 0$  (as  $\delta_0 = 0$ )

$$\delta_{\mathbf{k}} = \frac{1}{V\rho_0} \int_{C_L} (\rho(\mathbf{x}, t) - \rho_0) \exp(-i\mathbf{k} \cdot \mathbf{x}) d^3x \quad (2.157)$$

$$= \frac{1}{V\rho_0} \int_{C_L} \rho(\mathbf{x}, t) \exp(-i\mathbf{k} \cdot \mathbf{x}) d^3x. \quad (2.158)$$

where we have omitted the term  $\int_{C_L} \exp(-i\mathbf{k} \cdot \mathbf{x}) d^3x = V\delta_{\mathbf{k},0}^K$  with  $\delta_{\mathbf{k},0}^K$  the 3D Kronecker symbol. We can now split the box into  $N_D$  small domains ( $\Omega_\alpha$ ) of similar size in such a way that each of them contains at least a few particles. We calculate the centre of mass  $\mathbf{X}_\alpha$  in all of them. If we denote by  $R$  their size, we have for  $\mathbf{k} \ll 1/R$ ,

$$\delta_{\mathbf{k}} = \frac{1}{V\rho_0} \sum_{\alpha=1}^{N_D} \int_{\Omega_\alpha} \rho(\mathbf{x}, t) \exp(-i\mathbf{k} \cdot \mathbf{x}) d^3x \quad (2.159)$$

$$= \frac{1}{V\rho_0} \sum_{\alpha=1}^{N_D} \exp(-i\mathbf{k} \cdot \mathbf{X}_\alpha) \int_{\mathbf{y} + \mathbf{X}_\alpha \in \Omega_\alpha} \rho(\mathbf{X}_\alpha + \mathbf{y}, t) \exp(-i\mathbf{k} \cdot \mathbf{y}) d^3y \quad (2.160)$$

$$\approx \frac{1}{V\rho_0} \sum_{\alpha=1}^{N_D} \exp(-i\mathbf{k} \cdot \mathbf{X}_\alpha) \int_{\mathbf{y} + \mathbf{X}_\alpha \in \Omega_\alpha} \rho(\mathbf{X}_\alpha + \mathbf{y}, t) (1 - i\mathbf{k} \cdot \mathbf{y}) d^3y \quad (2.161)$$

$$= \frac{1}{V\rho_0} \sum_{\alpha=1}^{N_D} \exp(-i\mathbf{k} \cdot \mathbf{X}_\alpha) N_\alpha m \quad (2.162)$$

$$= \frac{1}{N} \sum_{\alpha=1}^{N_D} N_\alpha \exp(-i\mathbf{k} \cdot \mathbf{X}_\alpha), \quad (2.163)$$

where  $N_\alpha$  is the number of particles in the domain  $\Omega_\alpha$ . This means that up to terms of order  $(kR)^2$ ,  $\delta_{\mathbf{k}}$  depends only on the positions of the centres of mass  $\mathbf{X}_\alpha$  as if they were simply particles of different masses. As before, we can draw the conclusion that dynamics which do not change the positions of the centres of mass above a certain scale  $R$ , as it is the case when some particles collapse, have no effects on  $\delta_{\mathbf{k}}$  for  $\mathbf{k}$  much smaller than the inverse of this scale. But clearly, as before, this is true only if terms of order  $(kR)^2$  are really negligible compared to the right hand side of the last line of Eq. (2.161).

A conclusion which can be drawn from this discussion but which should be handled with care is the following: if at  $t = 0$ , for a fixed value of  $\mathbf{k}$  and a scale  $R$ , one has on the one hand

$$\delta_{\mathbf{k}} \approx \frac{1}{N} \sum_{\alpha=1}^{N_D} N_\alpha \exp(-i\mathbf{k} \cdot \mathbf{X}_\alpha) \quad (2.164)$$

as in Eq. (2.161), and on the other hand

$$4\pi G\rho_0\delta_{\mathbf{k}} + 4\pi G\rho_0 \sum_{\mathbf{q} \neq 0, \mathbf{k}} \frac{\mathbf{k} \cdot \mathbf{q}}{q^2} \delta_{\mathbf{k}} \delta_{\mathbf{k}-\mathbf{q}} - \frac{1}{N} \sum_{i=1}^N (\mathbf{k} \cdot \dot{\mathbf{x}}_i)^2 \exp(-i\mathbf{k} \cdot \mathbf{x}_i) \approx 4\pi G\rho_0\delta_{\mathbf{k}}, \quad (2.165)$$

then the evolution of  $\delta_{\mathbf{k}}$  will satisfy approximatively the equation

$$\ddot{\delta}_{\mathbf{k}} = 4\pi G\rho_0\delta_{\mathbf{k}}, \quad (2.166)$$

describing the motion of the centres of mass in the domains of size  $R$  as long as the clusters will have a size smaller than  $1/k \approx R$ , without being influenced by the complicated dynamics on smaller scales. According to Eq. (2.156) these dynamics have only negligible effects on centres of mass at a scale equal to  $R$ . For  $\mathbf{k}$  such that  $|\mathbf{k}| < 1/R$ , the simple linear fluid approach should be justified and if everything holds for all  $\mathbf{k}$  of similar size,  $\delta(\mathbf{x}, t)$  should also be described by the linear fluid theory at scales larger than  $R$ .

### The limit value $n = 4$ for the exponent of the power spectrum - model for newly forming clusters

In the following, we follow the derivation of Peebles [126] to determine the limit value  $n = 4$  for the exponent of the power-spectrum for the validity of linear perturbation theory.

We are interested in a distribution where the large-scale fluctuations are suppressed as much as possible, so the power spectrum will be taken to be

$$|\delta_{\mathbf{k}}|^2 \propto k^n \quad (2.167)$$

for small  $k < x_0^{-1}$ , where  $x_0$  represents the interparticle distance, and  $n > 0$ . At large scale the spectrum is similar to random. The fluctuations are just becoming nonlinear at scale  $x_0$ , signaling the incipient formation of a new generation of clusters on this scale. Since this generation has not yet formed, we shall suppose that the velocity term  $C$  in Eq. (2.144) may be neglected, and we shall estimate the size of the gravity term  $A$  in Eq. (2.144)

$$A = 4\pi G\rho_0 \sum_{\mathbf{q} \neq 0, \mathbf{k}} \frac{\mathbf{k} \cdot \mathbf{q}}{q^2} \delta_{\mathbf{k}} \delta_{\mathbf{k}-\mathbf{q}}, \quad (2.168)$$

$$A^* = 4\pi G\rho_0 \sum_{\mathbf{q} \neq 0, \mathbf{k}} \frac{\mathbf{k} \cdot \mathbf{q}}{q^2} \delta_{-\mathbf{k}} \delta_{\mathbf{q}-\mathbf{k}} \quad (2.169)$$

One then has to compare the mean of the square of  $A$ , *i.e.*  $\langle |A|^2 \rangle$  with the linear gravitational term  $4\pi G\rho |\delta_{\mathbf{k}}|^2$ . Peebles shown in [126] that  $\langle |A|^2 \rangle \sim k^4$ , whereas  $|\delta_{\mathbf{k}}|^2 \sim k^n$ . Then if  $n < 4$  the linear term is larger than  $A$  and we expect linear amplification to be valid, while if  $n \geq 4$  this will not be the case.

## 4 Background on Stochastic point processes

In the following we introduce the formalism used to describe density fields in cosmology: (infinite) statistically homogeneous and isotropic point processes which are uniform, *i.e.* have a well-defined non zero mean density.

### 4.1 Stochastic distributions

Let us consider a discrete random mass distribution represented by the microscopic density function  $\rho(\mathbf{r})$ . The quantity  $\rho(\mathbf{r})dV$  represents the number of particles contained in the infinitesimal volume  $dV$  around the point  $r$ . Assuming that the particles have unitary mass we can write

$$\rho(\mathbf{r}) = \sum_i \delta(\mathbf{r} - \mathbf{r}_i), \quad (2.170)$$

where  $\mathbf{r}_i$  is the position vector of the particle  $i$  of the distribution and  $\delta(\mathbf{r})$  is the Dirac delta function. The function  $\rho(\mathbf{r})$  can be thought as a realization of a stochastic process. It means that to any point  $\mathbf{r}$  is associated a positive random variable  $\hat{\rho}(\mathbf{r})$  whose “extracted” value is  $\rho(\mathbf{r})$ . The stochastic process is totally characterized by

the probability density functional  $P[\rho(\mathbf{r})]$  of the density field  $\rho(\mathbf{r})$ , that gives the probability to have the particular realization  $\rho(\mathbf{r})$  of the stochastic field  $\hat{\rho}(\mathbf{r}, t)$ . We will limit our analysis to ordinary or regular point processes, in which taking a small volume  $\Delta V$  in an arbitrary point of the space, the probability to have more than one point in this volume is of higher order of  $\Delta V$ .

We can compute the average value of any function of the density  $F[\rho(\mathbf{r})]$  in function of the probability density functional:

$$\langle F \rangle = \int D\rho(r) F[\rho(r)] P[\rho(r)], \quad (2.171)$$

where we have used a functional integral (see e.g. [71]).

We can smooth a discrete distribution to obtain a continuous one  $\bar{\rho}$  by averaging over small volumes  $\Delta V(\mathbf{r}_i)$  (centered around the position  $\mathbf{r}$ ) but containing a large amount of particles:

$$\bar{\rho}(\mathbf{r}, t) = \frac{1}{\Delta V(\mathbf{r})} \int_{\Delta V(\mathbf{r}')} d^3 r' \rho(\mathbf{r}', t). \quad (2.172)$$

Note that the density for discrete distribution Eq. (2.170) is a sum of distributions (and then non-smooth function) whereas the averaged density function defined in Eq. (2.172) is a smooth function.

In the probability density functional  $P[\rho(\mathbf{r})]$  all the information about the stochastic field is contained. In general, this information is much more than one wants manipulate. For this reason, one focuses on the  $\ell$ -point correlation functions of the stochastic field defined as

$$\langle \hat{\rho}(\mathbf{r}_1) \hat{\rho}(\mathbf{r}_2) \dots \hat{\rho}(\mathbf{r}_\ell) \rangle = \int D\rho(\mathbf{r}) P[\rho(\mathbf{r})] \hat{\rho}(\mathbf{r}_1) \hat{\rho}(\mathbf{r}_2) \dots \hat{\rho}(\mathbf{r}_\ell). \quad (2.173)$$

The quantity defined in Eq. (2.173), multiplied by  $[dV]^\ell$ , gives the a priori probability of finding simultaneously  $\ell$  particles, in a volume  $dV$  about the positions  $\mathbf{r}_1, \dots, \mathbf{r}_\ell$ , independently of the position of the remaining particles. For example, the 1-point correlation function is simply the local density function  $\langle \rho(\mathbf{r}) \rangle$ .

### Spatial averages and ergodicity

A typical assumption in the statistical analysis of stochastic fields is the so-called *ergodicity* of the stochastic process which generates the mass field both in the continuous and discrete case. In order to clarify the meaning of *ergodicity*, let us take a generic observable  $F = F(\rho(\mathbf{r}_1), \rho(\mathbf{r}_2), \dots)$  of the mass distribution  $\rho(\mathbf{r})$ . Ergodicity means that  $\langle F \rangle$  is equal to the spatial average  $\bar{F}$  given by:

$$\bar{F} = \lim_{V \rightarrow \infty} \frac{1}{V} \int_V d^3 r_0 F(\rho(\mathbf{r}_1 + \mathbf{r}_0), \rho(\mathbf{r}_2 + \mathbf{r}_0), \dots), \quad (2.174)$$

where  $V$  is the integration volume and  $\lim_{V \rightarrow \infty}$  means that the limit of the integration is taken over all space. Finally,  $\rho(\mathbf{r})$  is almost any realization of the mass distribution “extracted” from the probability functional  $P[\rho(\mathbf{r})]$ . This property is also referred to as the *self-averaging* property of the distribution. Note that if the

average in Eq. (2.174) is extended only to a finite sub-sample  $V$  of the whole space, then Eq. (2.174) is only an *estimator* of  $\langle F \rangle$  in the given sub-sample. In cosmology one typically has only such finite volume estimators. Therefore the assumption of ergodicity is necessary if we want to use these statistical estimators of some specific quantities to build or verify hypotheses and theories.

The assumption of *ergodicity* is based on a theorem of continuous stochastic processes: the ergodic theorem of Birkhoff-Khinchin which states that if  $\rho(\mathbf{r})$  has a well-defined average value  $\rho_0$ , then the volume average, in the infinite volume limit, converges with probability one to a well-defined limit [75].

### Statistically homogeneous and isotropic distributions

A stochastic process is statistically homogeneous when the probability density functional  $P[\rho(\mathbf{r})]$  is invariant under spatial translations. The consequence is that the complete  $\ell$ -point correlation function has the property

$$\langle \hat{\rho}(\mathbf{r}_1)\hat{\rho}(\mathbf{r}_2)\dots\hat{\rho}(\mathbf{r}_\ell) \rangle = \langle \hat{\rho}(\mathbf{r}_1 + \mathbf{r}_0)\hat{\rho}(\mathbf{r}_2 + \mathbf{r}_0)\dots\hat{\rho}(\mathbf{r}_\ell + \mathbf{r}_0) \rangle. \quad (2.175)$$

It therefore does not depend on  $\ell$  vector variables anymore but only on  $\ell - 1$  vector variables. For example, the large scale structure of the universe is assumed to be described by a stochastic density field which is statistically homogeneous, *i.e.* it is assumed that there is no privileged positions in the universe (this is the Cosmological principle).

A stochastic system is statistically isotropic if the probability density functional is invariant under rotations, in the sense that

$$P[\rho(\mathbf{r})] = P[\rho(\hat{R}\mathbf{r})], \quad (2.176)$$

where  $\hat{R}$  is any rotation. In the case of the universe, the Cosmological principle assumes statistical isotropy.

The working hypothesis of the current cosmological models are therefore to assume statistically homogeneity and isotropy. In this case, the 1-point correlation function does not depend on the position:

$$\langle \hat{\rho}(\mathbf{r}) \rangle = \rho_0. \quad (2.177)$$

We will also suppose, when the average is performed in an infinite volume, that  $\rho_0 > 0$ , what is called homogeneity or uniformity. It is distinct from the concept of statistical homogeneity or translational invariance discusses above. Homogeneity or uniformity means that if a local average density is performed in a finite volume, the result does not depend on the volume. Current observations indicate homogeneity on large scales in cosmology (see [71]).

### Homogeneity and Homogeneity scale

Let us now consider the meaning of *homogeneity* given by Eq. (2.177) in terms of the spatial average in a single realization of a stochastic mass distribution. The existence of a well-defined average positive density implies that

$$\lim_{R \rightarrow \infty} \frac{1}{||C(R; \mathbf{x}_0)||} \int_{C(R; \mathbf{x}_0)} \rho(\mathbf{r}) d^3r = \rho_0 > 0, \quad \forall \mathbf{x}_0, \quad (2.178)$$

where  $\|C(R; \mathbf{x}_0)\| \equiv 4\pi R^3/3$  is the volume of the sphere  $C(R; \mathbf{x}_0)$  of radius  $R$ , centered on an arbitrary point  $\mathbf{x}_0$ . When Eq. (2.178) is valid, *i.e.* a well-defined positive average density exists for the mass distribution, the characteristic *homogeneity scale*  $\lambda_0$  can be defined as the scale such that

$$\left| \frac{1}{C(R; \mathbf{x}_0)} \int_{C(R; \mathbf{x}_0)} d^3r \rho(\mathbf{r}) - \rho_0 \right| < \rho_0, \quad \forall R > \lambda_0, \quad \forall \mathbf{x}_0. \quad (2.179)$$

This scale gives basically the distance above which fluctuations can be considered small with respect to the mean density  $\rho_0$  and a perturbative approach can be appropriate to describe the physics of the system.

### Correlation Function

Using the hypothesis of homogeneity, we define the 2-point reduced correlation function as

$$C_2(r_{12}) = \langle (\hat{\rho}(\mathbf{r}_1) - \rho_0)(\hat{\rho}(\mathbf{r}_2) - \rho_0) \rangle, \quad (2.180)$$

where  $r_{12} = |\mathbf{r}_1 - \mathbf{r}_2|$ . The complete 2-point correlation function can be written as a function of the reduced 2-point correlation function as:

$$\langle \hat{\rho}(\mathbf{r}_1)\hat{\rho}(\mathbf{r}_2) \rangle = \langle \hat{\rho}(\mathbf{r}_1) \rangle \langle \hat{\rho}(\mathbf{r}_2) \rangle. \quad (2.181)$$

The reduced correlation function  $C_{12}$  (also called covariance function) gives the non-trivial part of this probability. It is usual to normalize the correlation function for density field as

$$\xi(r_{12}) = \frac{C_2(r_{12})}{\rho_0^2}. \quad (2.182)$$

### The Power Spectrum

In cosmology and Statistical Physics it is very usual to characterize distribution in Fourier space rather than in real space. In Cosmology a particular emphasis is placed on this representation because it is mathematically much easier to modelize theoretically the evolution of structures in Fourier space. We define the Fourier transform (FT) of a function  $f(\mathbf{r})$ , in a cubic volume of size  $L$  ( $V = L^d$ ), where  $d$  is the spatial dimension as:

$$\tilde{f}(\mathbf{k}) = \int_V d^d r f(\mathbf{r}) e^{-i\mathbf{k}\cdot\mathbf{r}}. \quad (2.183)$$

The inverse transform is therefore

$$f(\mathbf{r}) = \frac{1}{V} \sum_{\mathbf{k}} \tilde{f}(\mathbf{k}) e^{i\mathbf{k}\cdot\mathbf{r}}, \quad (2.184)$$

where the sum over the discrete  $k$  is restricted to those with components  $k_i = \frac{2m\pi}{L}$  with  $m \in \mathbb{Z}$ . In the limit of infinite  $d$ -dimensional Euclidian space the direct and inverse FT are defined as

$$\tilde{f}(\mathbf{k}) = FT[f(\mathbf{r})] = \int_{R^d} d^d r f(\mathbf{r}) e^{-i\mathbf{k}\cdot\mathbf{r}} \quad (2.185)$$

$$f(\mathbf{r}) = FT^{-1}[\tilde{f}(\mathbf{k})] = \frac{1}{(2\pi)^d} \int_{R^d} d^d k \tilde{f}(\mathbf{k}) e^{-i\mathbf{k}\cdot\mathbf{r}}. \quad (2.186)$$

From now on, for simplicity, we will denote by  $\rho(\mathbf{r})$  both the stochastic density field  $\hat{\rho}(\mathbf{r})$  and any realization of it. We define the fluctuation of the density field  $\delta_\rho(\mathbf{r})$  as

$$\delta_\rho(\mathbf{r}) = \rho(\mathbf{r}) - \rho_0. \quad (2.187)$$

Its Fourier transform in a volume  $V$  is

$$\delta_\rho(\mathbf{k}; V) = \int_V d^d r \delta_\rho(\mathbf{r}) e^{-i\mathbf{k}\cdot\mathbf{r}}. \quad (2.188)$$

Because  $\delta_\rho(\mathbf{r})$  is real,  $\delta_\rho(\mathbf{k}, V) = \delta_\rho^*(-\mathbf{k}; V)$ , where the asterisk denotes “complex conjugate”. We define the structure factor (SF) as

$$S(\mathbf{k}) = \frac{\langle |\delta_\rho(\mathbf{k}; V)|^2 \rangle}{V}. \quad (2.189)$$

It is obviously a positive-definite quantity. In the thermodynamic limit, one takes  $V \rightarrow \infty$  (with constant  $\rho_0$ ). The brackets  $\langle . \rangle$  in Eq. (2.189) indicate an average over realizations. In cosmology the SF is called Power Spectrum (PS) and it is defined as the infinite volume limit of the SF:

$$P(\mathbf{k}) = \lim_{V \rightarrow \infty} \frac{\langle |\delta_\rho(\mathbf{k}; V)|^2 \rangle}{V}. \quad (2.190)$$

If we assume statistical homogeneity, it is simple to show from their respective definitions that the 2-point correlation function and the SF are FT pairs:

$$S(\mathbf{k}) = FT[C_2(\mathbf{r})] \quad (2.191)$$

$$P(\mathbf{k}) = \rho_0^2 FT[\xi(\mathbf{r})]. \quad (2.192)$$

If we assume statistical isotropy an additional average over vectors  $\mathbf{k}$  with the same modulus can be performed, the SF depending then only on  $k = |\mathbf{k}|$ .

There is an important theorem in the theory of stochastic processes related with the PS. This is basically the Wiener-Khinchin theorem (see e.g. [71]), which states that, given a 2-point correlation function  $C_2(\mathbf{r})$ , it exists a statistically homogeneous continuous stochastic stationary process with this correlation, if and only if its PS is integrable and non-negative for all  $k$ , i.e.  $FT[C_2(\mathbf{r})] > 0$ . In the case of a point distribution this condition is only necessary. A corollary of this theorem is the property:

$$\xi(0) \geq \xi(\mathbf{r}). \quad (2.193)$$

Its proof is straightforward: the correlation function  $\xi(r)$  is the FT of the PS

$$\xi(\mathbf{r}) = \frac{1}{(2\pi)^d} \int_{R^d} P(\mathbf{k}) e^{i\mathbf{k}\cdot\mathbf{r}} d^d k. \quad (2.194)$$

Since by defintion,  $P(\mathbf{k}) \geq 0$  and  $\|\exp(i\mathbf{k}\cdot\mathbf{r})\| \leq 1$ , the inequality Eq. (2.193) is evident.

### Mass variance

Another convenient way to characterize stochastic distributions is via the fluctuations of mass in  $d$ -dimensional regions that we will denote  $\Lambda$ . The normalized mass variance is defined as

$$\sigma^2(\Lambda) = \frac{\langle M(\Lambda)^2 \rangle - \langle M(\Lambda) \rangle^2}{\langle M(\Lambda) \rangle^2}. \quad (2.195)$$

The average amount of mass in the region  $\Lambda$  is

$$\langle M(\Lambda) \rangle = \int_{R^d} W_\Lambda(\mathbf{r}) \langle \rho(\mathbf{r}) \rangle d^d r, \quad (2.196)$$

where we have introduced the window function  $W_\Lambda(\mathbf{r})$

$$W_\Lambda(\mathbf{r}) = \begin{cases} 1 & \text{if } \mathbf{r} \in \Lambda \\ 0 & \text{otherwise} \end{cases} \quad (2.197)$$

Further, the average of the square of the mass in the same region is

$$\langle M(\Lambda)^2 \rangle = \int \int_{R^d} d^d r_1 d^d r_2 W_\Lambda(\mathbf{r}_1) W_\Lambda(\mathbf{r}_2) \langle \rho(\mathbf{r}_1) \rho(\mathbf{r}_2) \rangle. \quad (2.198)$$

Using the above formulae and the defintion of correlation function Eq. (2.182) we can write

$$\sigma^2(\Lambda) = \frac{1}{V^2} \int \int_{R^d} d^d r_1 d^d r_2 W_\Lambda(\mathbf{r}_1) W_\Lambda(\mathbf{r}_2) \xi(|\mathbf{r}_1 - \mathbf{r}_2|), \quad (2.199)$$

where  $V$  is the volume of the region  $\Lambda = \int d^d r W_\Lambda(\mathbf{r})$ . Performing the FT of Eq. (2.199) we obtain

$$\sigma^2(\Lambda) = \frac{1}{(2\pi)^d} \int d^d k P(\mathbf{k}) |\tilde{W}_\Lambda(\mathbf{k})|^2, \quad (2.200)$$

where  $\tilde{W}_\Lambda(\mathbf{k})$  is the FT of  $W_\Lambda(\mathbf{r})$ . Very often the natural choice of volume  $\Lambda$  in which to compute the fluctuations is a sphere. It is simple to find that the FT of the window function is in three dimensions [71]

$$\tilde{W}_\Lambda(\mathbf{k}) = \frac{3}{(kR)^3} (\sin kR - kR \cos kR). \quad (2.201)$$

### Discrete versus continuous distributions

When performing numerical simulations in cosmology, evolution of continuous field is computed evolving discrete  $N$ -body particle distributions. In this context it is important to understand the differences between continuous and discrete distributions.

Discreteness introduces a kind of fluctuations that does not appear in continuous distributions. For example, it is possible to construct a continuous distribution with zero fluctuations, *i.e.* with  $C_{12}(\mathbf{r}) = 0$  for all  $\mathbf{r}$  (we assume statistical homogeneity). This is simply a distribution with constant density everywhere. In the case of discrete distributions there is always a fluctuation introduced by discreteness: a particle is correlated with itself, which introduces a singularity in  $C_{12}(\mathbf{r})$ . We can see that studying the uncorrelated (discrete) Poisson distribution.

**The Poisson distribution** We work for simplicity in  $d = 3$  dimensions. We divide the 3-dimensional real space in  $n = V/dV$  infinitesimal cells of volume  $dV$  and we define the stochastic density field in each cell as

$$\hat{\rho}(\mathbf{r}) = \begin{cases} \frac{1}{dV} & \text{with probability } \rho dV \\ 0 & \text{with probability } 1 - \rho dV \end{cases} \quad (2.202)$$

The average density (the 1-point correlation function) is trivially

$$\langle \hat{\rho}(\mathbf{r}) \rangle = \frac{n.(1/dV).\rho_0 dV + n.0.(1 - \rho_0 dV)}{n} = \rho_0. \quad (2.203)$$

The 2-point correlation function is

$$\langle \hat{\rho}(\mathbf{r}_1) \hat{\rho}(\mathbf{r}_2) \rangle = \langle \hat{\rho}(\mathbf{r}) \rangle^2 = \rho_0^2 \quad (2.204)$$

if  $\mathbf{r}_1 \neq \mathbf{r}_2$  and

$$\langle \hat{\rho}(\mathbf{r}_1) \hat{\rho}(\mathbf{r}_2) \rangle = \frac{n.(1/dV)^2.\rho_0 dV + n.0^2.(1 - \rho_0 dV)}{n} = \frac{\rho_0}{dV}, \quad (2.205)$$

if  $\mathbf{r}_1 = \mathbf{r}_2$ . Therefore, in the limit  $dV \rightarrow 0$  we obtain:

$$C_2(r_{12}) = \langle \hat{\rho}(\mathbf{r}_1) \hat{\rho}(\mathbf{r}_2) \rangle - \rho_0^2 = \rho_0 \delta(\mathbf{r}_1 - \mathbf{r}_2). \quad (2.206)$$

The discreteness of the distribution introduces a singularity in the correlation function  $C_{12}(r)$  at  $r = 0$  (and indeed for all  $\ell$ -point correlation functions). The density has an infinite discontinuity around any particle with finite mass, which is mathematically represented by a delta function in the correlation function. Note that this result is general for any particle distribution and not only for a Poisson distribution. The correlation function of a correlated particle distribution can be written therefore as the sum of two pieces:

$$C_{12}(\mathbf{r}) = \delta(\mathbf{r}) + \rho_0^2 h(\mathbf{r}), \quad (2.207)$$

where  $\delta(\mathbf{r})$  is the singularity introduced by discreteness and  $h(\mathbf{r})$  is a smooth function.

**Asymptotic behavior** It is important to know the permitted asymptotic behavior of the correlation function. The general condition to be a continuous stochastic process well defined are

- The distribution is no singular with regions with infinite density, *i.e.*

$$\int_{\epsilon} n_0(1 + \xi(r))dV < \infty, \quad (2.208)$$

where the integration is performed in any arbitrary small region  $\epsilon$ . It implies that if we consider a power-law behavior of the correlation function at small scales, we have

$$\lim_{r \rightarrow 0} \xi(r) \sim r^\alpha, \quad \alpha > -d. \quad (2.209)$$

- Regions at infinite distance are not correlated. Therefore

$$\lim_{r \rightarrow \infty} \xi(r) \sim r^\beta, \quad \beta < 0. \quad (2.210)$$

In the case of a discrete distribution the situation is very similar. At large scales, the correlation function remains unchanged and therefore condition Eq. (2.210) holds. At small scales, the divergence introduced by the discreteness give rise only to a finite contribution and the condition Eq. (2.209) has to be fulfilled now by the smooth function  $h(r)$ .

From above properties for the correlation function, it is simple to deduce the analogous permitted asymptotic behaviour of the PS. From Eq. (2.209), for a continuous distribution, we have the condition

$$\lim_{k \rightarrow \infty} P(k) = 0, \quad (2.211)$$

which implies that, if  $P(k \rightarrow \infty) \sim k^\gamma$ ,  $\gamma < 0$ . If, moreover, the stochastic process has finite variance (*i.e.*  $\xi(0) < \infty$ ), then

$$\lim_{k \rightarrow \infty} k^d P(k) = 0, \quad (2.212)$$

and then  $\gamma < -d$ . For a point-particle distribution we have the constraint

$$\lim_{k \rightarrow \infty} \left| P(k) - \frac{1}{\rho_0} \right| = 0, \quad (2.213)$$

*i.e.* if  $\left| P(k) - \frac{1}{\rho_0} \right| \sim k^\gamma$  then  $\gamma < 0$ . The small  $k$  behaviour of the PS is, from condition Eq. (2.210),

$$P(k \rightarrow 0) \sim k^\delta \quad (2.214)$$

then  $\delta > -d$ .

## 4.2 Classification of stochastic processes

In order to derive a complete classification of stochastic processes, let us consider Eqs. (??) and (2.201), and assume without loss of generality that  $P(k) = Ak^n f(k)$ , where  $A > 0$  and  $f(k)$  a cut-off function chosen such that (i)  $\lim_{k \rightarrow 0} f(k) = 1$ , and (ii)  $\lim_{k \rightarrow \infty} k^n f(k)$  is finite. We also require  $n > -3$  to have the integrability of  $P(k)$  around  $k = 0$ . It is convenient to rescale variables putting  $x = kR$  to rewrite

$$\sigma^2(R) = \frac{9A}{2\pi^2} \frac{1}{R^{3+n}} \int_0^\infty dx (\sin x - x \cos x)^2 x^{n-4} f\left(\frac{x}{R}\right). \quad (2.215)$$

By analyzing in detail this formula, we obtain (see a complete derivation in [71]) the following general relation between the large  $R$  behavior of  $\sigma^2(R)$  and the small  $k$  behavior of  $P(k)$ :

$$\sigma^2(R) \sim \begin{cases} R^{-(3+n)} & \text{for } -3 < n < 1 \\ R^{-4} \log R & \text{for } n = 1 \\ R^{-4} & \text{for } n > 1. \end{cases} \quad (2.216)$$

The argument used to derive Eq. (2.216) can be generalized to Euclidian spaces of any dimension  $d$ . Therefore supposing  $P(k) = Ak^n f(k)$  as above, it is possible to proceed to the following classification for the scaling behavior of the normalized mass-variance:

$$\sigma^2(R) \sim \begin{cases} R^{-(d+n)} & \text{for } -d < n < 1 \\ R^{-(d+1)} \log R & \text{for } n = 1 \\ R^{-(d+1)} & \text{for } n > 1. \end{cases} \quad (2.217)$$

Therefore

- For  $-d < n < 0$ , we have “super-Poisson” mass fluctuations typical of systems at the critical point of a second order phase transition.
- For  $n = 0$ , we have Poisson-like fluctuations, and the system can be called substantially Poisson. This behavior is typical of many common physical systems, e.g. an homogeneous gas at thermodynamic equilibrium at sufficiently high temperature.
- For  $n > 0$ , we have “sub-Poisson” fluctuations, and for this reason we name this class of systems super-homogeneous. This behaviour is typical, for example, of lattice-like point distributions where positively correlated regions are balanced by negatively correlated ones. Therefore the condition of  $P(0) = 0$  corresponds to a sort of underlying long-range order. This class of mass distributions play an important role in Cosmology.

### 4.3 Causal bounds on the Power spectrum

The consideration in section 3.3 above of the evolution of discrete self-gravitating system, which leads to the “limit” value  $n = 4$  for the applicability of fluid linear theory is in fact related to a much more general significance of this particular power spectrum. This arises when one considers the constraints imposed by *causality* on the power spectrum of density fluctuations which may be generated by a physical process in an expanding universe with a finite causal “horizon” (*i.e.* a finite distance up to which light can travel up to cosmic time  $t$ , as in standard FRW expanding models dominated by matter or radiation).

Zeldovich concluded, using a simple heuristic derivation, that in this case, if one assumes that the physics involved conserves *mass* and *momentum*, one obtains that, at small  $k$ ,  $P(k) \sim k^n$  with  $n \geq 4$  [160]. Indeed such fluctuations can only be correlated up to a finite distance ( $L_H$  say), *i.e.*  $\xi(r) = 0$  for  $r > L_H$ . By Fourier transform theory, this implies that the PS is analytic at  $k = 0$ . Then Taylor expansion about  $k = 0$  gives  $P(k) = P(0) + \frac{k^2}{2} P''(0) + O(k^4)$ . It can be shown quite rigorously that  $P(0) = 0$  follows from the condition of local mass conservation, and heuristic arguments suggest that  $P''(0) = 0$  follows from local “center of mass conservation” (*i.e.* momentum conservation). Specific constructions (see e.g. [69]) also show the apparent generality of the result.

Assuming non-linear structure formation through self-gravity to be an example of such a causal process (where the “horizon” is now the non-linear scale at the given time) one immediately comes to the conclusion of section 3.3, that non-linear clustering can create  $P(k \rightarrow 0) \sim k^4$ , which will overwhelm the linear amplification if the initial large scale fluctuations have  $P(k \rightarrow 0) \sim k^n$  and  $n > 4$ .

## 5 The non-linear regime: numerical simulation

In the current cosmological paradigm, structures grow through the gravitational instability of initial density fluctuations of collisionless dark matter. This occurs in a hierarchical way, with small-scale perturbations collapsing first and large-scale perturbations latter, *i.e.* the *bottom-up* formation scenario of the CDM model. Let us note, however, that different models were proposed in the late 1970s and early 1980s: the *hot dark matter* (HDM) models [131]. HDM models of cosmological structure formation led to a *top-down* formation scenario, in which superclusters of galaxies are the first objects to form after the big bang, with galaxies and clusters forming through a subsequent process of fragmentation. However, it was already becoming clear from observations that galaxies are much older than superclusters, contrary to what the HDM scenario implies, and such models were abandoned by the mid-1980s after cosmologists realized that if galaxies had formed early enough to agree with observations, their distribution would be much more inhomogeneous than is the case [154].

One of the most direct manifestations of this nonlinear process is the evolution of the power spectrum of the mass,  $P(k)$ , where  $k$  is the wavenumber of a given Fourier mode. Understanding this evolution of the power spectrum is one of the key problems in structure formation, being directly related to the abundance and clustering of galaxy systems as a function of mass and redshift. If the processes that contribute to the evolution could be captured in an accurate analytic model, this would open the way to using observations of the nonlinear mass distribution (from large-scale galaxy clustering or weak gravitational lensing) in order to recover the primordial spectrum of fluctuations. One such attempt at such analytic description of clustering evolution was the “stable clustering” hypothesis of Davis and Peebles [126] that assumes that a nonlinear collapsed object would decouple from the global expansion of the Universe to form an isolated system in virial equilibrium.

We provide a brief overview of the theoretical understanding of nonlinear evolution. In particular we introduce the stable clustering hypothesis and the halo model, as these ideas are central in the study of nonlinear clustering. We also discuss the scale-free models and their self-similarity properties.

### 5.1 *N*-body simulations

#### Equations of motion

Equation of motion in cosmological *N*-body simulations, introduced in Eq. (2.50), can be explicitly written

$$\ddot{\mathbf{x}}_i + 2 H(t) \dot{\mathbf{x}}_i = -\frac{Gm}{a^3} \sum_{j \neq i}^* \frac{\mathbf{x}_i - \mathbf{x}_j}{|\mathbf{x}_i - \mathbf{x}_j|^3} \quad (2.218)$$

where the notation  $\sum^*$  implicitly excludes the (badly defined) contribution due to the mean density, and where  $a(t)$  is the scale factor of the model considered, and  $H(t) = \dot{a}/a$  is the Hubble “constant”. For the EdS cosmology  $k = 0$ ,  $\Lambda = 0$ ,  $a(t) \propto t^{2/3}$  and  $H^2 = \frac{8\pi G}{3}\rho$ . The case  $H = 0$  defines a “static universe” limit.

### Algorithms and timestep

The basic idea for numerical integration is as follows. The equation of motion expresses the second derivative of position in terms of position, velocity and time. Position and velocity at later times are expressed in terms of position and velocity at earlier times using a truncated Taylor series. The key constraint in cosmological simulations is that force evaluation is very time consuming and one wishes to minimise the number of force evaluations per time step. Mainly for this reason, cosmological  $N$ -body simulations use the Leap-Frog method for integrating the equation of motion as it requires only one evaluation of force and the error is of order  $(\Delta t)^3$ , where  $\Delta t$  is the time step (see e.g. [59]).

The optimum value of the time step depends on the distribution of particles and it changes as this distribution evolves. It is common to use a time step that varies with time so that the  $N$ -body code does not use too small a time step when a smaller value is required for conserving integrals of motion. It is possible to generalise even further and choose a different time step for each particle as well, motivation for this being that a few particles in a very dense regions require a small  $\Delta t$  whereas most particles are not in such regions. There are several methods of implementing this in  $N$ -body simulations, and main consideration is to ensure that the positions and velocities of all particles are synchronised at frequent intervals. Using individual time steps can speed up  $N$ -body simulations by a significant amount (see e.g. [129, 132] and references therein).

### Calculation of force

The attractive gravitational force produces, during the evolution, smaller and smaller structures. The necessary to resolve the smallest possible scales. The combination of this necessity to resolve small scales in large regions implies the need to use the maximum number of particles.

The calculation of the force is the most time consuming task in  $N$ -body simulations. As a result, a lot of attention has been focused on this aspect and many algorithms and optimising schemes have been developed.

The direct calculation of the force is numerically costly -  $N^2$  operations for  $N$  particles - and even a modest  $10^4$  particles simulation needs considerable computer resources (while the largest current simulations use more than  $10^{10}$  particles). To solve this technical problem different approximations are used, such as the (for a review see e.g. [1]). In short, the first one smooths the particle mass on a grid to allow the use of FFT techniques, which speed up the computation. The  $P^3M$  method does almost the same but gains accuracy by computing directly (“Particle-Particle”) the force from nearby particles. Tree-codes build a hierarchy between the particles that resembles a “tree”. The gravitational force is calculated using the structure of the tree. The force between two close particles in the tree is computed almost exactly. The force between distant particles in the tree is computed using a whole branch as a single effective particle, as in a multipole expansion method (for details see [142]). Others refinements are used to improve the small scale resolution in the simulations. One of them is to use an adaptative mesh: in regions with higher density a mesh with more resolution is used, keeping a lower resolution in regions with small density. Another method is the technique of “re-simulation”: a first sim-

ulation is performed to localise regions with high density. Then, the simulation is performed again putting more particles in the region where the particles of the final high density regions were initially (for details, see e.g. [24, 46, 96, 141].

To mimic as closely as possible a truly infinite system, one uses an infinite periodic system, made of  $3-d$  cubic cells containing  $N$  particles. The forces on particles are then calculated considering not only the particles situated in the original box but also the particles of all the copies. Then if the  $i^{th}$  particle has coordinate  $r_i$ , its copies will have coordinates  $r_i + nL$ , where  $n$  is a vector with integer components. For the gravitational interaction

$$\phi(r_i) = \sum_{j,n}^* \frac{m_j}{|r_{ij} + nL|}, \quad (2.219)$$

where  $m_j$  is the mass of the particles and the asterisk denotes that the sum  $n = 0$  does not include the term  $i = j$ . As we have noted in section 3.1, this expression is badly defined, and its regularisation by subtraction of the contribution due to the mean density is implicit. A natural way of writing the sum in an explicitly convergent way taking this regularisation into account is to separate the potential into a short range and long range part by introducing a parameter-dependent damping function  $f(r; \alpha)$ :

$$\phi(r_i) = \sum_{j,n}^* m_j \left( \frac{f(r_{ij} + nL; \alpha)}{|r_{ij} + nL|} + \frac{1 - f(r_{ij} + nL; \alpha)}{|r_{ij} + nL|} \right). \quad (2.220)$$

The first term on the r.h.s of Eq. (2.220) is short-range (*i.e.* decays rapidly) and the second term is long-range. The procedure used in the *Ewald summation method* is to compute the first term in real space and the second in Fourier space [62]. If the parameter  $\alpha$  is appropriately chosen, the real part converges well taking only the sum over the closest image, and the part of the sum in Fourier part is rapidly convergent. Of course the sum of the two terms yields the original particle distribution. We write the potential energy then as:

$$\phi = \phi_r^{(s)} + \phi_k^{(l)}. \quad (2.221)$$

Further it is convenient to separate out the zero mode in the long-range part, writing

$$\phi_k^{(l)} = \phi_{k=0}^{(l)} + \phi_{k \neq 0}^{(l)}. \quad (2.222)$$

The function  $f(r; \alpha)$  is chosen in the Ewald summation so that  $\phi_r^{(s)}$  and  $\phi_{k \neq 0}^{(l)}$  are both rapidly convergent, and with a known analytical expression for its Fourier transform. The value of the term  $k = 0$  depends on how precisely the infinite sum in Eq. (2.219) is defined. In cosmology this term is simply removed, as this corresponds to subtracting the mean density.

## 5.2 Initial conditions

When one runs an  $N$ -body simulation, the first step is to generate adequate initial conditions (IC) with the correlations specified by some theoretical model. The most widely used method to generate such IC uses correlated displacement of particles initially placed on a lattice. The correlations of the displacement field are determined

to be such as to obtain a final distribution that has, approximately, the desired correlation properties (cf. [65]).

How this can be done can be understood, up to corrections coming from discrete nature of the distribution, using the Zeldovich approximation. As discussed in section above, this gives an approximation valid (at sufficiently short time) for the displacements of fluid elements from their initial position  $\mathbf{q}$

$$\mathbf{r}(\mathbf{q}, t) = \mathbf{q} + A(t) \mathbf{u}(\mathbf{q}) \quad \text{with} \quad \mathbf{u}(\mathbf{q}) = -\nabla \cdot \Phi(\mathbf{q}), \quad (2.223)$$

where  $A(t)$  is simply the growth factor associated with the growing mode in linear perturbative theory and  $\Phi(\mathbf{q})$  is the gravitational potential at the initial time created by the density fluctuations.

Now if we consider the points on the initial grid as defining the initial positions  $\mathbf{q}$  of the fluid elements, we can obtain the corresponding displacements (and velocities  $\frac{d\mathbf{u}}{dt} = -\dot{f}(t) \nabla \Phi(\mathbf{q})$ ) by determining the gravitational potential  $\Phi(\mathbf{q})$ , which can be inferred directly from the desired power spectrum  $P(k)$  through the Poisson equation. The latter is assumed to be a realization of a Gaussian process.

To set up IC for the  $N$  particles of a cosmological  $N$ -body simulation the procedure is then in summary [50]:

- one sets up a “pre-initial” configuration (usually a lattice) of the  $N$  particles.
- given an input theoretical PS  $P_{th}(k)$ , and fluctuations assumed Gaussian, the corresponding displacement field in the ZA is applied to the “pre-initial” point distribution.

In the following, we give a brief survey of basic results derived from cosmological  $N$ -body simulations.

### 5.3 Self-similarity

One of the important results from numerical simulations in the context of cosmology is that, for a *power-law* initial condition  $P(k) \sim k^n$ , the system reaches a kind of scaling regime, in which the temporal evolution is equivalent to a rescaling of the spatial variables. This spatio-temporal scaling relation is referred to as *self-similarity*: the 2-point correlation function  $\xi(x, t)$  scales as

$$\xi(x, t) \equiv \xi\left(\frac{x}{R_s(t)}\right) \quad (2.224)$$

where  $R_s(t)$  is a time dependent function derived from linear theory. In statistical physics such behaviour is known as *dynamical scaling*, and is observed for example in the ordering dynamics of quenched ferromagnetic systems.

Two necessary requirements for the evolution to be self-similar are usually identified

1. the background cosmological model should not possess any characteristic length or time-scales. Thus the universe must be spatially flat, with zero cosmological constant and a scale-free equation of state;

2. the initial density perturbation field should have no characteristic length scale. Its power spectrum must therefore have power law form.

There are then only two characteristic scales in the problem

- the homogeneity scale  $\ell(t)$  defined initially through the amplitude of the PS;
- an ultraviolet scale (cut-off in the PS at large  $k$ , provided in cosmological simulations by the lattice spacing).

Now if the second scale is irrelevant to the dynamics and the clustering it produces at sufficiently long times and large scales, one then necessarily must have

$$f(x, t) = f_0\left(\frac{x}{R_s(t)}\right) \quad (2.225)$$

where  $f$  is any dimensionless function characterizing the clustering in real space (*i.e.* the physical behavior of clustering at any scale can only be determined by its size compared to this single characteristic length scale), where  $R_s(t)$  is the temporal behavior of the scale  $\ell(t)$ . In  $k$ -space, likewise,  $f(k, t) = f_0(kR_s(t))$ . Further, if linear perturbation theory is valid, such behavior is indeed verified (and different scales decouple, the UV cut-off being irrelevant). This allows us to determine the function  $R_s(t)$ . The linear amplification gives

$$k^d P(k, t) = A^2(t) P(k, t_0) = (k R_s(t))^d P(k R_s(t), t_0), \quad (2.226)$$

which is satisfied for a power-law initial PS if

$$R_s(t) = A(t)^{2/(d+n)}. \quad (2.227)$$

In a flat, matter-dominated universe  $A(t) \propto t^{2/3}$  so one simply obtains

$$R_s(t) \propto t^{4/3(3+n)}. \quad (2.228)$$

If it is linear theory that drives structure formation, in a hierarchical process in which non-linear is generated through the collapse of the initial fluctuations, we would expect such behavior always to result. Given the analysis of the range of validity of linear theory, this means the range

$$-d < n < 4. \quad (2.229)$$

In the cosmological literature, different considerations have led various authors to restrict this range. If one naively considers the fact that the mass fluctuations becomes sensitive to the UV cut-off, one would limit this range to  $n < 1$ . Efstathiou et al. [51] suggested that  $-d < n < -d + 2$  could be excluded (in addition to  $n > 1$ ) because of the divergence of the displacements in the Zeldovich approximation in this case, which they thought would mean that evolution would depend in this case on the box size. Jain and Bertschinger [84, 85] argued that this would not be the case. Numerically only the case  $n \leq 1$  appear to have been studied in the literature for an expanding universe. As  $n$  decreases it becomes more difficult to determine whether self-similarity applies because the temporal range accessible is much shorter.

However numerical studies [39, 85] indicate the self-similarity does indeed hold for  $n = -2$  in  $d = 3$ .

Studies of the static limit have been performed which show that self-similarity is valid for  $n = 0$  and  $n = 2$  [11]. Note that in the cosmology literature self-similarity is argued to be associated to power-law behaviour of  $R_s(t)$  which arises in “scale-free” cosmologies like EdS — and related to the existence of scaling solutions to the Vlasov equation in this case. The arguments given above are much general and clearly apply also to a static model. Indeed, following [11], Eq. (2.226) gives for a static universe  $R_s(t) \propto \exp\left[\frac{2(t-t_{ref})}{(3+n)\tau_{dyn}}\right]$  if one considers the growing mode, where one has chosen for convenience  $R_s(t_{ref}) = 1$ .

## 5.4 From linear theory to stable clustering

In the non-linear regime where perturbation theory fails, it was proposed that clustering in the very non-linear regime might be understood by assuming that regions of high density contrast undergo virialization and subsequently maintain a *fixed proper density* [126]. Denoting  $x$  a comoving distance, the correlation function for a population of such systems would then simply evolve according to

$$\xi(x, t) \propto a^{-3}. \quad (2.230)$$

This evolution was termed *stable clustering*. Peebles went on to show that if the initial power spectrum was a pure power-law in  $k$  with spectral index  $n$ ,  $P(k) \propto k^n$ , and if  $\Omega = 1$ , then under the stable clustering hypothesis, the slope of the nonlinear correlation function would be directly related to the spectral index through the relation

$$\xi(r, t) \propto r^{-\gamma} \quad \text{with} \quad \gamma = \frac{3(3+n)}{5+n}. \quad (2.231)$$

where  $r$  is a proper distance. This can be simply derived if we link the results obtained in both comoving and physical coordinates, *i.e.*

$$a^3 \xi(x, t) \sim r^{-\gamma} \sim \left(\frac{r_0}{a R_s(t)}\right)^{-\gamma}, \quad (2.232)$$

which gives  $a^{3+\gamma} \sim R_s^\gamma(t) \sim t^{4\gamma/3(3+n)} \sim a^{2\gamma/(3+n)}$ . Hence, if stable clustering applies, then nonlinear density field retains some memory of its initial configuration, and in principle can be used to measure the primordial spectrum of fluctuations.

## 5.5 Halo models

We present now an approach which has its origins in papers by Neyman and Scott [119]. They were interested in describing the spatial distribution of galaxies. They argued that it was useful to think of the galaxy distribution as being made up of distinct clusters with a range of sizes. Since galaxies are discrete objects, they described how to study statistical properties of distribution of discrete points; the description requires knowledge of the distribution of cluster sizes, the distribution of points around the cluster center, and a description of the clustering of clusters.

The non-linear evolution of the dark matter distribution has been studied extensively using numerical simulations of the large scale structure clustering process. These simulations indicate that an initially smooth matter distribution evolves into a complex network of sheets, filaments and knots. The dense knots are often called dark matter halos. High resolution, but relatively small volume, simulations have been used to provide detailed information about the distribution of mass in and around such halos (*i.e.* the halo density profile [115, 116]), whereas larger volume, but lower resolution simulations have provided information about the abundance and spatial distribution of halos [37, 87]. Simulations such as these show that the halo abundance, spatial distribution and internal density profiles are closely related to the properties of the initial fluctuation field. When these halos are treated as the analogs of Neyman and Scott's clusters, their formalism provides a way to describe the spatial statistics of the dark matter density field from the linear to highly non-linear regimes.

Such a halo based description of the dark matter distribution of large scale structure is extremely useful because, following White and Rees [155], the idea that galaxies form within such dark matter halos has gained increasing credence. In this picture, the physical properties of galaxies are determined by the halos in which they form. Therefore, the statistical properties of a given galaxy population are determined by the properties of the parent halo population. There are now a number of detailed “semi-analytic” models which implement this approach [21, 38, 92, 140]; they combine simple physically motivated galaxy formation recipes with the halo population output from a numerical simulation of the clustering of the dark matter distribution to make predictions about how the galaxy and dark matter distributions differ.

In the following, we give a brief introduction of the ingredients building the halo model of large scale structure. The approach assumes that all the mass in the Universe is partitioned up into distinct units, the halos. If these halos are small compared to the typical distances between them, the statistics of the mass density field on small scales are determined by the spatial distribution within the halos; the precise way in which the halos themselves may be organized into large scale structures is not important. On the other hand, the details of the internal structure of the halos cannot be important on scales larger than a typical halo; on large scales, the important ingredient is the spatial distribution of the halos. This approximation, in which the distribution of the mass is studied in two steps (*i.e.* the distribution of mass within each halo and the spatial distribution of the halos themselves) is the key to what has come to be called the *halo model*.

The halo model assumes that, in addition to thinking of the spatial statistics in two steps, it is useful and accurate to think of the physics in two steps also. In particular, the model assumes that the regime in which the physics is not described by perturbation theory is confined to regions within halos, and that halos can be adequately approximated by assuming that they are in virial equilibrium.

### The spherical collapse model

The assumption that non-linear objects formed from a spherical collapse is a simple and useful approximation. The spherical collapse of an initially top-hat density perturbation was first study by Gunn and Gott [79].

In the top-hat model, one starts with a region of initial, comoving Lagrangian size  $R_0$ . Let  $\delta_i$  denote the initial density within this region. We will suppose that the initial fluctuations were Gaussian with an rms value on scale  $R_0$  which was much less than unity, *i.e.*  $|\delta_i| \ll 1$ . This means that the mass  $M_0$  within  $R_0$  is  $M_0 = \frac{4\pi}{3}\bar{\rho}(1 + \delta_i)R_0^3 \approx \frac{4\pi}{3}\bar{\rho}R_0^3$  where  $\bar{\rho}$  denotes the comoving background density.

As the Universe evolves, the size of this region changes. Let  $R$  denote the comoving size of the region at some later time. The density within the region is  $(R_0/R)^3 \equiv (1 + \delta)$ . In the spherical collapse model there is a deterministic relation between the initial comoving Lagrangian size  $R_0$  and density of an object, and its Eulerian size  $R$  at any subsequent time. For an EdS universe, one can obtain a parametric solution to  $R(z)$  in terms of  $\theta$ :

$$\frac{R(z)}{R_0} = \frac{(1+z)}{(5/3)|\delta_0|} \frac{(1 - \cos \theta)}{2}, \quad (2.233)$$

and

$$\frac{1}{1+z} = \left(\frac{3}{4}\right)^{2/3} \frac{(\theta - \sin \theta)^{2/3}}{(5/3)|\delta_0|}, \quad (2.234)$$

where  $\delta_0$  denotes the initial density  $\delta_i$  extrapolated using linear theory to the present time (see e.g. [126]). If  $\delta_i < 0$ , then  $(1 - \cos \theta)$  should be replaced with  $(\cosh \theta - 1)$  and  $(\theta - \sin \theta)$  with  $(\sinh \theta - \theta)$ .

In the spherical collapse model, initially overdense regions collapse: with  $\theta = 0$  at start, they “turnaround” at  $\theta = \pi$ , and have collapsed completely when  $\theta = 2\pi$ . Eq. (2.233) shows that the size of an overdense region evolves as

$$\frac{R_0}{R(z)} = \frac{6^{2/3}}{2} \frac{(\theta - \sin \theta)^{2/3}}{(1 - \cos \theta)}. \quad (2.235)$$

At turnaround,  $\theta = \pi$ , so  $[R_0/R(z_{ta})]^3 = (3\pi/4)^2$ ; when an overdense region turns around, the average density within it is about 5.55 times that of the background universe.

At collapse, the average density within the region is even higher: formally,  $R(z_{col}) = 0$ , so the density at collapse is infinite. In practice the region does not collapse to vanishingly small size: it virializes at some non-zero size. The average density within the virialized object is usually estimated as follows. Assume that after turning around the object virializes at half the value of the turnaround radius in physical, rather than comoving units. In the time between turnaround and collapse, the background universe expands by a factor of  $(1 + z_{ta})/(1 + z_{col}) = 2^{2/3}$ , so the virialized object is eight times denser than it was at turnaround (because  $R_{vir} = R_{ta}/2$ ). The background density at turnaround is  $(2^{2/3})^3 = 4$  times the background density at  $z_{vir}$ . Therefore the virialized object is

$$\Delta_{vir} \equiv (9\pi^2/16) \times 8 \times 4 = 18\pi^2 \quad (2.236)$$

times the density of the background at virialization.

What was the initial overdensity of such an object? Eq. (2.233) shows that if the region is to collapse at  $z$ , the average density within it must have had a critical value  $\delta_{sc}$  given by

$$\frac{\delta_{sc}}{1+z} = \frac{3}{5} \left(\frac{3\pi}{2}\right)^{2/3}. \quad (2.237)$$

Thus a collapsed object is one in which the initial overdensity, extrapolated using linear theory to the time of collapse, was  $\delta_{sc}(z)$ . At this time, the actual overdensity is significantly larger than the linear theory prediction. Although the formal overdensity is infinite, the virialisation argument just presented says that the object is about 178 times denser than the background.

There is an important feature of the spherical collapse model which is extremely useful. Since  $(1+\delta) = (R/R_0)^3$ , the equations above provide a relation between the actual overdensity  $\delta$  and that predicted by linear theory  $\delta_0$ , and this relation is the same for all  $R_0$ . That is to say, it is the ratio  $R/R_0$  which is determined by  $\delta_i$ , rather than the value of  $R$  itself. Because the mass of the object is proportional to  $R_0^3$ , this means that the critical density for collapse  $\delta_{sc}$  is the same for all objects, whatever their mass. In addition, the evolution of the average density within a region which is collapsing is also independent of the mass within it.

### The mass-function of the halos: the Press-Schechter formalism

Press and Schechter proposed a formalism to compute the average number of objects that collapsed from the primordial Gaussian density field [130]. They assumed that the dense objects seen at the present time are a direct result of the peaks in the initial density field. These small perturbations collapsed spherically under the action of gravity to form selfbound virialized objects.

In the primordial Gaussian field the probability that a given point lies in a region with the density contrast  $\delta$  greater than the critical density for collapse  $\delta_c$  is given by

$$p(\delta > \delta_c | R_f) = \frac{1}{2} \left[ 1 - \text{erf} \left( \frac{\delta_c}{\sqrt{2}\sigma(R_f)} \right) \right], \quad (2.238)$$

where  $\sigma(R_f)$  is the variance of the density field smoothed on the scale  $R_f$ . The Press-Schechter formalism assumes that this probability corresponds to the probability that a given point has ever been part of a collapsed object of scale  $> R_f$ . Then, the comoving number density of halos of mass  $M$  at redshift  $z$  is given by

$$\frac{dn}{dM}(M, z) = \sqrt{\frac{2}{\pi}} \frac{\bar{\rho}}{M^2} \frac{\delta_c(z)}{\sigma_m} \left| \frac{d \ln \sigma(M)}{d \ln M} \right| \exp \left( -\frac{\delta_c(z)^2}{2\sigma^2(M)} \right), \quad (2.239)$$

where  $\sigma(M)$  is the variance corresponding to a radius  $R_f$  containing a mass  $M$  and  $\delta_c(z) = \delta_c^0/D(z)$  is the critical overdensity linearly extrapolated to the present time. Here  $\delta_c^0 = \delta_c(z=0)$ . For an EdS universe the critical overdensity is  $\delta_c^0 = 1.69$ . There are approximations for other models and in general  $\delta_c^0$  has a weak dependence on  $\Omega_m$  (see e.g. [117]). Let us note, however, that Press and Schechter used an additional

ingredient to derive Eq. (2.239): the fraction of (dark) matter in halos above  $M$  is multiplied by an additional factor of 2 in order to ensure that every particle ends up as part of some halo with  $M > 0$ . This ad-hoc factor of 2 is necessary, since otherwise only positive fluctuations of  $\delta$  would be included.

One of the limitations of the Press-Schechter formalism is that it assumes over-dense perturbations to be perfectly spherically symmetric. In reality the situation is more complex. Bardeen et al. ([14]) extensively studied the statistics of peaks in a random density field. They showed that peaks in the primordial density field have a degree of flattening. This departure from a spherical distribution is amplified under the action of gravity affecting the final collapse of the object.

### Halo density profiles

To describe Halo density profiles, functions of the form

$$\rho(r) = \frac{\rho_s}{(r/r_s)^\alpha (1+r/r_s)^\beta} \quad \text{or} \quad \rho(r) = \frac{\rho_s}{(r/r_s)^\alpha [1+(r/r_s)^\beta]}, \quad (2.240)$$

have been extensively studied as models of elliptical galaxies [23,64]. Setting  $(\alpha, \beta) = (1, 3)$  and  $(1, 2)$  in the expression on the left gives the Hernquist and NFW profiles [116], whereas  $(\alpha, \beta) = (3/2, 3/2)$  in the expression on the right is the M99 profile [115].

The NFW and M99 profiles differ on small scales,  $r \ll r_s$ , and whether one provides a better description of the simulations than the other is still being hotly debated (see e.g. [116]). Both profiles are parametrized by  $r_s$  and  $\rho_s$ , which define a scale radius and the density at that radius, respectively. Although they appear to provide a two-parameter fit, in practice, one finds an object of given mass  $m$  and radius  $r_{vir}$  in the simulations, and then finds that  $r_s$  which provides the best fit to the density run. This is because the edge of the object is its virial radius  $r_{vir}$ , while the combination of  $r_s$  and the mass determines the characteristic density,  $\rho_s$ , following

$$m \equiv \int_0^{r_{vir}} dr \, 4\pi r^2 \, \rho(r). \quad (2.241)$$

For the NFW and M99 profiles,

$$m = 4\pi \rho_s r_s^3 \left[ \ln(1+c) - \frac{c}{1+c} \right] \quad \text{and} \quad m = 4\pi \rho_s r_s^3 \frac{2 \ln(1+c^{3/2})}{3} \quad (2.242)$$

where  $c \equiv r_{vir}/r_s$  is known as the concentration parameter. Note that we have explicitly assumed that the halo profile is truncated at  $r_{vir}$ , even though formally, the NFW and M99 profiles extend to infinity.

There is a very extensive literature not only on the numerical characterization of halos, but also developing theoretical models to explain these measured properties (see e.g. [116,121,128,152]). The cusps-core debate is indeed a rather subtle issue, as, for example, it emerges from recent numerical investigations [118,143] that the mass profile of  $\Lambda$ CDM halos deviates slightly but systematically from the form proposed by Navarro, Frenk and White in Eq. (2.240). This implies that the mass profile of  $\Lambda$ CDM halos are not universal: different halos cannot, in general, be rescaled to look identical.



# Chapter 3

## $1-d$ gravity in infinite point distributions

The development of clustering in initially quasi-uniform *infinite* distributions of point particles evolving purely under their Newtonian self-gravity has been the subject of extensive numerical study in cosmology over the last decades. However analytical understanding, which would be very useful in trying to extend the numerical results and also control their reliability, remains very limited. In attempts to progress in this direction it is natural to look to simplified toy models which may provide insight and qualitative understanding. Such models may also be interesting theoretically in a purely statistical mechanics setting, and specifically in the context of the investigation of out of equilibrium dynamics of systems with long-range interactions introduced in Chapter 1.

An obvious toy model for this full  $3-d$  problem is the analogous problem in  $1-d$ , *i.e.*, the generalization to an infinite space (static or expanding) of the so-called “sheet model”, which is formulated for finite mass distributions. In this latter model, which has been quite extensively investigated (see, e.g., [82, 110, 133, 134, 138, 148]), particles in  $1-d$  experience pair forces independent of their separation, like those between parallel self-gravitating sheets in  $3-d$  of infinite extent. Several groups of authors [7, 8, 10, 111–113, 135, 145, 150, 151, 157] have then discussed different variants on this model to develop the analogy with the  $3-d$  infinite space problem. Just as for the finite sheet model, these models have the particular interest of admitting exact solutions between sheet crossing, which means that they can be easily solved numerically to machine precision, and at modest numerical cost for quite large numbers of particles.

In this chapter we revisit the basics of these toy models (in either static or expanding universes), addressing the problem of their general formulation for infinite distributions. Indeed, as we will discuss, previous discussions have required, in their implementation, the imposition of symmetry about a point, or finite extent of the considered density perturbations<sup>1</sup>. Such a restriction on the class of point processes which can be considered, and notably the requirement that statistical translational invariance be broken, is not desirable. Indeed in the context of the cosmological problem, this latter property of the distributions usually considered

---

<sup>1</sup>This is not true of the treatments in [145, 157], which start directly from the fluid limit (rather than from a particle description). See further discussion below.

as initial conditions for simulations is very important, because of the “cosmological principle” which supposes that there are no preferred centres (see e.g. [71, 126]). Further the question of the extrapolation of the finite version of the model (which is what is simulated numerically) to the infinite system limit has, as we will discuss below, not been carefully examined. We will show that problems with the definition of the force (as used in these previous treatments) arise from a subtlety about how the so-called “Jeans’ swindle” is applied in one dimension. We draw here on the work of Kiessling in [95], where it has been shown that, in  $3 - d$ , the usual formulation of the “Jeans’ swindle” — subtraction of a compensating negative mass background in calculation of the potential — may be more physically formulated as a prescription for the calculation of the *force* in the infinite volume limit. It turns out, as we will see, that while in  $3 - d$  it is sufficient to prescribe that the force on a given particle is obtained by summing symmetrically about it (e.g. summing in spheres of radius  $R$  with centre at the particle, and then sending  $R$  to infinity), in  $1 - d$  this limiting procedure needs to be further specified. More specifically the force turns out to be defined in  $1 - d$  for a broader class of distributions — and notably for distributions without a centre — when the summation is performed by taking the unscreened limit of the same sum for a screened version of the interaction, rather than as the limit of the sum truncated to a finite symmetric “top-hat” interval.

## 1 From finite to infinite systems

### 1.1 Definitions

By gravity in one dimension we mean the pair interaction corresponding to an attractive force independent of separation, *i.e.*, the force  $f(x)$  on a particle at coordinate position  $x$  exerted by a particle at the origin is given by

$$f(x) = -g \frac{x}{|x|} = -g \operatorname{sgn}(x) , \quad (3.1)$$

where  $g$  is the coupling. Equivalently it is the pair interaction given by the pair potential  $\phi(x) = g|x|$  which satisfies the  $1 - d$  Poisson equation for a point source,  $\frac{d^2\phi}{dx^2} = 2g\delta_D(x)$  (where  $\delta_D$  is the Dirac delta function). Comparing with the  $3 - d$  Poisson equation shows the equivalence with the case of an infinitely thin plane of infinite extent and surface mass density  $\Sigma = g/2\pi G$ , which explains the widely used name “sheet model”. We will work in the one dimensional language, referring to “particles”. For convenience we will set the mass of these particles, which will always be equal here, to unity.

### 1.2 Finite system

Let us consider first the case of a finite system, consisting of a finite number  $N$  of particles (with either open boundary conditions, or contained in a finite box). Denoting by  $x_i$  the coordinate position of the  $i^{th}$  particle along the real axis, the force field  $F(x)$  (*i.e.* the force on a test particle) at the point  $x$  is

$$F(x) = g \sum_i \operatorname{sgn}(x_i - x) = g \int dy n(y) \operatorname{sgn}(y - x) , \quad (3.2)$$

where  $n(y) = \sum_i \delta_D(y - x_i)$  is the microscopic number density and the integral is over the real line<sup>2</sup>. Equivalently it may be written as

$$F(x) = g \left[ N_>(x) - N_<(x) \right]. \quad (3.3)$$

where  $N_>(x)$  ( $N_<(x)$ ) is the number of particles to the right (left) of  $x$ . The dynamics of this model, from various initial conditions and over different times scales, has been extensively explored in the literature (see references given above).

### 1.3 Infinite system limit

Let us consider now the infinite system limit, *i.e.*, an infinite uniform distribution of points<sup>3</sup> on the real line with some mean density  $n_0$  (e.g. a Poisson process). It is evident that the forces acting on particles are not well defined in this limit, as the difference between the number of particles on the right and left of a given particle depends on how the limit is taken. Formally we can write the force field of Eq. (3.2) as

$$F(x) = gn_0 \int dy \operatorname{sgn}(y - x) + g \int dy \delta n(y) \operatorname{sgn}(y - x), \quad (3.4)$$

where  $\delta n(y) = n(y) - n_0 = \sum_i \delta_D(y - x_i) - n_0$  represents the number density fluctuation. While the second term would, naively, be expected to converge if the fluctuations  $\delta n(y)$  can decay sufficiently rapidly, the first term, due to the mean density, is explicitly badly defined (as the integral is only semi-convergent). Precisely the same problem arises for gravity in infinite  $3 - d$  distributions. The solution, known as the “Jeans swindle”, is the subtraction of the contribution due to the mean density. As discussed by Kiessling in [95], rather than a “swindle”, this is, in  $3 - d$ , in fact a mathematically well-defined regularisation of the physical problem, corresponding simply to the prescription that the force be summed so that it vanishes in the limit of exact uniformity. The simplest form of such a prescription in  $3 - d$  is that the force on a particle be calculated by summing symmetrically about the particle (e.g. by summing about the considered point in spheres of radius  $R$ , and then sending  $R \rightarrow \infty$ ). This formulation needs no explicit use of a “background subtraction”, since the term due to the mean density does not contribute when the sum is performed symmetrically.

Applying the same reasoning to the  $1 - d$  case would lead to the prescription

$$F(x) = g \int dy \delta n(y) \operatorname{sgn}(y - x). \quad (3.5)$$

The question is whether this expression for the gravitational force is now well defined, and if it is, in what class of infinite point distributions. As we will detail in the next section of the chapter, this question may be given a precise answer, as in  $3 - d$ , by considering the probability density function of the force in such distributions, described as stochastic point processes in infinite space. In the rest of this section

<sup>2</sup>We use the standard convention that  $\operatorname{sgn}(0) = 0$ , which implies this same formula is valid for the force on a particle of the distribution (rather than a test particle) at  $x$ .

<sup>3</sup>By “uniform” we mean that the point process has a well defined *positive* mean density, *i.e.*, it becomes homogeneous at sufficiently large scales.

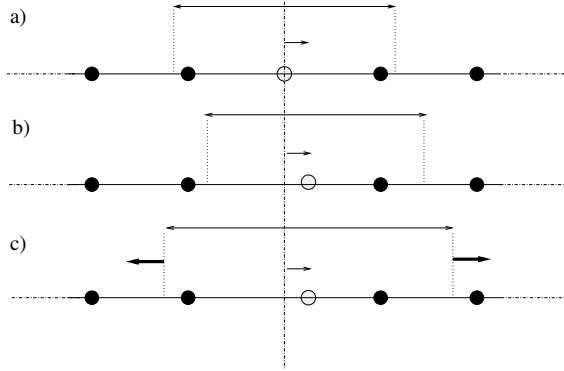


Figure 3.1: Calculation of the force using a top-hat regularisation centred on the point considered, *i.e.*, as defined in Eq. (3.7). In an unperturbed lattice (case a) the force on points of the lattice vanishes. However, as shown in b) and c), when a single point is displaced off lattice, the force becomes badly defined, oscillating between  $g$  and zero as the size of top-hat goes to infinity.

we will simply explain the problems which arise when the infinite system limit of expression Eq. (3.5) is taken using a simple top-hat prescription. This discussion motivates the use of a smooth version of this prescription, which we then show rigorously in the subsequent section to give a well defined force for a broad class of infinite perturbed lattices.

For Eq. (3.5) to be well defined in an infinite point distribution it must give the same answer no matter how it is calculated. Two evident top-hat prescriptions for its calculation are the following. On the one hand it may be written as

$$F(x) = g \lim_{L \rightarrow \infty} \int_{x-L}^{x+L} dy n(y) \operatorname{sgn}(y - x) , \quad (3.6)$$

or, equivalently,

$$F(x) = g \lim_{L \rightarrow \infty} [N(x, x+L) - N(x-L, x)] , \quad (3.7)$$

where  $N(x, y)$  is the number of points between  $x$  and  $y$ , *i.e.*, the force is proportional to the difference in the number of points on the right and left of  $x$  inside a *symmetric interval centred on  $x$* , when the size of the interval is taken to infinity. On the other hand, we can write

$$F(x) = g \lim_{L \rightarrow \infty} \int_{-L}^{+L} dy \delta n(y) \operatorname{sgn}(y - x) , \quad (3.8)$$

or, equivalently,

$$F(x) = g \lim_{L \rightarrow \infty} [N(x, L) - N(-L, x)] + 2gn_0x , \quad (3.9)$$

*i.e.*, we integrate the mass density fluctuations in a top-hat centred *on some arbitrarily chosen origin*.

That these expressions are both badly defined in an infinite Poisson distribution is easy to see: in this case the fluctuation in mass on the right of any point is

uncorrelated with that on the left, giving a typical force proportional to the square root of the mass in a randomly placed window of size  $L$ , which grows in proportion to  $\sqrt{L}$  (and thus diverges). Calculating the force with Eq. (3.7) it has been shown in [65] that it is in fact not well defined either in a class of more uniform distributions of points, randomly perturbed lattices<sup>4</sup>. Why this is so can be understood easily by considering, as illustrated in Fig. 3.1, the calculation of the force using Eq. (3.7) in such configurations. While on the unperturbed lattice (case a) the force on all points of the lattice is well-defined (and vanishing, as it should be), this is no longer true when a particle is displaced: the force on the displaced particle now oscillates deterministically (between  $g$  in case b, and zero in case c) and does not converge as  $L \rightarrow \infty$ .

For the same case, of a single particle displaced off an infinite perfect lattice, the prescription Eq. (3.9) for the force does, however, give a well-defined result if one chooses as origin a point of the *unperturbed* lattice: since the first (“particle”) term is unchanged by the displacement of the particle, the only non-vanishing contribution comes from the second (“background”) term, giving a finite force

$$F(u) = 2gn_0u , \quad (3.10)$$

where  $u$  is the displacement of the particle from its lattice site (and we assume  $u$  is smaller than the lattice spacing). If we consider now, however, applying random displacements of small amplitude (compared to the interparticle spacing) to the other particles of the lattice, the problem of the first prescription Eq. (3.7) reappears: at any given  $L$  the first term in Eq. (3.9) picks up a stochastic fluctuation which varies discretely between  $\pm g$  and zero, and does not converge as  $L \rightarrow \infty$ . This will evidently be the case for any such configuration generated by displacing particles off a lattice, and more generally for any stochastic particle distribution in  $1 - d$ , unless some additional constraint is applied to make this surface contribution to the force vanish.

The previous literature on this model employ top-hat prescriptions equivalent to Eq. (3.9) to calculate the force, adding such a constraint. On the one hand, Aurell et al. in [10] restrict themselves to the study of an infinite perfect lattice off which only a *finite* number are initially displaced. In this case the problematic surface fluctuation vanishes for sufficiently large  $L$ . On the other hand [7, 112, 135, 150] impose exact symmetry in the displacements about some chosen point, which is then taken as the origin of the symmetric summation interval. A particle entering (or leaving) at one extremity of the interval is then always compensated by one doing the same at the other extremity.

We note that it is only in [10] that the problem of the infinite system limit is actually considered. In the other works the authors do not discuss this limit explicitly: they consider and study in practice a finite system, with a prescription for the force equivalent to Eq. (3.9) where  $2L$  is the system size, *i.e.*, without the explicit limit  $L \rightarrow \infty$ . Symmetry about the origin is imposed because this allows one to use periodic boundary conditions. Such a *finite* periodic system of period  $2L$  is equivalent to a finite system of size  $L$  with reflecting boundary conditions.

---

<sup>4</sup>The force is, however, shown to be well defined in this class of point distributions using the analogous definition for any power law interaction in which the pair force decays with separation. See [65] for details.

The dynamics of such a system is of course always well defined, for any (finite) initial distribution of the points in the box. This does not, however, mean that this dynamics can be defined in the limit that the size of the system is taken to infinity. This is the question we focus on here, as the definition of such a limit is essential if a proper analogy is to be made with the cosmological problem in  $3 - d$ : in this case the gravitational force is well defined in the infinite system limit, for a class of statistically translationally invariant distributions representing the initial conditions of cosmological models<sup>5</sup>.

The problems with the top-hat prescriptions arise, as we have seen, from non-convergent fluctuations at the surface of a top-hat window, which will be generic in statistically translationally invariant point processes. It is thus natural to consider smoothing the summation window, and specifically a prescription for Eq. (3.5) such as:

$$F(x) = g \lim_{\mu \rightarrow 0} \int dy n(y) \operatorname{sgn}(y - x) e^{-\mu|x-y|}, \quad (3.11)$$

or, equivalently,

$$F(x) = g \lim_{\mu \rightarrow 0} \sum_i \operatorname{sgn}(x_i - x) e^{-\mu|x_i-x|}, \quad (3.12)$$

where the sum runs over all particles in the (infinite) distribution. Rather than a smoothing of the summation window, this can be interpreted more physically in terms of the screening of the gravitational interaction, *i.e.*, the pair force law of Eq. (3.1) is replaced by

$$f_\mu(x) = -g \operatorname{sgn}(x) e^{-\mu|x|}, \quad (3.13)$$

and the gravitational force in the infinite system limit is defined as that obtained when the screening length is taken to infinity, *after* the infinite system is taken<sup>6</sup>. This treatment is borrowed from the class of infrared problems well known in quantum field theory. The standard procedure of handling infrared divergences is to apply an infrared regularization, to solve the regularized problem, and to remove the regularization at the end of the calculation, perhaps involving a renormalization.

For the case of a single particle displaced off a perfect lattice discussed above it is simple to calculate the force using Eq. (3.11). Denoting the lattice spacing by  $\ell$ , and the displacement by  $u$ , we have

$$F(u) = g \lim_{\mu \rightarrow 0} \sum_{n \neq 0} \operatorname{sgn}(n\ell - u) e^{-\mu|n\ell-u|}. \quad (3.14)$$

For  $|u| \leq \ell$  the sum gives

$$2 \sinh(\mu u) \left( \sum_{n>0} e^{-\mu n\ell} \right). \quad (3.15)$$

---

<sup>5</sup>Numerically one treats, of course, a periodic system, but it is an *infinite* periodic system, *i.e.*, the force is calculated by summing over the particles in the finite box and all its (infinite) copies. This is the so-called “replica method”, used also widely in equilibrium systems such as the one component plasma [19]. The infinite sum is usually calculated using the Ewald sum method. To obtain results independent of the chosen periodic box, the prescription for the force must converge in the appropriate class of infinite point distributions.

<sup>6</sup>Although we will not use the interparticle potential in our calculations, we note that  $f_\mu(x) = -d\phi_\mu/dx$  where  $\phi_\mu(x) = -ge^{-\mu|x|}/\mu$  is the solution of  $\frac{d^2\phi_\mu}{dx^2} - \mu^2\phi_\mu = 2g\delta_D(x)$ .

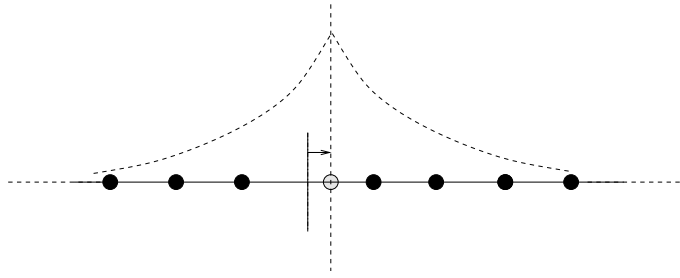


Figure 3.2: Schematic representation of the smooth screening of the force (or, equivalently, summation window).

Expanding this in powers of  $\mu$  we obtain

$$F_\mu(u) = \frac{2gu}{\ell} + O(\mu). \quad (3.16)$$

Taking the limit  $\mu \rightarrow 0$  gives Eq. (3.10), *i.e.*, the result obtained using the top-hat prescription Eq. (3.9). The equivalence of the two prescriptions can likewise be shown to apply when displacements are applied to a *finite* number of particles on the lattice (which leave the forces unchanged, and equal to Eq. (3.10), if there are no crossings). Thus the only difference between the prescriptions is how they treat the contribution from particles at arbitrarily large distances when the infinite system limit is taken.

We will show rigorously in the next section that, for a class of infinite perturbed lattices in which particles do not cross, the prescription Eq. (3.11) simply removes the problematic surface contribution present in the top-hat prescriptions (without applying any additional constraint of symmetry). This gives a force on each particle equal to Eq. (3.10) where  $u$  is the displacement of the particle, the only difference with respect to the case of a finite number of displaced particles being that the origin of this displacement may be redefined by a net translation of the whole system induced by the infinite displacements. The force felt by each particle is thus equivalent to that exerted by an inverted harmonic oscillator about an (unstable) equilibrium point. We note that this expression for the force is in fact what one would expect from a naive generalization of the analogous results in  $3 - d$ . In the latter case it can be shown [66] that the force on a single particle displaced off an infinite lattice by a vector  $\mathbf{u}$  is, to linear order in  $|\mathbf{u}|$ , simply

$$\mathbf{F}(\mathbf{u}) = 4\pi G\rho_0 \mathbf{u}/3. \quad (3.17)$$

This force is simply that which is inferred, by Gauss's law, as due to a uniform background of mass density  $-\rho_0$  (*i.e.* due to the mass of such a background contained in a sphere of radius  $|\mathbf{u}|$ ). The  $1 - d$  result is exactly analogous, as  $2n_0|u|$  is simply the mass inside the interval of "radius"  $|u|$ . While this result is valid, in  $3 - d$ , only at linear order and for the case of a single displaced particles, it is exactly valid in  $1 - d$  in absence of particle crossings and for a broad class of displacement statistics. The reason is simply that in  $1 - d$  the force on a particle is unaffected by displacements of other particles, unless the latter cross the considered particle.

## 2 Forces in infinite perturbed lattices

In this section we calculate, using the definition Eq. (3.12), the gravitational force on particles in a class of infinite perturbed lattices. To do this we describe these point distributions as generated by a stochastic process in which the particles are displaced<sup>7</sup>. The force on a particle (or the force field at a point in space) is then itself a stochastic variable, taking a different value in each realization of the point process, and the question of its definedness can be cast in terms of the existence of the probability distribution function (PDF) of the force. We thus calculate here the PDF of the force on a particle with a given displacement  $u$ , in the ensemble of realizations of the displacements of the other particles. The result is that, for the class of stochastic displacement fields in which displacements are such that particles do not cross, this force PDF becomes simply a Dirac delta function. This gives the anticipated result, that the only force which results is that due to the particle's own displacement given by Eq. (3.10), modulo an additional term describing a contribution from the coherent displacement of the whole infinite lattice if the average displacement is non-zero.

### 2.1 Stochastic perturbed lattices

Let us consider first an infinite  $1 - d$  regular chain of unitary mass particles with lattice spacing  $\ell > 0$ , *i.e.*, the position of the  $n^{\text{th}}$  particle is  $X_n = n\ell$ , and the microscopic number density can be written as

$$n_{in}(x) = \sum_{n=-\infty}^{+\infty} \delta_D(x - n\ell). \quad (3.18)$$

We now apply a stochastic displacement field  $\{U_n\}$  to this system, in which the displacement  $U_n$  is applied to the generic  $n^{\text{th}}$  particle with  $n \in \mathbb{Z}$ . Let us call  $\{u_n\}$  the single realization of the stochastic field  $\{U_n\}$ . The corresponding realization of the point process thus has microscopic number density

$$n(x) = \sum_{n=-\infty}^{+\infty} \delta_D(x - n\ell - u_n). \quad (3.19)$$

This displacement field is completely characterized by the joint displacement PDF  $\mathcal{P}(\{u_n\})$  where  $\{u_n\}$  is the set of all particle displacements with  $n \in \mathbb{Z}$ . We will further assume that this stochastic process is statistically translationally invariant, *i.e.*  $\mathcal{P}(\{u_n\}) = \mathcal{P}(\{u_{n+l}\})$  for any integer  $l$ . This implies in particular that the one displacement PDF (for the displacement applied to a single particle) is independent of the position of that particle, *i.e.*, the function

$$p_m(u) \equiv \int \prod_n du_n \mathcal{P}(\{u_n\}) \delta_D(u - u_m) \quad (3.20)$$

---

<sup>7</sup>For an introduction to the formalism of stochastic point processes *i.e.* stochastic spatial distributions of point-particles with identical mass, see, e.g., [71].

is independent of  $m$ , *i.e.*  $p_m(u) = p(u)$ . Moreover the joint two-displacement PDF

$$q_{nm}(u, v) = \int \prod_n du_n \mathcal{P}(\{u_n\}) \delta_D(u - u_m) \delta_D(v - u_n)$$

depends parametrically on the lattice positions  $n, m$  only through their relative distance  $(m - n)$ .

## 2.2 Mean value and variance of the total force

Let us denote in general by  $F_\mu(x_0)$  the total gravitational force, with finite screening  $\mu$ , acting on the particle at  $x_0$  and due to all the other particles placed at  $x_n$ :

$$F_\mu(x_0) = g \sum_{n \neq 0} \operatorname{sgn}(x_n - x_0) e^{-\mu|x_n - x_0|}. \quad (3.21)$$

Writing now  $x_n = n\ell + u_n$  in Eq. (3.21), we can write the total screened force on the particle at  $x_0 = u_0$  in a perturbed lattice for a given realization of the displacement field:

$$F_\mu(u_0) = g \sum_{n \neq 0} \operatorname{sgn}(n\ell + u_n - u_0) e^{-\mu|n\ell + u_n - u_0|}. \quad (3.22)$$

Note that, given the assumed statistical translational invariance of the field  $\{U_n\}$  the statistical properties of the force are the same for all particles in the system. If, further, we assume now that the displacements from the lattice are such that *particles do not cross*, *i.e.*  $\operatorname{sgn}(n\ell + u_n - u_0) = \operatorname{sgn}(n)$  for  $n \neq 0$ , this can be written as

$$F_\mu(u_0) = g \sum_{n=1}^{\infty} e^{-\mu n \ell} f_n, \quad (3.23)$$

where we define for,  $n \geq 1$ ,

$$f_n \equiv f_n(\mu) = e^{-\mu(u_n - u_0)} - e^{-\mu(u_0 - u_{-n})}.$$

We now take the average of Eq. (3.23) over all realizations of the displacements of all particles, except the chosen one  $u_0$ , which we consider as fixed. We denote this conditional average as  $\langle \cdot \rangle_0$ , while we use  $\langle \cdot \rangle$  for the unconditional average. In order to do this we need the conditional PDF of  $U_n$  to  $U_0$ , which by definition of conditional probability is

$$P_n(u; u_0) = \frac{q_{n0}(u, u_0)}{p(u_0)}. \quad (3.24)$$

By using this function we can write

$$\langle f_n(\mu) \rangle_0 = e^{\mu u_0} \tilde{P}_n(\mu; u_0) - e^{-\mu u_0} \tilde{P}_{-n}(-\mu; u_0) \quad (3.25)$$

and therefore

$$\langle F_\mu(u_0) \rangle_0 = g \sum_{n=1}^{\infty} \left[ e^{\mu u_0} \tilde{P}_n(\mu; u_0) - e^{-\mu u_0} \tilde{P}_{-n}(-\mu; u_0) \right] e^{-\mu n \ell} \quad (3.26)$$

where we have defined

$$\begin{aligned}\tilde{P}_n(\mu; u_0) &= \int_{-\infty}^{\infty} du P_n(u; u_0) e^{-\mu u}, \\ &= \sum_{k=0}^{\infty} \frac{(-\mu)^k \langle U_n^k \rangle_0}{k!}.\end{aligned}\quad (3.27)$$

The latter equality is valid when all the moments  $\langle U_n^k \rangle_0$  of  $P_n(u; u_0)$  are finite. Note that, given the assumption that particles do not cross, it follows from the definition (3.24) that  $q_{n0}(u, u_0) = 0$  for  $u + n \leq u_0$  respectively for  $n \geq 0$ . Therefore  $P_n(u; u_0)$  is always zero for some sufficiently negative  $u_0$  dependent value of  $u$  if  $n > 0$ , and likewise for sufficiently positive values if  $n < 0$ . This ensures that the integral in Eq. (3.27) is indeed finite.

In order to study the behavior of Eq. (3.26) for  $\mu \rightarrow 0$ , we will assume that

$$q_{nm}(u, v) \xrightarrow{|n-m| \rightarrow \infty} p(u)p(v). \quad (3.28)$$

This corresponds to the assumption that the displacement field is a well defined stochastic field, which requires (see e.g. [71]) that the two-displacement correlations vanish as the spatial separation diverges. We will discuss in the next section the restriction this corresponds to on the large scale behaviour of the density perturbations, which is of particular relevance when one considers the analogy to 3 – d cosmological simulations.

Assuming Eq. (3.28) we can write

$$P_n(u; u_0) = p(u) + r_n(u; u_0),$$

where  $r_n(u; u_0)$  is a function vanishing for  $|n| \rightarrow \infty$  and with zero integral over  $u$  for any  $n$ . As a consequence

$$\tilde{P}_n(\mu; u_0) = \tilde{p}(\mu) + \tilde{r}_n(\mu; u_0), \quad (3.29)$$

where we used the definition analogous to Eq. (3.27) for  $\tilde{p}(\mu)$  and  $\tilde{r}_n(\mu; u_0)$ , and the latter vanishes for  $\mu \rightarrow 0$  and/or  $n \rightarrow \infty$ . If we now suppose that both  $\langle U \rangle$  and  $\langle U_n \rangle_0$  are finite, with evidently  $\langle U_n \rangle_0 \rightarrow \langle U \rangle$  for  $n \rightarrow \infty$ , we can write at lower order:

$$\begin{aligned}\tilde{p}(\mu) &= 1 - \mu \langle U \rangle + o(\mu), \\ \tilde{r}_n(\mu; u_0) &= \mu(\langle U \rangle - \langle U_n \rangle_0) + o(\mu).\end{aligned}\quad (3.30)$$

It is now simple, by substituting Eqs. (3.29) and (3.30) into Eq. (3.26), to show that, if  $(\langle U \rangle - \langle U_n \rangle_0)$  decays in  $n$  as a negative power law or faster, we have

$$\langle F(u_0) \rangle_0 \equiv \lim_{\mu \rightarrow 0} \langle F_\mu(u_0) \rangle_0 = 2gn_0(u_0 - \langle U \rangle). \quad (3.31)$$

We will now show that both for uncorrelated displacements, and then more generally for correlated displacements with decaying correlations, this average force is in fact the exact force in every realization. We do so by simply showing that

$$\lim_{\mu \rightarrow 0} \left[ \langle F_\mu^2(u_0) \rangle_0 - \langle F_\mu(u_0) \rangle_0^2 \right] = 0. \quad (3.32)$$

This implies that the variance of the conditional PDF of the total force  $F$  acting on the particle in  $u_0$  vanishes, *i.e.*, it is a Dirac delta function at the average value given by Eq. (3.31). Compared to the simple case of a single displaced particle we analysed above, the only effect of the (infinite number of) other displacements is to possibly shift the centre of mass of the whole (infinite) distribution with respect to which the displacement of the single particle is defined.

In order to show Eq. (3.32) we note first that the second conditional moment of  $F$  may be written

$$\begin{aligned} \langle F_\mu^2(u_0) \rangle_0 &= g^2 \sum_{n,m}^{1,\infty} e^{-\mu(n+m)\ell} \langle f_n f_m \rangle_0 \\ &= \langle F_\mu(u_0) \rangle_0^2 + g^2 \sum_{n=1}^{\infty} e^{-2\mu n \ell} A_n(\mu) \\ &\quad + g^2 \sum_{n,m}^{1,\infty}' e^{-\mu(n+m)\ell} B_{nm}(\mu), \end{aligned} \quad (3.33)$$

with

$$\begin{aligned} A_n(\mu) &= \langle f_n^2 \rangle_0 - \langle f_n \rangle_0^2, \\ B_{nm}(\mu) &= \langle f_n f_m \rangle_0 - \langle f_n \rangle_0 \langle f_m \rangle_0 \quad (m \neq n), \end{aligned} \quad (3.34)$$

and where  $\sum'_{n,m}$  as usual indicates the sum over  $m$  and  $n$  with the exception of the  $n = m$  terms. To prove Eq. (3.32) it is sufficient to show that the last two terms in Eq. (3.33) go continuously to zero as  $\mu$  does so.

### 2.3 Lattice with uncorrelated displacements

We consider first the case that the displacements are uncorrelated and identically distributed, *i.e.*,

$$\mathcal{P}(\{u_n\}) = \prod_{n=-\infty}^{+\infty} p(u_n). \quad (3.35)$$

We refer to this as a “shuffled lattice” configuration (following [71]). In this case conditional and unconditional averages coincide. Given the assumption that the displacements do not make particles cross, we must have that  $p(u) = 0$  for  $|u| > \ell/2$ , implying that all the moments of  $p(u)$  are necessarily finite.

In this case the  $u_n$  are statistically independent and identically distributed random variables. Given the definition Eq. (3.24), it follows that the  $f_n$  also have this property, *i.e.*,

$$\langle f_n f_m \rangle = \langle f_n \rangle \langle f_m \rangle, \quad (3.36)$$

and thus that  $B_{nm}(\mu) = 0$ . Further  $A_n(\mu)$  is independent of  $n$  and can be expressed explicitly as

$$A_n(\mu) = e^{2\mu u_0} [\tilde{p}(2\mu) - \tilde{p}^2(\mu)] - e^{-2\mu u_0} [\tilde{p}(-2\mu) - \tilde{p}^2(-\mu)]. \quad (3.37)$$

Expanding this expression in  $\mu$  about  $\mu = 0$ , we find that the leading non-vanishing term is at order  $\mu^2$ . The desired result, Eq. (3.32), follows as

$$\sum_{n=1}^{\infty} e^{-2\mu nl} = \frac{e^{-2\mu l}}{1 - e^{-2\mu l}} = O(\mu^{-1}) \quad \text{for } \mu \rightarrow 0,$$

where  $O(\mu^l)$  means as usual a term of order  $l$  in  $\mu$ .

## 2.4 Lattice with correlated displacements

We now consider the case where the displacements are non-trivially correlated. In order to calculate  $A_n(\mu)$  and  $B_{nm}(\mu)$  we need both the conditional single displacement PDF  $P_n(u; u_0)$  and the conditional two-displacement PDF  $Q_{nm}(u, v; u_0)$ , both conditioned to the fixed value  $u_0$  of the stochastic displacement  $U_0$ . The function  $Q_{nm}(u, v; u_0)$  is defined by the rules of conditional probability as

$$Q_{nm}(u, v; u_0) = \frac{s_{nml}(u, v, u_0)}{p(u_0)},$$

where  $s_{nml}(u, v, w)$  is the joint three displacement PDF of having the three displacements  $u, v, w$  respectively at the lattice sites  $n, m, l$ .

Let us start from the evaluation of  $A_n(\mu)$ . From its definition it is simple to show that

$$\begin{aligned} \langle f_n^2(\mu) \rangle_0 = & e^{2\mu u_0} \tilde{P}_n(2\mu; u_0) + e^{-2\mu u_0} \tilde{P}_{-n}(-2\mu; u_0) \\ & - 2\tilde{Q}_{n-n}(\mu, -\mu; u_0), \end{aligned} \quad (3.38)$$

where

$$\tilde{Q}_{nm}(\mu, \nu; u_0) = \int \int_{-\infty}^{+\infty} du dv Q_{nm}(u, v; u_0) e^{-(\mu u + \nu v)}.$$

In order to study the limit  $\mu \rightarrow 0$  we have to expand  $\tilde{P}_n(\mu; u_0)$  and  $\tilde{Q}_{nm}(\mu, \pm\mu; u_0)$  in powers of  $\mu$ . Assuming that at least the first two moments of the displacement statistics are finite, we can write

$$\begin{aligned} \tilde{P}_n(\mu; u_0) &= 1 - \mu \langle U_n \rangle_0 + \frac{\mu^2}{2} \langle U_n^2 \rangle_0 + o(\mu^2), \\ \tilde{Q}_{nm}(\mu, \pm\mu; u_0) &= 1 - \mu (\langle U_n \rangle_0 \pm \langle U_m \rangle_0) + \frac{\mu^2}{2} (\langle U_n^2 \rangle_0 \\ &\quad + \langle U_m^2 \rangle_0 \pm \langle U_n U_m \rangle_0) + o(\mu^2). \end{aligned} \quad (3.39)$$

Using this result and Eqs. (3.25) and (3.38) in the definition (3.34) of  $A_n(\mu)$ , it is simple to show that

$$\begin{aligned} A_n(\mu) = & \mu^2 [e^{2\mu u_0} (\langle U_n^2 \rangle_0 - \langle U_n \rangle_0^2) \\ & + e^{-2\mu u_0} (\langle U_{-n}^2 \rangle_0 - \langle U_{-n} \rangle_0^2) \\ & + 2 (\langle U_n U_{-n} \rangle_0 - \langle U_n \rangle_0 \langle U_{-n} \rangle_0)] + o(\mu^2). \end{aligned} \quad (3.40)$$

Note that for  $|n| \rightarrow \infty$  we have  $\langle U_n \rangle_0 \rightarrow \langle U \rangle$ ,  $\langle U_n^2 \rangle_0 \rightarrow \langle U^2 \rangle$  and  $\langle U_n U_{-n} \rangle_0 \rightarrow \langle U \rangle^2$ . Therefore we can write

$$A_n(\mu) \xrightarrow{n \rightarrow \infty} \mu^2 (\langle U^2 \rangle - \langle U \rangle^2) (e^{2\mu u_0} + e^{-2\mu u_0}),$$

where we have used the fact that, as the coefficients of the higher order contributions in  $\mu$  to  $A_n(\mu)$  are non-diverging, they can be neglected. This is sufficient to conclude that

$$\sum_{n=1}^{\infty} e^{-\mu n} A_n(\mu) = O(\mu), \quad (3.41)$$

where  $O(\mu^l)$  as usual means a term of order  $\mu^l$ , and therefore the sum vanishes as  $\mu$  for  $\mu \rightarrow 0$ .

Let us now move to analyze the last sum in Eq. (3.33). We study the behavior of  $B_{nm}(\mu)$  as defined by Eq. (3.34). It is simple to show that

$$\begin{aligned} \langle f_n f_m \rangle_0 &= e^{-2\mu u_0} \tilde{Q}_{nm}(\mu, \mu; u_0) + e^{2\mu u_0} \tilde{Q}_{-n-m}(-\mu, -\mu; u_0) \\ &\quad - \tilde{Q}_{n-m}(\mu, -\mu; u_0) - \tilde{Q}_{-nm}(-\mu, \mu; u_0). \end{aligned} \quad (3.42)$$

Using this equation together with Eqs. (3.34), (3.25) and (3.39), we can write

$$\begin{aligned} B_{nm}(\mu) &= \mu^2 [e^{-2\mu u_0} g(n, m; u_0) + e^{2\mu u_0} g(-n, -m; u_0) \\ &\quad - g(n, -m; u_0) - g(-n, m; u_0)] + o(\mu^2), \end{aligned} \quad (3.43)$$

where we have called

$$g(n, m; u_0) = \langle U_n U_m \rangle_0 - \langle U_n \rangle_0 \langle U_m \rangle_0,$$

i.e., the conditional displacement covariance matrix. Since this is a “conditional” correlation it does not depend simply on  $n - m$ , but on both  $n$  and  $m$  in a non-trivial way. However for both  $|n|, |m| \rightarrow \infty$  the conditional averages coincide with the unconditional ones and therefore we can write

$$g(n, m; u_0) = c(|n - m|)[1 + h(n, m; u_0)], \quad (3.44)$$

where  $c(|n - m|) = \langle U_n U_m \rangle - \langle U \rangle^2$  is the unconditional displacement covariance matrix, and  $h(n, m; u_0) \rightarrow 0$  for  $|n|, |m| \rightarrow \infty$ . In order to analyze the asymptotic behavior for small  $\mu$  of

$$I(\mu) \equiv \sum_{n,m}^{1,\infty} e^{-\mu(n+m)} B_{nm}(\mu), \quad (3.45)$$

it is sufficient to study the behavior of the sum coming from the first term (or equivalently the second) of  $B_{nm}(\mu)$  in Eq. (3.43) as it is the most slowly convergent one, i.e., basically to study the following sum:

$$J(\mu) = \sum_{n,m}^{1,\infty} e^{-\mu(n+m)} g(n, m; u_0).$$

Since  $h(n, m; u_0) \rightarrow 0$  for  $|n|, |m| \rightarrow \infty$ , the small  $\mu$  scaling behavior of  $J(\mu)$  is the same if we replace  $g(n, m; u_0)$  by  $c(|n - m|)$ :

$$J(\mu) \simeq \sum_{n,m}^{1,\infty} e^{-\mu(n+m)} c(|n - m|). \quad (3.46)$$

This can be also shown by the following argument: assuming that  $h(n, m; u_0)$  is bounded, say  $|h(n, m; u_0)| \leq A$ , we can write

$$\begin{aligned} |J(\mu)| &\leq \sum_{n,m}^{1,\infty} e^{-\mu(n+m)} |g(n, m; u_0)| \\ &\leq (1 + A) \sum_{n,m}^{1,\infty} e^{-\mu(n+m)} |c(|n - m|)|. \end{aligned}$$

Therefore the convergence to zero of  $\mu^2$  times the right-hand side of Eq. (3.46) is a sufficient condition to have the variance of  $F$  to vanish for  $\mu \rightarrow 0$ .

Let us now analyze the right-hand side of Eq. (3.46). We can write

$$\begin{aligned} &\sum_{n,m}^{1,\infty} e^{-\mu(n+m)} c(|n - m|) \\ &= \sum_{n,m}^{1,\infty} e^{-\mu(n+m)} c(|n - m|) - c(0) \frac{1}{e^{2\mu} - 1}, \end{aligned} \quad (3.47)$$

where  $c(0)$  is the single displacement variance. Note that the second term is of order  $\mu^{-1}$  at small  $\mu$  and therefore gives rise to a term at linear order in  $\mu$  in Eq. (3.45). Let us introduce the Fourier transform  $\tilde{c}(k)$  of  $c(n)$ , defined by

$$c(n) = \int_{-\pi}^{\pi} \frac{dk}{2\pi} \tilde{c}(k) e^{ikn}.$$

Using this in the right-hand side of Eq. (3.47) we get

$$\begin{aligned} &\sum_{n,m}^{1,\infty} e^{-\mu(n+m)} c(|n - m|) \\ &= \int_{-\pi}^{\pi} \frac{dk}{2\pi} \tilde{c}(k) \frac{1}{e^{2\mu} + 1 - 2e^{\mu} \cos k}. \end{aligned} \quad (3.48)$$

The small  $\mu$  limit of this integral is dominated by the behavior at small  $k$  of the integrand. In this limit the following approximation holds  $(e^{2\mu} + 1 - 2e^{\mu} \cos k) \simeq (\mu^2 + k^2)$ . Let us also assume that  $c(n) \sim n^{-\alpha}$  at large  $n$  (with in general  $\alpha > 0$ )<sup>8</sup> which implies at small  $|k|$   $\tilde{c}(k) \sim |k|^{\alpha-1}$  for  $0 < \alpha \leq 1$  (with logarithmic corrections for  $\alpha = 1$ ) and  $\tilde{c}(k) \sim |k|^{\beta}$  with  $\beta \geq 0$  for  $\alpha > 1$ . Therefore the small  $\mu$  behavior of Eq. (3.48) is the same as that of the simple integral

$$\int_{-\pi}^{\pi} \frac{dk}{2\pi} \frac{\tilde{c}(k)}{\mu^2 + k^2} \sim \begin{cases} \mu^{\alpha-2} & \text{for } 0 < \alpha \leq 1, \\ \mu^{\beta-1} & \text{for } \alpha > 1. \end{cases} \quad (3.49)$$

<sup>8</sup>The case of a decay faster than any power, e.g. exponential decay, can be included for  $\alpha \rightarrow \infty$ .

Taking also into account the second term in Eq. (3.47), we can therefore conclude that

$$\sum_{n,m}^{1,\infty}' B_{nm}(\mu) e^{-(n+m)\mu} \sim \begin{cases} \mu^\alpha & \text{for } 0 < \alpha < 1, \\ \mu & \text{for } \alpha \geq 1. \end{cases} \quad (3.50)$$

This, together with the results for the first sum in Eq. (3.33), it follows that at small  $\mu$

$$\langle F_\mu^2(u_0) \rangle_0 - \langle F_\mu(u_0) \rangle_0^2 \sim \begin{cases} \mu^\alpha & \text{for } 0 < \alpha < 1, \\ \mu & \text{for } \alpha \geq 1, \end{cases} \quad (3.51)$$

*i.e.* it vanishes in the  $\mu \rightarrow 0$  limit and the PDF of the total force acting on a particle displaced by  $u_0$  from its lattice position is  $W(F; u_0) = \delta[F - 2g(u_0 - \langle U \rangle)]$ . In other words, even in the case of spatially correlated displacements, the total force acting on a particle is a deterministic quantity equal to  $2g(u_0 - \langle U \rangle)$  with no fluctuations. This value depends only on the displacement of the particle on which we are calculating the force and not on the displacements of other particles as it does in  $3 - d$  [66].

### 3 Dynamics of 1d gravitational systems

In the previous section we have shown the prescription Eq. (3.11) for the  $1 - d$  gravitational force to give a well defined result in a class of infinite displaced lattice distributions. This result can be used in the construction of different toy models, through different prescriptions for the dynamics associated to these forces. In this section we discuss two such models, analogous to the  $3 - d$  cases of gravitational clustering in an infinite static or expanding universe, respectively. In the last subsection we discuss in detail the relation of these models to previous treatments of such models in the literature.

As motivation let us first comment on the reason for our interest in the case of perturbed lattices: in  $3 - d$  cosmological  $N$ -body simulations precisely such configurations are used as initial conditions. The reason is that by displacing particles from a lattice in this way, one can represent accurately, at sufficiently large scales, low-amplitude density perturbations about uniformity with a desired power spectrum  $P(k)$  (for a detailed discussion see e.g. [71] or [88]). This algorithm is strictly valid in the limit of very small relative displacements of particles, so that the assumption that particles do not cross in our derivation is a reasonable one (although not, as we will discuss in our conclusions, rigorously valid). The further assumption Eq. (3.28) we have made, on the decay of correlations, corresponds, also to a reasonable restriction on the class of initial power spectra. Indeed it can be shown easily that it corresponds, in  $d$  dimensions, to the assumption that  $P(k)/k^2$  be integrable at  $k = 0$ . In  $3 - d$  this corresponds to  $P(k \rightarrow 0) \sim k^n$  with  $n > -1$ , which is strictly satisfied in typical cosmological models which are characterised by an exponent  $n = 1$  at asymptotically small  $k$ .

#### 3.1 Toy models: static

The simplest such model is the conservative Newtonian dynamics associated to the derived force law, *i.e.*, with equation of motion

$$\ddot{x}_i = F_i(\{x_j, j = 0.. \infty\}, t), \quad (3.52)$$

where  $F_i$  is the gravitational force on the  $i$ -th particle of the distribution, with position  $x_i$  at time  $t$  (and dots denote derivatives with respect to  $t$ ), calculated using the prescription Eq. (3.12), *i.e.*,

$$\ddot{x}_i = -g \lim_{\mu \rightarrow 0} \sum_{j \neq i} \operatorname{sgn}(x_i - x_j) e^{-\mu|x_i - x_j|}. \quad (3.53)$$

We have shown that, for the case of an infinite lattice subjected to displacements which (i) do not make the particles cross, and (ii) satisfy Eq. (3.28), the force on the right-hand side is simply given deterministically as proportional to the particle's displacement (when  $\langle U \rangle$ , the average displacement, is zero). Denoting then the displacements of the  $i$ -th particle by  $u_i$ , *i.e.*  $x_i = ia + u_i$ , the equation of motion is therefore

$$\ddot{u}_i(t) = 2gn_0 u_i(t), \quad (3.54)$$

*i.e.*, simply that of an inverted harmonic oscillator. The same equation is valid in the case that  $\langle U \rangle \neq 0$  if we define  $x_i = ia + \langle U \rangle + u_i$ . This equation of motion is valid, of course, only as long as the non-crossing condition is satisfied. While it is in principle straightforward to generalize our calculation of the force to incorporate the effects of a finite number of crossings, it is much more convenient to make use of the following fact, which we recalled above: particles crossings in  $1 - d$  are equivalent, up to exchange of particle labels, to elastic collisions between particles, in which velocities are exchanged. This means that if we are interested in properties of the model which do not depend on particle labels, the model of  $1 - d$  self-gravitating particles is *equivalent* to a model in which particles bounce elastically. In this case the particles displacements from their original lattice sites are *at all times* such that there is no crossing of particles, and Eq. (3.54) remains valid, except exactly at "collisions". The dynamics of this model is therefore equivalent to that of an infinite set of inverted harmonic oscillators centred on the sites of a perfect lattice which bounce elastically, exchanging velocities, when they collide. To avoid any confusion, let us underline that these collisions *are no way analogous* to "2-body collisions" which formally appear in the Boltzmann equation, and which cause relaxation towards equilibrium. As in the finite "sheet model" the equation of motion may be integrated exactly. Defining, for convenience, time in units of the characteristic "dynamical" time  $\tau_{dyn} = 1/\sqrt{2gn_0}$ , the evolution between collisions is given exactly by

$$u_i(t_0 + t) = u_i(t_0) \cosh t + v_i(t_0) \sinh t, \quad (3.55)$$

$$v_i(t_0 + t) = u_i(t_0) \sinh t + v_i(t_0) \cosh t, \quad (3.56)$$

where  $u_i(t_0)$  ( $v_i(t_0)$ ) is the position (velocity) after the preceeding collision. The solution of the dynamics requires simply the determination of the next crossing time, which involves the solution of a quadratic equation (in  $e^t$ ), followed by an appropriate updating of the velocities of the colliding particles.

## 3.2 Toy models: expanding

The model we have just discussed is the  $1-d$  analogy for the problem of gravitational clustering in an infinite static universe, with equations of motion

$$\ddot{\mathbf{r}}_i = -Gm \sum_{j \neq i}^J \frac{\mathbf{r}_i - \mathbf{r}_j}{|\mathbf{r}_i - \mathbf{r}_j|^3}, \quad (3.57)$$

for identical particles of mass  $m$ . We use the superscript  $J$  on the sum to indicate that the sum is calculated using the “Jeans swindle”. As we have discussed this “swindle” in  $3 - d$  can be implemented by summing symmetrically about the point  $i$  either in a top-hat (*i.e.* sphere) or using the limiting procedure with a screening.

The equations of motion for particles in an infinite *expanding*  $3 - d$  universe are usually written in the form

$$\ddot{\mathbf{x}}_i + 2H\dot{\mathbf{x}}_i = -\frac{Gm}{a^3} \sum^J \frac{\mathbf{x}_i - \mathbf{x}_j}{|\mathbf{x}_i - \mathbf{x}_j|^3}, \quad (3.58)$$

where  $\mathbf{x}_i$  are the so-called *comoving coordinates* of the particles,  $H(t) = \dot{a}/a$  is the Hubble “constant”, and  $a(t)$  is the scale factor which is a solution of the equations

$$H^2 = \left(\frac{\dot{a}}{a}\right)^2 = \frac{8\pi G}{3a^3} \rho_0 + \frac{C}{a^2}, \quad (3.59)$$

$$\frac{\ddot{a}}{a} = -\frac{4\pi G}{3a^3} \rho_0, \quad (3.60)$$

where  $\rho_0$  is the mean mass density when  $a = 1$ , and  $C$  is a constant of integration<sup>9</sup>.

Note that these equations can be derived entirely in a Newtonian framework, and correspond simply to a different regularisation of the infinite system limit than that employed in the Jeans’ swindle: instead of discarding the effect of the mean mass density, the force is regularised so that the mean density sources a homologous expansion (or contraction) of the whole system. This corresponds to taking equations of motion

$$\ddot{\mathbf{r}}_i = -Gm \lim_{R \rightarrow \infty} \sum_{j \neq i, |\mathbf{r}_j| < R} \frac{\mathbf{r}_i - \mathbf{r}_j}{|\mathbf{r}_i - \mathbf{r}_j|^3}, \quad (3.61)$$

*i.e.* with the sum for the force calculated by summing symmetrically *about a chosen origin*. Dividing the sum into a term due to the mean mass density and a term due to fluctuations about this density, this may be written as

$$\ddot{\mathbf{r}}_i = -\frac{4\pi G\rho}{3}\mathbf{r}_i - Gm \sum^J \frac{\mathbf{r}_i - \mathbf{r}_j}{|\mathbf{r}_i - \mathbf{r}_j|^3}, \quad (3.62)$$

Neglecting the second term (*i.e.* taking only the force due to the mean density) gives an equation of motion admitting solutions of the form  $\mathbf{r}_i(t) = a(t)\mathbf{r}_i(t_0)$ , with  $a(t)$  satisfying Eqs. (3.59) and (3.60). Changing to comoving coordinates defined by  $\mathbf{r}_i = a(t)\mathbf{x}_i$  in Eq. (3.61) [or in Eq. (3.62)], and using Eq. (3.60), then gives Eq. (3.58).

Note that setting  $a(t) = 1$  in Eq. (3.58) gives exactly the static case Eq. (3.57), *i.e.*, the “Jeans’ swindle” in static space corresponds *formally* to the non-expanding limit of an expanding FRW universe. This static solution  $a(t) = 1$  is, however, a solution to Eqs. (3.59) and (3.60) only if  $\rho_0 = 0$  (and  $C = 0$ ), *i.e.*, it is not a *physical* limit of the expanding case but corresponds to the different prescription, Eq. (3.57),

---

<sup>9</sup> $C = 0$  corresponds to the flat Einstein de Sitter universe,  $C > 0$  to a closed universe, and  $C < 0$  to an open universe. In the Newtonian derivation of these equations, given below,  $C$  can be expressed in terms of the physical particle velocities at some initial time.

for calculating the force in the infinite volume limit. While almost all numerical studies are of the expanding case (for a review, see e.g., [12]), a recent study [11] of the static case for such initial conditions has shown that the evolution of clustering is, in essential respects, qualitatively similar in both cases. This suggests that it may be possible to understand essential qualitative features of the dynamics of structure formation in the universe in the conceptually simpler framework in which there is no expansion.

With the  $3 - d$  equation of motion in the form of Eq. (3.58) it is evident how the static  $1 - d$  model discussed above is naturally modified to mimic the  $3 - d$  expanding case: one can simply replace the force term due to the infinite  $3 - d$  distribution [*i.e.* the sum on the right-hand side of Eqs. (3.58)] by that due to the  $3 - d$  distribution consisting of infinite sheets. The summation prescription implementing the Jeans' swindle for the general  $3 - d$  case, *i.e.* spherical top-hat summation, is then, as we have discussed at length above, most appropriately replaced by the smooth prescription we have given. Thus we take the following  $1 - d$  equation for the positions  $x_i$  of the particles (sheets):

$$\ddot{x}_i + 2H\dot{x}_i = -\frac{2\pi G\Sigma}{a^3} \lim_{\mu \rightarrow 0} \sum_{j \neq i} \operatorname{sgn}(x_i - x_j) e^{-\mu|x_i - x_j|}, \quad (3.63)$$

where the sum extends over the infinite distribution of sheets, and we have explicitly made the identification  $g = 2\pi G\Sigma$  (where  $\Sigma$  is the mass per unit surface).

With initial conditions in the class of  $1 - d$  infinite perturbed lattices for which we have shown the sum for the force to be well defined and given by Eq. (3.10), we then have

$$\ddot{u}_i + 2H\dot{u}_i = \frac{4\pi G\rho_0}{a^3} u_i, \quad (3.64)$$

where we have used that the mean comoving mass density  $\rho_0 = \Sigma n_0$  (*i.e.* physical mass density when  $a = 1$ ). As in the static case, this equation of motion remains valid at all times if we exchange the labels of particles when they cross, so that they bounce instead of passing through one another.

For the case of an Einstein de Sitter (EdS) universe, which corresponds to  $C = 0$  in Eq. (3.59),  $a(t) = (6\pi G\rho_0)^{1/3}t^{2/3}$  and Eqs. (3.64) simplify to

$$\ddot{u}_i + \frac{4}{3t}\dot{u}_i = \frac{2}{3t^2}u_i \quad (3.65)$$

of which the independent solutions are  $u_i(t) \propto t^{2/3}$  and  $u_i(t) \propto t^{-1}$  [which are simply the well known growing and decaying solutions for small perturbations to a self-gravitating fluid in an EdS universe (see, e.g., [126])]. The evolution in between “collisions” is thus given by

$$\begin{aligned} u_i(t) &= u_i(t_0) \left[ \frac{3}{5} \left( \frac{t}{t_0} \right)^{2/3} + \frac{2}{5} \left( \frac{t}{t_0} \right)^{-1} \right] \\ &\quad + v_i(t_0)t_0 \left[ \frac{3}{5} \left( \frac{t}{t_0} \right)^{2/3} - \frac{3}{5} \left( \frac{t}{t_0} \right)^{-1} \right]. \end{aligned} \quad (3.66)$$

Note that, from Eq. (3.66) the determination of the crossings in these models, instead of a quadratic equation in the static model, thus involves the solution of a fifth order equation (for  $t^{1/3}$ ).

### 3.3 Discussion of previous literature

#### Static models

A few previous studies [10, 150, 151] have considered static  $1 - d$  toy models, defining the force on the right hand side of Eq. (3.52) as the derivative of a potential, which is the sum of the contribution from the sheets in a finite system of size  $L$ , and an additional one due to a uniform negative background. This is exactly the “naive” version of the Jeans swindle discussed above, and corresponds exactly to the prescription Eq. (3.9) for the calculation of the force (with  $L$  finite). The authors of [10] discuss explicitly the problems associated with taking the infinite system limit. As a result they limit their analysis only to a case for which their prescription gives a unique and finite result: a finite number of particles displaced off an infinite perfect lattice, modelling a finite localized perturbation embedded in an otherwise uniform universe. It is simple to verify that equation of motion for these displacements is then exactly Eq. (3.54), which we have now shown to be valid for the infinite lattice with perturbations which do not break the lattice translational invariance.

In [150, 151], on the other hand, the dynamics is formulated for a system of finite  $L$ , and the problem of the definedness of the force in the infinite system limit is not explicitly addressed. Instead it is dealt with implicitly by assuming that the finite system is symmetric about some point. Taking this latter point as origin of coordinates, the top-hat prescription Eq. (3.9) for the force at coordinate position  $x$  may then be rewritten as

$$F(x) = -2gN(0, x) + 2gn_0x, \quad (3.67)$$

in which the size of the system does not explicitly appear. Labelling the particles by their position with respect to the origin ( $i = 1 \dots N$ ), the force on the  $i$ -th particle may then be written

$$F_i = 2gn_0 \left[ x_i - \left( \frac{L}{N} \right) (i - 1) \right], \quad (3.68)$$

where  $x_i$  is the position of the particle. For any *finite* system the quantity in brackets can be considered as the displacement  $u_i$  of the particle  $i$  from its “original” lattice site [at  $(i - 1)L/N$ ]. Thus the equation of motion for the particles is again identical to that we have derived.

We note again that we have derived this force law without the assumption of symmetry (and without the explicit introduction of a background). Further, and most crucially, we have shown it to remain valid for a certain class of distributions when the infinite volume limit is taken — perturbed lattices without crossing and displacements of finite variance. In this respect we underline, as we have done in Sect. 1, that while in the formulation of [150] the same equations of motion Eq. (3.54) are valid for the particles in *any* finite symmetric system, this does not mean that the infinite system limit is well defined, even with the assumed symmetry. It is illustrative to see what “goes wrong” when the infinite system limit is taken, for example, for the case of a Poisson distribution, *i.e.*, when we consider a system of size  $L$  in which we distribute  $N$  particles randomly, and take  $L \rightarrow \infty$  at fixed  $n_0 = N/V$ . The problem is that forces, although defined at any finite  $L$ , by Eq. (3.68), diverge as  $L$  does. This can be seen by considering the statistics of the displacements as a function of  $L$  — the variance diverges, violating a crucial

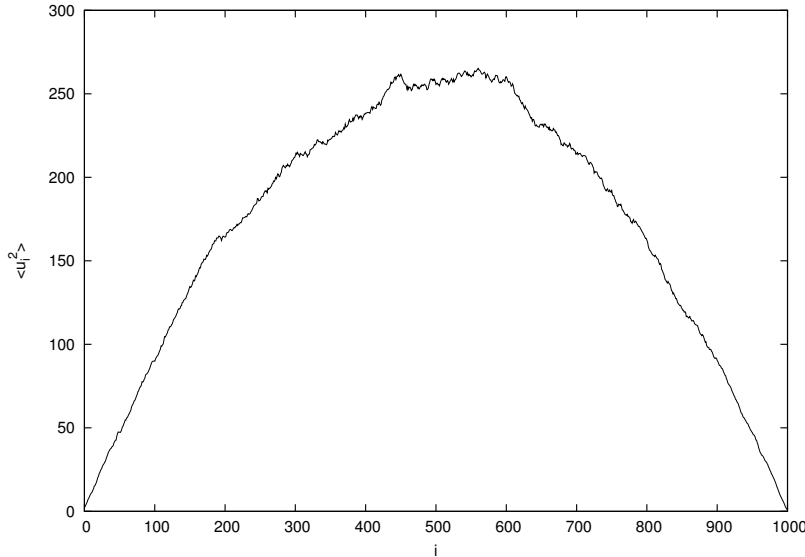


Figure 3.3: The variance of the displacement  $u_i$  (see text) as a function of a particle’s ordered position  $i$ , calculated for one thousand realizations of one thousand particles randomly placed in an interval.

assumption in our derivation — or more directly from the force written as Eq. (3.67): the force on a particle at  $x$ , as it is proportional to the fluctuation in the number of particles in the interval  $[0, x]$  about its average value, grows in proportion to  $\sqrt{x}$ . This means that the typical force on a particle not only diverges as  $L$  does, but that in a finite system *its typical value depends on the position of the particle with respect to the boundaries*. This is illustrated in Fig. 3.3, which shows the variance of the displacement  $u_i$  (as defined above as a function of  $i$ , as measured in one thousand realizations of one thousand randomly thrown particles. In a typical realization the force on a particle in the centre of the box is thus much larger than on a particle at the boundaries. In practice this means that the evolution of clustering in a symmetric finite system of initially Poisson distributed particles is, right from the initial time, global in character, and explicitly size dependent. Such behaviour can be seen in  $1 - d$  simulations reported in [151] from such initial conditions, which contrasts qualitatively with the local clustering characteristic of the  $1 - d$  (and cosmological) simulations which we will describe in the next section.

### Expanding models

We note first that Eq. (3.64) coincides exactly with that obtained in the so-called Zeldovich approximation (see, e.g., [29, 126]), when  $u_i$  is replaced by a vector function  $\mathbf{u}(\mathbf{x})$ . This approximation describes the evolution of displacement fields  $\mathbf{u}(\mathbf{x})$  engendering small amplitude fluctuations to a self-gravitating *fluid* in an expanding universe, and can be obtained rigorously by a perturbative treatment of the full fluid equations [29] in the lagrangian formalism<sup>10</sup>. For the case of one-dimensional perturbations it is well known (see [126] and references therein) that this approximation becomes exact, up to the time when caustics form, corresponding to the crossing

<sup>10</sup> $\mathbf{x}$  is a lagrangian coordinate and the fluid is exactly uniform when  $u(\mathbf{x}) = 0$ .

of “sheets” of fluid (*i.e.* particles in our case). It is thus, perhaps, not surprising, *a posteriori*, that we recover exactly the Zeldovich approximation for the motion of *discrete* sheets up to the time they cross: as the pair force between sheets is independent of separation, the only way a sheet can “see” that the force sourcing its motion is discrete, rather than continuous (as in the fluid limit), is when it crosses other sheets.

Eq. (3.64) can equally be derived [89, 105] using a perturbative treatment of the dynamics of an infinite perturbed lattice (in  $3 - d$ ) of *particles*. For plane wave displacements of the particles with a wave-vector orthogonal to one of the lattice planes, the amplitude of the displacement wave obeys exactly this equation in the limit that the discreteness of the mass distribution in these orthogonal planes is neglected. This latter assumption is weaker than that used in this framework to derive the Zeldovich approximation for a general perturbation, which would require also that the displacement be of long wavelength compared to the discreteness scale in the direction parallel to it.

In the studies of [145, 157], the authors study exactly the equations of motion Eq. (3.64) for the displacements of sheets perturbed off a perfect lattice (as in cosmological simulations). They adopt these equations arguing that they represent the fluid limit for  $1 - d$  perturbations in a  $3 - d$  expanding universe. While *before* sheet crossing (*i.e.* the formation of caustics), as discussed above, this is indeed known to be true — these equations are just the Zeldovich approximation which is, in this regime, exact — the extension to longer times is argued to be valid because the “collisionless” sheets of fluid will simply pass through one another. Our derivation of these equations shows that this in fact corresponds to the *discrete* particle/sheet model. Indeed we have *not* taken the fluid limit in our derivation, and the equations do not represent the fluid limit of this model. It simply happens to be the case that in this model, before crossing, the equations correspond with those in the fluid limit, for the physical reasons we have mentioned above. After crossing this equivalence breaks down, and the prescription used by [157] to “analytically continue” the fluid model beyond its regime of validity actually maps onto this discrete particle/shell model.

The other two groups who have considered  $1 - d$  toy models incorporating  $3 - d$  expansion have, as in this article, worked in a particle/sheet framework. Both the original model, proposed in [135] and studied further in [111], and the subsequent one proposed and studied in [7, 8] and [112], derive their (different) equations of motion by following, formally, the steps described above leading from Eq. (3.61) to Eq. (3.58). The force on the right hand side of Eq. (3.57) is simply that due to the sheets, calculated in the analogous manner<sup>11</sup>, *i.e.*,

$$\ddot{r}_i = 2\pi G \sum_{L \rightarrow \infty} \sum_{r_j \in [-L, L]} \text{sgn}(r_j - r_i). \quad (3.69)$$

The change to comoving coordinates, when assumed also to rescale the mass in the

---

<sup>11</sup>In [135] the force term is simply denoted  $E_i$ , without an explicit prescription for calculating it. It can be inferred from the description given subsequently of the numerical simulations that the implicit summation is the symmetric top-hat centred at the spatial origin. In [7, 8], on the other hand, the top-hat regularisation is explicated.

sheets in the orthogonal direction (so that  $\Sigma \rightarrow \Sigma/a^2$ ), gives

$$\ddot{x}_i + 2H\dot{x}_i = \frac{2\pi G\Sigma}{a^3} \left[ \lim_{L \rightarrow \infty} \sum_{x_j \in [-L, L]} \text{sgn}(x_j - x_i) + 2n_0 x_i \right], \quad (3.70)$$

provided that  $a(t)$  obeys the equation

$$\frac{\ddot{a}}{a} = -\frac{4\pi G}{a^3} \rho_0. \quad (3.71)$$

As above  $\rho_0 = \Sigma n_0$  is the mass density (in  $3 - d$ ) when  $a = 1$ .

The Eqs. (3.70) are those adopted by [7, 8, 111, 112, 135]. The term which we have written on the right hand side of the equation corresponds exactly to the prescription Eq. (3.9) for the calculation of the force. It incorporates the required subtraction of the effect of the background, so that motion in comoving coordinates is sourced only by perturbations to uniformity. Just as in the static models of [10, 150] discussed above, which are obtained formally by setting  $a = 1$  in Eq. (3.70), this force is well defined only if symmetry is assumed about the chosen origin in the point distribution. This is indeed the assumption made in the numerical studies of [7, 8, 111, 112, 135].

The difference between the models of [111, 135] and of [7, 8] (studied also in [112]) arises only in what they assume about the scale factor  $a(t)$ . The former authors impose an EdS cosmology behaviour for the scale factor,  $a(t) \propto t^{2/3}$ , and require that it is a solution of Eq. (3.71). Comparing Eq. (3.71) and Eq. (3.59) we see that it corresponds to imposing a Hubble expansion sourced by a mean density three times the physical mass density of the sheet (or, equivalently, assuming that the gravitational constant is not the same for the background as for the perturbations). Refs. [7, 8], on the other hand, simply impose that  $a(t)$  be the EdS expansion, with the right normalization. This amounts to adding “by hand” a term to the derived equation [112]. It corresponds effectively to simply replacing the “Jeans swindle”  $3 - d$  force term in Eq. (3.58) by the prescription Eq. (3.9). This differs from the “derivation” we have given above for Eqs. (3.63) only in the form of the Jeans swindle adopted. For the case that symmetry about the origin is assumed, we have the same equations of motion. In a finite system Eq. (3.68) is valid and so the equations of motion in their numerical simulations reduce exactly to Eqs. (3.64).

In conclusion the equations of motion Eqs. (3.64) are exactly the same as those used by [145, 157], and by [7, 8, 112]. The only difference in practice between all these studies are the initial conditions adopted and also the analysis of the resultant clustering given. Rather than working in the cosmological time variables, the latter authors define, a new time coordinate  $\tau = \sqrt{2/3} \ln t$ . Eqs. (3.65), for the case of an EdS universe, then take the very simple form

$$\frac{d^2 u_i}{d\tau^2} + \frac{1}{\sqrt{6}} \frac{du_i}{d\tau} = u_i. \quad (3.72)$$

In these variables the model is thus equivalent to an infinite set of inverted oscillators which bounce elastically, with an additional *constant* damping. Because of the

fifth order equation which must be solved to determine the crossings (now for the parameter  $t^{1/3} = e^{\tau/\sqrt{6}}$ ), the model has been dubbed the “quintic” model by the authors of [8].

The model of [111, 135], on the other hand does not impose on the sheets the physical  $3 - d$  expansion. Following the same approach as for the quintic model previously defined, we obtained an equation of motion

$$\frac{d^2 u_i}{d\tau^2} + \frac{1}{\sqrt{2}} \frac{du_i}{d\tau} = u_i. \quad (3.73)$$

Then it simply corresponds to Eq. (3.72) with a different damping term.

we note however that, in the derivation of [135], any function  $a(t)$  satisfying Eq. (3.71) can be adopted with the same consistency. The only way in fact in which the derivation of the  $3 - d$  equations can be rigorously adapted to  $1 - d$  is by using the  $1 - d$  expansion law derived from Eq. (3.69) in the limit of uniformly distributed sheets. This is

$$a(t) = 1 + H_0 t - 2\pi G n_0 t^2, \quad (3.74)$$

where  $H_0 = H(t = 0)$ , i.e., free fall in a constant gravitational field of strength  $4\pi G n_0$ . As this is very different to the  $3 - d$  expansion law it is probably not a variant of the toy model which is of practical interest.

## 4 Conclusion

We have revisited in this chapter a basic question concerning the definition of the gravitational force in  $1 - d$  in infinite point distributions. Previous definitions of this quantity in the literature have required the assumption of the existence of a special point (centre) in the distribution, i.e., explicit breaking of statistical translational invariance which is typically a feature of the infinite distributions one instead wishes to study. We have noted that the problem, associated with the non-converging surface fluctuations in such distributions, may be solved by employing a definition using a smooth screening which is sent to zero at the end of the calculation. We have then shown explicitly that this leads to a well defined force for a specific class of infinite perturbed lattices — those subject to perturbations of finite variance which do not make particles cross. In this case, when the mean displacement of particles is also assumed to vanish, the force on each particle take a unique value which is simply proportional to its own displacement from its lattice site. We note that we have assumed also that variance of the displacement fields is finite, which restricts to initial density fluctuations which have a sufficiently rapidly decaying power spectrum at small wavenumber (specifically, such that  $P(k \rightarrow) \sim k^n$  where  $n > 1$ , analagous to the same condition with  $n > -1$  in  $3 - d$ ).

We have then discussed different dynamical toy models which incorporate this definition of the force — the simple conservative Newtonian dynamics and one which incorporates a damping term mimicking the effect of  $3 - d$  expansion (the quintic and the RF models). Since the crossing of particles is equivalent, up to labels, to elastic collisions with exchange of velocities, the configurations generated by such dynamics, at any finite time, are always in the class of infinite perturbed lattices for which the force is defined (provided such a configuration is the initial condition). This is the

case because, at any finite time, collisions/crossings may only correlate particles up to a finite distance, and the correlation properties of displacements at asymptotically large separations therefore always obey the required conditions. The equations of motion are then simply those of an infinite set of inverted harmonic oscillators (with damping in the expanding case) with centres on the original lattice sites, and which bounce elastically when they collide. In this context we have also discussed in detail the different formulations of these models in the previous literature.

# Chapter 4

## Dynamics of infinite one dimensional self-gravitating systems: self-similarity and its limits

In the previous chapter we have defined gravitational forces in  $1 - d$  in an infinite system of particles. We have shown that for a particular class of initial conditions, *i.e.* a class of perturbed infinite lattices, which are point processes relevant to cosmological  $N$ -body simulations, the dynamics is that of particles in inverted harmonic oscillator potential centred at the lattice sites, which bounce elastically when they collide. The effect of cosmological expansion analogous to  $3 - d$  simulations in cosmology can be described by a simple fluid damping term. In this chapter, we present the results of a numerical investigation of the dynamical evolution of these toy models.

In the next section, we start by introducing the numerical simulation: integration of the dynamics, choice of units and initial conditions. In section 2, we present results of this  $1-d$  numerical investigation, which shows that these toy models are physically interesting in so far as they present very strong qualitative similarities with the evolution of the analogous  $3 - d$  systems. Indeed, using as initial condition the particular class of stochastic point processes whose power spectra are simple power-laws  $P_{init}(k) \propto k^n$  with  $n = 0$  and  $2$ , the  $1 - d$  system exhibits interesting features as the hierarchical nature of the clustering, the mechanism of linear amplification determining the growth of the non-linearity scale, as well as “self-similar” behaviour. We also observe a qualitative difference between static and expanding cases, like those which can be seen in  $3 - d$ . This is brought to light through the study of the temporal evolution of statistical measures such as the normalized mass variance, the correlation function and its Fourier transform, the power spectrum. We consider also the qualitative behavior of the shape of the correlation function as a function of  $n$ , the exponent of the initial power spectra, and the nature of the model (static or expanding case), and find again similar behaviours as in  $3 - d$ .

In the rest of the chapter, we then explore aspects of these behaviors which one cannot easily probe with  $3-d$  numerical simulations due to numerical difficulties. We study in particular, in section 3, structure formation for the particular class of initial condition corresponding to “causal fluctuations”, *i.e.*  $P_{init}(k) \propto k^4$ . We investigate the absence or presence of linear amplification, particularly whether self-similarity

applies in this case and how the non-linearity scale grows.

In the last section, we explore further what can be learnt about the strongly clustered regime, and in particular the exponents which characterize it. The advantage of the  $1 - d$  toy model is that it allows us to probe the development of self-similarity at smaller scale. In  $3 - d$ , in contrast, this is not possible because of the presence of a smoothing at small scales, which limits spatial resolution. Numerical investigation allows us to identify the lower cut-off of the self-similar regime, and to identify its behaviour. We observe that our results, for the expanding (*i.e.* damping) models suggest that a “stable-clustering” hypothesis can be made, analogous to that sometimes proposed in  $3 - d$ . Using this hypothesis we derive a simple analytical prediction for the exponent of the power spectrum in the self-similar regime. Excellent agreement is observed with the results of the simulations for a range of  $n$  and different values of the damping term modeling expansion.

## 1 Numerical simulation

In this section, we outline how our  $1 - d$   $N$ -body simulations are performed. We start by explaining the *heap algorithm* we use to integrate the dynamical equations of our systems. We present the way we generate numerically the different initial conditions, both for the particles positions and velocities. We define the estimators of statistical quantities used to study the dynamical evolution of  $1 - d$  self-gravitating systems: correlation function, mass variance and power spectrum. We also introduce the appropriate unit of time based on the characteristic timescales of the system. Not only  $1 - d$  toy model presents the interest of being “exact”, *i.e.* limited only by the machine precision, but also, as we will see, gives the opportunity to probe a much larger range of scale than in analogous  $3 - d$  simulations.

### 1.1 Integration of dynamics

In the  $1 - d$  case, we have studied in Chapter 3 that for a class of perturbed lattices (which are the configurations used as initial conditions in cosmological simulations) the force is given exactly as a trivial function only of the particle displacement. Thus, to simulate numerically the evolution of a  $1 - d$  infinite system, the step in which the force is calculated is trivial, and does not involve any approximation of an infinite sum as in  $3 - d$  (see Chapter 2). The only question which arises is how to treat the boundary conditions of the finite sub-system of this infinite system which one can simulate. Periodic boundary conditions, *i.e* particles which leave the finite interval on one side enter at the other side, are the evident simple choice, as they have advantage of maintaining (discrete) translational invariance. We could however, easily use other boundary conditions (e.g. simply neglecting mass loss, or injecting mass in a stochastic manner to compensate average loss). Our results should not depend on this choice, just as they should not depend on the size of the periodic box.

We start with a subsystem of  $N$  particles initially distributed in a  $1 - d$  regular lattice, with lattice spacing  $\ell > 0$ , *i.e.* the position of the  $n^{th}$  particles is  $X_n = n\ell$ , with  $n \in [0, (N - 1)]$ . We then apply a displacement field  $U_n$  to this system: the position of the  $n^{th}$  particle then becomes  $X_n = n\ell + U_n$ .

As far as the dynamical evolution of the displacement field in the static and expanding cases is concerned, we have defined in Chapter 3 the generic expression for the equations of motion for our  $1-d$  toy model between particle collisions/crossings:

$$\frac{d^2 u_i}{dt^2} + \Gamma \frac{du_i}{dt} = u_i, \quad (4.1)$$

where

- $\Gamma = 0$  corresponds to the static model, where  $t \equiv t_s$  with  $t_s$  the *static time variable* defined in the units of  $\tau_{dyn} \equiv \frac{1}{\sqrt{2g n_0}}$ ,
- $\Gamma = \frac{1}{\sqrt{6}}$  corresponds to the quintic model (*i.e.* “EdS” like), where  $t \equiv \sqrt{\frac{2}{3}} \ln(t_E/t_0)$  is a dimensionless time variable with  $t_E$  the *expanding time variable* defined in the units of  $t_0$ .
- $\Gamma = \frac{1}{\sqrt{2}}$  corresponds to the RF model, where  $t \equiv \frac{\sqrt{2}}{3} \ln(t_E/t_0)$  is a dimensionless time variable with  $t_E$  the *expanding time variable* defined in the units of  $t_0$ .

As we consider a system of colliding particles, each particle keeps its own label  $i$ . The effect of the collisions is to exchange the velocities of the couple of particles concerned. Between collisions, the solutions of these equations are given by

$$u_i^S(t_s) = e^{t_s/\tau_{dyn}} \left( \frac{u_i(0) + v_i(0)}{2} \right) + e^{-t_s/\tau_{dyn}} \left( \frac{u_i(0) - v_i(0)}{2} \right), \quad (4.2)$$

$$u_i^Q(t_e) = \left( \frac{t_e}{t_0} \right)^{2/3} \frac{3(u_i(t_0) + t_0 v_i(t_0))}{5} + \left( \frac{t_e}{t_0} \right)^{-1} \frac{(2u_i(t_0) - 3t_0 v_i(t_0))}{5}, \quad (4.3)$$

$$u_i^{RF}(t_e) = \left( \frac{t_e}{t_0} \right)^{1/3} \frac{(2u_i(t_0) + 3t_0 v_i(t_0))}{3} + \left( \frac{t_e}{t_0} \right)^{-2/3} \frac{(u_i(t_0) - 3t_0 v_i(t_0))}{3}, \quad (4.4)$$

where  $u_i^S(t_s)$ ,  $u_i^Q(t_e)$  and  $u_i^{RF}(t_e)$  represent the displacement of the  $i^{th}$  particle of the lattice between collisions in the static, quintic and RF models. The subsequent crossing is determined at each time, and the positions and velocities of the crossing particles are updated accordingly. For numerical efficiency we have implemented the optimized *heap-algorithm* (see e.g. [120] for a detailed study):  $1-d$  systems have the important characteristic that the set of positions is well-ordered. This means that all  $(N-1)$  possible collisions between  $N$  particles can be easily enumerated and that the neighbors of two colliding particles can be found in  $O(1)$  operations if we keep the particles sorted by position. It is then possible to build an *event-driven algorithm* to simulate a set of particles by finding the minimum of all possible collision times, evolving all particles up to that time and repeating the procedure. At first sight this involves  $O(N)$  operations per collision. However, in  $1-d$ , it is possible to update only the states of the two colliding particles and their next collision times with their two nearest neighbors. Also, by using a *heap structure*, we can find the minimum of the set of collision times using  $O(\log N)$  operations per collision.

The basic idea of a heap structure is to put the key elements in a binary tree and ensure that they satisfy the heap condition: the value in any tree node is smaller than the value in its “child” nodes. This does not completely order the set, but is enough to warrant that the smallest value in the heap is at the root. Also, the

heap condition can be maintained efficiently: if a node value is modified so that the heap condition is violated, we exchange the value with its parent node (if the value decreased) or with the smallest of its child nodes (if the value increased) and we repeat the procedure, moving up or down the tree until the heap condition is satisfied again, or we reach the root or leaves of the tree.

We now explain how the heap-algorithm is implemented in our  $N$ -body simulation. We consider the motion of  $N$  colliding particles in  $1 - d$ , and require that the equations of motion for particles can be integrated in between two successive collisions. We construct arrays of size  $N$  which contain the states of the particles, such as position, velocity and acceleration, at the time of their last collision, stored in increasing order of the spatial coordinates. An additional state variable associated to each particle is  $\tau_j$ , the time it last experienced a collision.

The algorithm starts by computing the collision time of each particle with its neighbor to the right, and the results are stored in an array of size  $(N - 1)$ , which is then turned into a heap. So that we do not need to move the whole particles state while processing the heap, we introduce an indexing array, *Particle-Heap* ( $PH[.]$ ), mapping the position in the heap to the rank in space of the leftmost of the two particles ( $j$  and  $j + 1$ ) involved in that collision (see Fig. 4.1). To update the list of predicted collision times of neighbors particles, we also need the index array inverse to *Particle-Heap*, which we call *Heap-Particle* ( $HP[.]$ ). Hence for all  $j$  in the range 1 to  $(N - 1)$ ,  $PH[HP[j]] = j$  and  $HP[PH[j]] = j$ . This condition will be preserved at all times while we update the heap. Note that the collision times are directly present in the heap, and that the two indexing arrays then realize exactly the functions needed to implement the algorithm.

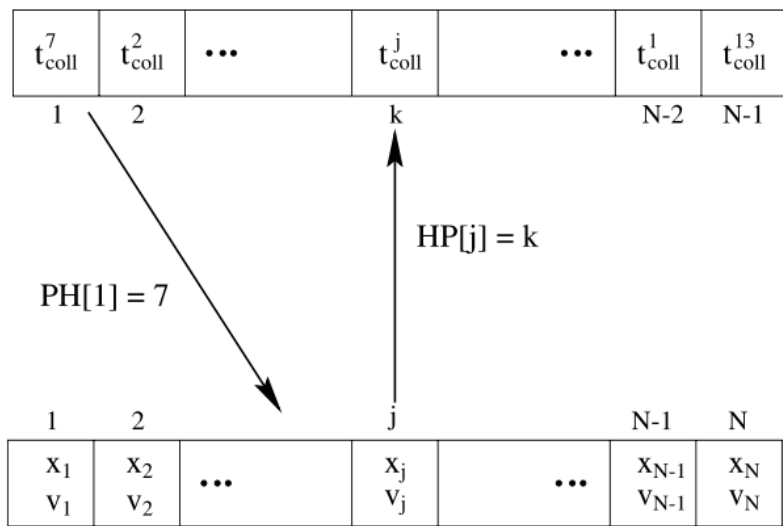


Figure 4.1: Representation of the structure of the heap algorithm implemented in our  $1 - d$   $N$ -body simulation (from [120]). It represents the two arrays  $PH[.]$  and  $HP[.]$ . The first array in the figure only contains the predicted collision times ordered as a heap, while the second contains the particle states stored in increasing order of spatial positions. The two indexing arrays allow to move back and forth between the two sets.

Once the heap has been built, the minimum collision time  $t_{min}$  is at the root. The particles involved in the first collision,  $j = PH[1]$  and  $(j + 1)$ , are selected and their states evolved up to time  $t_{min}$  where they are rearranged by the collision (momenta simply exchanged in the case of elastic collision), and  $\tau_j$  and  $\tau_{j+1}$  are set equal to  $t_{min}$ . Next the new predicted collision time between  $j$  and  $(j + 1)$  is computed and replaces the one at the root of the tree. The root might now not fulfill the heap condition, so the heap array is re-arranged by sifting down the root value, using at most  $O(\log N)$  operations.

The next collision times of particles  $j$  and  $(j + 1)$  with their other nearest neighbor,  $(j - 1)$  and  $(j + 2)$ , respectively, also need to be re-computed (see Fig. 4.2). To do this, particles  $(j - 1)$  and  $(j + 2)$  are temporarily moved forward in time up to  $t_{min}$ , where their new collision times are computed and put into the heap at  $HP[j - 1]$  and  $HP[j + 1]$ , replacing the old ones. As a consequence, the heap has to be re-arranged two more times, again at a cost of at least  $O(\log N)$  for each modification.

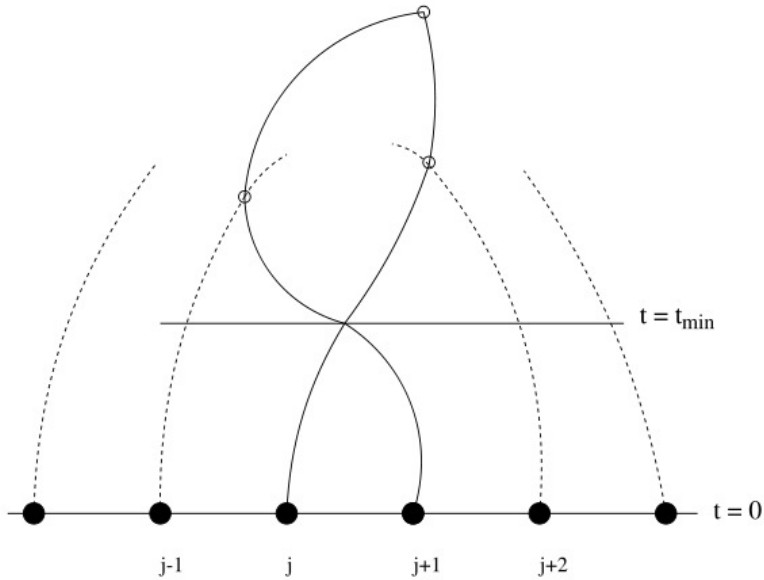


Figure 4.2: Intersection of the trajectories of particles  $j$  and  $j + 1$  at time  $t = t_{min}$  (from [120]). The ringed intersections are the collisions/crossings that need to be recomputed.

The heap is now again in a consistent state with the next collision time at the root, and the whole procedure can be repeated. The evolution can be stopped either after some fixed number of collisions  $Z$ , or when the predicted time for the next collision becomes larger than some chosen final time  $T_{end}$ . At the end, all particles are moved forward in time from their own  $\tau_j$  to the final time which is either  $T_{end}$  or the time of the last collision. The complexity of the algorithm is then in the worst-case  $O(Z \log N)$  plus lower-order terms  $O(Z)$  and  $O(N)$ .

## 1.2 Initial conditions

As the structure of the algorithm which explains the numerical integration of the equations of motions has been introduced, we present the classes of initial conditions we study.

As discussed in Chapter 2, perturbed lattice initial condition allows one to produce a stochastic point process with a desired power spectrum, up to contribution coming from the original lattice structure. As in general studies in cosmology we will consider a class of lattices in which  $P_{init}(k) \propto k^n$ , where  $n$  is a constant for  $k \leq k_N$  (where  $k_N = \frac{\pi}{\ell}$  is the Nyquist frequency). Around and above  $k_N$ ,  $P(k)$  becomes dominated by terms associated with the “pre-initial lattice”. Such initial conditions are often referred to as “scale-free” in cosmology - because of the scale-free power law behaviour - but it is important to underline that such initial condition *do* contain at least two characteristic scales:

- the lattice spacing, which leads in  $k$  space to the deviation from the power-law behaviour at  $k_N$ ;
- the homogeneity scale at which the amplitude of the fluctuations are of order one.

If the dynamics does not depend on the ultraviolet scale, such as the lattice spacing, there is only one relevant characteristic scale in the initial conditions. If the dynamics introduces no further scale (*i.e.* once the transients due to UV cut-off have gone) one expects to find *asymptotically* the “self-similar” behaviour we have discussed in Chapter 2. In  $3-d$  it was shown, using the BBGKY hierarchy, describing the matter in the fluid limit, that in such a specific case (EdS and power law PS) one can find solution of this kind for the phase space density. We will consider here a range of  $n$  that corresponds to different relevant subclasses of initial conditions:

- $n = 0$  corresponds to a specific class of infinite perturbed lattices for which the variance of the displacement field is infinite (see Chapter 3). Therefore, it leads to a divergent force, analogous to the range  $-3 < n < -1$  in  $3-d$ , which is regulated therefore by the box size. However, this divergence of the force does not prevent the dynamics of formation of structures from setting, as it has been shown in [3] that what does really matter is the convergence of *the difference of the force* between particles.
- $n = 2$  corresponds to a specific class of infinite perturbed lattice, the shuffled lattice, for which the variance of the uncorrelated displacements is finite (see Chapter 3), and which leads to a convergent force, analogous to the range  $-1 < n < 4$  in  $3-d$ ,
- $n = 4$  represents the limit of “causal process” which locally conserves mass. This corresponds to the power generated by the “newly forming structures” mechanism introduced by Peeble in [126] and discussed in Chapter 2.

**Flat power spectrum:**  $P_{init}(k) \propto k^0$  **at small  $k$**

To generate the intial PS  $P_{init}(k) \propto k^0$  at small  $k$ , we consider the canonical method introduced in Chapter 2, which is based on the so-called Zeldovich approximation.

The procedure is the following (see e.g. [49, 137]): i) we set up a “pre-initial” configuration of the  $N$  particles: a simple regular lattice; ii) given an input theoretical PS  $P_{th}(k) \propto k^0$ , the corresponding displacement field in the Zeldovich approximation is applied to the “pre-initial” point distribution. The cosmological IC are usually taken to be Gaussian, and the displacements are determined by generating a realization of the gravitational potential

$$\Phi(q) = \sum_k a_k \cos(k \cdot q) + b_k \sin(k \cdot q), \quad (4.5)$$

with  $a_k = R_1 \frac{\sqrt{P_{th}(k)}}{k^2}$  and  $b_k = R_2 \frac{\sqrt{P_{th}(k)}}{k^2}$ , where  $R_1$  and  $R_2$  are Gaussian random numbers of mean zero and dispersion unity. We have seen in Chapter 2 that this corresponds to generating a realization of a stochastic displacement field with PS  $\hat{g}(k) = P_{th}(k)/k^2 \propto 1/k^2$ . The motivation for the choice of this algorithm instead of a simple Poissonian initial condition (*i.e.* particles randomly distributed in the simulation box) consists in the fact that we can control the amplitude of the initial condition, as it is done in  $3 - d$  simulations.

### The shuffled lattice IC: $P_{init}(k) \propto k^2$ at small $k$

Following [71], we use the term SL to refer to the infinite point distribution obtained by randomly perturbing a perfect lattice: each particle on the lattice, of lattice spacing  $\ell$ , is moved randomly (“shuffled”) about its lattice site, each particle independently of all others. A particle initially at the lattice site  $R$  is thus at  $x(R) = R + u(R)$ , where the random displacements  $u(R)$  are specified by the factorised joint probability density function

$$P[u(R)] = \prod_R p(u(R)). \quad (4.6)$$

The distribution is thus entirely specified by  $p(u)$ , the probability density function for the displacement of a single particle. We study evolution from SL with the following PDF:

$$p(u) = \begin{cases} 2\Delta & \text{if } u \in [-\Delta, \Delta] \\ 0 & \text{otherwise} \end{cases} \quad (4.7)$$

Each particle is therefore moved randomly in an interval of side  $2\Delta$  centered on the corresponding lattice site by taking into account the periodicity of the system. The resulting distribution is a shuffled lattice. We assume that  $\Delta \leq \ell$ . The average displacement of a particle is  $\langle u \rangle = 0$  and the variance of the shuffling  $\langle u^2 \rangle = \int du u^2 p(u) = \Delta^2$ .

We can now estimate the PS of a SL. Defining the Fourier transform  $\delta_k$  of the density contrast  $\delta_x = \frac{n(x)-n_0}{n_0}$  as

$$\delta_k = \begin{cases} 0 & \text{if } k = 0 \\ \frac{1}{N} \sum_{i=1}^N \exp(-ikx_i) & \text{otherwise} \end{cases} \quad (4.8)$$

we obtain

$$\delta_k = \frac{1}{N} \sum_n \exp[-ik(\ell n + u_n)], \quad (4.9)$$

where  $n$  is an integer labelling the particles of the system and where  $u_n$  is the displacement of the particle on the site  $n$ . For  $k$  such that  $(k u_n) \ll 1$ , we obtain, by using the approximation  $\exp(ix) \approx 1 - ix - x^2/2$  and  $\langle u_n \rangle = 0$ , that the PS is given by

$$P(k) = \langle |\delta_k|^2 \rangle \approx \frac{1}{N^2} \sum_{n_1, n_2} \exp[-i\ell k(n_1 - n_2)] \left\{ 1 - \frac{1}{2} \langle [k(u_{n_1} - u_{n_2})]^2 \rangle \right\}. \quad (4.10)$$

The independence of  $u_{n_1}$  and  $u_{n_2}$  if  $n_1 \neq n_2$  implies that

$$\langle [k(u_{n_1} - u_{n_2})]^2 \rangle = 2\Delta^2 k^2 (1 - \delta_{n_1, n_2}), \quad (4.11)$$

with  $\delta_{n_1, n_2} = 1$  if  $n_1 = n_2$  and 0 otherwise. Therefore

$$P(k) \approx \frac{k^2 \Delta^2}{N} + \frac{1 - \Delta^2 k^2}{N^2} \sum_{n_1, n_2} \exp[-i\ell k(n_1 - n_2)]. \quad (4.12)$$

Limiting our analysis to the leading order in the behavior for small values of  $k$ , we obtain

$$P(k) \approx \frac{1}{N} \Delta^2 k^2 \quad (4.13)$$

when  $k$  is small. The SL configurations are therefore specified by two parameters: the lattice constant  $\ell$  and the shuffling parameter  $\Delta$ . An alternative convenient characterization would be given by  $\ell$  and the adimensional ratio  $\Delta/\ell$ .

### Causal power spectrum: $P_{init}(k) \propto k^4$ at small $k$

To generate the intial PS in  $k^4$  at small  $k$ , we follow the argument in [2]: we start with an arbitrary uniform spatial point-particle distribution with a known PS. We suppose that each of these particles, called “mother” particles in [2], splits into a “cloud” of  $m$  identical “daughter” particles, where  $m$  is a constant. Each daughter particle is then assumed to be displaced from its mother position by a stochastic displacement which may, or may not, be correlated with the displacement of other particles. In other words each set of  $m$  particles initially lying at the same spatial point “explodes” forming a “cloud” of particles around it; this procedure was called in [2], *a stochastic cloud process*.

We suppose that the displacements applied to different particles belonging to the same mother are symmetrically distributed with arbitrary pair correlations. One can choose, for instance, these correlations in order to fix certain moments of the mass dispersion of each cloud. To generate a  $k^4$  initial condition, we apply this result to the specific case that the mother distribution is a regular lattice, and we thus derive, following [2], the interesting small  $k$  behaviour of the PS of the daughter distribution.

For a mother distribution corresponding to a regular lattice, we can write the microscopic particle density as

$$n(x) = \sum_R \delta(x - R), \quad (4.14)$$

where  $R$  is the generic lattice site. In this case, the PS of  $n(x)$  is

$$S_n(k) = 2\pi n_0 \sum_{H \neq 0} \delta(k - H), \quad (4.15)$$

where the sum is over all the vectors  $H$  of the reciprocal lattice but  $H = 0$ . Note that this vanishes identically in the first Brillouin zone, and therefore in this region of the  $k$ -space the following relation holds exactly:

$$S_\rho(k) = 1 + (m-1) \sum_{l=0}^{+\infty} (-ik)^l \frac{\overline{(u-v)^l}}{l!} - m \left| \sum_{l=0}^{+\infty} (-ik)^l \frac{\overline{u^l}}{l!} \right|^2, \quad (4.16)$$

where  $\rho = mn$  is the microscopic particle density of the daughter particles distribution, and where  $u$  and  $v$  are the displacements applied to two different particles belonging to the same cloud. Expanding the terms  $(u-v)^l$  in Eq. (4.16), we obtain

$$S_\rho(k) = \sum_{l=1}^{+\infty} \frac{(-ik)^l}{l!} \sum_{j=0}^l (-1)^j \binom{l}{j} \left[ (m-1) \overline{u^j \times v^{l-j}} - m \overline{u^j} \times \overline{v^{l-j}} \right]. \quad (4.17)$$

Making the additional assumption of statistical symmetry in the displacements,  $p(u) = p(-u)$ , all the terms with odd  $l$  in Eq. (4.17) vanish.

Let us now analyse in detail Eq. (4.17), denoting by  $O_n(k)$  its term proportional to  $k^n$ . The lowest order non-zero term is  $n = 2$ :

$$O_2(k) = \left[ \overline{u^2} + (m-1) \overline{u \times v} \right] k^2. \quad (4.18)$$

It is simple to verify that  $[\overline{u^2} + (m-1) \overline{u \times v}] \geq 0$  always, as required from the fact that  $S_\rho(k)$  is a PS. This quantity, however, given our symmetry hypotheses about the displacement distribution, is nothing other than

$$\overline{\left( \sum_{i=1}^m u_i \right)^2} = m \left[ \overline{u^2} + (m-1) \overline{u \times v} \right]. \quad (4.19)$$

Consequently the condition to have an identically vanishing  $O_2(k)$  term, and therefore a small  $k$  PS of order greater than two, is  $\overline{(\sum_{i=1}^m u_i)^2} = 0$ , or in other words,

$$\sum_{i=1}^m u_i = 0, \quad (4.20)$$

with probability one. This means that the center of mass of each cloud does not move away from the mother particle when the displacements are applied. Clearly, for  $m = 1$ , this condition can only be trivially satisfied by applying no displacement, in which case the daughter distribution is the original lattice distribution. For  $m = 2$ , it can be satisfied non-trivially: choosing the displacement of a first point with the PDF  $p(u)$ , the other particle is then displaced deterministically by  $(-u)$ . The method we use in this thesis then consists in starting with a distribution of  $N$  particles on a regular lattice of lattice spacing  $\ell$ . We divide the total set of  $N$  particles ( $N$  even) into  $N/2$  subsets of couple of particles. Let us denote these subsets  $(i, i+1)$  where  $i = 2k + 1$  with  $k \in [0; \frac{N}{2} - 1]$ . We then displace particle  $i$  with the PDF  $p(u_i)$  such that

$$p(u_i) = \begin{cases} \ell & \text{if } u_i \in [-\frac{\ell}{2}; \frac{\ell}{2}] \\ 0 & \text{otherwise.} \end{cases} \quad (4.21)$$

Its neighbours  $(i+1)$  is then displaced deterministically by  $u_{i+1} = -u_i$ .

### Initial velocities

To complete information about the initial conditions, we must choose the initial velocities. One possible choice would be to consider the system of particles at rest, *i.e.*  $v_i = 0$  for all  $i \in [0, N - 1]$ . However, in exploring the analogy with cosmological simulation there is another choice which is natural. This is that corresponding to that given by the Zeldovich approximation (which becomes exact in  $1 - d$ ) discussed in Chapter 2. This consists in the purely growing mode of the displacement field in Eqs. (4.2), (4.3) and (4.4) at early time, *i.e.* obtained by setting the coefficients of the second term in these equations to zero, such that

$$u_i^S(t_s) = e^{t_s/\tau_{dyn}} \left( \frac{u_i(0) + v_i(0)}{2} \right), \quad (4.22)$$

$$u_i^Q(t_e) = \left( \frac{t_e}{t_0} \right)^{2/3} \frac{3(u_i(t_0) + t_0 v_i(t_0))}{5}, \quad (4.23)$$

$$u_i^{RF}(t_e) = \left( \frac{t_e}{t_0} \right)^{1/3} \frac{(2u_i(t_0) + 3t_0 v_i(t_0))}{3}, \quad (4.24)$$

where  $u_i^S(t_s)$ ,  $u_i^Q(t_e)$  and  $u_i^{RF}(t_e)$  represent the displacement of the  $i^{th}$  particle of the lattice between collisions in the static, quintic and RF models. Its only effect on the dynamical evolution will be to make the transient to self-similarity, which we will discuss below, slightly shorter. We then obtain the conditions on the initial velocity field

$$v_i^S(0) = u_i^S(0), \quad (4.25)$$

$$v_i^Q(t_0) = \frac{2}{3t_0} u_i^Q(t_0), \quad (4.26)$$

$$v_i^{RF}(t_0) = \frac{1}{3t_0} u_i^{RF}(t_0). \quad (4.27)$$

Whe then have, up to the first crossing/collision

$$u_i^S(t_s) = u_i(0) e^{t_s/\tau_{dyn}}, \quad (4.28)$$

$$u_i^Q(t_e) = u_i(t_0) \left( \frac{t_e}{t_0} \right)^{2/3}, \quad (4.29)$$

$$u_i^{RF}(t_e) = u_i(t_0) \left( \frac{t_e}{t_0} \right)^{1/3}. \quad (4.30)$$

### 1.3 Choice of units

We now explain our choice of units of length, mass and time for the  $1 - d$  system. We simply fix our unit of mass equal to the particle mass,  $m = 1$ . As unit of length we choose the initial lattice spacing  $\ell = L/N = 1$ , where  $L$  is the size of the simulation box and  $N$  the total number of particles in the system. To follow the dynamical evolution of the  $1 - d$  toy model, we choose the unit of time considering Eq. (4.1) and the discussion below it. Indeed, Eq. (4.1) simply incorporates the choice of the different time units: in the static case we choose the so called dynamical time  $\tau_{dyn} = \frac{1}{\sqrt{2g_{n0}}}$  and in the expanding case (quintic and RF) we consider the dimensionless time variable  $\tau_\Gamma = \frac{1}{3\Gamma} \ln \left( \frac{t_E}{t_0} \right)$ . For convenience, we fix  $\tau_{dyn} = 1 = t_0$ .

Below we will compare the dynamical evolution in the static and expanding cases. To do so it is necessary to define the relation between the different time variables in the two cases (as there is a priori no connection between the two). An evident possible choice of mapping is given by the very early time evolution (before first crossing) of the displacement given by Eqs. (4.28), (4.29) and (4.30). If we choose

$$t_s/\tau_{dyn} = \frac{2}{3} \ln(t_e/t_0) \quad \text{and} \quad t_s/\tau_{dyn} = \frac{1}{3} \ln(t_e/t_0), \quad (4.31)$$

in each case (quintic and RF) we map so that these early two displacements are identical in each case. This mapping Eq. (4.31) allows us to associate to any expanding simulation (corresponding to a certain value of  $\Gamma$ ) a “static time variable”  $t_s$ .

In the continuum approximation, the displacements of the particles are related to the density perturbation through the continuity equation  $\delta \propto \nabla u$ . Considering Eqs. (4.28), (4.29) and (4.30) and the definition of the PS  $P(k) \propto \langle |\delta_k|^2 \rangle$ , we simply obtain then

$$P_s(k, t_s) = P(k, 0) e^{2t_s/\tau_{dyn}}, \quad (4.32)$$

$$P_Q(k, t_e) = P(k, t_0) \left( \frac{t_e}{t_0} \right)^{4/3}, \quad (4.33)$$

$$P_{RF}(k, t_e) = P(k, t_0) \left( \frac{t_e}{t_0} \right)^{2/3}. \quad (4.34)$$

Considering that the PS in the static and expanding cases are initially identical, *i.e.*  $P(k, 0) = P(k, t_0)$  we obtain the same relation as in Eq. (4.31). This means that, with this mapping in these time variables, the linear regimes in the static and expanding cases (quintic and RF) are identical at early time. The physical meaning of this mapping extends however, as we will see, for beyond early time: the growth of displacements reflects exactly that of the PS in the linearised approximation (cf. Chapter 2). The mapping in fact relates times in different models (with identical initial conditions) at which the PS will be identical, *if* linear amplification is valid. We will see below that, as in  $3 - d$ , linear amplification does indeed hold at all time at sufficiently small  $k$ . The mapping of time chosen therefore relates evolved configurations which remain approximately the same at the large scales where density fluctuations are small.

In the following, we will only refer to the static time  $t_s$  to compare the different analysis in both the static and expanding cases. Let us note that we can derive a generic relation between  $t$  (*i.e.* the time variable in Eq. (4.1)) and the reference time  $t_s$  in the growing mode. We simply obtain from Eqs. (4.1) and (4.2) with  $\tau_{dyn} = 1$

$$t_s = D(\Gamma) t, \quad (4.35)$$

where  $D(\Gamma) = \frac{1}{2} \left( -\Gamma + \sqrt{\Gamma^2 + 4} \right)$ . This gives in the quintic and RF models respectively

$$t = \sqrt{\frac{3}{2}} t_s \quad \text{and} \quad t = \sqrt{2} t_s. \quad (4.36)$$

## 1.4 Statistical measures

In the previous chapters, we have talked about ensemble averages, that is averages on all possible realizations of a stochastic process  $\rho(x, t)$ . In practice, what we have is only one or at most a few realizations of such a stochastic process. While in statistical mechanics, ergodicity refers to equality between time average and ensemble average, here it implies equality between space average and ensemble average. Therefore, we have seen in Chapter 2 that if the stochastic process is ergodic, one (infinite) realization suffices to obtain an ensemble average. Thus if we consider a quantity  $F$  depending on the stochastic process  $\rho(x, t)$  at some positions  $y_1, \dots, y_n$ , we denote  $\langle F \rangle$  its ensemble average and  $\bar{F}$  its estimator in the space average. We will use this notation in the following.

### The reduced two-point correlation $\tilde{\xi}$

In order to estimate the reduced two-point correlation function  $\tilde{\xi}$  defined in Chapter 2, we calculate first an estimate of the conditional average density  $\langle \rho(x) \rangle_p$ : we choose randomly  $N_c$  particles (centres) in the distribution resulting from one realization of the considered stochastic process and for each of them we calculate the average density in  $1-d$  “spherical shells” of different radii, taking into account the periodicity. This can be summarised by the following formula

$$\overline{\rho(x, t)_p} \equiv \frac{1}{N_c} \sum_{i=1}^{N_c} \frac{m}{V(x, \delta x)} N_i(x, \delta x), \quad (4.37)$$

where  $V(x, \delta x)$  is the “volume” of the symmetric interval centered on the  $i^{\text{th}}$  particle of a subset of  $N_c < N$  particles randomly chosen among the  $N$  particles of the system. Clearly the result is a function which does not depend on the sign of  $x$  but only on its absolute value. An estimation of  $\tilde{\xi}(x, t)$  for  $x \neq 0$  is then

$$\tilde{\xi}(x, t) \approx \frac{\overline{\rho(x, t)_p}}{\rho_0} - 1. \quad (4.38)$$

Note that we will generally restrict ourselves to scales where  $|x| < L/2$  in order to avoid effects coming from the periodicity of the system. Actually if one looks at larger scales, the estimators  $\overline{\rho(x, t)_p}$  gives always a value close to  $\rho_0$ .

### The power spectrum

For the power spectrum  $P(k, t) = P(|k|, t)$ , we use the following quantity to estimate it:

$$P(k, t) \approx \frac{1}{N_q} \sum_{k \leq q \leq k + \delta k} |\delta(q, t)|^2, \quad (4.39)$$

where  $N_q$  is simply the number of vector  $q$  considered in the sum. Note that to speed up the calculation, not all the vector  $q$  for a given modulus are taken into account: at large  $k$  the density of vectors considered is smaller than at small  $k$ . Numerically we simply use a logarithmic separation of the vector  $k$  to represent the PS.

### The normalized mass variance

In the case of the normalized variance, we choose  $N_r$  random points in the system (*i.e.* not necessarily particles of the distribution) and calculate the mass inside spheres centred on them: if  $N_i(R)$  is the number of particles in the sphere centred on the point  $i$  and  $\overline{N}(R, t)$  its average, *i.e.*

$$\overline{N}(R, t) = \frac{1}{N_r} \sum_{i=1}^{N_r} N_i(R), \quad (4.40)$$

then

$$\sigma^2(R, t) \approx \frac{\frac{1}{N_r} \sum_{i=1}^{N_r} N_i^2(R) - \overline{N}(R, t)^2}{\overline{N}(R, t)^2}. \quad (4.41)$$

## 2 Basic results: comparison with $3 - d$

In this section, we focus our analysis on the dynamical evolution of a static and  $1-d$  equivalent of an expanding “EdS” universe (*i.e.* quintic model), starting with initial PS  $P_{init}(k) \propto k^0$  and  $k^2$ . We present basic results, and underline the very strong qualitative similarities with  $3 - d$ .

### 2.1 Visual inspection

The evolution of clustering can firstly be illustrated by a visual inspection in configuration space as well as in one-particle phase space (also called  $\mu$ -space). Shown in Figs. 4.3, 4.4, 4.5 and 4.6 are snapshots of different initial conditions and evolved configurations at increasing time for initial PS  $P_{init}(k) \propto k^0$  and  $k^2$ , in a static and expanding (quintic) universe, for a system of  $N = 10^5$  particles. The plots in the left-hand panels show the number of particles  $N(i)$  in each lattice cell at each time, which is proportional to the mass density in each cell. Defining the number density contrast as

$$\delta(x) = \frac{n(x) - n_0}{n_0}, \quad (4.42)$$

where  $n(x) = \sum_{i=1}^N \delta_D(x - x_i)$  is the microscopic number density and  $n_0$  is the mean microscopic density, the plots represent the evolution of  $\bar{\delta}(x) + 1$ , where the bar indicates an average over the unit lattice cell. In the phase space plots, in the right-hand panels, each point represents simply one particle.

One sees clearly that, in both the static and expanding cases, the evolution appears to proceed in a “bottom-up” manner: overdensities first develop at small scales and subsequently at larger scales. This is typical of what is termed in  $3 - d$  the *hierarchical* formation of structures.

We note a difference between the case corresponding to an initial PS  $P_{init}(k) \propto k^0$  and the one corresponding to  $P_{init}(k) \propto k^2$ . In the latter case, we see clearly the appearance of voids in the simulation box whose size grows monotonically in time, and which separate overdense regions. In the case of an initial PS  $P_{init}(k) \propto k^0$ , on the other hand, we see that, while one can distinguish clearly overdensities which emerge at increasing scale with time, they are not separated by voids. We will

return in Chapter 5 to these differences in the context of a multifractal analysis of the clustering in each case.

Furthermore, the sense in which the system is representative of the evolution of an infinite system is manifest visually in the fact that the system does not appear to have a preferred center - clusters form in apparently random locations without sensitivity to the boundaries. Indeed we do not follow the evolution for longer times than those shown precisely because the system then begins to be dominated by a single non-linear structure. This is a regime in which we are not interested since it is evidently strongly affected by finite size effects. The maximal time to reach this regime depends not only on the number of particles  $N$  in the system (or size  $L$  of the simulation box), but also on the amplitude of the displacements.

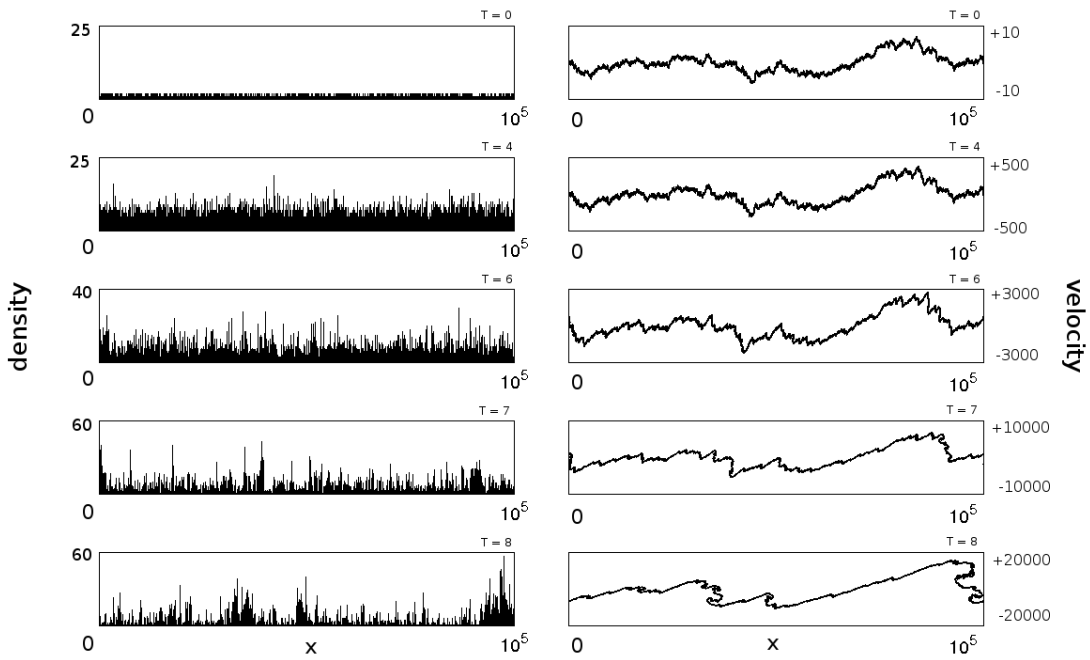


Figure 4.3: Evolution in configuration space (left hand panels) and in one particle phase space -  $\mu$ -space - (right hand panels) starting with an initial PS  $P_{init} \propto k^0$  for the static model at time  $t_s = 0, 4, 6, 7, 8$ . The unit of length is given by the initial lattice spacing  $\ell = L/N$  and thus  $L = N = 10^5$ .

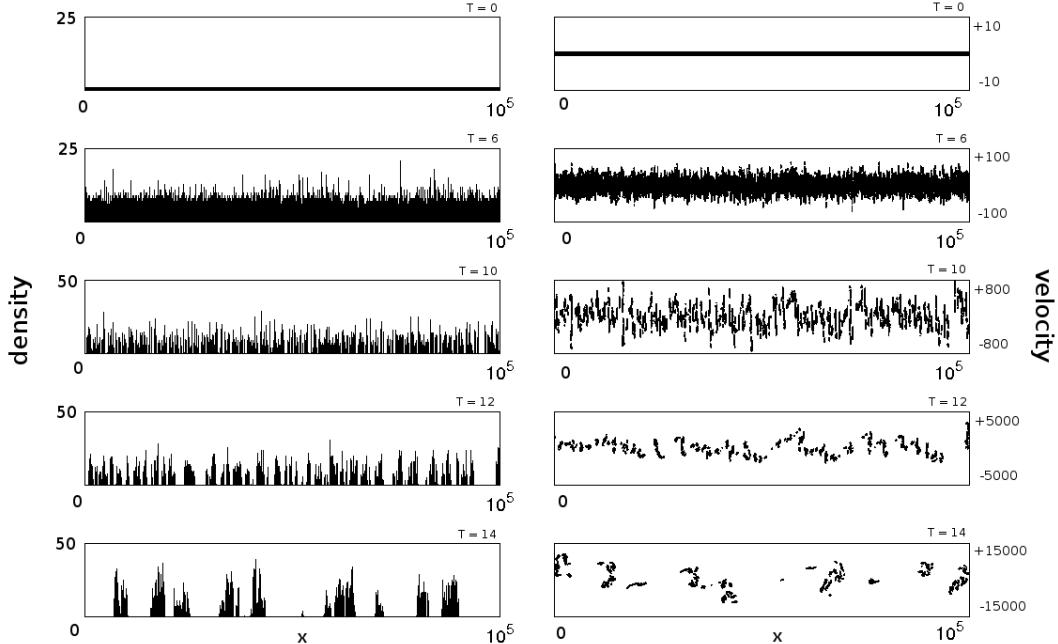


Figure 4.4: Evolution in configuration space (left hand panels) and in one particle phase space -  $\mu$ -space - (right hand panels) starting with an initial PS  $P_{init} \propto k^2$  for the static model at time  $t_s = 0, 6, 10, 12, 14$ . The unit of length is given by the initial lattice spacing  $\ell = L/N$ , and thus  $L = N = 10^5$ .

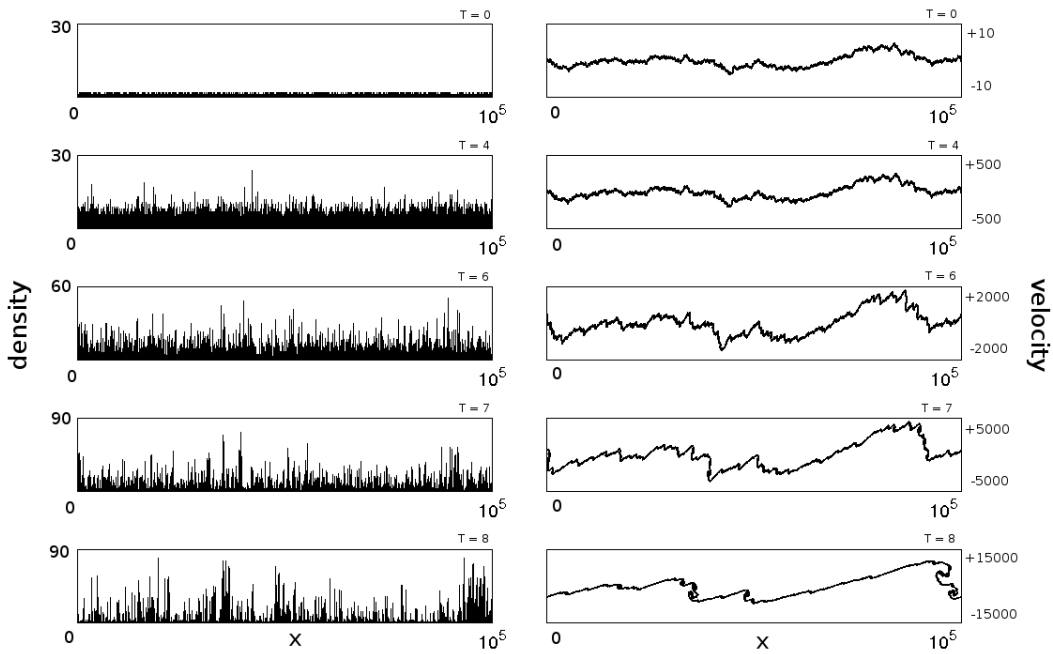


Figure 4.5: Evolution in configuration space (left hand panels) and in one particle phase space -  $\mu$ -space - (right hand panels) starting with an initial PS  $P_{init} \propto k^0$  for the expanding (quintic) model at time  $t_s = 0, 4, 6, 7, 8$ . The unit of length is given by the initial lattice spacing  $\ell = L/N$ , and thus  $L = N = 10^5$ .

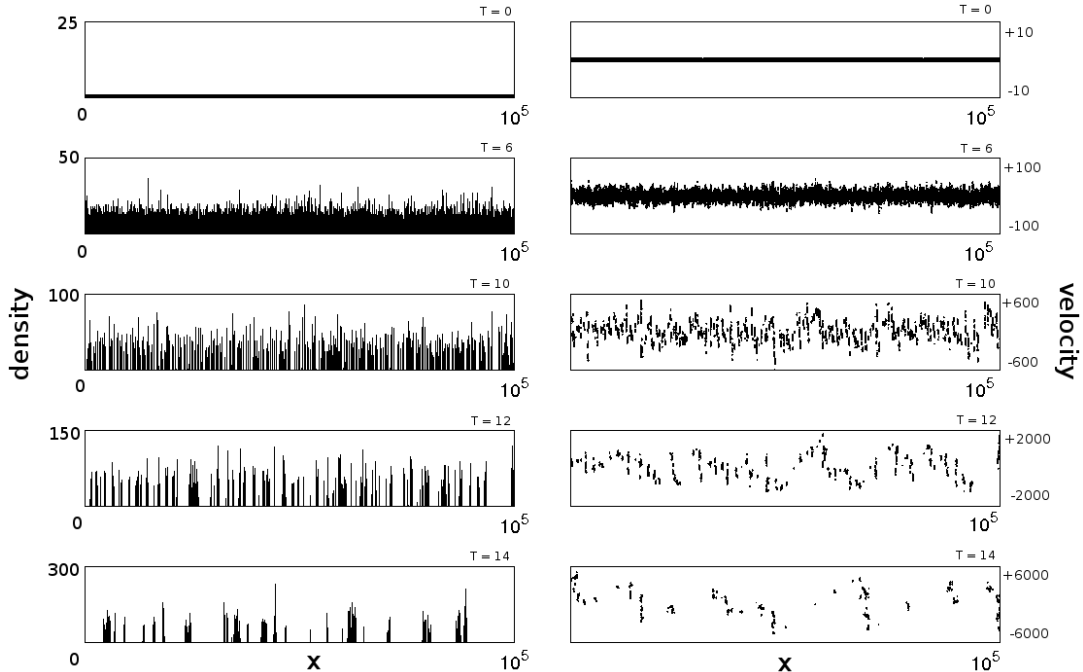


Figure 4.6: Evolution in configuration space (left hand panels) and in one particle phase space -  $\mu$ -space - (right hand panels) starting with an initial PS  $P_{init} \propto k^2$  for the expanding (quintic) model at time  $t_s = 0, 6, 10, 12, 14$ . The unit of length is given by the initial lattice spacing  $\ell = L/N$ , and thus  $L = N = 10^5$ .

## Memory of initial conditions

It is interesting to compare visually the evolution of clustering in the two cases (static and expanding). Note that the simulations are started for each value of  $n$  from identical initial conditions (*i.e.* the same realization of the displacements). We show in Figs. 4.7 and 4.8 the evolution of the density field, smoothed, as in previous plots, at the scale of initial lattice spacing, for initial PS  $P_{init}(k) \propto k^0$  and  $k^2$ .

We see that the principal structures are formed approximately at the same spatial locations in the two cases. That our choice of “time correspondence” Eq. (4.31) is appropriate is, as we will see below, reflected in the fact that, if we smooth the structures on large scale, the two configurations strongly resemble one another. This is indicative of the central role of the linear amplification of density fluctuation discussed in Chapter 2, which leads to the development of structures from the “seed” overdensities in the initial conditions. The amplitude of the density field in the expanding case (blue representation in Figs. 4.7 and 4.8) is clearly typically higher than that in the static case (red representation in Fig. 4.7 and 4.8). This can be explained by the fact that in the expanding case there is simply an additional damping term: as we will discuss in detail below, the effect of this term is that it simply causes, in the highly clustered regions, the structures to “shrink” in size compared to the static case. This “shrinking” is induced by the “cooling” associated with the damping term.

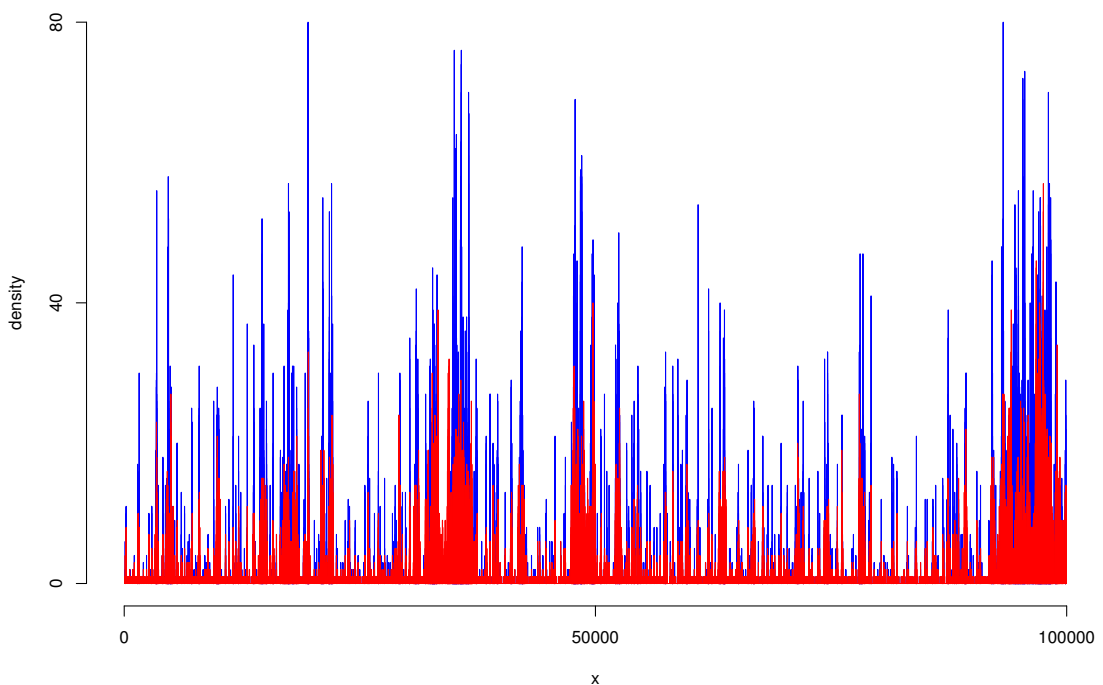


Figure 4.7: Density field (smoothed on initial lattice spacing) for the static (red) and expanding (blue) models obtained from identical initial condition for an initial PS  $P_{init}(k) \propto k^0$  at  $t_s = 8$ .

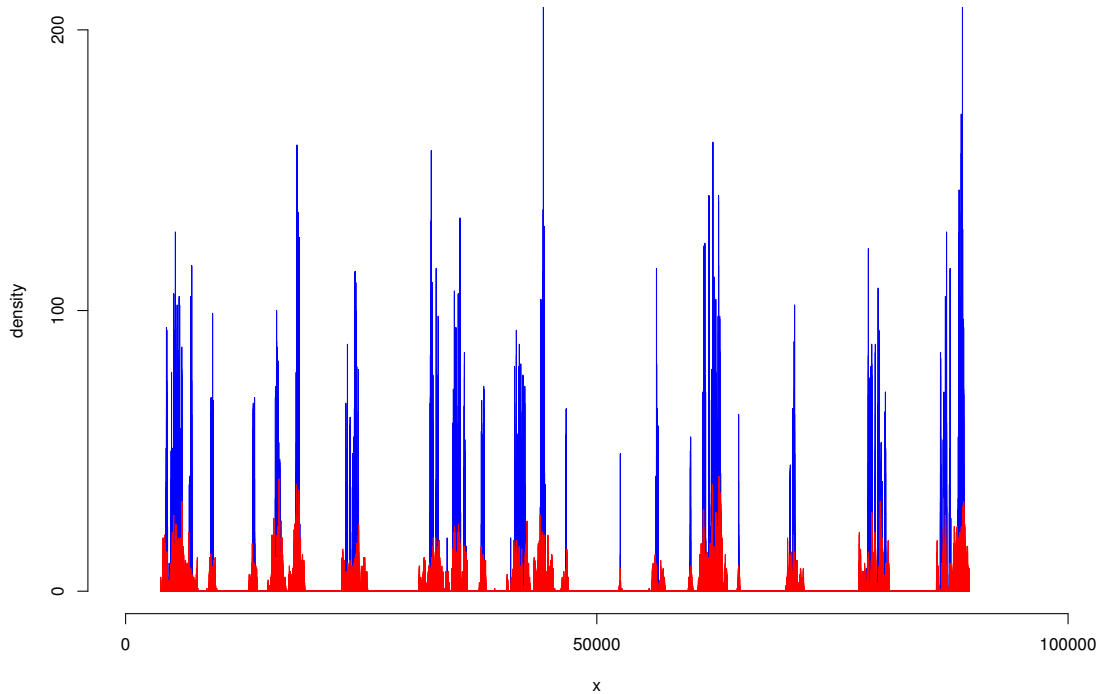


Figure 4.8: Density field (smoothed on initial lattice spacing) for the static (red) and expanding (blue) models obtained from identical initial condition for an initial PS  $P_{init}(k) \propto k^2$  at time  $t_s = 14$ .

We show in Fig. 4.9, a spatial zoom in the case of  $P_{init}(k) \propto k^2$ : starting with a subsystem of width of approximately  $3.10^4$  (in units where the size of the box  $L = N = 10^5$ ) selected out from the simulation box, we perform a zoom, between each plot, by about a factor of five, *i.e.* each plot shows a small part of the previous one, the scale on the  $x$ -axis being multiplied in each case by this factor. Although we are limited in this particular representation by the chosen resolution (we have fixed the size of the bin in the histogram equal to the initial lattice spacing), we see that our numerical simulation gives the opportunity to resolve non-trivial clustering in the system over a large range of scale (in  $3 - d$  it is typically limited to two or at very most three orders of magnitude). At large scales, we observe that the structures are formed at the same places in the static and expanding cases. However, when we zoom in, we see that this correspondence is lost. This is a reflection of the fact that the non-linear physics, which comes into play at smaller scales, wipes out memory of the initial condition.

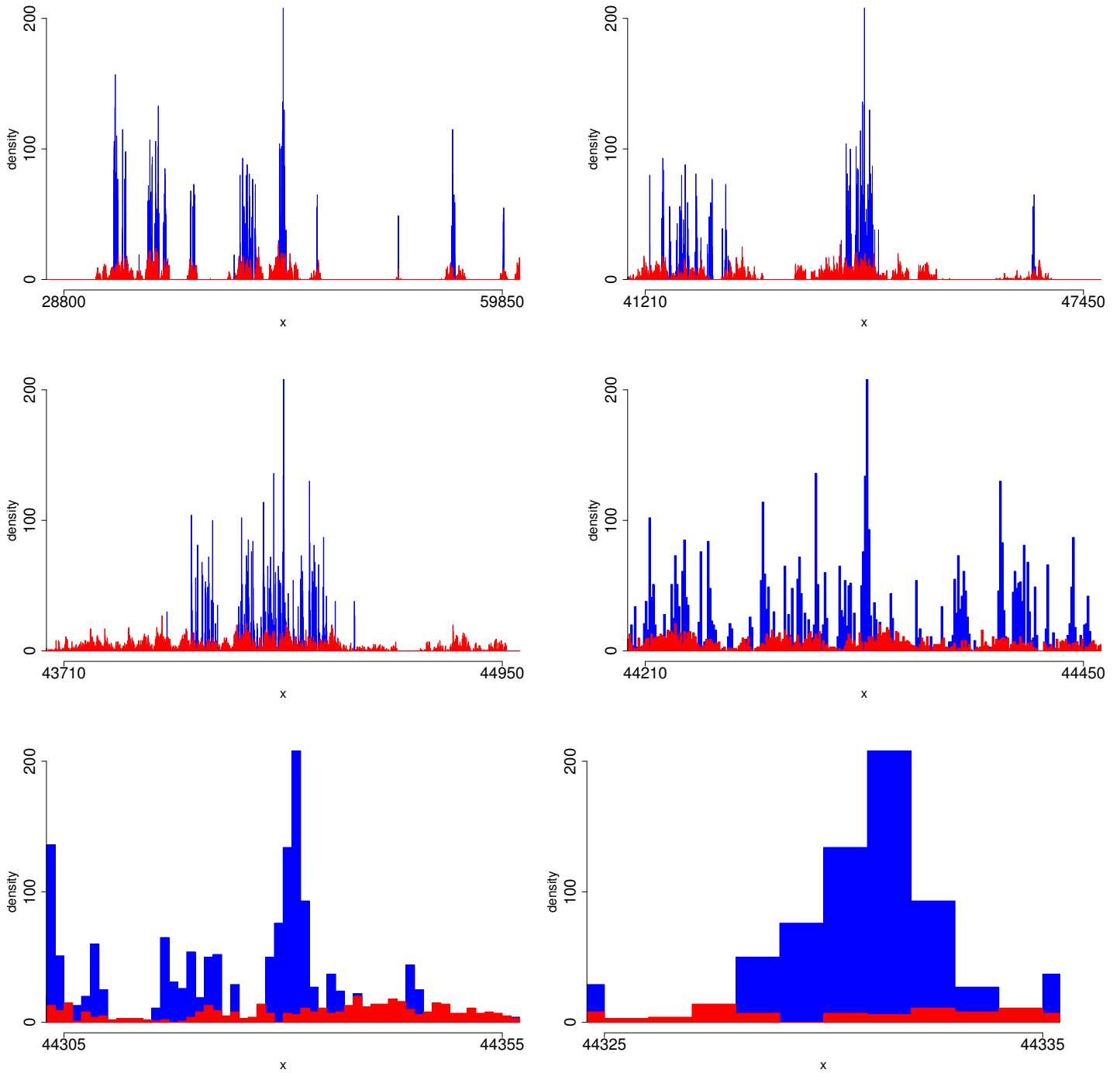


Figure 4.9: Representation of the superposition of the density field in the static (red) and expanding (blue) cases for an initial power PS  $P_{init}(k) \propto k^2$ . Between each pictures a “zoom” of factor 5 is applied, *i.e.* each plot shows a small part of the previous one, the scale on the  $x$ -axis being multiplied in each case by this factor. We are limited by the resolution chosen.

## 2.2 Development of fluctuations in real space: hierarchical clustering

In order to distinguish the *non-linear* regime of large fluctuations from the *linear* regime of small fluctuations (in which the linear fluid theory introduced in Chapter 2 is expected to be valid), it is useful to consider, just as in  $3 - d$ , the normalized variance of particle number (or mass) in intervals, defined in Chapter 2, section 4. The homogeneity scale, already defined in Chapter 2, and denoted  $\lambda_0$ , marks this cross-over from large to small fluctuations. An alternative definition of  $\lambda_0$  is the length-scale at which the normalized mass variance is of order unity, *i.e.*

$$\sigma^2(\lambda_0) \simeq 1, \quad (4.43)$$

and  $\sigma^2(x) < 1$  for  $\forall x > \lambda_0$  (this definition of the homogeneity scale can however be misleading when the average density is not a well-defined property of the system, as in fractal particle distributions (see e.g. [71]), but is appropriate here where the mean density is indeed non-zero and known exactly). Through the study of the normalized mass variance we will probe in the following the validity of the linearized fluid theory as well as the hierarchical nature of the clustering.

We start here with the analysis of the temporal evolution of  $\sigma^2(x)$ . We show in Figs. 4.10, 4.11, 4.12 and 4.13 its temporal evolution in the static and expanding (quintic) cases, starting with initial PS  $P_{init}(k) \propto k^0$  and  $k^2$ . In each case, we can distinguish three distinct regimes: at large scales we see a simple amplification of the initial functional behaviour. In the case of  $P_{init}(k) \propto k^n$  with  $n > 1$ , this corresponds to  $\sigma^2(x) \propto x^{-2}$ . This behaviour simply corresponds, as explained in Chapter 2, to unnormalized mass fluctuations independent of scale, which is the most rapid decay (proportional to the surface) possible in any spatially homogeneous point distribution, *i.e.*  $\sigma^2(x) \propto x^{-d+1}$  where  $d$  represents the dimension of the Euclidean space ( $d = 1$  in our model). In the case  $P(k) \propto k^n$  with  $n < 1$  the large scales behaviour simply corresponds to  $\sigma^2(x) \propto x^{-d+n}$ , with  $d = 1$ . Thus for  $n = 0$  we have  $\sigma^2(x) \propto x^{-1}$ .

At small scales, we observe in all cases  $\sigma^2(x) \propto x^{-1}$ . This is the shot noise behaviour intrinsic to any such distribution at small scales. The range of scales between these two limiting behaviours is that of the *non-linear* clustering. We see qualitatively that the “cross-over” to this non-linear regime from the linear regime occurs approximately where the amplitude of the fluctuations is of order unity.

To study the validity of the linear theory and illustrate the “hierarchical” nature of the clustering, we consider further the temporal evolution of the scale  $\lambda(\alpha, t)$  defined by the relation

$$\sigma^2(\lambda(\alpha, t), t) = \alpha, \quad (4.44)$$

where  $\alpha$  is a chosen constant. Let us note that if we fix  $\alpha = 1$ , we recover the definition for the homogeneity scale Eq. (4.43). We represent in Figs. 4.14 and 4.15 the temporal evolution of the scale  $\lambda(\alpha, t)$  for different values of  $\alpha$  and for different initial PS  $P_{init}(k) \propto k^0$  and  $k^2$ . For  $\alpha < 1$ , which corresponds to the regime of small fluctuations, we see that the scale  $\lambda(\alpha, t)$  increases in time, *i.e.* the scale at which linear theory would be expected to remain valid increases. This means that, as non-linearity develops at small-scale, homogeneity is still valid at larger scale for

which we are still in the regime of small fluctuations. This is completely analogous to what is observed in  $3 - d$  simulations of hierarchical clustering, which is generic in the evolution of  $3 - d$  simulations starting from this kind of initial condition: the initial small fluctuations at a given “non-linear” scale are amplified, as described by linear theory, until the fluctuations in overdense regions collapse forming structures.

For an initial condition with a PS with  $n < 1$  it is simple to derive the prediction which follows from linear theory alone for the growth of the scale  $\lambda(\alpha, t)$  for  $\alpha < 1$ . Indeed, we have seen in Chapter 2 that for  $n < 1$ ,  $\sigma^2(x, t) \sim k^d P(k, t) \Big|_{k \sim x^{-1}}$ . Thus the linear amplification of  $P(k, t)$  discussed in Chapter 2, *i.e.*  $P(k, t) = A(t) P(k, 0)$  for sufficiently small  $k$ , where  $A(t)$  may be inferred in each case from the set of Eqs. (4.32), implies

$$\sigma^2(x, t) = A(t) \sigma^2(x, 0) \quad (4.45)$$

*i.e.* the variance in real space is amplified linearly also. For  $P(k) \propto k^n$ , we have  $\sigma^2(x, t) \sim \frac{1}{x^{n+1}}$ , thus

$$\sigma^2(\lambda(\alpha, t), t) = \alpha = A(t) \sigma^2(\lambda(\alpha, t), 0) = A(t) \left( \frac{\lambda(1, 0)}{\lambda(\alpha, t)} \right)^{1+n}, \quad (4.46)$$

which gives

$$\lambda(\alpha, t) \propto A^{1+n}(t) = R_s(t). \quad (4.47)$$

where  $R_s(t)$  is the scaling factor derived in Chapter 2 in the discussion of self-similarity. We see in Figs. 4.14 and 4.15 that these behaviours in fact fit well the behaviour of  $\lambda(\alpha, t)$  not just for  $n < 1$  and  $\alpha < 1$ , but they work also for  $n > 1$  and, at sufficiently long times, for  $\alpha > 1$  for both cases. This is a result of the *self-similar* evolution of the system which we discuss in the following section in detail. Note that, for  $n = 2$ , we have  $\sigma^2 \propto \frac{1}{x^2}$  at large  $x$ , and thus  $\sigma^2(x, t) \sim R_s^2(t) \sigma^2(x, 0) \not\propto A(t) \sigma^2(x, 0)$  at large  $x$ , *i.e.* we do not obtain the amplification of Eq. (4.46).

Let us note that the fact that in the case  $n = 0$ , for  $\alpha = 0.1$  which correspond to a scale of small fluctuations, the points at early time do not match the linear amplification prediction (the line symbolizing  $R_s(t)$ ) can be simply explained by the fact that the mass-variance  $\sigma^2(x, t)$  is dominated at early times by large  $k$ .

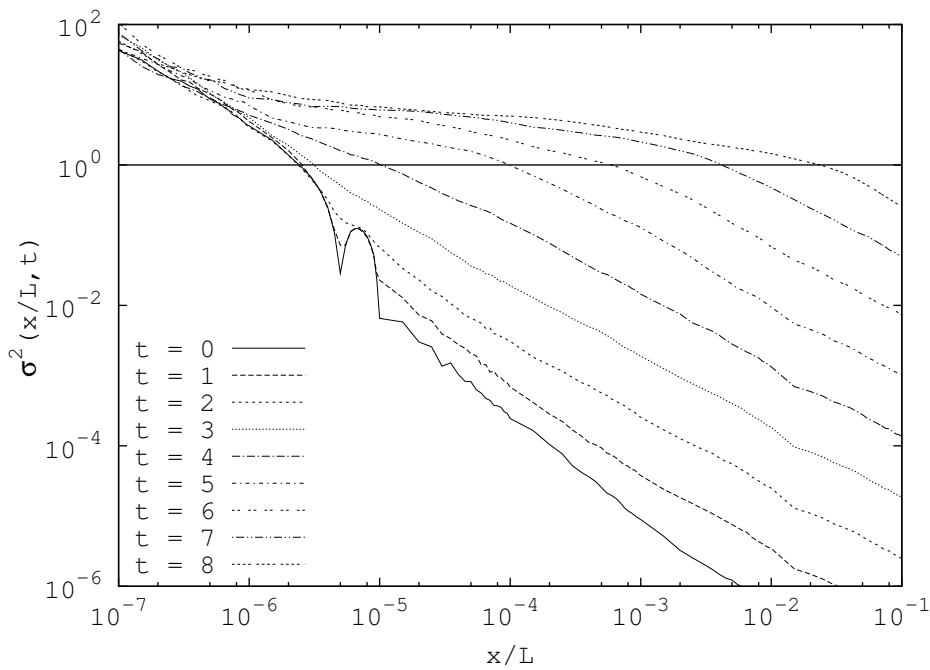


Figure 4.10: Evolution of the mass variance in the static case starting with an initial PS  $P_{init}(k) \propto k^0$  at  $t_s = 0, 1, 2, 3, 4, 5, 6, 7, 8$ . The  $x$ -axis is normalized by the box size.

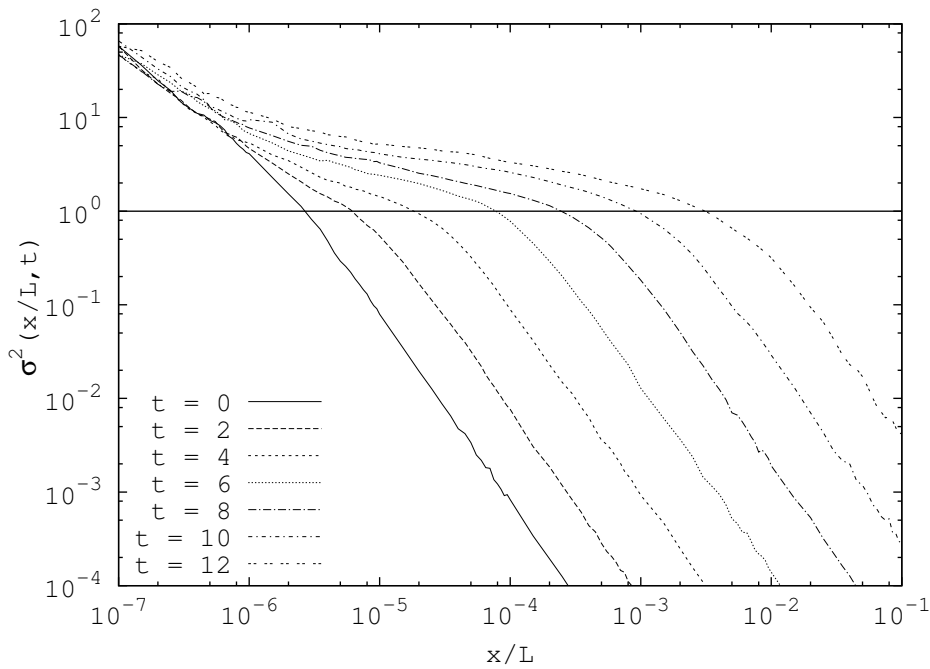


Figure 4.11: Evolution of the mass variance in the static case starting with an initial PS  $P_{init}(k) \propto k^2$  at  $t_s = 0, 2, 4, 6, 8, 10, 12$ . The  $x$ -axis is normalized by the box size.

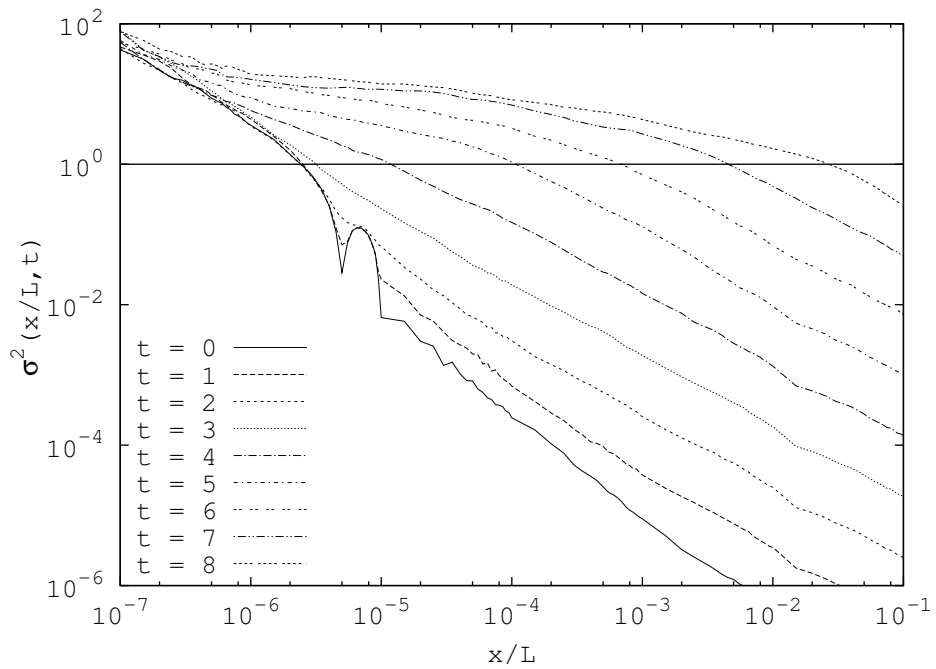


Figure 4.12: Evolution of the mass variance in the expanding (quintic) case starting with an initial PS  $P_{init}(k) \propto k^0$  at  $t_s = 0, 1, 2, 3, 4, 5, 6, 7, 8$ . The  $x$ -axis is normalized by the box size.

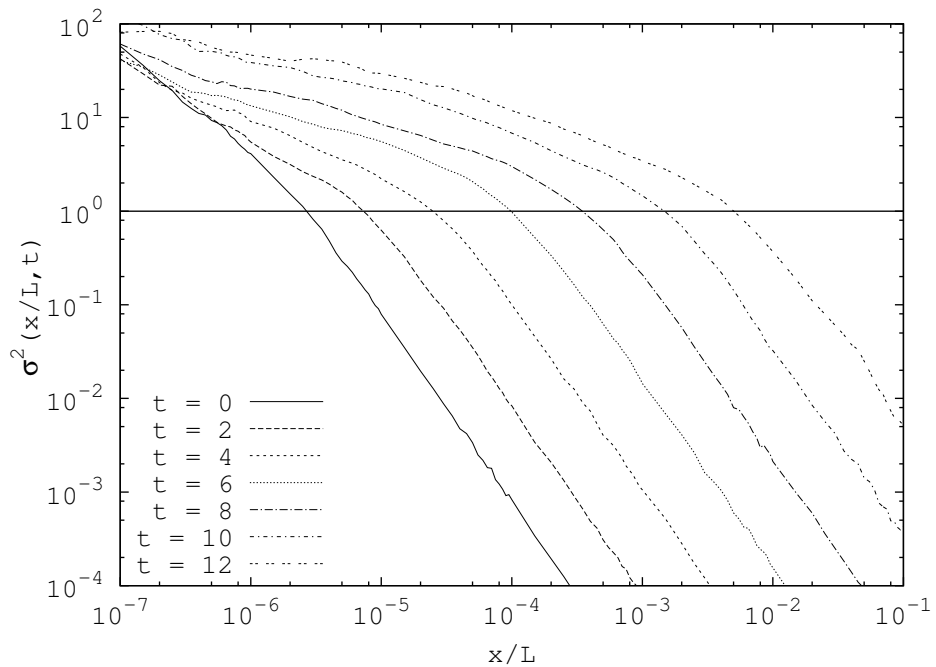


Figure 4.13: Evolution of the mass variance in the expanding (quintic) case starting with an initial PS  $P_{init}(k) \propto k^2$  at  $t_s = 0, 2, 4, 6, 8, 10, 12$ . The  $x$ -axis is normalized by the box size.

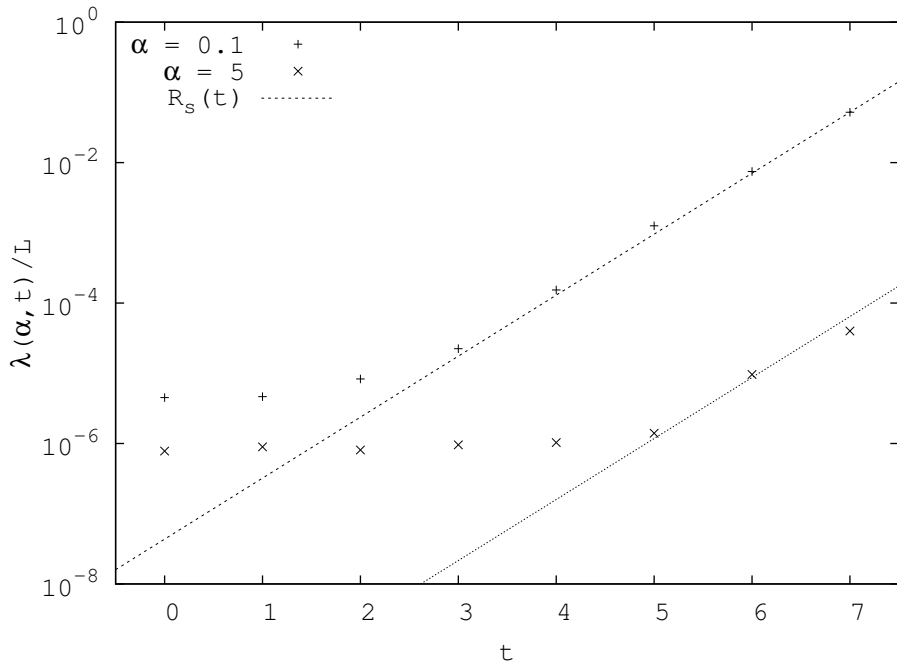


Figure 4.14: Evolution of the scale  $\lambda(\alpha, t)$  defined in Eq. (4.44) starting with an initial PS  $P_{init}(k) \propto k^0$  in the static case.

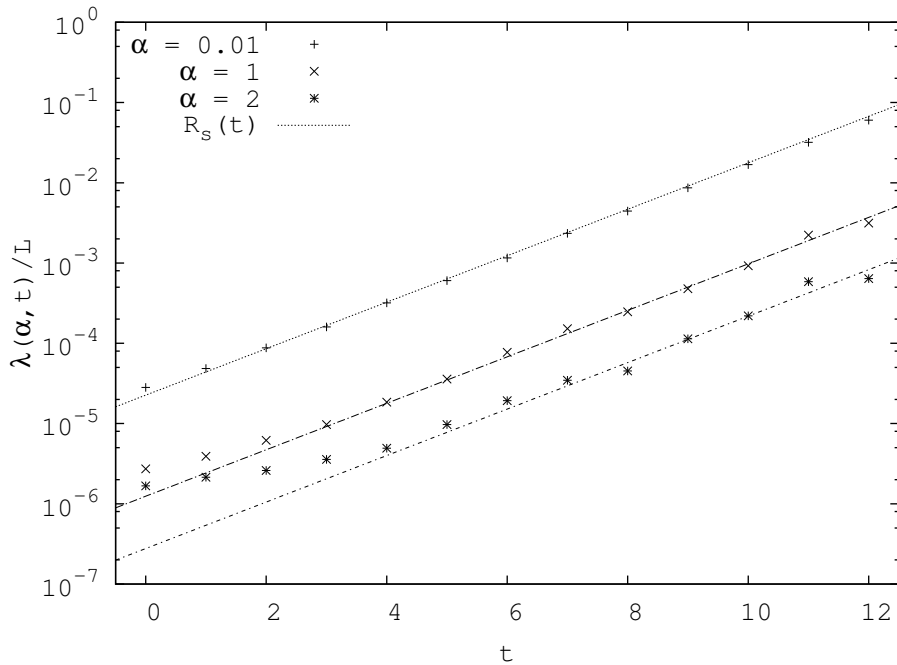


Figure 4.15: Evolution of the scale  $\lambda(\alpha, t)$  defined in Eq. (4.44) starting with an initial PS  $P_{init}(k) \propto k^2$  in the static case.

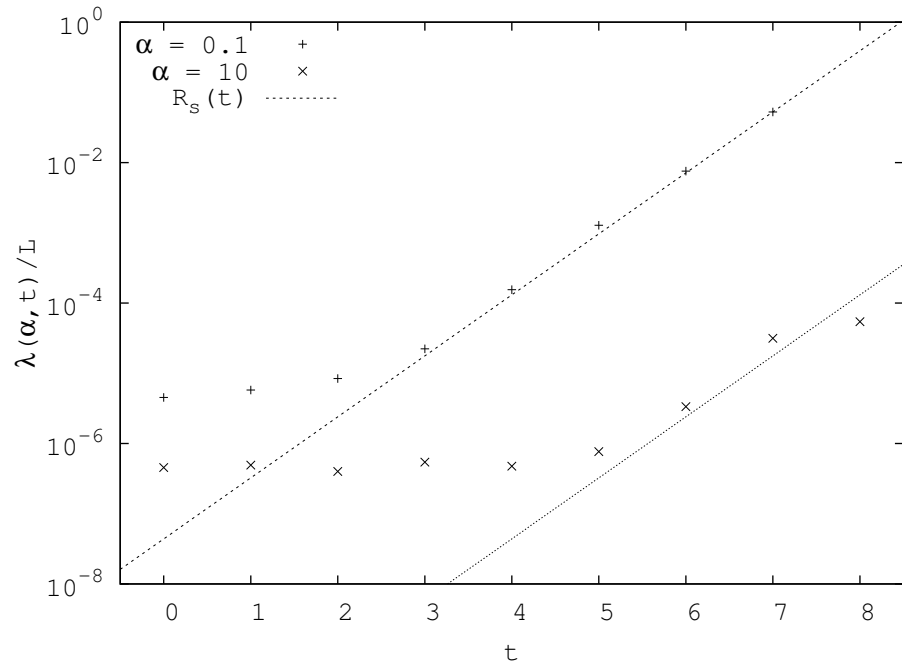


Figure 4.16: Evolution of the scale  $\lambda(\alpha, t)$  defined in Eq. (4.44) starting with an initial PS  $P_{init}(k) \propto k^0$  in the expanding (quintic) case.

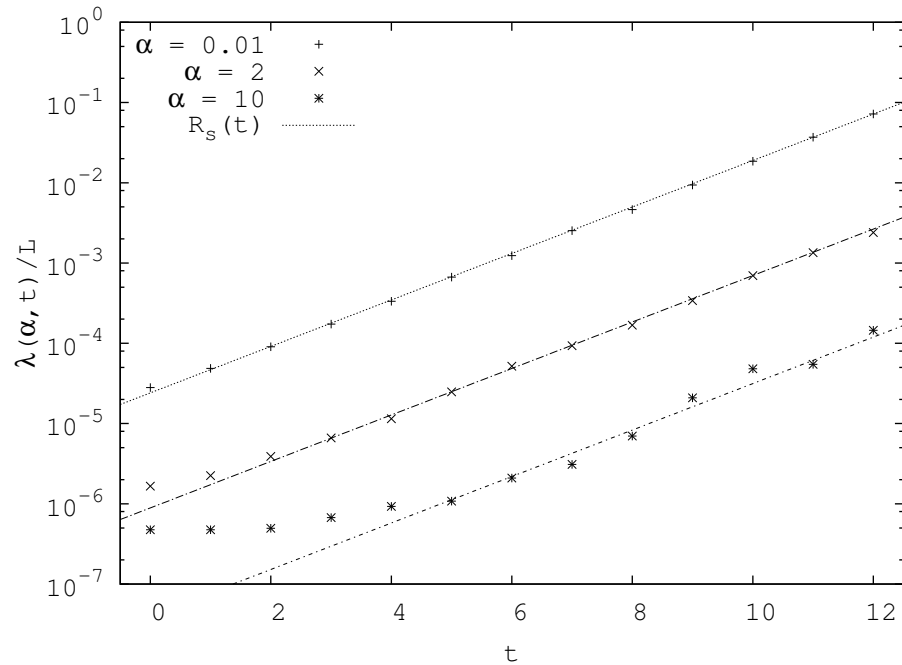


Figure 4.17: Evolution of the scale  $\lambda(\alpha, t)$  defined in Eq. (4.44) starting with an initial PS  $P_{init}(k) \propto k^2$  in the expanding (quintic) case.

## 2.3 Development of correlation in real space: self-similarity

We next consider the evolution of clustering in real space as characterized by the reduced two-point correlation function,  $\xi(x)$ , introduced in Chapter 2.

In Figs. 4.18, 4.19, 4.20 and 4.21, we show the evolution of  $|\xi(x, t)|$ , the absolute value of the correlation function in a log-log plot. As expected from the study of the temporal evolution of the normalized mass variance, we observe that starting from  $\xi(x) \leq 1$  everywhere, non-linear clustering (*i.e.*  $\xi(x) \gg 1$ ) first develops around the initial interparticle distance, and then progressively develops both at larger and smaller scales. At any given scale the amplitude of correlation grows in time monotonically. In particular, the scale of non-linear clustering which we can define by  $\xi(\lambda_{NL}) = 1$  monotonically grows, reflecting again the hierarchical nature of the clustering discussed in the previous sections.

Once the correlation has evolved in all cases a  $\xi$  emerges in which one can identify three distinct regimes:

1. an approximately flat (constant)  $\xi(x, t) = \xi_{max}(t)$  at small scale, below a scale  $x_{min}$ ;
2. a region of strong clustering  $\xi$  with approximately power law behaviour;
3. a region of weak clustering,  $\xi < 1$ , where the clustering signal becomes very noisy.

Let us now turn to the question of whether the evolution is *self-similar*. As discussed in Chapter 2, this means that the system evolves towards a behaviour

$$\xi(x, t) \approx \Xi(x/R_s(t)), \quad (4.48)$$

*i.e.* towards a dynamical scaling behaviour of the correlation function, where  $R_s(t)$  is the scaling factor predicted by the linearized fluid theory. To test this we show in Figs. 4.22, 4.23, 4.24 and 4.25 the appropriately rescaled version of the previous figures, *i.e.* we represent the absolute value of the correlation function  $|\xi(x, t)|$  as a function of  $x/R_s(t)$  where  $R_s(t) = \exp\left(\frac{2(t_s - t_{ref})}{n+1}\right)$  in  $1-d$ , with  $t_{ref}$  some arbitrary time, has been introduced in Chapter 2. We observe that in all cases the curves indeed superimpose well in a range of scale which grows monotonically in time, *i.e.* the spatial range in which self-similarity is valid becomes more and more extended. The “break” from self-similarity at small scales is clearly associated with a plateau at these scales in the correlation function. Indeed such a plateau can only be consistent with self-similarity if its amplitude does not evolve, which is clearly not the case. At large scale the noise in  $\xi$  makes it difficult to assess whether self-similarity applies. We will see in the next section that it does indeed apply as expected at large scales where it reflects the validity of linear theory.

In the non-linear regime, and where self-similarity is valid, the correlation function fits to a good approximation in all cases

$$\Xi(x) \propto x^{-\gamma}, \quad (4.49)$$

where  $\gamma(n, \Gamma)$  depends on the index  $n$  of the initial PS and on the value of the damping term  $\Gamma$ . We give in Table 2.3 the values of the power index  $\gamma(n, \Gamma)$  obtained

| initial PS | static ( $\Gamma = 0$ )  | quintic ( $\Gamma = 1/\sqrt{6}$ ) | RF ( $\Gamma = 1/\sqrt{2}$ ) |
|------------|--------------------------|-----------------------------------|------------------------------|
| $n = 0$    | $\gamma = 0.18 \pm 0.03$ | $\gamma = 0.20 \pm 0.05$          | $\gamma = 0.25 \pm 0.02$     |
| $n = 2$    | $\gamma = 0.18 \pm 0.03$ | $\gamma = 0.34 \pm 0.03$          | $\gamma = 0.50 \pm 0.02$     |

Table 4.1: power index  $\gamma(n, \Gamma)$  of the correlation function in the self-similar regime  $\Xi_{SS}(x) \propto x^{-\gamma}$ , for the different values of  $n$  and  $\Gamma$  indicated. We consider both the static and expanding (quintic and RF) cases. The different values of  $\gamma$  and the corresponding error bars are obtained with a linear interpolation. We see that the power index  $\gamma$  depends on the index  $n$  of the initial power spectrum and the damping term  $\Gamma$ .

with a linear interpolation.

Note that in  $3 - d$  similar trends are observed:

- $\gamma$  is independent of  $n$  for static model (see e.g. [11]);
- $\gamma$  increases with  $n$  in expanding (EdS) model (see e.g. [139]).

A striking difference between the static and expanding cases is that  $x_{min}$  decreases very significantly in the expanding case, while it remains roughly constant in the static case. We will come back to study more carefully these behaviours in section 4 below.

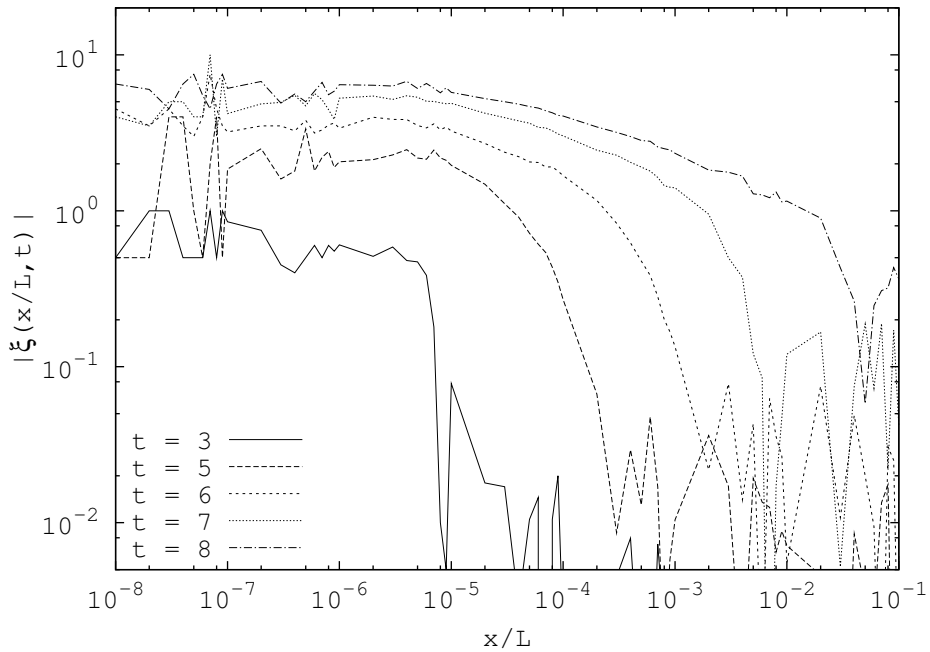


Figure 4.18: Evolution in time of the reduced 2-point correlation function starting with an initial PS  $P_{init}(k) \propto k^0$  in the static model. The  $x$ -axis is normalized by the box size.

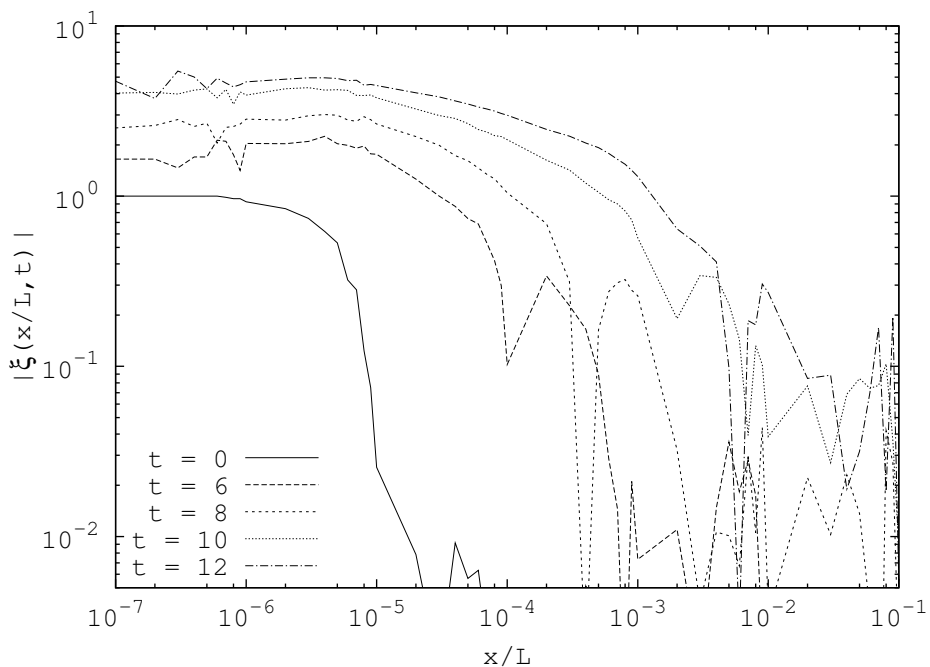


Figure 4.19: Evolution in time of the reduced 2-point correlation function starting with an initial PS  $P_{init}(k) \propto k^2$  in a static universe. The  $x$ -axis is normalized by the box size.

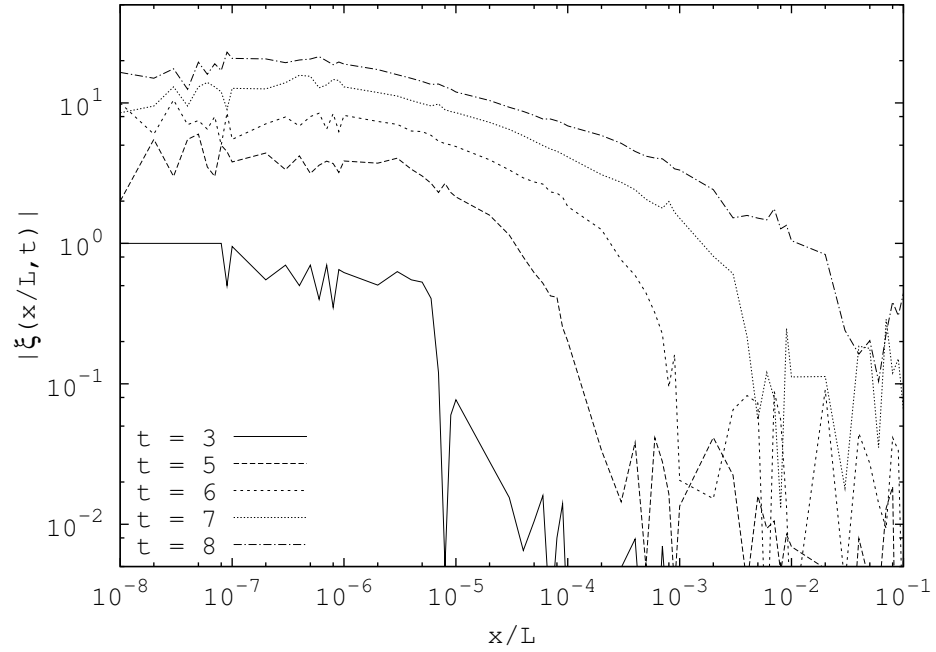


Figure 4.20: Evolution in time of the reduced 2-point correlation function starting with an initial PS  $P_{init}(k) \propto k^0$  in an expanding (quintic) universe. The  $x$ -axis is normalized by the box size.

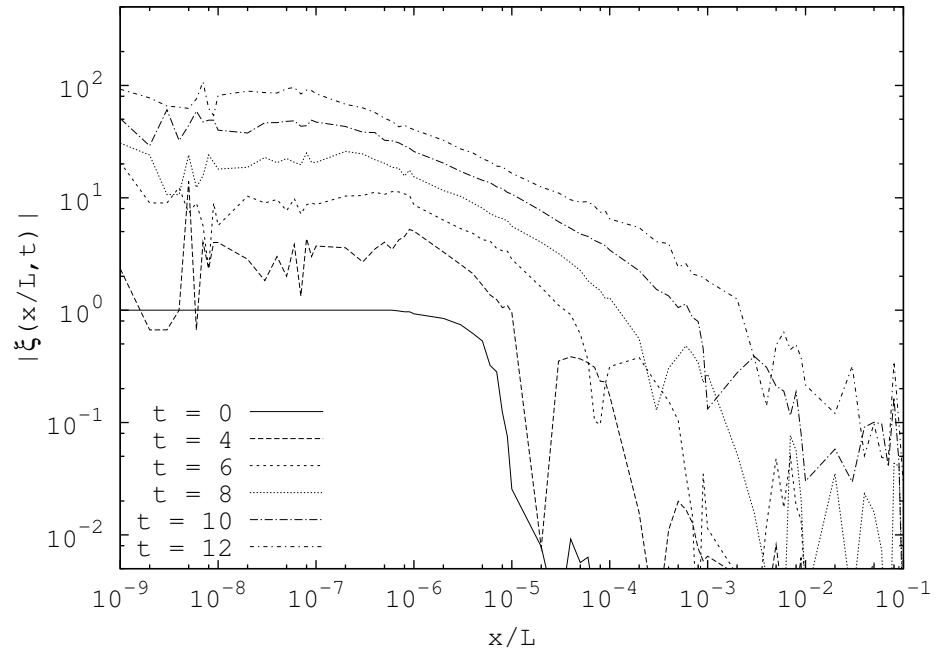


Figure 4.21: Evolution in time of the reduced 2-point correlation function starting with an initial PS  $P_{init}(k) \propto k^2$  in an expanding (quintic) universe. The  $x$ -axis is normalized by the box size.

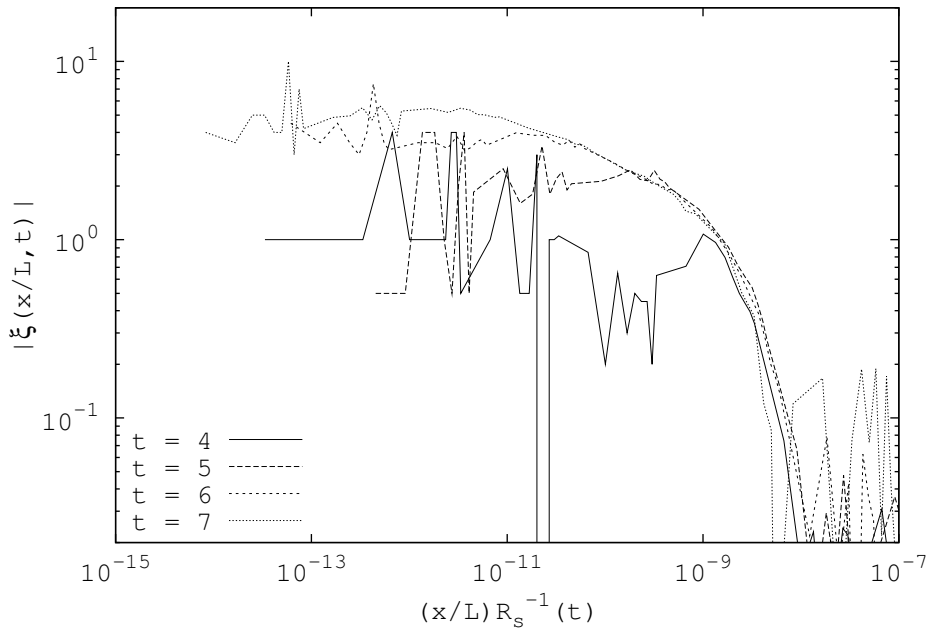


Figure 4.22: Evolution in time of the correlation function as a function of  $x/R_s(t)$  starting with an initial PS  $P_{init}(k) \propto k^0$  in a static universe. The  $x$ -axis is normalized by the box size.

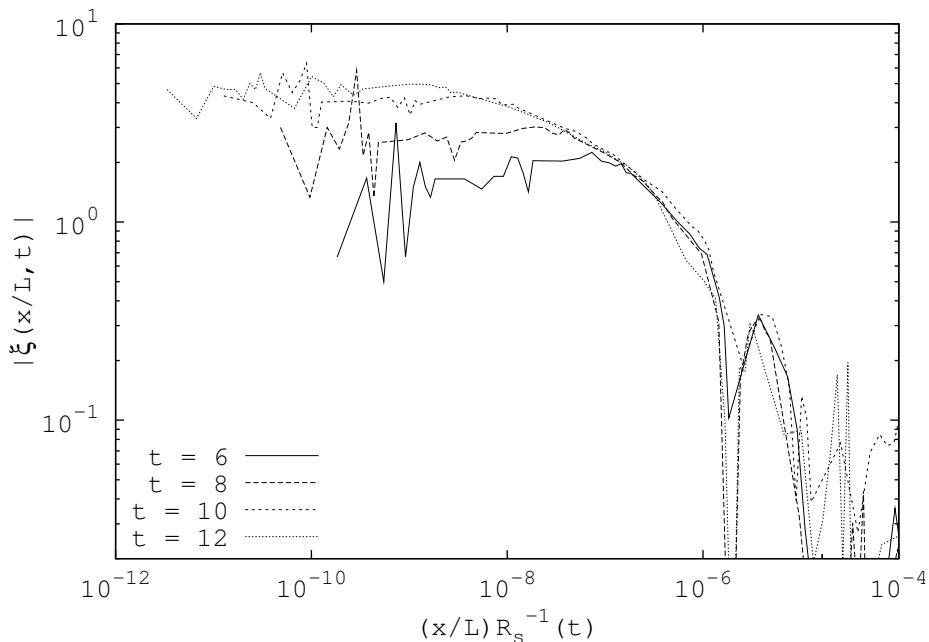


Figure 4.23: Evolution in time of the correlation function as a function of  $x/R_s(t)$  starting with an initial PS  $P_{init}(k) \propto k^2$  in a static universe. The  $x$ -axis is normalized by the box size.

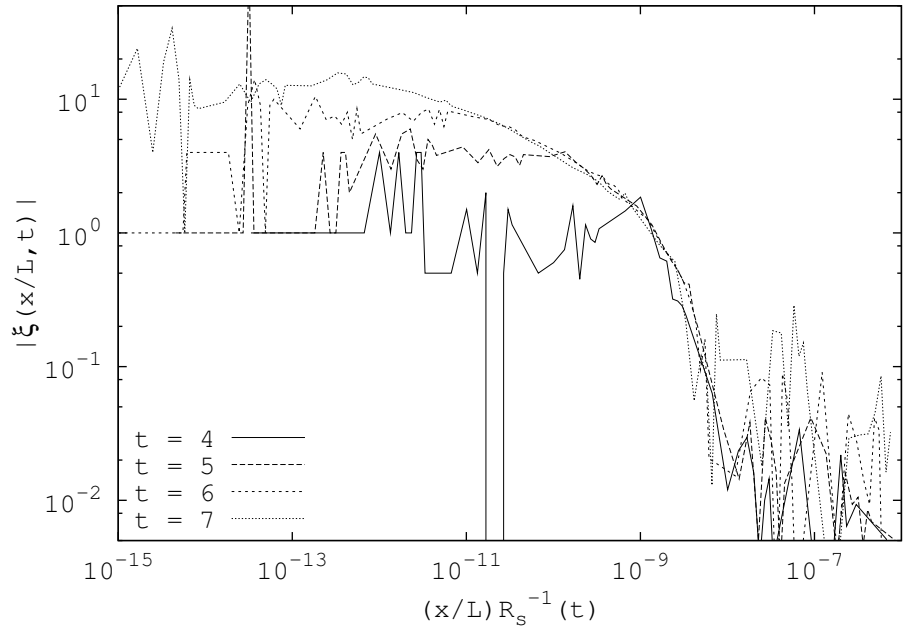


Figure 4.24: Evolution in time of the correlation function as a function of  $x/R_s(t)$  starting with an initial PS  $P_{init}(k) \propto k^0$  in an expanding (quintic) universe. The  $x$ -axis is normalized by the box size.

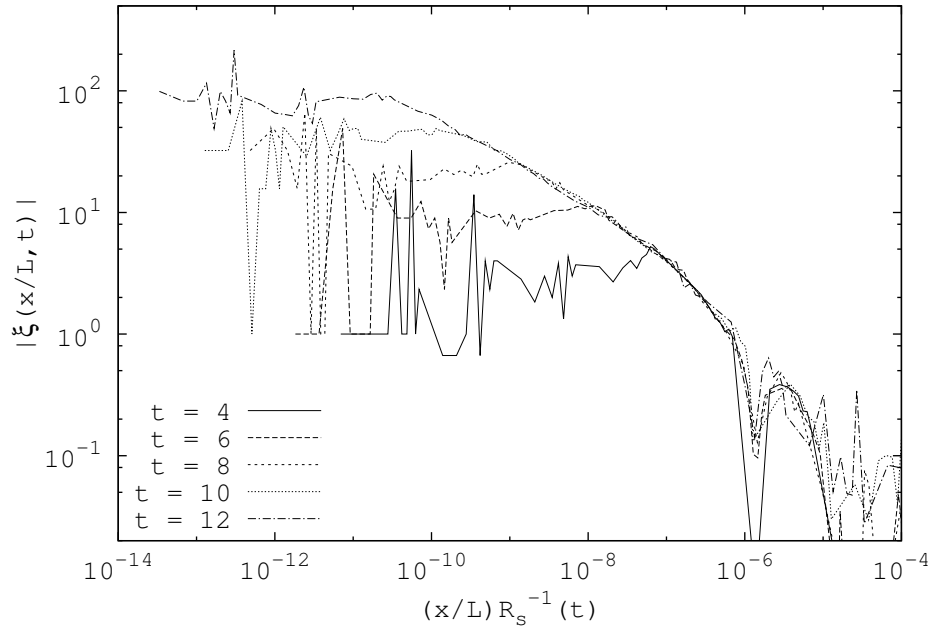


Figure 4.25: Evolution in time of the correlation function as a function of  $x/R_s(t)$  starting with an initial PS  $P(k) \propto k^2$  in an expanding (quintic) universe. The  $x$ -axis is normalized by the box size.

## 2.4 Development of correlations in reciprocal space

We next analyse the evolution of correlation as characterized by the PS for the same cases.

Shown in Figs. 4.27, 4.28, 4.29 and 4.30 are the evolution of the PS in each of the same four cases above. We observe in each case that

- at small  $k$ , there is a simple amplification of the initial fluctuation which has indeed the appropriate simple power law form. This amplification corresponds to the behaviour expected from the linearized treatment of the equation for a self-gravitating fluid, *i.e.* the linear amplification. This can be simply written in the growing mode

$$P(k, t) = P(k, 0) \exp(2t_s), \quad (4.50)$$

where the relation is written in the reference time units  $t_s$ ;

- the range in which the initial PS shape is maintained, *i.e.* over which simple amplification is observed, becomes more reduced as time progresses. This simple amplification, indeed, is observed in a range of  $k < k_{NL}(t)$ , where  $k_{NL}(t)$  is a wave number which decreases as a function of time. The monotonic decrease of  $k_{NL}(t)$  just reflects the hierarchical nature of the clustering. This is precisely the qualitative behavior one would anticipate as linear theory is expected to hold only above a scale which, in real space, because of clustering, increases with time;
- at all times, the PS converges at large wave-numbers ( $k \geq k_N$ , where  $k_N = \frac{\pi}{\ell}$  is the Nyquist frequency) to the asymptotic value  $1/n_0$ . This is simply a reflection of the necessary presence of shot noise fluctuations at small scales due to the particle nature of the distribution.

The effect of expansion (*i.e.* the damping term in the equation of motion Eq. (4.1)) is illustrated more clearly in Fig. 4.26. It shows, at  $t_s = 8$ , the PS in the static and expanding (quintic and RF) models starting with identical initial conditions (*i.e.* the same realization of the displacements). We clearly see that the linear regimes are superposed as expected with the growing mode. This also reflects the effect of the damping term in the expanding cases. In the intermediate range of  $k$ , *i.e.*  $k_{NL}(t) < k \leq k_N$ , the evolution is quite different than that given by linear theory. This is the regime of nonlinear clustering in which the density fluctuations are large in amplitude.

Let us now examine how the self-similarity discussed in previous section manifests itself in the behaviour of the PS. In  $1 - d$  this corresponds to the relation

$$k P(k, t) = k R_s(t) \times P(k R_s, t_{ref}), \quad (4.51)$$

where  $R_s(t)$  is the time dependent rescaling of length, normalized by at some arbitrary time  $t_{ref}$ . As explained previously in Chapter 2, the small  $k$  behaviour of the PS taken together with the fact that it is amplified at small  $k$  as given by linear

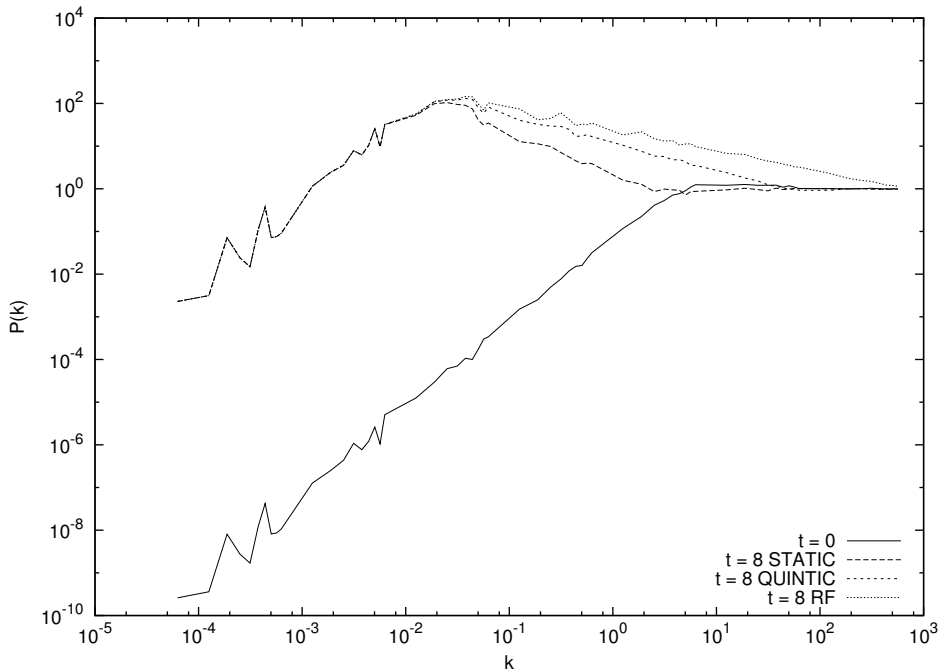


Figure 4.26: Illustration of effect of the damping term on the evolution of the scale  $k_{max}$ . We choose for comparison the evolved configuration of the static ( $\Gamma = 0$ ), the quintic ( $\Gamma = 1/\sqrt{6}$ ) and the RF ( $\Gamma = 1/\sqrt{2}$ ) models at time  $t_s = 8$ . We clearly see that the linear regimes are superposed as expected with the growing mode, and that the scale  $k_{max}$  increases when the parameter  $\Gamma$  (*i.e.* the damping) increases.

theory then imply that the self-similar scaling will be characterized in  $1 - d$  by the function

$$R_s(t) = \exp\left(\frac{2}{n+1}\frac{t_s - t_{ref}}{\tau_{dyn}}\right). \quad (4.52)$$

To assess the validity of this in our system, we show in Figs. 4.31, 4.32, 4.33 and 4.34 the temporal evolution of  $k \times P(k, t)$  as a function of the dimensionless parameter  $k \times R_s(t)$ , and taking  $t_{ref} = 0$ . At small  $k$ , we see that right from the initial time the self-similarity is indeed followed (as the rescaled curves are always superimposed at these scales). This is simply a check on the result validity of linear theory in this regime for an index  $n < 4$ , as anticipated above. As time progresses we see the range of  $k$  in which the curves are superimposed increases, extending further with time into the non-linear regime. This is precisely what is observed in the analogous 3- $d$  simulations. Note that the behavior at asymptotically large  $k$  is constrained to be proportional to  $k/n_0$  at all times, corresponding to the shot noise present in all particle distributions with average density  $n_0$  and which, by definition, does not evolve in time (and therefore cannot manifest self-similarity).

We must however notice that in the study of the temporal evolution of the PS, the behavior at asymptotically large  $k$  (proportional to  $1/n_0$ ) is different from the result that we might expect naively from the study of the correlation function. Indeed, we found that the correlation function reaches at small scales a plateau whose amplitude would correspond to an asymptotically large  $k$  behavior of the PS proportional to  $1/n_{plat} \ll 1/n_0$ . This difference can be explained by the fact that the PS contains

| intial PS | static                  | quintic                 | RF                      |
|-----------|-------------------------|-------------------------|-------------------------|
| $n = 0$   | $\beta = 0.02 \pm 0.01$ | $\beta = 0.14 \pm 0.02$ | $\beta = 0.25 \pm 0.02$ |
| $n = 2$   | $\beta = 0.01 \pm 0.01$ | $\beta = 0.35 \pm 0.02$ | $\beta = 0.50 \pm 0.02$ |

Table 4.2: power index  $\beta(n, \Gamma)$  of  $k \times P(k) \propto k^\beta$  in the self-similar regime, when  $n$  the index of the initial PS is  $n = 0$  and  $n = 2$ , and  $\Gamma$  the damping term. We consider both the static and expanding (quintic and RF) cases. The different values of  $\beta$  and the corresponding error bars are obtained with a linear interpolation. We see the dependance of  $\beta$  in  $n$  and  $\Gamma$  as observed in the correlation function.

a term proportional to  $1/n_0$  which “drowns” the signal at small scales which we can discern in the correlation function.

Defining the parameter  $\beta$  through the power-law relation

$$k \times P(k) \propto k^\beta \quad (4.53)$$

in the self-similar regime for the static and expanding models, we can extract from Figs. 4.31, 4.32, 4.33 and 4.34 the different values measured for this power index. The results are presented in table 2.4. We show in the non-linear regime, in the static and expanding models, that just as for the correlation function, the exponents  $\beta$  do not depend on  $n$  in the static case, but do show such a dependence in the expanding cases.

As the PS is the Fourier transform of the correlation function (cf. Chapter 2), we expect the power indexis  $\beta(n, \Gamma)$  and  $\gamma(n, \Gamma)$ , for a pure power law, to be equal. It is then interesting to compare the results presented in Table 2.3 and Table 2.4. We see that the values of the two different exponents are in agreement within the standard numerical error in the expanding (quintic and RF) cases. In the static case, however, we see that  $\beta$  and  $\gamma$  do not tally. We note that this difference is not limited to the  $1 - d$  study, as the same disagreement is also observed in  $3 - d$  [11] in which case  $P(k) \propto k^{-3}$  and  $\xi(r) \propto r^{-0.2}$  in the self-similar regime.

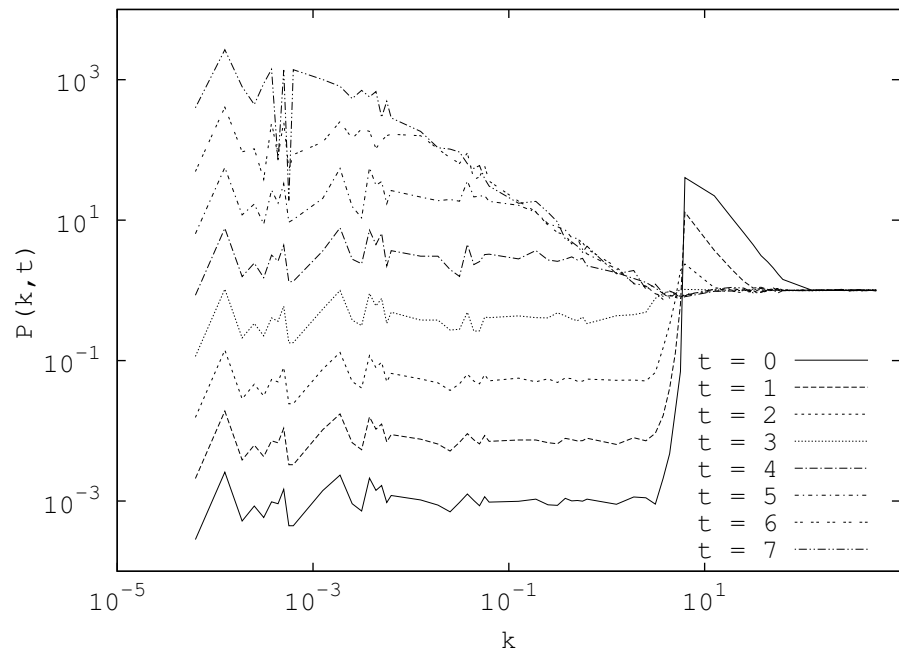


Figure 4.27: Evolution in time of the PS starting with an initial PS  $P_{init}(k) \propto k^0$  in the static case.

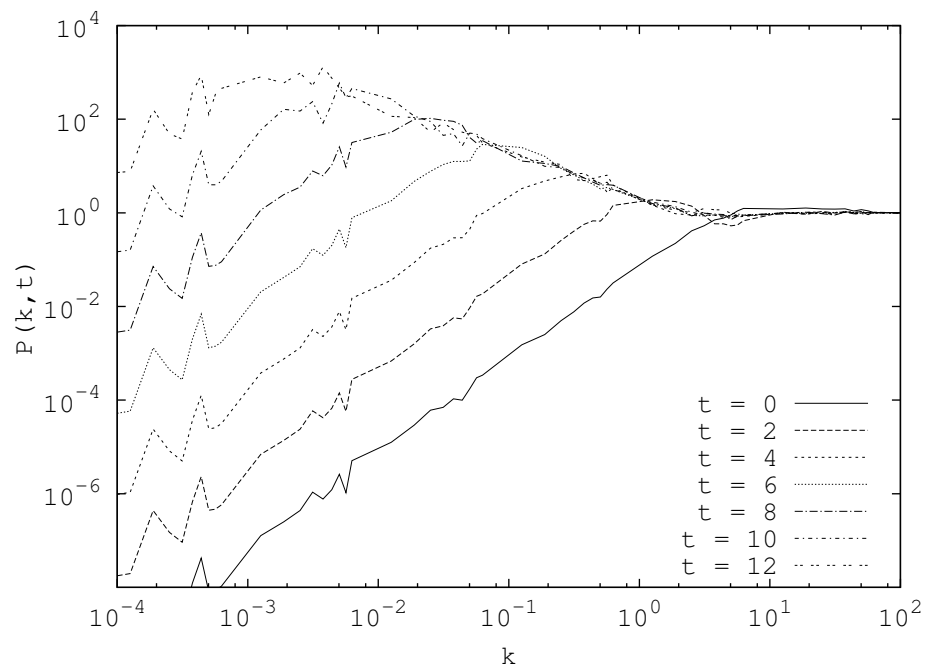


Figure 4.28: Evolution in time of the PS starting with an initial PS  $P_{init}(k) \propto k^2$  in the static case.

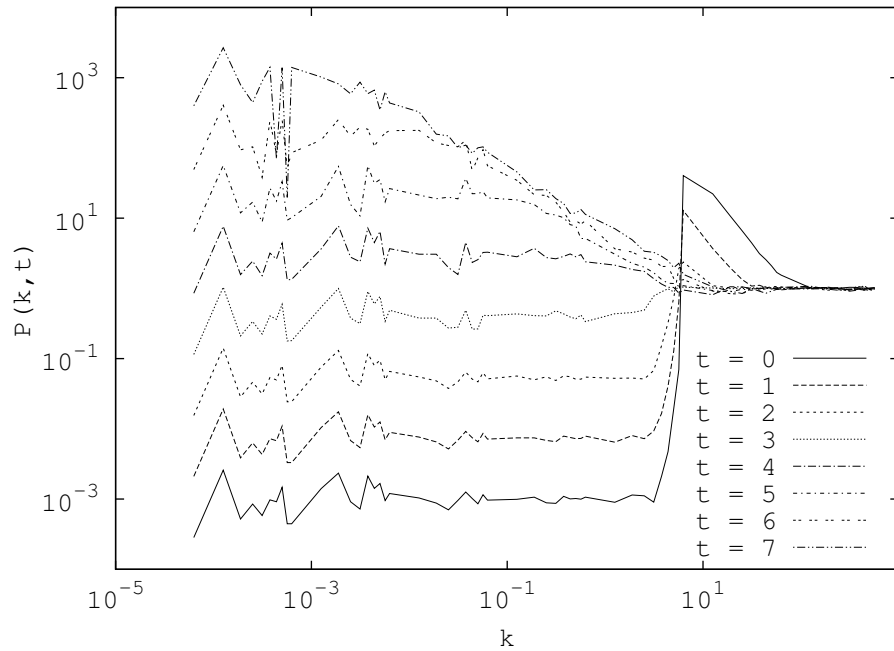


Figure 4.29: Evolution in time of the PS starting with an initial PS  $P_{init}(k) \propto k^0$  in the expanding (quintic) case.

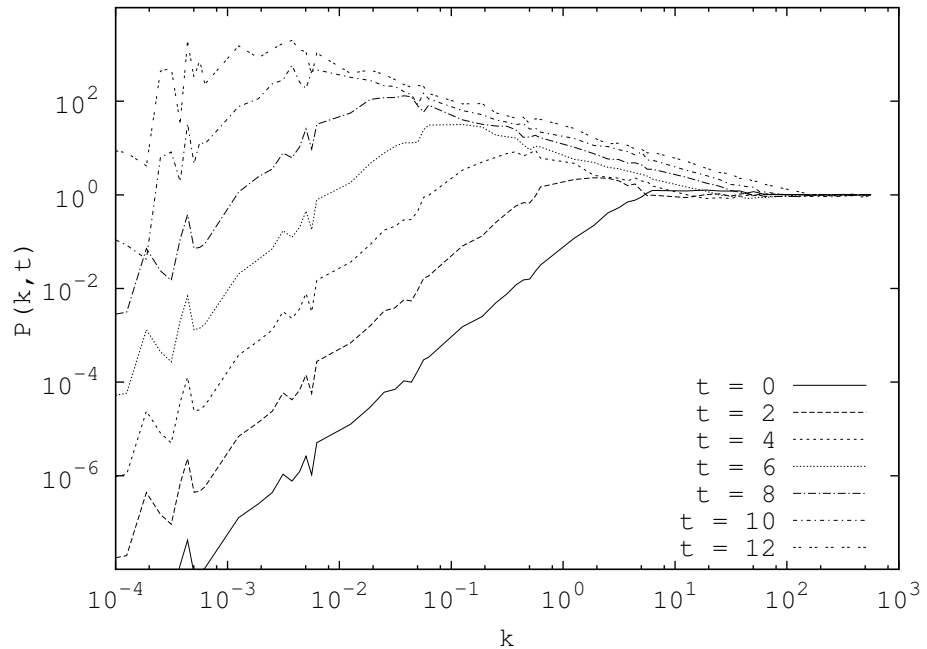


Figure 4.30: Evolution in time of the PS starting with an initial PS  $P_{init}(k) \propto k^2$  in the expanding (quintic) case.

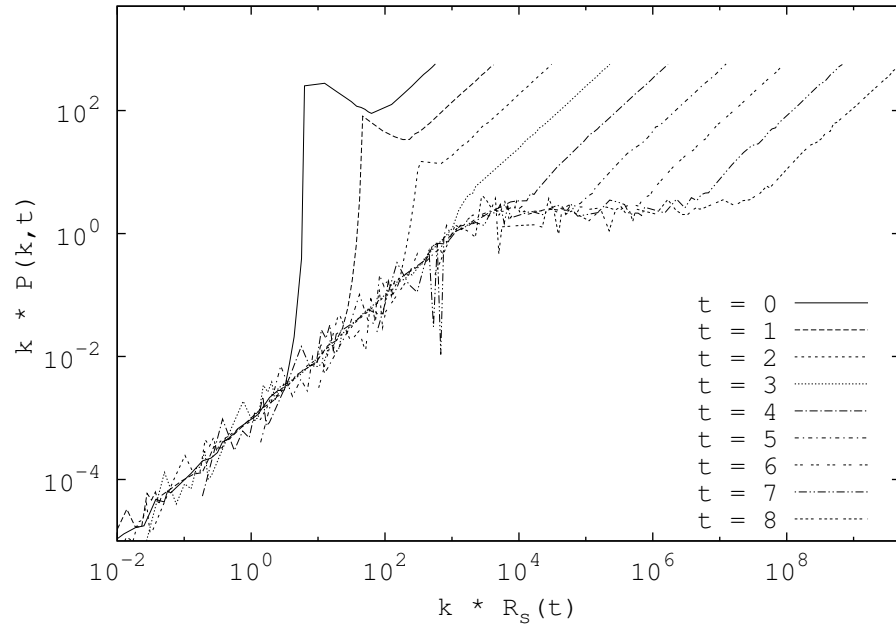


Figure 4.31: Evolution of  $k \times P(k, t)$  as a function of  $k \times R_s(t)$  where  $R_s(t)$  is given in Eq.4.52 starting with an initial PS  $P_{init}(k) \propto k^0$  in the static case.

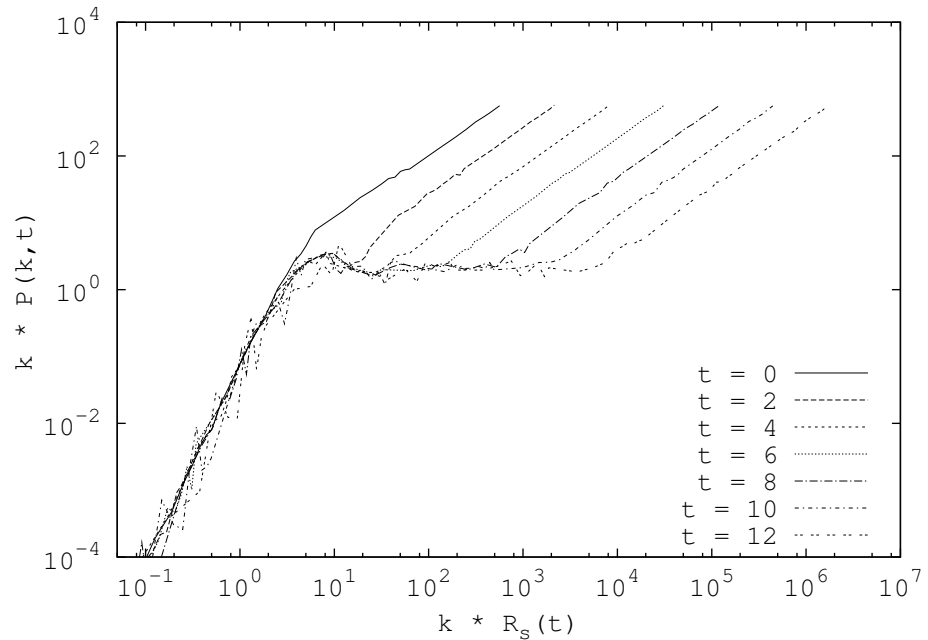


Figure 4.32: Evolution of  $k \times P(k, t)$  as a function of  $k \times R_s(t)$  where  $R_s(t)$  is given in Eq.4.52 starting with an initial PS  $P_{init}(k) \propto k^2$  in the static case.

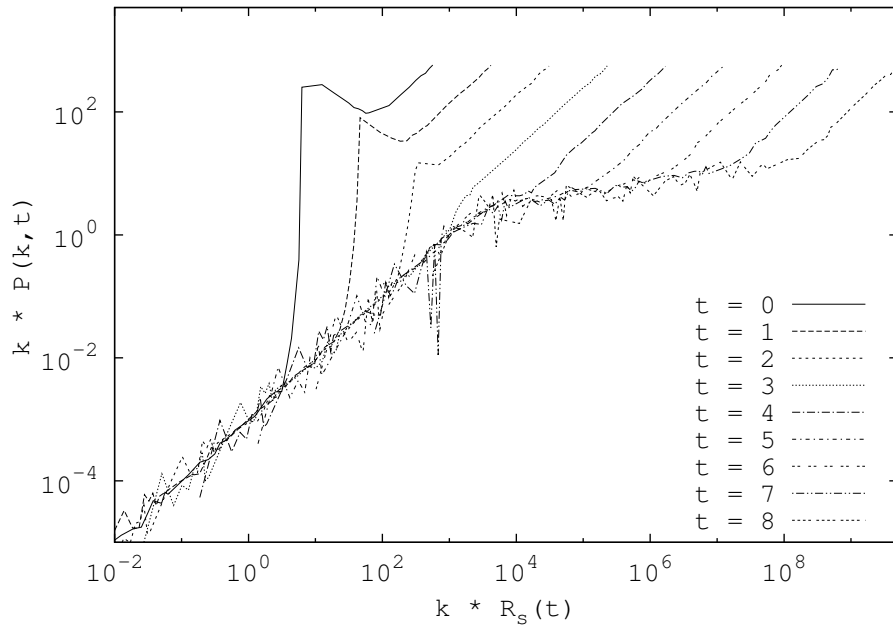


Figure 4.33: Evolution of  $k \times P(k, t)$  as a function of  $k \times R_s(t)$  where  $R_s(t)$  is given in Eq.4.52 starting with an initial PS  $P_{init}(k) \propto k^0$  in the expanding (quintic) case.

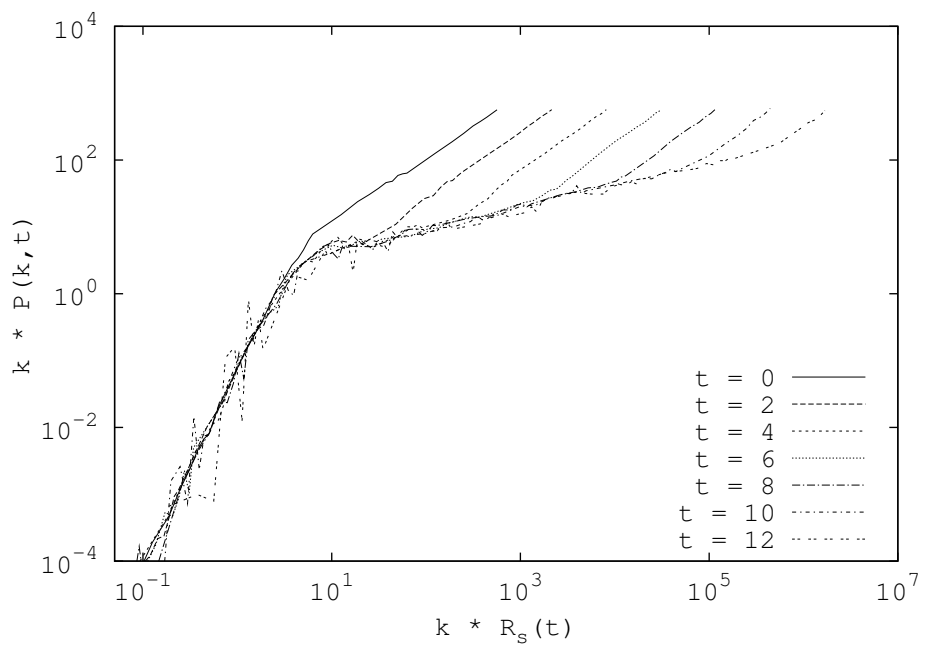


Figure 4.34: Evolution of  $k \times P(k, t)$  as a function of  $k \times R_s(t)$  where  $R_s(t)$  is given in Eq.4.52 starting with an initial PS  $P_{init}(k) \propto k^0$  and  $k^2$  in the expanding (quintic) case.

### Summary of comparison with $3 - d$

As far as the expanding (EdS) case is concerned in  $3 - d$ , self-similarity is expected to be valid, as explained in Chapter 2, in a range of  $n$ , the index of the initial PS, such that  $-3 < n < 4$ . While there has been considerable discussion of the case  $-3 < n < -1$  in the literature, with different conclusions about the observed degree of self-similarity (see e.g. [51] and [139]), the case  $n \geq 1$  has remained open. The reason why the case  $n > 1$  has not been studied numerically appears to be twofold:

- firstly, it is not of direct interest to “real” cosmological models which describe PS with exponents in the range  $-3 < n < -1$ ;
- secondly, such initial conditions are considered “hard to simulate” (see e.g. [139]).

In the static case, a qualitative similarity seems to emerge from the  $1 - d$  and  $3 - d$   $N$ -body simulations: self-similarity is observed in  $3 - d$  even for  $n > 1$  ( $n = 2$  in [11]), and the slope of the PS in the self-similar regime appears to be independant of the initial spectrum.

In the expanding case, our  $1 - d$  results show the same tendency as the result observed in  $3 - d$  (see e.g. [139]): the slope of the PS in the self-similar regime shows dependence on the initial spectrum. When the index of the initial spectrum increases, the slope of the PS in the self-similar regime increases also.

## 3 Evolution from causal density seeds

We now consider the case where the initial PS is  $P_{init}(k) \propto k^4$ . We treat this case separately because, as discussed in Chapter 2, it corresponds to the power-law behaviour at which one expects linear theory, which we have seen is the “driving force” of the dynamics in the cases above, to break down. One thus expects a qualitatively different mechanism for the formation of structures. As explained also in Chapter 2, this corresponds to the so-called “causal seeds”, *i.e.* density perturbations at large scale, which could be produced by some small scale physics obeying simply to conservation of mass and momentum. It has not been studied in  $3 - d$ , the principal reason being probably the considerable numerical accuracy needed: any spatially uncorrelated random error introduces a  $k^2$  contribution to the PS which can become dominant at small  $k$ . We follow the same approach as in the case  $k^0$  and  $k^2$ , starting with visual inspection.

### 3.1 Visual inspection

In Figs. 4.36 and 4.37, the plots in the left-hand panels again show the number of particles  $N(i)$  in each lattice cell at each time, which is proportional to the mass density in each cell. In the phase space plots, in the right-hand panels, each point represents simply one particle.

One sees clearly that, as in the case with initial PS  $P_{init} \propto k^0$  and  $k^2$ , in both the static and expanding cases, the evolution appears again to proceed in a “bottom-up” manner. As before, the system is representative of the evolution of an infinite system: it does not appear to have a preferred center - clusters form in apparently

random locations without sensitivity to the boundaries.

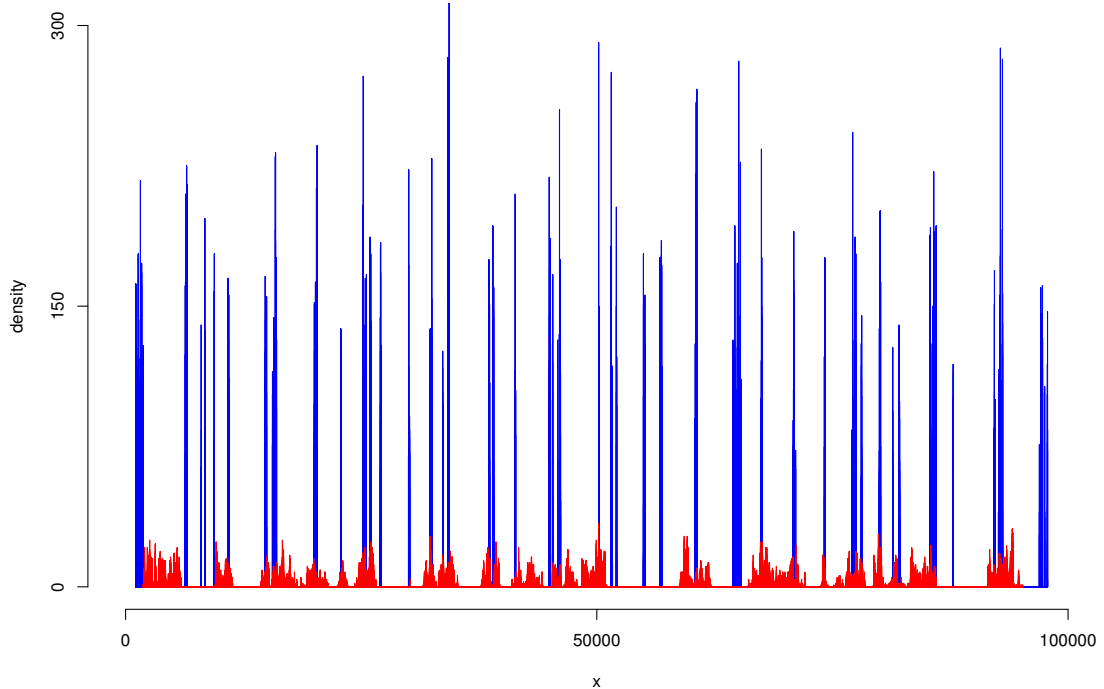


Figure 4.35: Superposition of the cases static (red) and expanding (blue) for an initial PS  $P_{init}(k) \propto k^4$ , at time  $ts = 22$ . In both cases, the initial displacement configurations are exactly the same.

The system shows however a qualitative difference compared to the previous analysis. We compare qualitatively in Fig. 4.35 the evolved configurations in the static and expanding cases. As in the previous plot, the figure shows the density distribution smoothed on initial lattice spacing. The simulations are started with exactly the same density perturbation and  $P_{init}(k) \propto k^4$ . We see that the correlation between the location of the structures is, contrary to  $n = 0$  and  $n = 2$ , not so strong at all. In the former cases the strong correlation was explained to be the result of the validity of linear theory at large scales: the structures at large scales are the amplified seed fluctuations. The fact that this is not the case when  $n = 4$  is then not surprising; indeed this case is precisely expected to be very different because linear amplification is no longer valid.

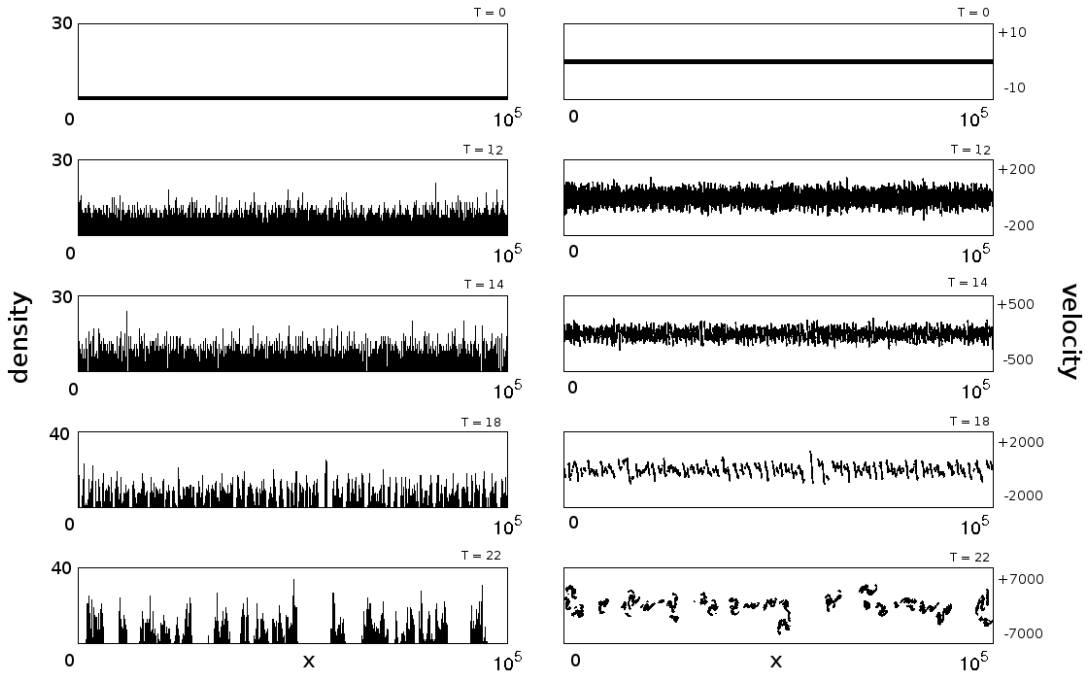


Figure 4.36: Evolution in the configuration space and in the one particle phase space ( $\mu$ -space) of our one-dimensional toy model, starting with an initial PS  $P_{init}(k) \propto k^4$  in a static case at time  $t_s = 0, 12, 14, 18, 22$ . The unit of length is given by the initial lattice spacing  $\ell = L/N$  with  $L = N = 10^5$ .

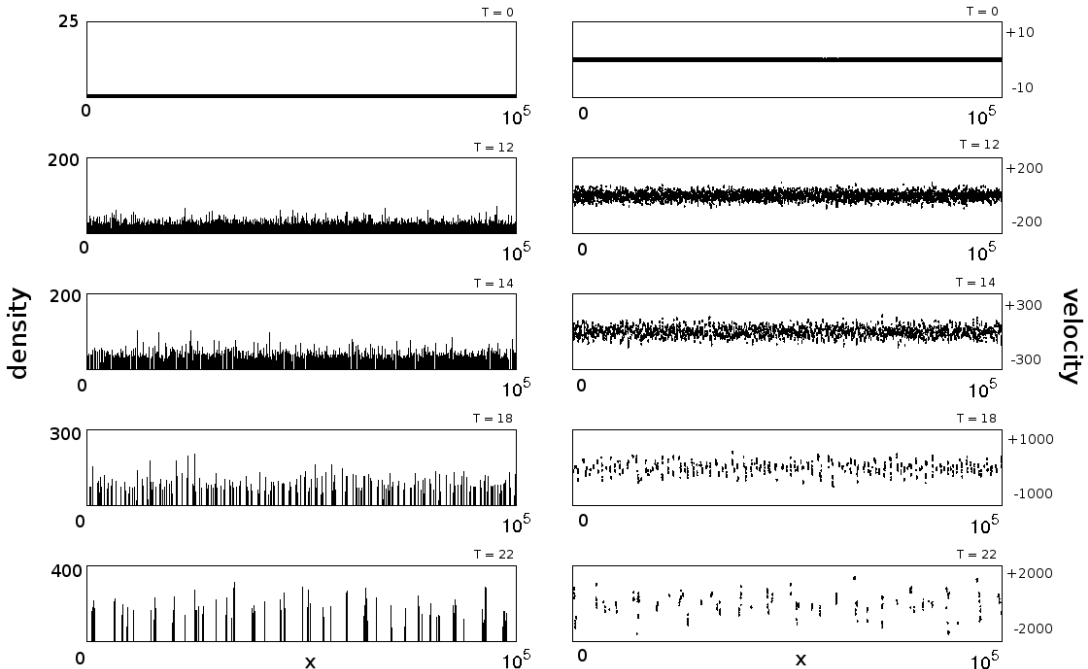


Figure 4.37: Evolution in the configuration space and in the one particle phase space ( $\mu$ -space) of our one-dimensional toy model, starting with an initial PS  $P_{init}(k) \propto k^4$  in an expanding case at time  $t_s = 0, 12, 14, 18, 22$ . The unit of length is given by the initial lattice spacing  $\ell = L/N$  with  $L = N = 10^5$ .

### 3.2 The power spectrum

We now study the PS as the qualitative differences anticipated are most evident in  $k$  space. Shown in Figs. 4.39 and 4.40 are the temporal evolution of the PS in both the static and expanding (quintic) cases.

We note that at small wave-numbers the PS shows a temporal amplification in  $k^4$ . The regime in which this temporal amplification is valid decreases with time and is observed in a range  $k < k_{NL}(t)$ , where  $k_{NL}(t)$  is a wave number which decreases as a function of time. At all times, the PS still converges at large wave-numbers to the asymptotic value  $1/n_0$ . However, this amplification is not the one predicted by linear theory. This is illustrated in Fig. 4.38 where we plot  $\left[ \frac{P(k,t)}{P(k,0)} \right]$  at small  $k$ . In dashed line is plotted for comparison the behaviour expected naively from linear theory, *i.e.*  $A(t) = R_s^{n+1}(t)$  with  $n = 4$ . As anticipated we see that the linear theory is not followed as the points are not superimposed with the linear prediction. We will come back to this result in the following with the study of self-similarity.

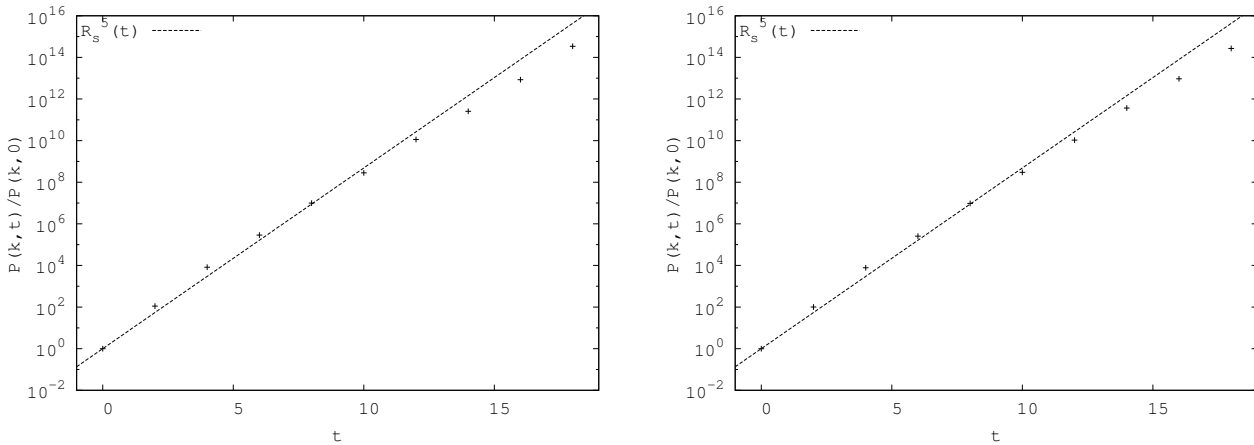


Figure 4.38: Temporal evolution of  $\frac{P(k,t)}{P(k,0)}$  for  $k = 10^{-3}$ , *i.e.* in the regime where a simple amplification is observed, in the static (left panel) and expanding (quintic) models (right panel). We also represent the function  $A(t) = R_s^{n+1}(t)$  with  $n = 4$ , where  $R_s(t)$  is the scaling factor predicted naively by the linearized fluid theory for  $n = 4$ .

We observe the same difference between the static and the expanding cases as in the case  $k^0$  and  $k^2$ : the scale  $k_{max}$  at which the PS reaches its asymptotic value  $1/n_0$  stays approximately constant in the static case, while it translates to the right in the expanding case.

As in the previous section, to assess whether self-similarity applies, we show in Figs. 4.41 and 4.42 the temporal evolution of  $k \times P(k,t)$  as a function of the dimensionless parameter  $k \times R_s(t)$ , where  $R_s(t)$  is the scaling factor predicted by linear theory for  $n = 4$ , and taking  $t_{ref} = 0$ .

In both the static and the expanding cases, we see that right from the initial time the self-similarity is not followed at small  $k$  (as the rescaled curves are never superimposed). This is representative of the non-validity of the linear amplification in the particular case  $k^4$ , as expected in Chapter 2. However, as time progresses,

we see a non-linear range of  $k$  in which the curves *are* superimposed and where this range of  $k$  increases with time: this means that as non-linearity develops in this limit case, we recover the self-similarity in the non-linear range with the scaling factor  $R_s(t)$  predicted by linear theory.

Defining the parameter  $\beta$  as in Eq. (4.53) in the self-similar regime for the static and expanding models, we can extract from Figs. 4.41 and 4.42, using linear interpolation, the different values measured for this power index. We obtain  $\beta = 0.43 \pm 0.01$  and  $\beta = 0.62 \pm 0.01$  in the quintic and RF models and  $\beta = 0.01 \pm 0.02$  in the static case.

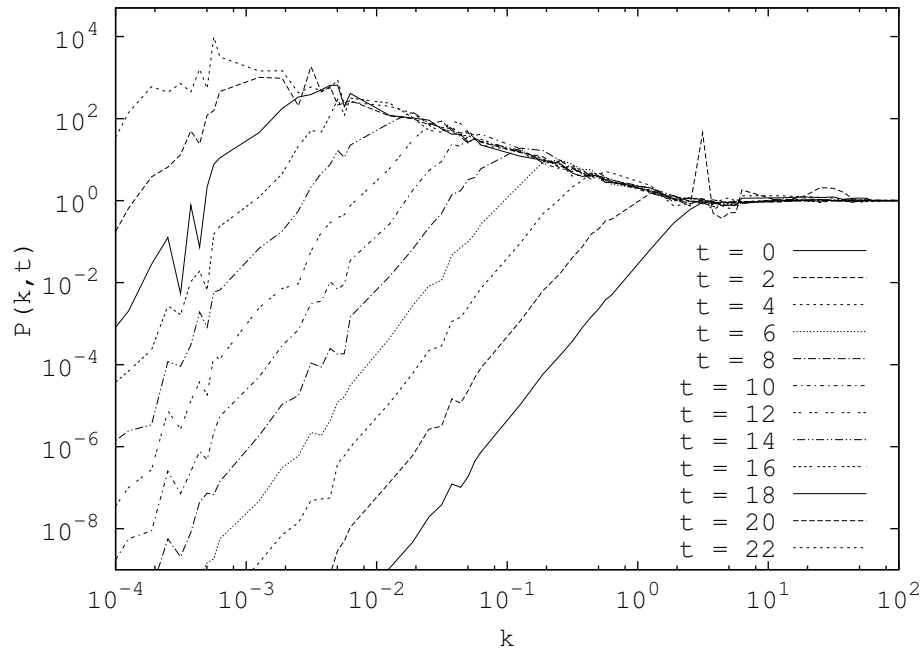


Figure 4.39: Temporal evolution of the PS starting with an initial PS  $P_{init}(k) \propto k^4$  for the static model at time  $t_s = 0, 2, 4, 6, 8, 10, 12, 14, 16, 18, 20, 22$ .

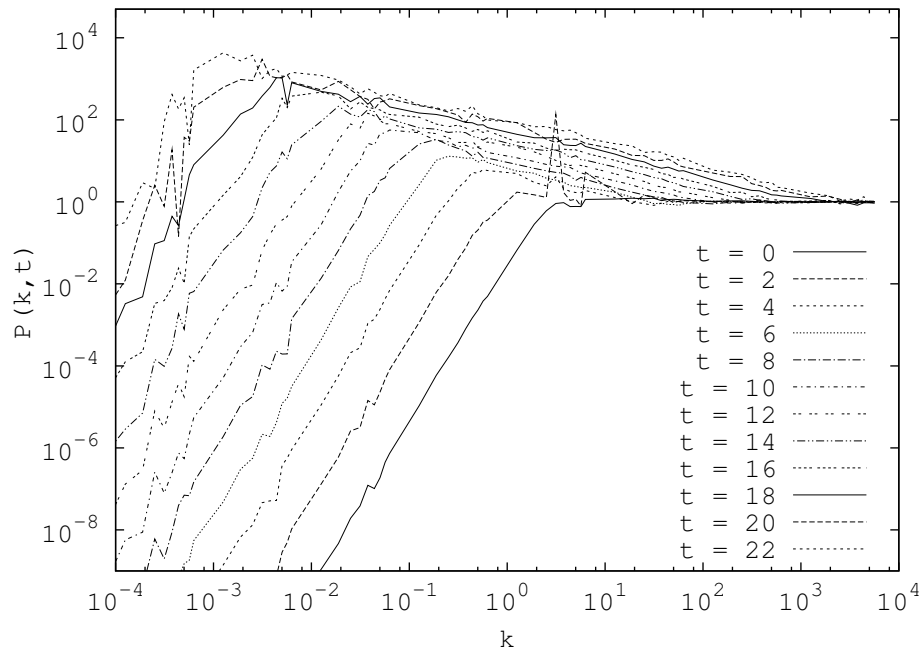


Figure 4.40: Temporal evolution of the PS starting with an initial PS  $P_{init}(k) \propto k^4$  for the expanding (quintic) model at time  $t_s = 0, 2, 4, 6, 8, 10, 12, 14, 16, 18, 20, 22$ .

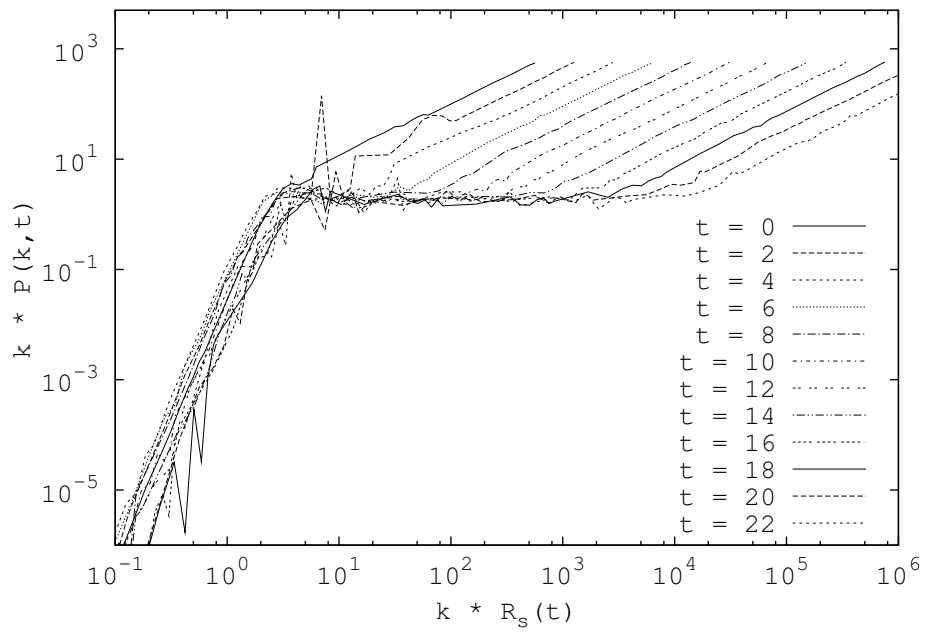


Figure 4.41: Temporal evolution of  $k \times P(k, t)$  as a function of  $k \times R_s(t)$  where  $R_s(t)$  is given in Eq. (4.52), starting with an initial PS  $P_{initi}(k) \propto k^4$  for the static model at time  $t_s = 0, 4, 8, 12, 16, 20$ .

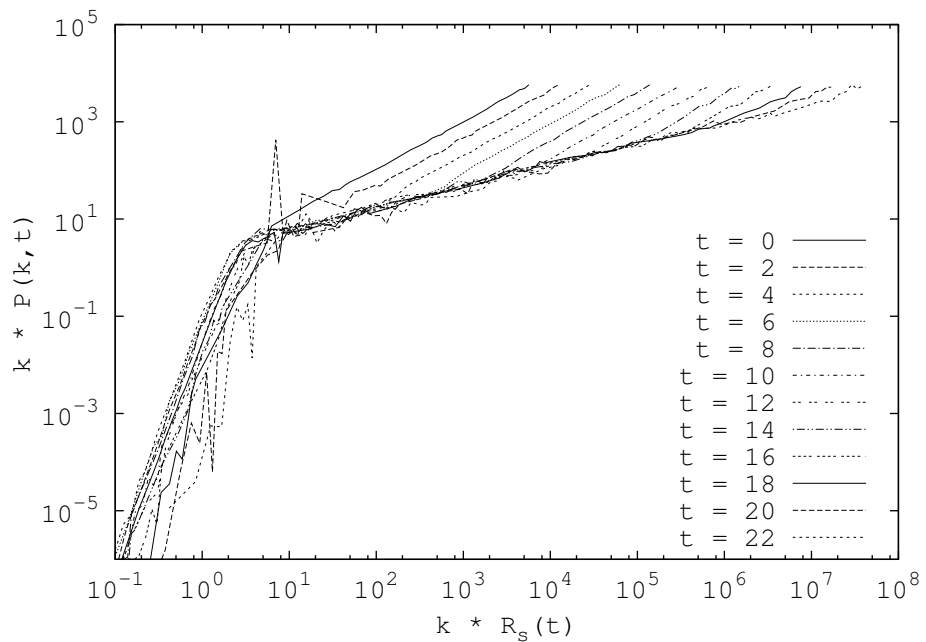


Figure 4.42: Temporal evolution of  $k \times P(k, t)$  as a function of  $k \times R_s(t)$  where  $R_s(t)$  is given in Eq. (4.52), starting with an initial PS  $P_{init}(k) \propto k^4$  for the expanding (quintic) model at time  $t_s = 0, 4, 8, 12, 16, 20$ .

### 3.3 Correlation function

In Figs. 4.43 and 4.44 we show the temporal evolution of the absolute value  $|\xi(x)|$  in a log-log plot just as in the case  $n < 4$ . We observe a qualitative similar behaviour as previously obtained for  $n < 4$ : starting from  $\xi(x) \leq 1$  everywhere, non-linear correlations develop first at scales smaller than the intial inter-particle distance, and after few dynamical times the clustering develops at smaller scales.

From Figs. 4.45 and 4.46 it appears that once significant non-linear correlations are formed, the evolution of the correlation function  $\xi(x)$  can be described, approximately, by the same simple translation in time described in Eq. (4.48). Let us note, however, that in Fig. 4.45 the different curves do not perfectly superpose themselves. This is not surprising as we expect from our study of the PS above that self-similarity does not apply at large  $x$ . Then, as the reduced 2-point correlation function is simply the FT of the PS, the correlation function in the static model (where the non-linear regime is less developped than in the expanding model) is dominated by large  $x$ .

Starting with an initial PS  $P_{init}(k) \propto k^4$ , we measure the values of the exponent  $\gamma = 0.15 \pm 0.05$  in the static model,  $\gamma = 0.46 \pm 0.03$  in the quintic model and  $\gamma = 0.63 \pm 0.01$  in the RF model, using a linear interpolation. We notice again that the rescaled correlation functions are superimposed above a scale  $x_{min}$  where a “plateau” of amplitude  $\xi_{max}$  is reached and shows the same qualitative behaviour as observed for  $n < 4$ .

As we did previously in the case where the initial PS  $P_{init} \propto k^0$  and  $k^2$ , we can compare the power index  $\beta$  and  $\gamma$ . We see that they are in agreement within the standard numerical error in the expanding cases (quintic and RF). However, as in the case  $k^0$  and  $k^2$ , they do not agree again in the static case.

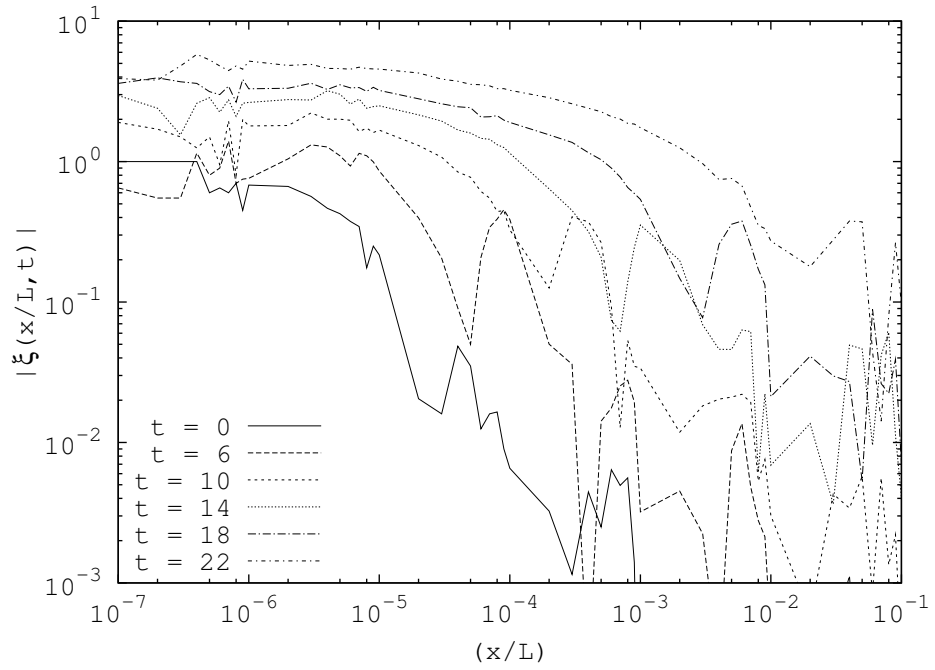


Figure 4.43: Temporal evolution of the correlation function, starting with an initial PS  $P_{init}(k) \propto k^4$  for the static model at time  $t_s = 0, 6, 10, 14, 18, 22$ .

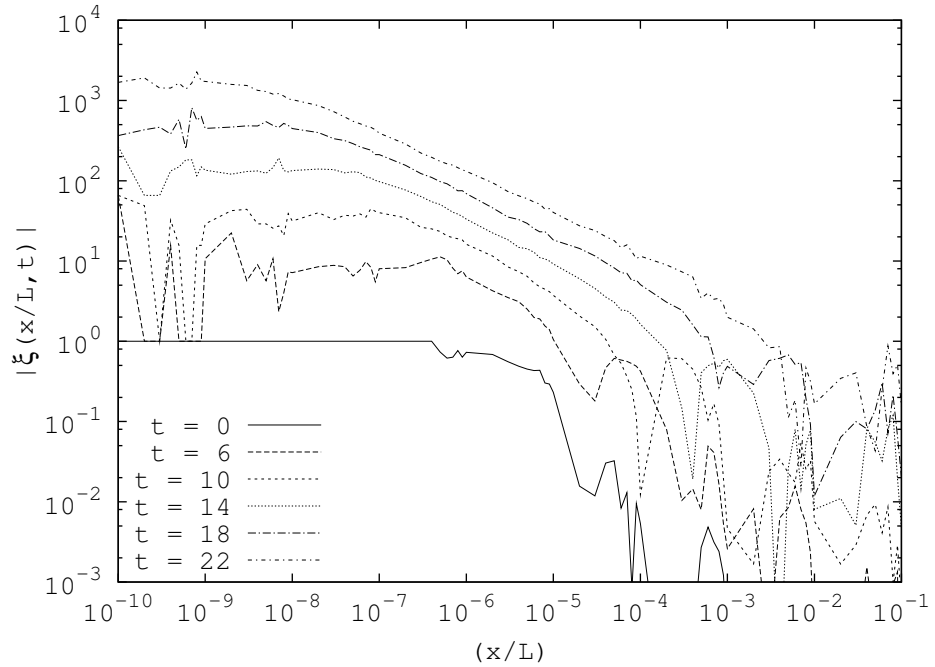


Figure 4.44: Temporal evolution of the correlation function, starting with an initial PS  $P_{init}(k) \propto k^4$  for the expanding (quintic) model at time  $t_s = 0, 6, 10, 14, 18, 22$ .

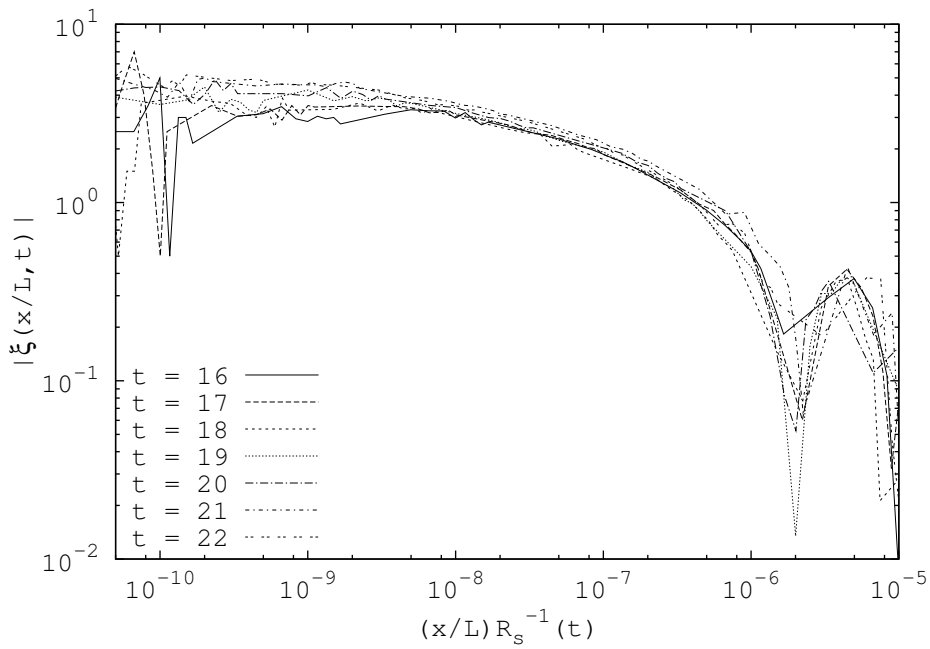


Figure 4.45: Temporal evolution of the correlation function as a function of  $x/R_s(t)$ , starting with an initial PS  $P_{init}(k) \propto k^4$  for the static model at time  $t_s = 16, 17, 18, 19, 20, 21, 22$ .

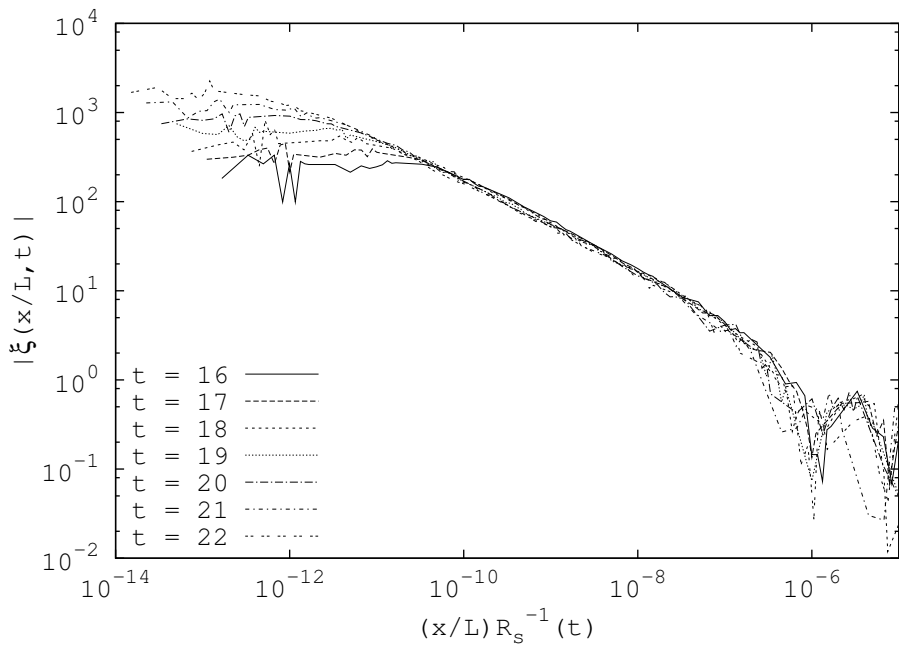


Figure 4.46: Temporal evolution of the correlation function as a function of  $x/R_s(t)$ , starting with an initial PS  $P_{init}(k) \propto k^4$  for the expanding (quintic) model at time  $t_s = 16, 17, 18, 19, 20, 21, 22$ .

### 3.4 Normalized mass variance

We show in Figs. 4.47 and 4.48 the temporal evolution of  $\sigma^2(x)$ . Its qualitative behaviour is very similar to that observed in the case  $n = 0$  and  $n = 2$ : at large scales we see a temporal amplification of the initial functional behaviour, which corresponds to  $\sigma^2(x) \propto x^{-2}$ . As we explained in Chapter 2, this behaviour simply corresponds to mass fluctuations independent of scale, which is the most rapid decay possible in any spatially homogeneous point distribution.

At small scales, we observe  $\sigma^2(x) \propto x^{-1}$  which is the shot noise behaviour intrinsic to any such distribution at small scales. The range of scales between these two limiting behaviours is still that of the non-linear clustering. Note that the amplification of the variance at large separation seen in Figs. 4.47 and 4.48 is not a result of linear amplification, just as discussed for the case  $n = 2$  in section above. Indeed, as for  $n = 2$ ,  $\sigma^2 \sim \frac{1}{x^2}$ , so that self-similarity implies  $\sigma^2 \sim R_s(t) \sim A(t)\sigma^2(x, 0)$ .

To probe in real space the self-similar behaviour we consider in Figs. 4.49 and 4.50 the temporal evolution of the scale  $\lambda(\alpha, t)$  defined in Eq. (4.44).

We see in Figs. 4.49 and 4.50 that, in both the static and expanding cases, despite the absence of linear amplification of PS, self-similarity seems to emerges with the behaviour that this would predict. Indeed, considering an initial PS  $P_{init} \propto k^n$  with  $n < 1$ , we have seen in Chapter 2 that  $\sigma^2(x) \propto k P(k) \Big|_{k=x^{-1}}$ . Then linear amplification of the PS implies consequently linear amplification of the normalized mass variance. However, for  $n > 1$ , which corresponds to the case where  $P_{init}(k) \propto k^4$ , the relation between the PS and the normalized mass variance is different. Following the argument developped in [11], the integral in Eq. (2.200) in Chapter 2 with  $P(k) \propto k^n$  with  $n > 1$  diverges at all  $k$ , and an ultraviolet cut-off is required to regulate it. The authors of [11] have shown that this cut-off is clearly in the range in which the amplification in  $k$  space is non-linear. Thus the evolution of this quantity, even at very large scales, is determined by modes in  $k$  space which are in the non-linear regime.

Furthermore, as in the case  $k^0$  and  $k^2$ , we see that in both the static and the expanding cases, we see that self-similarity propagates in time to non-linear ranges, as expected from the analysis of the PS.

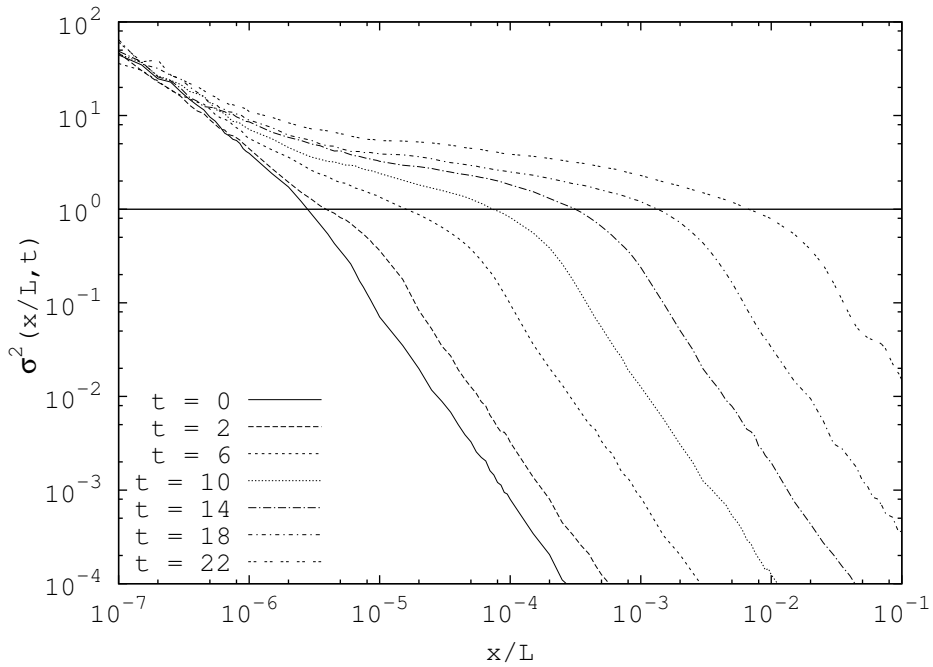


Figure 4.47: Evolution of the mass variance starting with an initial PS  $P_{init}(k) \propto k^4$  for the static model at time  $t = 0, 2, 6, 10, 14, 18$  and  $22$ .

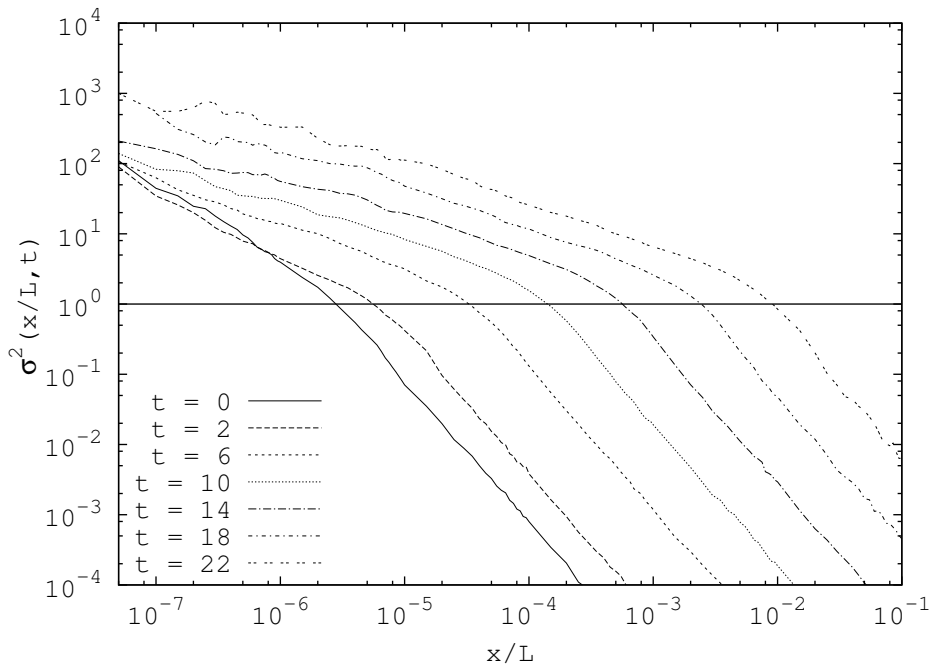


Figure 4.48: Evolution of the mass variance starting with an initial PS  $P_{init}(k) \propto k^4$  for the expanding (quintic) model at time  $t = 0, 2, 6, 10, 14, 18$  and  $22$ .

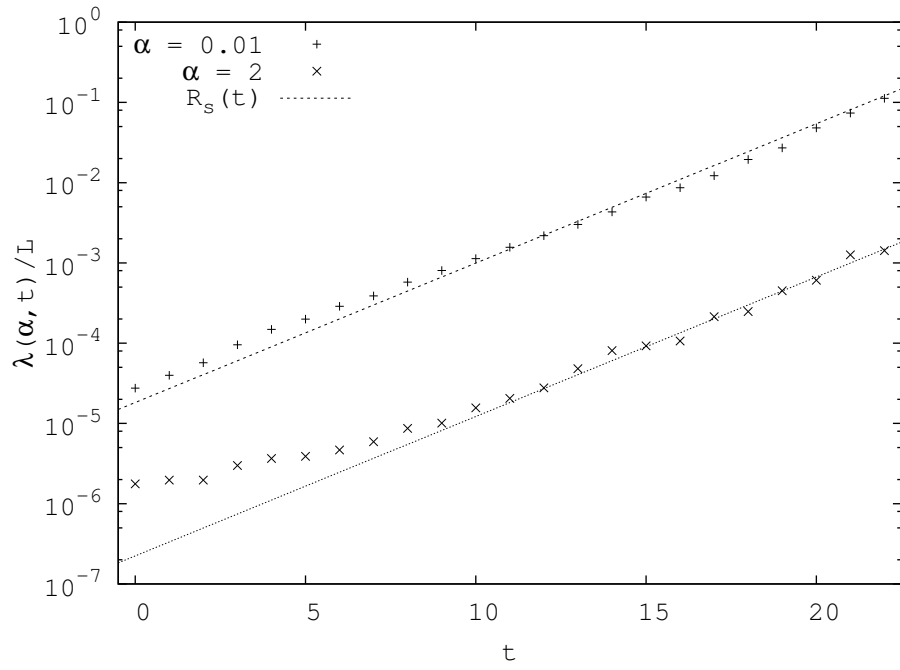


Figure 4.49: Temporal evolution of the scale  $\lambda(\alpha, t)$  defined in Eq. (4.44) starting with an initial PS  $P_{init}(k) \propto k^4$  for the static model.

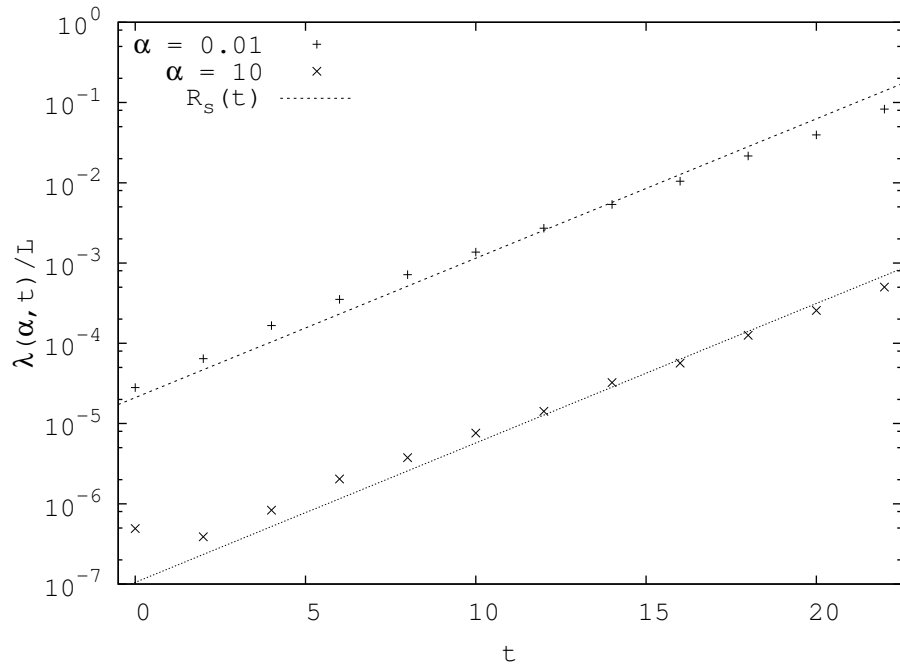


Figure 4.50: Temporal evolution of the scale  $\lambda(\alpha, t)$  defined in Eq. (4.44) starting with an initial PS  $P_{init}(k) \propto k^4$  for the expanding (quintic) model.

## 4 Development of the range of self-similarity and characteristic exponents

As we have already emphasized in section 1, one of the particularly interesting features of the  $1 - d$  self-gravitating model is the absence of smoothing at small scales analogous to that used in  $3 - d$  simulations. This means that we can study fully the development of clustering at small scales unimpeded by such a cut-off. We have already seen that the results above allow us to identify a lower-cut-off to self-similarity which we denoted  $x_{min}$ , and the existence of a regime below this scale where there is non-trivial clustering. We first study numerically the evolution of this scale  $x_{min}$  and of the corresponding approximate plateau  $\xi_{max}$ . In the expanding case we observe that there is a simple relation between them, with  $\xi_{max} \propto x_{min}^{-1}$ . Noting that this suggests the validity of a “stable clustering” hypothesis for the evolution at small scales, like that in  $3 - d$  which we discussed in Chapter 2, we determine precisely what the prediction of this hypothesis is in our  $1 - d$  models. This leads us to an analytic prediction for the exponent characterizing non-linear (and self-similar) clustering as a function of  $n$  and  $\Gamma$ . We compare then the exponents measured numerically with this prediction, finding good agreement.

### 4.1 Evolution of the spatial extent of non-linear SS clustering

We have seen in the previous section that the evolution of the lower cutoff to self-similarity in configuration space ( $x_{min}$ ) is different in the static and the expanding cases: while in both cases the correlation function appears to reach a plateau with an amplitude which grows in time, the scale  $x_{min}$  remains approximately constant in the static case but decreases monotonically in the expanding case. Let us focus in the following on the expanding case. We will come back to the study of the static case at the end of this section.

We show in Fig. 4.52 the evolution of  $x_{min}$  and  $\xi_{max}$  as a function of the reference time  $t_s$  for the quintic model and an initial condition  $P_{init}(k) \propto k^2$ . Fig. 4.51 illustrates the method we use to extract this information: we consider the same “collapse plot” used to test for self-similarity of  $\xi(x, t)$  in the previous section in which we rescale the  $x$ -axis by the time-dependent factor  $R_s(t)$ . We thus locate simply the temporal evolution of the scale marking the departure from the self-similar regime (represented in Fig. 4.51 by the small arrows)  $x_{min}$ , and then determine also the amplitude of the corresponding plateau  $\xi_{max}$  in the correlation function at each time.

The semi-log representation of Fig. 4.52 shows an exponential decrease of  $x_{min}$  and an exponential increase of  $\xi_{max}$ . We observe that the result approximately satisfies the relation

$$x_{min} \propto \xi_{max}^{-1} \propto \exp(-\epsilon t_s), \quad (4.54)$$

where we measure the parameter  $\epsilon = 0.33 \pm 0.03$  in the quintic model ( $\Gamma = 1/\sqrt{6}$ ) and  $\epsilon = 0.66 \pm 0.03$  in the RF model ( $\Gamma = 1/\sqrt{2}$ ), whatever is the value of  $n$  ( $n = 0, 2$  and  $4$ ). Thus, the parameter  $\epsilon$  appears not to depend on the power index of the initial PS, but only on the value of the damping term  $\Gamma$ .

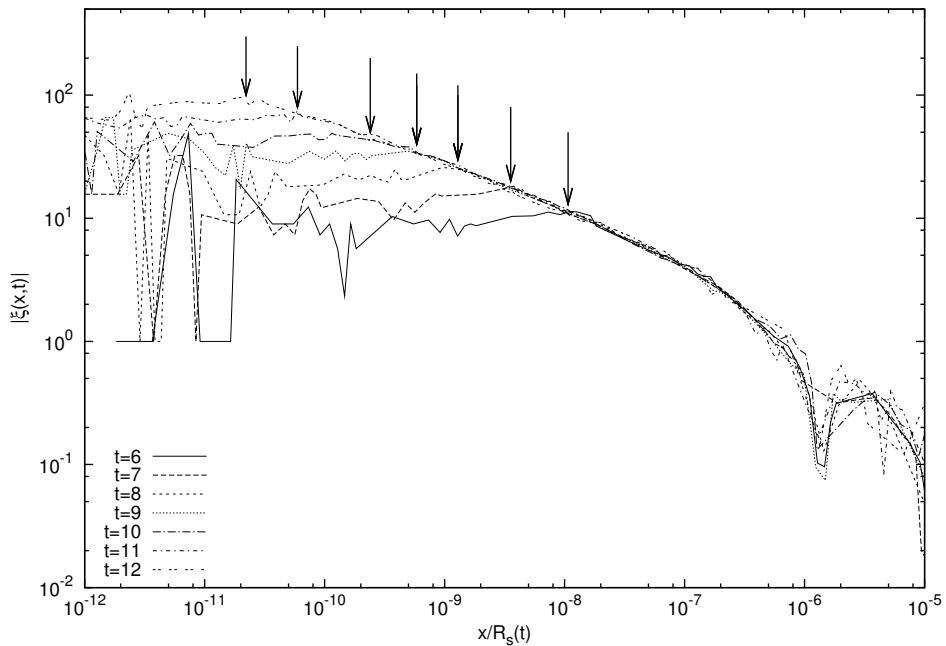


Figure 4.51: Determination of the temporal evolution of the non-linear scale  $x_{min}$  (and the amplitude of the corresponding plateau  $\xi_{max}$ ) in the quintic model with an initial condition  $P_{init}(k) \propto k^2$ . We use a “collapse plot” of  $|\xi(x, t)|$ : for each time, we rescale the  $x$ -axis by the time-dependent factor  $R_s(t)$  to superimpose all the curve as closely as possible. We then locate simply by arrows the temporal evolution of the departure from the self-similar regime.

The simple relation between  $x_{min}$  and  $\xi_{max}$  and the independence of  $n$  suggest that this result might be related to the so-called “stable clustering” hypothesis proposed sometimes in  $3 - d$  for the strongly clustered regime and discussed in Chapter 2 [126]: in this case one envisages that, in the strongly non-linear regime, the distribution at small scales remains frozen (*i.e.* “stable”) in physical coordinates, which are related to the comoving coordinates of the simulation by a simple rescaling ( $\mathbf{r}_{phys} = a(t) \mathbf{x}_{com}$ ) as discussed in Chapter 2. Thus in comoving coordinates, the conditional density (*i.e.* the mean density in a region  $r$  about a given point) scales as  $a^3(t)$ . In comoving coordinates the mean density is fixed so one obtains also  $\xi(x) \propto a^3(t)$ . If we now suppose here that  $x_{min}$  also remains fixed in physical coordinates, we have  $x_{min} \propto 1/a$  and  $\xi_{max} \propto 1/x_{min}^3$ .

If we adopt this argument naively to  $1 - d$  we would obtain  $\xi_{max} \propto 1/x_{min}$ , *i.e.*  $x_{min}$ , which is a characteristic scale of the clustering (breaking scale invariance), is constant in comoving coordinates. To do so, however, we must clarify what we mean by “stable clustering” in our  $1 - d$  models, because in deriving these models, we never made use of a transformation between physical and comoving coordinates as in  $3 - d$ .

“Stable clustering” can indeed be given meaning without reference to physical/comoving coordinates in  $1 - d$  through the following formulation: it is the behaviour expected by supposing that the clustering evolves as if it were that of a distribution made of *isolated virialized systems*. In the following section we consider

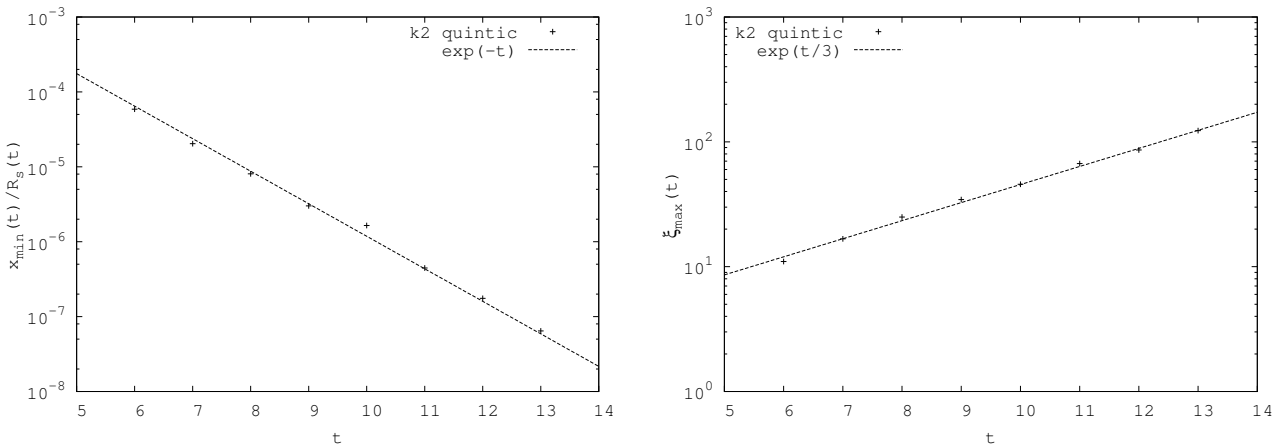


Figure 4.52: Evolution of the non-linear scale  $x_{min}$  and the amplitude of the plateau  $\xi_{max}$  in the quintic model with an initial condition  $P_{init}(k) \propto k^2$

what this behaviour is.

## 4.2 Stable clustering in one dimension

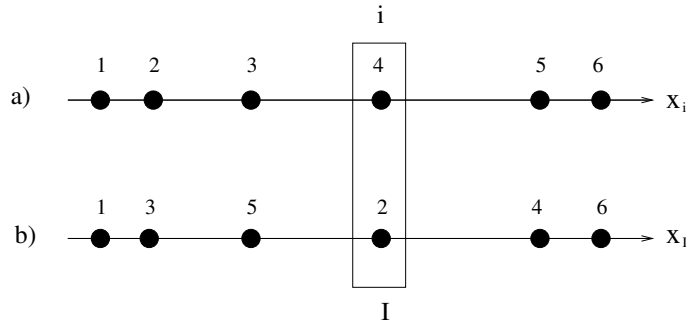
The meaning of an “isolated” subsystem in  $1 - d$  is much more exactly defined than in  $3 - d$  (where it means *tidal forces due to far away matter may be neglected*): if the particles of a given subsystem do not cross (or collide) with other particles, their evolution is indeed completely independent of the rest of the system. If this isolation is maintained for a sufficient time, one would expect the subsystem to equilibrate (just as any LRI systems) and virialize.

### Equations of motion for an isolated subsystem

To see what exactly this implies it is convenient to transform our equation back to the labelling in which particles cross rather than bounce: to derive analogy of the usual virial relation ,discussed in Chapter 2, we need a potential which is strictly a power law, which is only the case *at all times* in the labelling in which particles cross. In the colliding labelling we have seen in section 1 that we simply have, by appropriate choice of time variable

$$\frac{d^2 u_i}{dt^2} + \Gamma \frac{du_i}{dt} = u_i, \quad (4.55)$$

where  $i = 1 \dots M (< N)$ . The assumption of *isolation* means we can decouple these  $M$  equations from the other  $N - M$  particles in the system (with  $N \rightarrow \infty$ ). Let us now transform these equations back to the “crossing labelling”. At some initial time  $t = 0$ , both labellings coincide; at  $t > 0$  we show in Fig. 4.53 the two labellings which now differ. To illustrate the difference of labelling between a system  $S_{cross}$  of particles crossing and a system  $S_{coll}$  of particles colliding, we denote by  $a_i = a_0 + i\ell$  the original position of the  $i^{th}$  particle in  $S_{coll}$  on a regular lattice, where  $a_0$  represents an arbitrary origin of the  $x$ -axis and  $\ell = 1/n_0$  is the lattice spacing. We then write  $x_i$  the position of the particle  $i$  in  $S_{coll}$  , i.e.  $x_i < x_{i+1} \forall i$


 Figure 4.53: Correspondance between a)  $S_{coll}$  and b)  $S_{cross}$ 

and  $x_I$  the position of the “same” particle expressed in the different labelling  $S_{cross}$ . In Fig. 4.53 is illustrated the simple correspondence between  $S_{coll}$  and  $S_{cross}$ . We then have the relation  $i = I + \Delta N_I$  where  $\Delta N_I$  is the difference between the number of particles crossed by particle  $I$  from the left in the time interval and the number of particles which have crossed the particle  $I$  from the right in the same interval. Since we clearly have

$$\Delta N_I = \left( \frac{N_I^<(t) - N_I^>(t)}{2} \right) - \left( \frac{N_I^<(0) - N_I^>(0)}{2} \right), \quad (4.56)$$

where  $N_I^<(t)$  (respectively  $N_I^>(t)$ ) represents the number of particles on the left (respectively on the right) of the particle  $I$  at time  $t$ , we can rewrite the force on the particle as

$$\begin{aligned} F_i = F_I &= u_i = x_i - a_i = x_I - a_i = x_I - a_{I+\Delta N_I} \\ &= x_I - a_I - \left[ \left( \frac{N_I^<(t) - N_I^>(t)}{2} \right) - \left( \frac{N_I^<(0) - N_I^>(0)}{2} \right) \right] \ell. \end{aligned} \quad (4.57)$$

Denoting by  $x_{CM} = \frac{1}{M} \sum_{I=1..M} x_I$  the position of the center of mass of the system, and noting that  $\frac{1}{M} \sum_{I=1..M} \left( \frac{N_I^<(t) - N_I^>(t)}{2} \right) = 0$  we obtain

$$\frac{d^2}{dt^2}(x_I - x_{CM}) + \Gamma \frac{d}{dt}(x_I - x_{CM}) = \left( \frac{N_I^>(t) - N_I^<(t)}{2 n_0} \right) + (x_I - x_{CM}). \quad (4.58)$$

The gravitational contribution thus divides into two terms:  $f_{grav} = (N_I^>(t) - N_I^<(t))/2 n_0$  just as in the finite  $1-d$  system; the only effect of the infinite system is thus the appearance of the background with  $f_{back} = (x_I - x_{CM})(t)$ . We also denote the damping term by  $f_\Gamma = \Gamma \frac{d}{dt}(x_I - x_{CM})$ .

### Evolution of an isolated overdensity

Let us consider now an *overdense* isolated subsystem, *i.e.*  $\frac{M}{L_s} = n_s \gg n_0$  (where  $L_s$  is the spatial extent of the subsystem of  $M$  particles). It is simple to see that in this case, assuming  $\Gamma \sim 1$ , one expects the evolution to be characterized by quite

different time scales associated with the terms  $f_{grav}$ ,  $f_\Gamma$  and  $f_{back}$ . For  $f_{grav}$  the characteristic time scale can be expected to be  $\tau_{grav} \sim \sqrt{\frac{L_s n_0}{M}} \sim \sqrt{\frac{n_0}{n_s}} \ll 1$ . One then has to compare it with the timescales associated to  $f_\Gamma$ , *i.e.*  $\tau_\Gamma \sim \frac{1}{\Gamma} \sim 1$  and  $f_{back}$  *i.e.*  $\tau_{back} \sim 1$ . The timescale associated with the gravitational term is thus much shorter than that associated with the damping (expansion) and the background.

Now Eq. (4.58) without  $f_{back}$  and  $f_{grav}$  is simply the equation of motion of  $M$  particles of a finite  $1 - d$  self-gravitating system, which are known to evolve to a virialized QSS on the timescale  $\tau_{grav}$  [90, 158]. We would then expect to be able to treat the full system in an adiabatic approximation, in which we assume that the damping (and background) term causes the system to evolve while remaining virialized at all times. Let us neglect for the moment the background term. Given that the term  $f_{grav}$  is a conservative force, we can then define the associated mechanical energy  $E = K + U$ , where  $K$  and  $U$  are respectively the kinetic and the potential energies, and write for the full system,

$$\frac{dE}{dt} = -\Gamma \left( \frac{dx_I}{dt} \right)^2 = -2\Gamma K. \quad (4.59)$$

Considering now the adiabatic approximation discussed above, *i.e.* assuming that the system is always virialized, we have  $\langle E \rangle = \langle K \rangle + \langle U \rangle = 3 \langle K \rangle$  since we have the virial relation  $2 \langle K \rangle + \langle U \rangle = 0$ . We can approximate Eq. (4.59)

$$3 \frac{d\langle K \rangle}{dt} = -2\Gamma \langle K \rangle \quad (4.60)$$

which gives in the appropriate choice of time variable

$$\langle K \rangle \propto \exp\left(-\frac{2}{3}\Gamma t\right) \quad \text{and} \quad \langle U \rangle \propto \exp\left(-\frac{2}{3}\Gamma t\right). \quad (4.61)$$

By simple dimensional analysis we infer that

$$\langle v_I^2 \rangle \propto \exp\left(-\frac{2}{3}\Gamma t\right) \quad \text{and} \quad \langle L_s \rangle \propto \exp\left(-\frac{2}{3}\Gamma t\right), \quad (4.62)$$

*i.e.* the effect of the damping is simply to rescale the whole system slowly in space and velocity. Thus our  $1 - d$  models behave as if there is an “effective” physical coordinate related to the comoving one through the relation  $x_{phys} = \exp\left(-\frac{2}{3}\Gamma t\right) x_{com}$ .

Let us compare the result obtained in Eq. (4.61) with those given through the study of the dynamical evolution of  $x_{min}$ . Using the relations derived in section 1.3 which introduces the relation between the appropriate time variable and the static time  $t_s$  we obtain

$$\langle L_s \rangle \propto \exp\left(-\frac{t_s}{3}\right) \quad \text{and} \quad \langle L_s \rangle \propto \exp\left(-\frac{2}{3}t_s\right) \quad (4.63)$$

in the quintic and RF models respectively. This is in agreement within the numerical errors with the values of the parameter  $\epsilon$ , defined in Eq. (4.54), given above, and also with the exponent measured by Aurell et al. in [9] directly for an isolated structure. We have then identified the behaviour expected of a finite virialized structure with that observed to fit  $x_{min}$ . We thus make the hypothesis that, up to this scale, the distribution is well described as a set of virialized independent clusters (of size  $x_{min}$ ).

### Numerical simulation of an isolated subsystem

It is straightforward to test numerically the accuracy of this prediction for the behaviour of an isolated subsystem: we simply evolve the same infinite system we have been considering, but now for an initial condition containing only a single localized overdensity. More specifically we consider  $N = 10^3$  particles initially distributed in a region of size  $L_c = 10^3$  in a box of size  $L = 10^7$ , *i.e.*  $n_0 = \frac{N}{L} = 10^{-4}$  and  $n_c = \frac{N}{L_c} = 1$  so that it corresponds to an overdensity of magnitude  $n_c/n_0 = 10^4$ . This initial condition make the background term, as well as the damping term, negligible in comparison with the gravitational term ( $f_{\text{back}}/f_{\text{grav}} \propto 10^{-4}$  in both the static and the expanding cases). It also clearly separates the timescale  $\tau_\Gamma$  and  $\tau_{\text{grav}}$  as  $\tau_\Gamma/\tau_{\text{grav}} \sim 10^2\Gamma$ . To complete the numerical description of our system it is convenient to use different time units to those previously considered. We then define a *finite dynamical time unit*

$$t_{\text{dyn}}^{\text{finite}} = \sqrt{\frac{1}{gn_c}}, \quad (4.64)$$

where  $g = 1/2 n_0$ , which is the characteristic time for the finite overdensities' evolution under the mean field force. It is interesting to compare this time with the *infinite* dynamical time  $\tau_{\text{dyn}}$  we defined for the *reference* time we used in our analysis above, *i.e.*

$$\tau_{\text{dyn}}^{\text{finite}} = \sqrt{2 \frac{n_0}{n_c}} \sim 10^{-2} \tau_{\text{dyn}}. \quad (4.65)$$

For convenience in the simulation we choose our coordinate system such that the centre of mass of the system is at rest (*i.e.* after distributing the particles in our initial condition we add a spatial translation and a constant velocity to all particles to satisfy this condition).

### Temporal evolution of the dynamical observables

For the initial condition just described, we study the evolution of different observables: the kinetic energy  $K$ , the potential energy  $U$ , the virial ratio  $V = \frac{2K}{U}$  and a parameter  $\phi = \frac{\langle xv \rangle}{\langle x \rangle \langle v \rangle} - 1$  introduced in [90]. In a typical quasi-stationary state this parameter is constant and different from zero.

In Figs. 4.55 and 4.56 are represented the evolution of the virial ratio and the parameter  $\phi$  as a function of time in both the static and the expanding cases. We clearly see two stages in the macroscopic evolution (cf. Chapter 1): a first stage of violent relaxation during which all quantities fluctuate strongly before settling down to behaviours which appear to fluctuate about a well defined average, and specifically about unity for the virial ratio and about a value different from zero for the parameter  $\phi$ . This last parameter is clearly non-zero on much longer time scales than that characterizing the virialization and indicating a dynamical equilibrium which is not the thermodynamic equilibrium of this model (cf. [90]).

In Fig. 4.54 we see that the kinetic and the potential energies of the static model reach a value independent of time, which is illustrated in the phase space evolution by a virialized structure of constant size. A different behaviour is observed in Fig. 4.54 for the expanding (quintic) model: kinetic and potential energies decreases in time as  $\exp(-\tau_{\text{finite}}/3) \propto \exp(-t_s/3)$ . This is in agreement with our derivation of  $\langle v_I^2 \rangle$  and  $\langle L_s \rangle$  in Eq. (4.62) above and with the values of the parameter  $\epsilon$ .

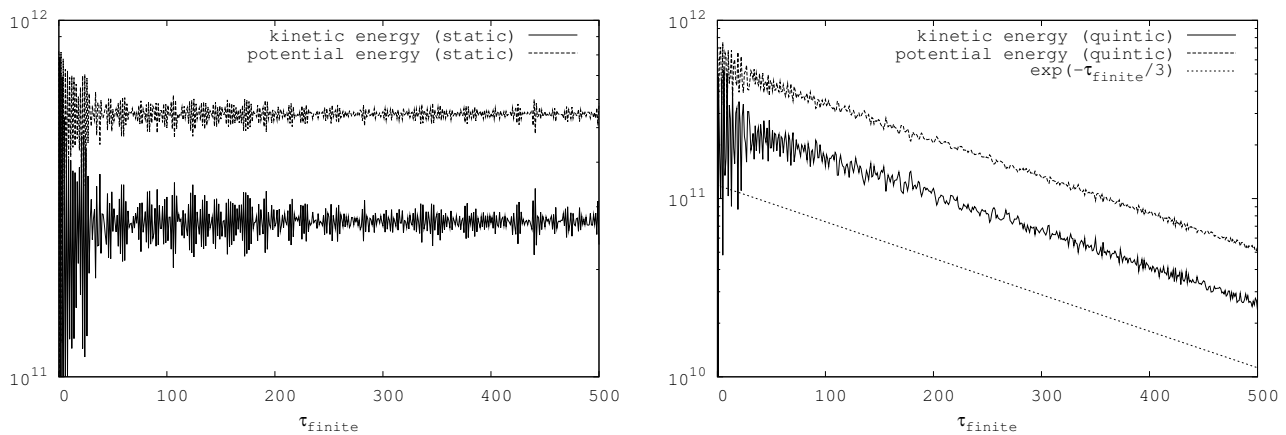


Figure 4.54: Evolution of the kinetic and the potential energy in the static and expanding (quintic) cases as a function of time  $\tau_{finite}$  in units of  $t_{dyn}^{finite}$ .

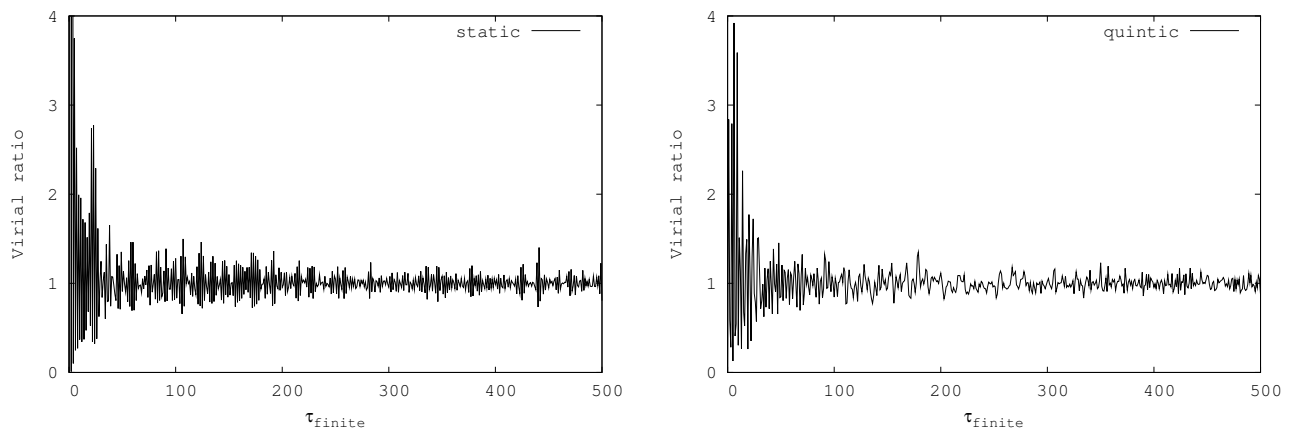


Figure 4.55: Evolution of the virial ratio in the static and expanding (quintic) cases as a function of time  $\tau_{finite}$  in units of  $t_{dyn}^{finite}$ .

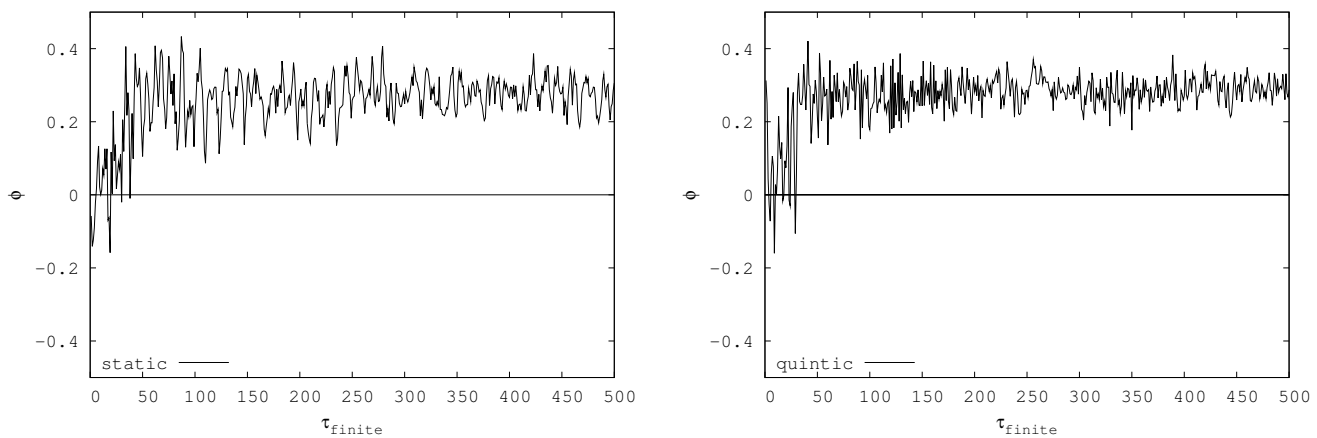


Figure 4.56: Evolution of the intrication parameter in the static and expanding (quintic) cases as a function of time  $\tau_{finite}$  in units of  $t_{dyn}^{finite}$ .

### 4.3 Prediction of exponents of power-law clustering (expanding case)

We derive now the exponent predicted by this “stable clustering” hypothesis. Assuming the power-law behaviour  $\xi_{SS}(x) \propto x^{-\gamma}$  (which corresponds to a PS  $P_{SS}(k) \propto k^{\beta-1}$  with  $\beta = \gamma$ ) for the reduced 2-point correlation function in the non-linear self-similar regime, we focus on the study of the evolution of the scales  $x_{min}$ , marking the break from power-law behaviour at small scales. The evolution of  $x_{NL}$  is given by the self-similar behaviour  $x_{NL}(t) \propto R_s(t)$  and  $\xi_{NL}(t) \approx 1$ . Through the hypothesis that clustering up to the scale  $x_{min}$  is produced essentially by isolated virialized structures, we have shown that  $x_{min}(t) \propto \xi_{max}^{-1}(t) \propto \exp(-\frac{2}{3}\Gamma t)$ .

Assuming that  $x_{NL} = x_{min}$  at the initial time, it is then possible to determine the value of the exponent  $\gamma$  (and consequently  $\beta$ ) through the relation

$$\gamma(n, \Gamma) = - \left( \frac{\ln(\xi_{max}(t)) - \ln(\xi_{NL}(t))}{\ln(x_{min}(t)) - \ln(x_{NL}(t))} \right). \quad (4.66)$$

which gives the general expression

$$\gamma(n, \Gamma) = \frac{\frac{2}{3}\Gamma/D(\Gamma)}{\frac{2}{3}\Gamma/D(\Gamma) + \frac{2}{n+1}}, \quad (4.67)$$

since  $R_s(t) \sim (e^{ts})^{2/(1+n)} \sim (e^{D(\Gamma)t})^{2/(1+n)}$  and  $x_{min} \sim e^{-\frac{2}{3}\Gamma t} \sim \xi_{max}^{-1}$ . We simply obtain in the quintic and RF models respectively

$$\gamma(n, 1/\sqrt{6}) = \frac{n+1}{n+7} \quad \text{and} \quad \gamma(n, 1/\sqrt{2}) = \frac{n+1}{n+4}. \quad (4.68)$$

We see in Tab. 4.3 that this result agrees with the numerical prediction of  $\beta$  and  $\gamma$ . This shows that we can explain very well the exponent characterizing clustering for the expanding case.

| intial PS | Quintic         | RF             | Quintic (simulation)     | RF (simulation)          |
|-----------|-----------------|----------------|--------------------------|--------------------------|
| $n = 0$   | $\gamma = 1/7$  | $\gamma = 1/4$ | $\gamma = 0.14 \pm 0.02$ | $\gamma = 0.25 \pm 0.02$ |
| $n = 2$   | $\gamma = 1/3$  | $\gamma = 1/2$ | $\gamma = 0.35 \pm 0.02$ | $\gamma = 0.50 \pm 0.02$ |
| $n = 4$   | $\gamma = 5/11$ | $\gamma = 5/8$ | $\gamma = 0.43 \pm 0.01$ | $\gamma = 0.62 \pm 0.01$ |

Table 4.3: Theoretical and numerical values of the parameter  $\gamma(n, \Gamma)$ , the exponent of the power-law behaviour of the reduced 2-point correlation function in the self-similar regime. We consider the expanding (quintic and RF) models. We see that theoretical results and numerical measures are in agreement within the standard numerical error.

### 4.4 Exponent of the power-law clustering in the static limit

Let us now return to the analysis of the static model and underline its difference with the expanding one. We expect from our analysis that in the static model, the absence of damping ( $\Gamma = 0$  in Eq. (4.1)) prevents the system from shrinking. Then

the size of the smaller structures should remain unchanged. This is what is observed in the analysis of the correlation function in section 2.3 where the scale  $x_{min}$  stays roughly fixed during the dynamical evolution of the system. However, the amplitude of the plateau,  $\xi_{max}$ , increases. Thus Eq. (4.54) is not followed in the static limit. If we compare the increase of the amplitude  $\xi_{max}$  in the static and expanding cases, we see that this amplitude increases by a factor of less than 10 in the static case, while it increases by a factor of more than 100 in the expanding case. This suggests that the increase of  $\xi_{max}$  in the static limit would be due to a “second order” effect, compared of Eq. (4.54), which is negligible in the expanding cases (for sufficiently large  $\Gamma$ ). Considering our numerical result for the exponent  $\gamma$  in Tab. 2.3, we could postulate a generalization of Eq. (4.67). Given that in the static limit the observed  $\gamma$  is independent of  $n$ , one might suppose a generalization to

$$\gamma(n, \Gamma) = \frac{\frac{2}{3}\Gamma/D(\Gamma) + \nu \frac{2}{n+1}}{\frac{2}{3}\Gamma/D(\Gamma) + \frac{2}{n+1}}. \quad (4.69)$$

where  $\nu$  is simply the  $n$ -independent exponent measured for the static case in Tab. 2.3, *i.e.*  $\nu = \gamma(n, 0) = 0.18 \pm 0.03$ . Such an ansatz would correspond to an amplification of  $\xi_{max}$  (additional to stable clustering) proportional to  $R_s(t)$ , *i.e.*  $\xi_{max} \sim e^{\frac{2}{3}\Gamma t} R_s(t)^{\gamma(0)}$ .

## 5 Conclusion

In this chapter, we have presented the results of the numerical investigation of the dynamical evolution of  $1 - d$  self-gravitating toy models, starting with a class of initial conditions analogous to those studied in cosmology: lattices perturbed to produce an initial PS  $P_{init}(k) \propto k^n$  at small  $k$ . We found that, when the index  $n$  of the initial PS is equal to 0 and 2, there are very strong qualitative similarities between the evolution of the  $1 - d$  and  $3 - d$  systems. We have observed specifically the hierarchical nature of the clustering and brought to light the mechanism of linear amplification determining the growth of non-linearity scale. Moreover, we have shown that “self-similarity” is indeed observed in  $1 - d$  system in both the static and expanding (quintic and RF) cases just as in  $3 - d$ .

An interesting result is that qualitative differences can be identified between the static and expanding cases. The shape of the correlation function (or the power spectrum) has appeared to be a function of the index  $n$  of the initial PS in the expanding case, and is independent of this index in the static case. Moreover the value of the damping term  $\Gamma$ , whose different values correspond to different expanding model ( $\Gamma = 1/\sqrt{6}$  and  $\Gamma = 1/\sqrt{2}$  represent the quintic and RF models respectively), has an influence on the shape of the correlation function or the power spectrum, and then on the exponent of these two statistical measures in the self-similar regime. This again coincides with  $3 - d$  results.

The  $1 - d$  self-gravitating model has also given us the opportunity to investigate easily structure formation in the limit of “causal fluctuations”, *i.e.*  $P(k) \propto k^4$  at small  $k$ , a numerically difficult case which has not been explored in  $3 - d$ . We have shown that, differently to the case where  $P(k) \propto k^0$  or  $k^2$  at small  $k$ , the amplification of the PS at small  $k$  is not the one we could expect from a naive linear

theory. However, despite the non-validity of the linear amplification of the small  $k$  PS, the non-linear structure formation does show asymptotically a self-similar evolution.

The  $1 - d$  toy model allowed us to probe the development of self-similarity at smaller scales and its range of validity. Such a study is impossible in  $3 - d$  due to the presence of smoothing at small scale. This investigation allowed us to identify the lower cut-off  $x_{min}$  marking the end of the self-similar regime at small scale. We have shown that this cut-off was explained naturally by a “stable clustering” hypothesis and we have shown that the exponent observed is in fact that expected for this case. Then as we know the temporal behaviour of the lower and upper cut-off, we can then determine the exponent in self-similar regime in terms of the index  $n$  of the initial PS and the damping term  $\Gamma$ .

We must however discuss the comparaison we made with  $3 - d$  stable clustering: in  $1 - d$  model, we envisage virialization only as valid up to the scale  $x_{min}$ , *i.e.* only smallest virialized structures can be supposed to be stable (at the same scale where the self-similarity break down, and not in the self-similar regime itself). This will be explored further in the next chapter. We will see that we can in fact consider, in a statistical sense, the structures in the self-similar regime to be virialized, but the stable clustering does not apply because they are not isolated.



# Chapter 5

## Dynamics of infinite one dimensional self-gravitating systems: scale invariance, halos and virialization

In this chapter we explore and characterize further the properties of the particle distributions produced in the  $1 - d$  self-gravitating models we have studied in the previous chapter. In particular we focus our analysis on two distinct approaches.

We start with a classical fractal analysis which is useful in particular to answer the following question: does the power-law behaviour observed in the correlation function correspond to a fractal-type distribution in this range of scales? In agreement with previous work of Miller et al. [112–114] we find that the answer is in the positive, and we extend some of the results which they have reported notably to the case where the initial power spectrum  $P_{init}(k) \propto k^4$  at small  $k$ .

In a second approach, we perform an analysis analogous to that now used canonically in  $3 - d$   $N$ -body simulations in cosmology in which the distribution is described as a collection of finite “halos”. As discussed in the introductory chapter 2, these are envisaged to be smooth virialized structures with properties given by a few parameters. Such a description, as it clearly *does not* correspond to a distribution with scale invariant properties, is at odds with the fractal description which emerges from the first part of this chapter. We will see that a description in terms of *approximately virialized* substructures may nevertheless be valid, precisely in the regime where there is fractal clustering. The substructures are, however, not smooth structures with a characteristic size; they must be defined as a function of an arbitrarily chosen scale. We interpret our results to mean that in the regime of non-linear fractal clustering the distribution can be said to correspond to a kind of “virialized hierarchy”.

### 1 Tools for fractal analysis

Fractals have been invoked to describe many physical phenomena which exhibit self-similarity (see e.g. [123]). Fractal geometry deals with the objects which are highly irregular and cannot be handled by the tools of differential geometry. A geometric object can in general be described in terms of its topological dimension which is an integer that defines the number of coordinates needed to specify the geometric

object. Loosely speaking a fractal is a shape that tends to have a scaling property, implying that the degree of its irregularity and/or fragmentation is identical at all scales. A single definition of fractal would be restrictive and it would be best to consider fractals as a collection of techniques and methods applicable in the study of the irregular, broken and self-similar geometrical patterns [104]. It seems best to regard a fractal as a set that has properties such as those described below: when we refer to a set as a fractal, we will typically keep in mind that this set has a fine structure, *i.e.* one has to look for detail on all accessible scales. It is too irregular to be described in traditional geometrical language, both locally and globally. This set which we call a fractal, often has some form of self-similarity, approximate or statistical. Although the concept of non differentiable geometry has been subsequently used in many physical and mathematical application, the concept of fractal object has been explicitly introduced and formalized by Mandelbrot (see e.g. [104]). A given fractal shape can be characterized by more than one definition of fractal dimension, and they do not necessarily need to coincide with each other. Therefore, an important aspect of studying a fractal structure (once it is characterized as self-similar in some way) is the choice of a definition for fractal dimension that best applies to, or is derived from, the case in study.

The approach we use in the following is a multifractal analysis of our simulated distribution of points [80]. A multifractal is an extension of the concept of fractal. It includes the possibility that the self-similar behaviour of particle distributions may be different in different density environments.

## 1.1 The Hausdorff Dimension

One of the most basic aspects of a set is its dimension which gives a quantitative characterization of its geometrical structure. An important step in the understanding of fractal dimensions is the *Hausdorff dimension* [104]. It can take non-integer values and was found to coincide with many other definitions. Hausdorff used the idea of defining measures using covers of point sets. To define the Hausdorff dimension of a subset  $S \subset \mathbb{R}^p$ , let us consider a covering of the set by  $p$ -dimensional neighborhoods, the  $i^{th}$  of which has a linear size  $\epsilon_i$ . The Hausdorff dimension  $D_H$  is the critical dimension which the Hausdorff measure  $H_d(\epsilon)$  passes from zero to an infinite value:

$$H_d(\epsilon) = \inf \sum_i \epsilon_i^d \rightarrow \begin{cases} 0 & \text{if } d > D_H \\ \infty & \text{if } d < D_H \end{cases} \quad (5.1)$$

and where the infimum extends over all the possible coverings subject to the constraint that any  $\epsilon_i \leq \epsilon$ .

The definition proposed by Mandelbrot for a fractal [104] is “*A fractal is a set for which the Hausdorff dimension strictly exceeds the topological dimension*”. The topological dimension can be simply defined as the number of independent directions in which one can move around a given point of the set. Smooth idealized forms like a plane and a cube, where the topological dimension equals the Hausdorff dimension, are non-fractal and are commonly called *homogeneous* or *compact*. Whenever a set has a non-integer Hausdorff dimension it is a fractal. This is sufficient but not a necessary condition [71].

The Hausdorff dimension defined so far provides a definition of fractal dimension for deterministic fractals, *i.e.* classical fractal sets in a *mathematical* idealized way. Although some of these classical fractals can be used to model physical structures, what is necessary is to discuss structures that are statistically self-similar, which are encountered in natural phenomena. The first tool to extract information is the *box-counting dimension*, also called the *capacity* of the set. It provides a relatively simple and appealing way of assigning a dimension to a set in such a way that certain kinds of sets are assigned a dimension which is not an integer.

## 1.2 Box Counting Dimension

In this approach the irregular distribution of particles is covered with a set of cells of size  $\ell_{cell}$ , and the number of cells are counted which contain part of the fractal. This size  $\ell_{cell}$  is varied over a range, and the resulting number of cells required to cover the distribution of points gives the number  $N(\ell_{cell})$ . Obviously  $N(\ell_{cell})$  will increase as the size  $\ell_{cell}$  decreases. If we proceed this way and find  $N(\ell_{cell})$  for smaller values of  $\ell_{cell}$ , we are able to plot a graph of  $N(\ell_{cell})$  versus  $\ell_{cell}$ , for different grid sizes. If asymptotically in the limit of small  $\ell_{cell}$  we reach the relation

$$N(\ell_{cell}) \propto \ell_{cell}^{-D}, \quad (5.2)$$

we can define the fractal dimension  $D$ . To accomplish the determination of this fractal dimension we find the slope of  $\ln(N(\ell_{cell}))$  plotted as a function of  $\ln(\ell_{cell})$ . We then get the expression for the box-counting dimension

$$D_b \equiv \lim_{\ell_{cell} \rightarrow 0} \frac{\ln(N(\ell_{cell}))}{\ln(1/\ell_{cell})}. \quad (5.3)$$

If the limit does not exist then one must talk about the *upper* box-counting dimension and the *lower* box-counting dimension which correspond to the upper limit and lower limit respectively in the expression above. In other words, the box-counting dimension is strictly defined only if the upper and lower box-counting dimension are equal. The box counting dimension  $D_b$  is, in essence, a scaling rule comparing how a pattern's detail changes with the scale at which it is considered. It is the most commonly used method of calculating dimensions. Its advantage lies in the easy and automatic computability provided by the method, as it is straightforward to count cells and maintain statistics allowing dimension calculation.

Note that the box-counting dimension deals only with the number of required coverings. This definition has no regard to the number of points contained inside each of the covering cells. In this sense, such a dimension depends on the “shape” of the distribution. In this way they provide a purely geometrical description, while no information is given about the clumpiness, as by correlation functions, discussed in Chapter 2, do.

In order to extend the description in terms of fractal dimensions, so as to include the clustering properties of a distribution, we need to introduce a probability measure, so that adequate information about the clustering of the distribution is available.

### 1.3 Generalized dimension

The definition of fractal dimension just introduced represents a particular case of a continuous sequence of scaling indices, known as the multifractal spectrum of generalized dimensions [80]. To define it, let us partition each space into cells of length  $\ell_{cell}$ . At each time of observation in the simulation, a measure  $\mu_i(t) = N_i(t)/N_T$  is assigned to cell  $i$ , where  $N_i(t)$  is the population of cell  $i$ , *i.e.* the number of particles in the cell, at time  $t$  and  $N_T$  is the total number of particles in the simulation. We thus define the sum over all occupied cells, *i.e.* the effective partition function

$$C_q = \sum_i \mu_i^q = \sum_i \left( \frac{N_i}{N_T} \right)^q. \quad (5.4)$$

If in some range of  $\ell_{cell}$  the quantity  $C_q$  has a scaling behaviour

$$C_q \propto \ell_{cell}^{\tau(q)}, \quad (5.5)$$

with a coefficient depending possibly on  $q$  but not on  $\ell_{cell}$ , its exponent  $\tau(q)$  is defined as the constant value, in this range, of

$$\tau(q) = \lim_{\ell_{cell} \rightarrow 0} \frac{\ln C_q}{\ln \ell_{cell}}. \quad (5.6)$$

The generalized dimension of order  $q$ , named also the *Renyi dimension*, is defined as

$$D_q \equiv \frac{\tau(q)}{q-1} = \frac{1}{q-1} \lim_{\ell_{cell} \rightarrow 0} \frac{\ln C_q}{\ln \ell_{cell}}, \quad (5.7)$$

and appears as a generalization of the Hausdorff dimension. The *box-counting dimension*  $D_b$  is simply obtained putting  $q = 0$  in Eq. (5.7) and is called  $D_0$ .

To take into account the different natural measures of the cells it is usual to introduce notably the quantities  $D_1$ , obtained by taking properly the limit  $q \rightarrow 1$ , and  $D_2$ .  $D_1$  is called the *information dimension* since it is related to the information entropy of the measure, *i.e.* it is related to the rate of information loss as the resolution scale increases [71]. It gives the fractal dimension of the points on which the measure is mostly concentrated.  $D_2$  is the *correlation dimension*, originally introduced by Grassberger and Procaccia (see e.g. [77]), and gives an important characterization of the scale-invariant properties of a fractal set. The correlation dimension can be easily related to the measured power-law shape of the 2-point correlation function defined in Chapter 2. As a complete statistical description of a given point distribution requires the knowledge of correlations or moments of any order, a complete characterization of the scaling properties of a fractal set should require the introduction of the hierarchy of scaling indices. Thus, as  $q$  increases above 0, the  $D_q$  provide information on the geometry of cells with higher population. It is well established that, for an homogeneous fractal, all of the generalized dimension are equal, while for an inhomogeneous fractal it is a decreasing function of its argument, *i.e.* the existence of several values for  $D_q$  as a function of  $q$  in a given range of  $\ell_{cell}$ , reveals different scaling behaviours for cells of the same size lying in dense or in underdense regions (see e.g. [123]).

In practice, it is not possible to take the limit  $\ell_{cell} \rightarrow 0$  with a finite sample. Instead, one looks for a scaling relation over a substantial range of  $\ln(\ell_{cell})$  with the hope that a linear relation between  $\ln C_q$  and  $\ln(\ell_{cell})$  occurs, suggesting power law dependence of  $C_q$  on  $\ell_{cell}$ . Then, in the most favorable case, the slope of the linear region should provide the correct power and, after dividing by  $q - 1$ , the generalized dimension  $D_q$ . Following [107], if scaling can be found, either from experiment or computation, *over three decades* of  $\ell_{cell}$  then we typically infer that there is a good evidence of fractal structure.

## 1.4 Relation to 2-point analysis

Part of our goal is to illustrate how the fractal analysis can be related to the study of the clustering properties of the distribution of points through statistical tools such as the reduced correlation function. In our study of the scale-invariant properties of the fractal set, we followed the temporal evolution of the correlation dimension  $D_2$ . As this can be related to the measured power-law shape of the 2-point correlation function, it is interesting to compare the values obtained for  $D_2$  with the exponents  $\beta$  and  $\gamma$  defined in chapter 4 generated by the PS and the correlation function respectively of the self-similar regime, *i.e.*  $P(k) \propto k^{\beta-1}$  and  $\xi(x) \propto x^{-\gamma}$ . It is easy to show this relation. Let us consider the probability  $C_i(r)$  of finding  $n_i(< r)$  points out of the  $N$  points of a set within a distance  $r$  from  $x_i$ ,

$$C_i(r) = \frac{1}{N} \sum_{j \neq i=1}^N \Theta(r - |x_i - x_j|) = \frac{n_i(r)}{N}, \quad (5.8)$$

where  $\Theta(x)$  represents the well-known Heaviside step function. We then introduce the correlation integral

$$C(r) = \frac{1}{N} \lim_{N \rightarrow \infty} \sum_{i=1}^N C_i(r), \quad (5.9)$$

whose scaling in the limit  $r \rightarrow 0$  defines the correlation dimension,  $D_2$ , according to  $C(r) \propto r^{D_2}$ . Following the definition of the 2-point correlation function given in [71], it is easy to see that it can be related to the correlation integral according to

$$C(r) = \int_0^r dr \left( 1 + \xi(r) \right). \quad (5.10)$$

As the correlation function behaves as a power-law  $\xi(x) \propto x^{-\gamma}$  we obtain the relation,

$$D_2 = 1 - \gamma = \beta, \quad (5.11)$$

where the second equality simply comes from the fact that the PS is the Fourier transform of the correlation function.

## 2 Fractal analysis of evolved self-gravitating distributions

We now apply the tools described in the previous section to analyse the clustering in real space which emerges in the toy models we have studied in the previous chapter.

We explore the same range of initial conditions as in the previous chapter (*i.e.* initial PS with  $P_{init}(k) \propto k^n$  at small  $k$  for  $n = 0, 2$  and  $4$ ) and the same range of models (static, quintic and RF), and analyse exactly the same simulations with  $N = 10^5$  particles. We also compare our results with those reported previously by Miller et al [112–114]. All our results apply to the same simulations with  $N = 10^5$  particles reported in the previous chapter.

If it exists, a scaling range of  $\ell_{cell}$  is defined as the interval on which plots of  $\ln C_q$  versus  $\ln(\ell_{cell})$  are linear. For the special case of  $q = 1$  we plot  $-\sum_i \mu_i \ln \mu_i$  versus  $\ln(\ell_{cell})$  to obtain the information dimension. If a scaling range can be found,  $D_q$  is obtained by taking the appropriate derivative. To probe the multifractal property, we limit our analysis to the generalized dimension  $D_q$  for  $q = 0, 1, 2$  and  $10$ . This latter large value of  $q$  has been chosen arbitrarily to probe for the multifractality of the distributions.

## 2.1 Algorithm

To perform the numerical fractal analysis, we simply follow the recipe introduced in section 1.3, *i.e.* we partition the configuration space into cells of length  $\ell_{cell}$  (at a given time of observation). For each length of cell  $\ell_{cell}$ , we assigned a measure  $\mu_i(t) = N_i(t)/N_T$  to cell  $i$ , where  $N_i(t)$  is the population of cell  $i$  and  $N_T$  is the total number of particles in the simulation. We thus perform the sum over all occupied cells, *i.e.* the effective partition function  $C_q = \sum_i \mu_i^q = \sum_i \left(\frac{N_i}{N_T}\right)^q$  defined previously.

We start with a single cell whose size is the same as the box size. We then decrease the size  $\ell_{cell}$  of the cell, increasing the number of cells  $N_{cell}$  in the box, and satisfying the relation  $L = N_{cell} \times \ell_{cell}$ , where  $L$  is the total size of the simulation box. We simply decrease the size of the cell by a factor 2, *i.e.* the number of cells in covering the configuration space is  $N_{cell} = 2^n$ , where  $n$  is an integer which counts the number of iterations. As we will discuss immediately below, the distribution itself defines a lower cutoff to the value  $\ell_{cell}$  we should consider in any case.

## 2.2 Temporal evolution of the generalized dimensions

We are interested in the temporal evolution of the generalized dimension in the configuration space. In Figs. 5.1 and 5.2 we consider the correlation dimension  $D_2$ , starting with an initial PS  $P_{init}(k) \propto k^2$  in the static and expanding (quintic) cases.

As time progresses three different regimes can be clearly distinguished:

- for very small  $\ell_{cell}$ , below a scale we indicate in Figs. 5.1 and 5.2 as  $\ell_{spar}$ , we have a trivial scaling behavior indicative of the so-called *sparseness* limit, *i.e.*  $\ell_{cell}$  is sufficiently small so that no box contains more than one point. Below the scale denoted by  $\ell_{spar}$  in Figs. 5.1 and 5.2,  $N_i(t) = 0$  or  $1$  and the number of occupied boxes is equal to the total number of particles  $N_T$  in the system. Thus  $C_q = \sum_{i=1}^{N_T} \left(\frac{1}{N_T}\right)^q$ . The slope of  $\frac{1}{q-1} \ln C_q$  versus  $\ln(\ell_{cell})$  is then zero;
- for the largest value of  $\ell_{cell}$ , above the scale  $\ell_{unif}$  in Figs. 5.1 and 5.2, we have a trivial scaling behavior indicative of the large scale uniformity of the

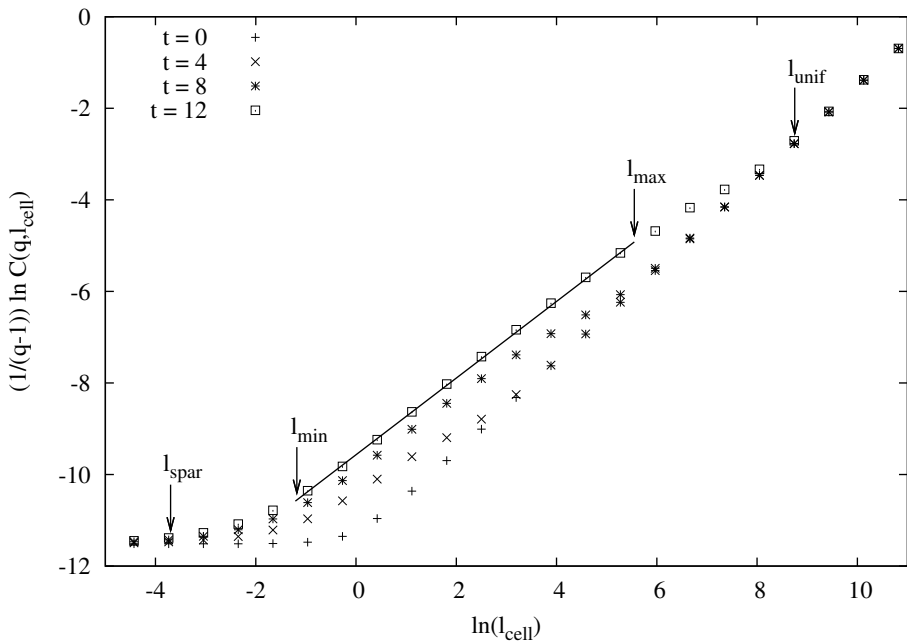


Figure 5.1: Temporal evolution of  $\frac{1}{q-1} \ln(C(q, \ell_{cell}))$  versus  $\ln(\ell_{cell})$  in configuration space for the static model for  $q = 2$ , and starting with an initial PS  $P_{init}(k) \propto k^2$ .

distribution. Above  $\ell_{unif}$ ,  $N_i(t) \approx \frac{N_T}{\ell_{cell}}$  and the number of occupied cells is simply equal to the number of cells  $N_{cell} = L/\ell_{cell}$ . The slope of  $\frac{1}{q-1} \ln C_q$  versus  $\ln(\ell_{cell})$  is then equal to unity;

- intermediate between these two regions, between the scales  $\ell_{min}$  and  $\ell_{max}$ , we have a scaling behavior which corresponds to the range where non-trivial non-linear clustering develops, and in which we focus our multifractal analysis: the slope of  $\frac{1}{q-1} \ln C_q$  versus  $\ln(\ell_{cell})$  then takes an intermediate value between zero and one in the range  $\ell_{min} \leq \ell_{cell} \leq \ell_{max}$  (see Figs. 5.1 and 5.2). The emergence of a scaling regime would indicate a fractal behaviour of the non-linear clustering. We expect that this range to correspond to the range of scale invariant clustering indicated by the analysis of the 2-point correlation function.

We note that there are also two distinct transient regimes between these three different scaling regions. Firstly, there is a range of  $\ell_{cell}$  between the sparseness limit and the self-similar regime, *i.e.*  $\ell_{spar} \leq \ell_{cell} \leq \ell_{min}$ , which would correspond in the 2-point correlation analysis in Chapter 4 to the clustering signal present at scales below those of the scaling regime, and where the correlation function is flat. The second transient regime corresponds to a range of  $\ell_{cell}$  between the self-similar regime and the scale of uniformity, *i.e.*  $\ell_{max} \leq \ell_{cell} \leq \ell_{unif}$ , and would correspond to the “quasi-linear” regime where the amplitude of the relative density fluctuations is of order unity or a little larger (see e.g. [22]).

A qualitative inspection shows that the observed size of each scaling range defined previously depends on the elapsed time into the simulation, as  $\ell_{min}$  and  $\ell_{max}$  evolve

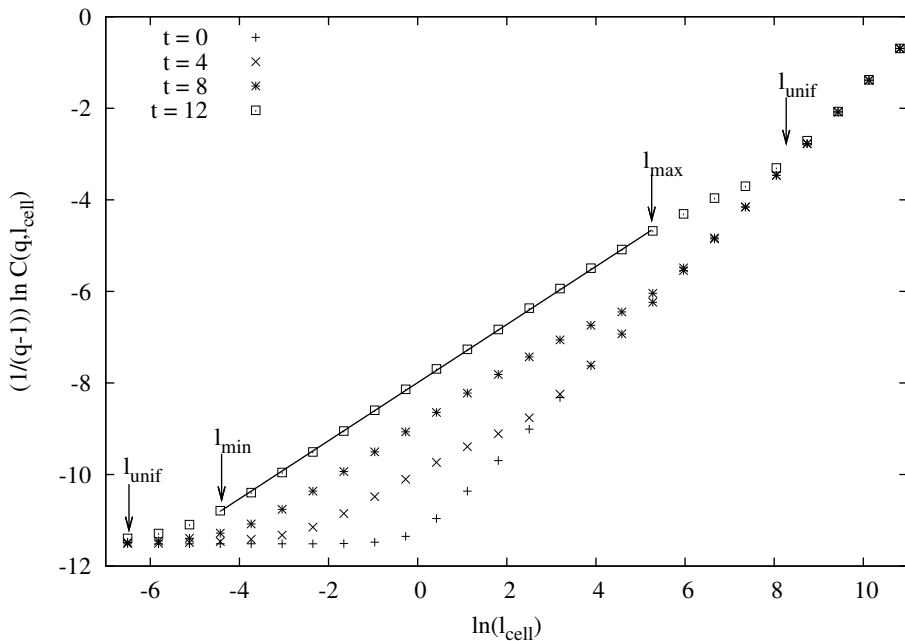


Figure 5.2: Temporal evolution of  $\frac{1}{q-1} \ln(C(q, \ell))$  versus  $\ln(\ell)$  in configuration space for the quintic model for  $q = 2$ , and starting with an initial PS  $P_{init}(k) \propto k^2$ .

in time. This evolution, however, is different in the static and expanding cases: the scale  $\ell_{min}$  clearly decreases in time in the expanding case, whereas it stays approximately constant in the static case. Basing our investigation on the 2-point analysis of Chapter 4, we expect the scale  $\ell_{max}$  to correspond to the scale of non-linearity, above which one crosses over to a uniform distribution, and the scale  $\ell_{min}$  to match with the lower cut-off to self-similarity,  $x_{min}$ , introduced in Chapter 4.

Shown in Fig. 5.4 and 5.3 are the evolution of the scales  $\ell_{min}$  and  $\ell_{max}$  for the initial PS  $P_{init}(k) \propto k^2$  in the static and expanding (quintic) cases, defined with the use of a linear regression of the correlation dimension in the self-similar range. As anticipated, these behaviors are precisely those we have observed in the previous chapter for the scale of self-similarity,  $\ell_{min} \propto \exp(-\frac{2}{3}\Gamma t)$  in the expanding case, and for the scale of non-linearity,  $\ell_{max} \propto R_s(t)$  in both the static and expanding cases, which follows the behavior predicted from linear theory.

## 2.3 Dependence of exponents on initial conditions and model

We focus now our analysis on the numerical assessment of the different fractal dimensions  $D_q$  in the range where clustering is non-linear and self-similar. To guarantee that the fractal structure is fully developed, we consider the most evolved configurations in time in which the range of non-linear clustering is greatest. We will see that it is possible to find good scaling over more than three decades in  $\ell_{cell}$ .

Following the definition of the generalized dimension in Eq. (1.3), we give first in Tab. 5.1 the different values of  $D_q$  in the self-similar regime, obtained with the use of a linear regression, and for different initial PS  $P_{init}(k) \propto k^2$  and  $k^4$  in the static and expanding (quintic and RF) cases. We discuss separately the case where the

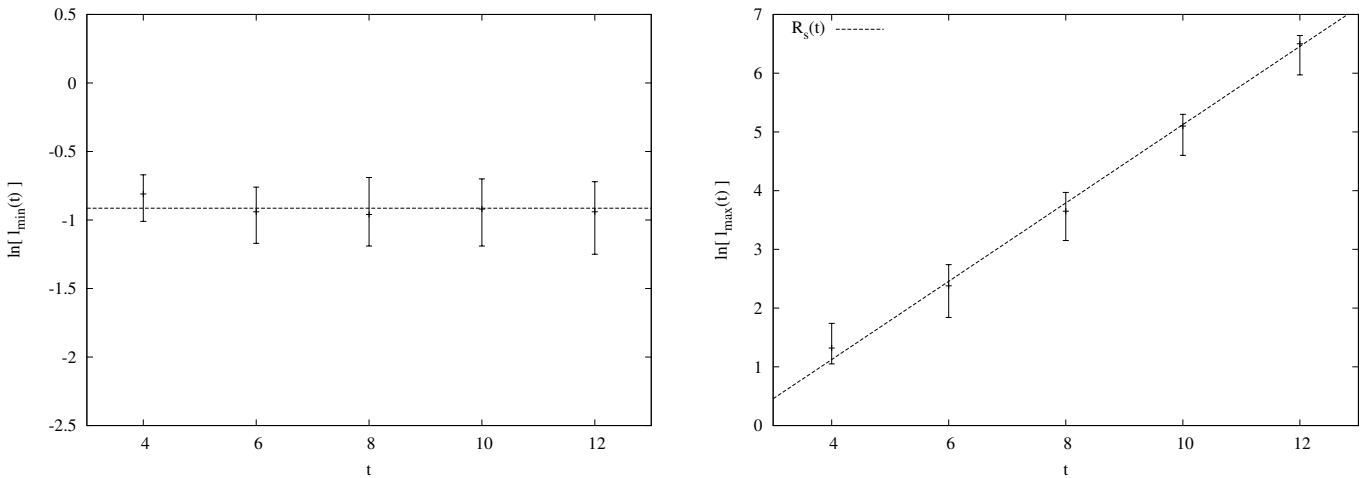


Figure 5.3: Evolution of the scales  $\ell_{\min}$  and  $\ell_{\max}$  in the static case for an initial PS  $P_{init} \propto k^2$ . We define these scales with the use of a linear regression of the reduced correlation dimension in the self-similar regime. We observe that  $\ell_{\min}$  stays slightly constant whereas  $\ell_{\max} \propto R_s(t)$ . The error bars represent the uncertainty of the linear regression.

initial PS  $P_{init}(k) \propto k^0$  in Tab. 5.2 for the same models. We restrict our analysis to the dimensions  $D_q$  with  $q = 0, 1, 2$  and  $10$ . The higher value of  $q$  has been chosen to shed light on the potential multifractal behaviour of the system. Inspecting the results in Tab. 5.1 we draw the following conclusions:

- the results for the correlation dimension  $D_2$  are in agreement, within the standard numerical error, with the exponents derived in the previous chapter (see Tabs. 2.3 and results in Chapter 4 section 3.3) from the 2-point correlation analysis, as given by Eq. (5.11);
- the systems are definitely fractal as the box-counting dimension  $D_0$  is different from unity. Moreover, all results for the generalized dimensions  $D_q$  are consistent with the constraint which applies to fractal behavior, *i.e.*  $D_{q_1} \geq D_{q_2}$  for  $q_1 \leq q_2$ ;
- a clear difference between static and expanding cases is evident: in the latter cases there is a significant variation of the exponent (*i.e.* non-trivial spectrum of multi-fractal exponents) while in the static case the results appear consistent with the hypothesis of a homogeneous fractal;
- further in the static case the exponents depend very weakly, if at all, on the initial condition (*i.e.* on the exponent  $n$  of the initial PS); in the expanding cases, all measured exponents show the same trend with the exponent  $n$  as shown by  $D_2$ , *i.e.* greater is  $n$ , smaller is the exponent.

We note that these results are partly in agreement with the investigation of Miller et al. in [113, 114] where a multifractal analysis has been performed in both the configuration space and the phase space. We clearly obtain the same qualitative behaviour for the generalized dimension in the expanding cases, as a multifractal

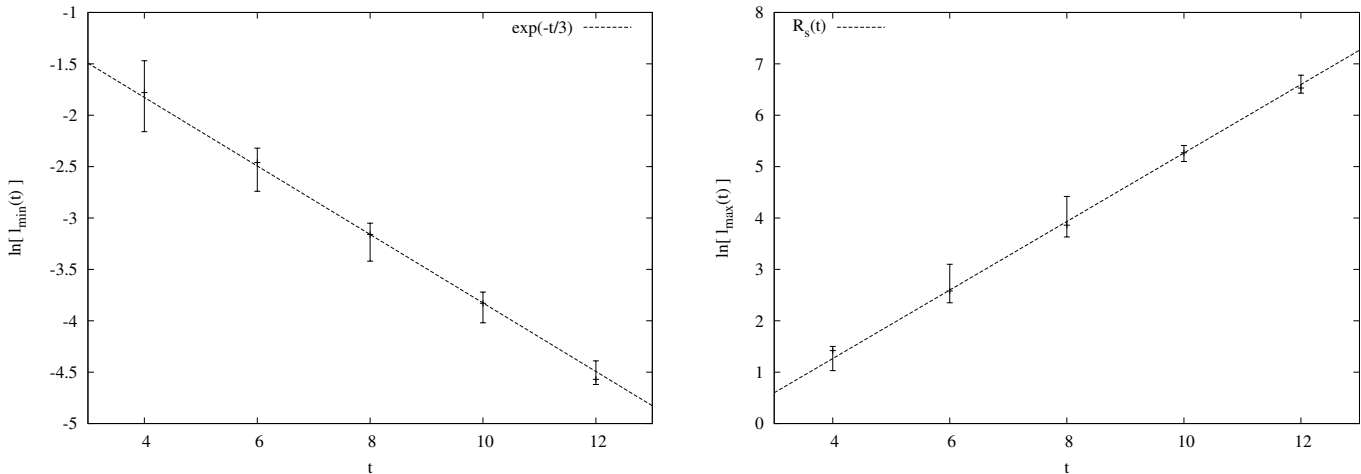


Figure 5.4: Evolution of the scales  $\ell_{\min}$  and  $\ell_{\max}$  in the quintic case for an initial PS  $P_{\text{init}}(k) \propto k^2$ . We define these scales with the use of a linear regression of the reduced correlation dimension in the self-similar regime. We observe that  $\ell_{\min} \propto \exp(-\frac{2}{3}\Gamma t)$  with  $\Gamma = 1/\sqrt{6}$ , and  $\ell_{\max} \propto R_s(t)$ . The error bars represent the uncertainty of the linear regression.

behavior is observed. However, we do not reach the same conclusion as in [113] as far as the static case is concerned: As our numerical investigation shows that the systems are in agreement, within the numerical error, with a mono-fractal behavior, *i.e.*  $D_q$  remains approximately constant for  $q \in [0, 10]$ , Miller et al. claim that the behavior of  $D_q$  in the static case is qualitatively similar to the expanding (quintic) case, but with less robust scaling ranges.

Furthermore, considering the measure of the correlation dimension  $D_2$  in [114] for an initial condition which corresponds to the choice of an initial PS  $P_{\text{init}}(k) \propto k^2$  at small  $k$ , we can compare quantitatively our results with those obtained by Miller et al. We see that they are in agreement within our numerical error in both the quintic and RF models. We obtain the same dependence on the initial condition, *i.e.* on the index of the initial PS. We now return to the case where the initial PS

|         | initial PS | $D_0$           | $D_1$           | $D_2$           | $D_{10}$        |
|---------|------------|-----------------|-----------------|-----------------|-----------------|
| static  | $k^2$      | $0.87 \pm 0.03$ | $0.88 \pm 0.02$ | $0.83 \pm 0.04$ | $0.84 \pm 0.03$ |
|         | $k^4$      | $0.89 \pm 0.03$ | $0.87 \pm 0.03$ | $0.85 \pm 0.02$ | $0.86 \pm 0.03$ |
| quintic | $k^2$      | $0.64 \pm 0.02$ | $0.65 \pm 0.02$ | $0.64 \pm 0.02$ | $0.59 \pm 0.03$ |
|         | $k^4$      | $0.56 \pm 0.02$ | $0.56 \pm 0.02$ | $0.53 \pm 0.02$ | $0.46 \pm 0.04$ |
| RF      | $k^2$      | $0.49 \pm 0.02$ | $0.50 \pm 0.02$ | $0.49 \pm 0.01$ | $0.45 \pm 0.01$ |
|         | $k^4$      | $0.39 \pm 0.03$ | $0.38 \pm 0.02$ | $0.37 \pm 0.01$ | $0.32 \pm 0.02$ |

Table 5.1: Generalized dimension  $D_q$  for  $q = 0, 1, 2$  and  $10$  in the static, quintic and RF cases (*i.e.*  $\Gamma = 0, 1/\sqrt{6}$  and  $1/\sqrt{2}$ ). We analyse the different initial condition characterized with different initial PS  $P_{\text{init}} \propto k^2$  and  $k^4$ .

$P_{\text{init}} \propto k^0$  for the same three different models. We give in Tab. 5.2 the different values of  $D_q$  for the same values of  $q$  as above. A difference emerges compared to

the case  $P_{init}(k) \propto k^2$  and  $k^4$ . While in an inhomogeneous fractal the generalized dimension  $D_q$  is a decreasing function of its argument, we see that in the three different models (static, quintic and RF)  $D_0$  is smaller than  $D_1$ . This puzzling result can be explained by the fact that such a distribution (*i.e.* initial spectrum  $n = 0$ ) is not as *strongly clustered* as the others, *i.e.* not all the particles are concentrated in the overdense regions. This was already noted in our visual inspection in Figs. 4.3 and 4.5 in Chapter 4. Then undersampling effects lead to lowering of the box-counting dimension. This paradoxical result was already discussed by Borgani in its study of the multifractal behaviour of  $3 - d$  hierarchical density distributions [27] and Dubrulle et al. in their multifractal analysis of  $3 - d$  galaxy catalogs with box-counting methods [48]. This illustrates that the box-counting method should be used with caution when analyzing discrete sets like galaxy distributions.

| $k^0$   | $D_0$           | $D_1$           | $D_2$           | $D_{10}$        |
|---------|-----------------|-----------------|-----------------|-----------------|
| static  | $0.71 \pm 0.04$ | $0.85 \pm 0.02$ | $0.84 \pm 0.02$ | $0.82 \pm 0.06$ |
| quintic | $0.62 \pm 0.02$ | $0.79 \pm 0.02$ | $0.80 \pm 0.02$ | $0.72 \pm 0.03$ |
| RF      | $0.48 \pm 0.02$ | $0.69 \pm 0.02$ | $0.71 \pm 0.02$ | $0.61 \pm 0.04$ |

Table 5.2: Generalized dimension  $D_q$  for  $q = 0, 1, 2$  and  $10$  in the static, quintic and RF cases (*i.e.*  $\Gamma = 0, 1/\sqrt{6}$  and  $1/\sqrt{2}$ ). We analyse the initial condition with PS  $P_{init}(k) \propto k^0$ .

### 3 Halos and virialization

In this section, we explore the possibility of describing the clustered distributions obtained in the toy models we have studied as a collection of “halos”, *i.e.* as a collection of approximately independent virialized structures. As discussed in Chapter 2, it is now standard to use such a description to characterize the structures obtained in cosmological simulations in  $3 - d$ . As we noted in the introduction, the fractality we have found in these models in the preceding sections would seem to be clearly at odds with such a description: these halos are considered to have smooth density profiles and clearly do not have scale invariant properties.

In the following, we first introduce and employ a simple “Friend-of-Friend” (FoF) algorithm which allows one to select out a set of (candidate) halos in a manner wholly analogous to how it is done in  $3 - d$  simulations. We analyse the properties of the selected halos and the degree to which their statistical properties reflect or not the scale invariance (in a certain range of scales) of the distribution. We then turn to the question of whether these halos, or at least a certain appropriately selected subclass of them, may actually be considered as roughly independent objects dynamically. This in practice is probed by testing whether they show a tendency to be virialized. This leads us then to analyze in detail the distribution of the measured virial ratios, testing whether, for halos selected with characteristic sizes in the range of scale-invariant clustering, there is evidence for a stable PDF of the virial ratio peaked about unity.

#### 3.1 Halo selection: The Friend-of-Friend algorithm

To define candidate “halos”, we follow the simplest method which consists in a *structure-finding* algorithm called the *FoF-algorithm* (see e.g. [58, 74, 108]). As illustrated in Fig. 5.5, this purely geometrical method consists in introducing an arbitrary linking length  $\ell_{\text{fof}}$  that represents the distance below which two neighboring particles belong to the same FoF-group. The collection of linked particles forms a group,

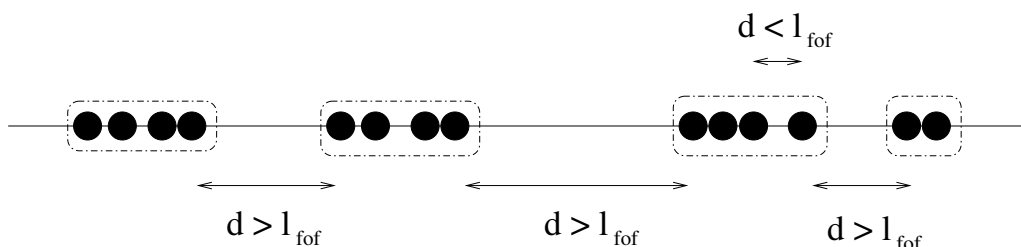


Figure 5.5:  $1 - d$  schematic representation of the FoF-algorithm: if and only if the distance  $d$  between two particles is less than the linking length  $\ell_{\text{fof}}$  these two particles are grouped together in the same FoF-halo (dashed line).

which we refer to an “FoF-halo”. In the following we discard isolated particles.

One way of describing what the algorithm does is that it simply selects out regions in which the density, smoothed on scale of local interparticle distance, is greater than a threshold density given by  $1/\ell_{\text{fof}}$ . Note that since the mean density is simply  $1/\ell$ , where  $\ell$  is the initial lattice spacing, if  $\ell_{\text{fof}} < \ell$  we select out regions

which are necessarily overdensities. Equivalently, the algorithm can be thought in  $1 - d$  as simply breaking the distribution into finite pieces by “cutting” it at any empty regions (*i.e.* voids) greater than  $\ell_{fov}$ .

In relation to the physical motivation - which is to try to define finite subsystems which have some dynamical independence - the limitation of the algorithm is that it picks out such subsystems in an extremely elementary way, without using any dynamical criterion notably. If there are such subsystems or finite structures, the algorithm will, for example, clearly put two of them together which “happen to be” closeby at the time considered. In the context of cosmology this has led to the development of various alternative algorithms (see e.g. [101, 102]).

A crucial feature of the algorithm is, evidently, that it includes one free parameter,  $\ell_{fov}$ , and the candidate “halos” one picks out depend on it. In  $3 - d$  cosmological simulations a *single* value of this is chosen by hand, corresponding to a threshold in the density a few times the mean density, the idea being to select out all groups of particles which have undergone together non-linear evolution<sup>1</sup>.

Here we will study carefully the dependence of the halos on this free parameter  $\ell_{fov}$ . In particular we will examine whether a choice of  $\ell_{fov}$  a little smaller than  $\ell$ , as used in cosmological simulations, has any physical justification or meaning. This latter point essentially concerns the question of whether there is a particular choice of  $\ell_{fov}$  which selects out structures which are (typically) virialized. Such virialization is what indicates that they are of dynamical significance considered on their own (because virialization is one of the distinguishing characteristics of finite isolated structures).

In the rest of the section we consider first the basic properties of the structures selected out by the FoF-algorithm, specifically

- the distribution of their size  $L_c$ , *i.e.* their spatial extent;
- the distribution of their mean densities  $n_c$ ;
- the distribution of the number of points they contain (known as their *mass function* in the cosmological context).

Provided  $\ell_{fov}$  is significantly smaller than the size of the system, such distributions may be assumed to be sampled from some underlying PDF which contains inevitably a certain kind of information about the distribution in the infinite system limit. The question which interests us is how these PDF depend on the single parameter  $\ell_{fov}$ . In general we would expect them to depend on how  $\ell_{fov}$  compares with the characteristic scales in the system. In the case of scale-invariant clustering in the distribution, which we have found appears to be the case of those considered here, one might expect appropriate properties of the FoF-halos to be independent of  $\ell_{fov}$ . If this is the case such an analysis is a suitable instrument for revealing scale-invariant properties.

---

<sup>1</sup>In other variants of the algorithm employed in cosmology at least one parameter, or often several such parameters must be introduced, and they are ascribed essentially ad-hoc values given similar kinds of physical motivation.

We present here only results for a single chosen case: initial conditions with PS in  $k^4$  (“causal fluctuations”) evolved up to  $t_s = 22$ , in the quintic model. We choose this case because it is one of those where the range of scales over which both non-linear clustering and, in particular, scale-invariant clustering is greatest. In Fig. 5.6 is recalled the reduced 2-point correlation function as it develops in time in this case up to the final time at which we analyse it here. For what follows it will be important to have present the scales characterising the clustering at the final time: as addressed in Chapter 4, the *scale-invariant power-law clustering* regime stretches in this case over approximately five orders of magnitude, *i.e.* between the scales  $x_{min} \sim 10^{-3}\ell \sim 10^{-8}$  and  $x_{max} \sim 10^2\ell \sim 10^{-3}$  where  $\ell$  is the initial lattice spacing. In the following, we will use the normalized parameter  $\Lambda = \ell_{fov}/\ell$  in studying the behaviors of the different observables. In this variable the region of scale invariance then corresponds to  $\Lambda = 10^{-3}$  to  $10^2$ . In our analysis, we do not consider values of  $\Lambda > 10$  as in this case, the number of FoF-halos is too small to give a significant statistics.

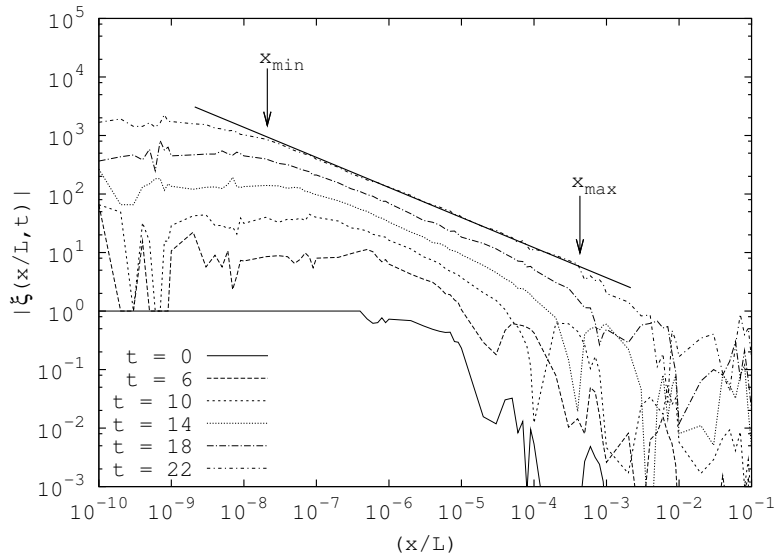


Figure 5.6: Evolution of the absolute value of the reduced 2-point correlation function  $|\xi(x, t)|$  in the quintic case, starting with an initial PS  $P_{init}(k) \propto k^4$ . Considering the evolved time  $t_s = 22$ , we see that the self-similar regime is well developed.

Just as in the fractal analysis of the previous section using box counting, we note at the outset that we expect to see limiting behaviours of the PDF of FoF-halos for very large or small values of  $\ell_{fov}$ :

- when  $\ell_{fov}$  becomes sufficiently small, the probability of having more than two particles becomes negligible and one has essentially just pairs of nearest-neighbor particles;
- when  $\ell_{fov}$  becomes comparable to the scale of non-linearity, we will link together the whole system and the result would be trivial.

We will show here only results up to  $\ell_{fov} = 10 \ell$  because the number of FoF-halos becomes so small that the measures of the PDF we consider become too noisy. Indeed, at  $\ell_{fov} = 10^2 \ell$  there are only a couple of FoF-halos.

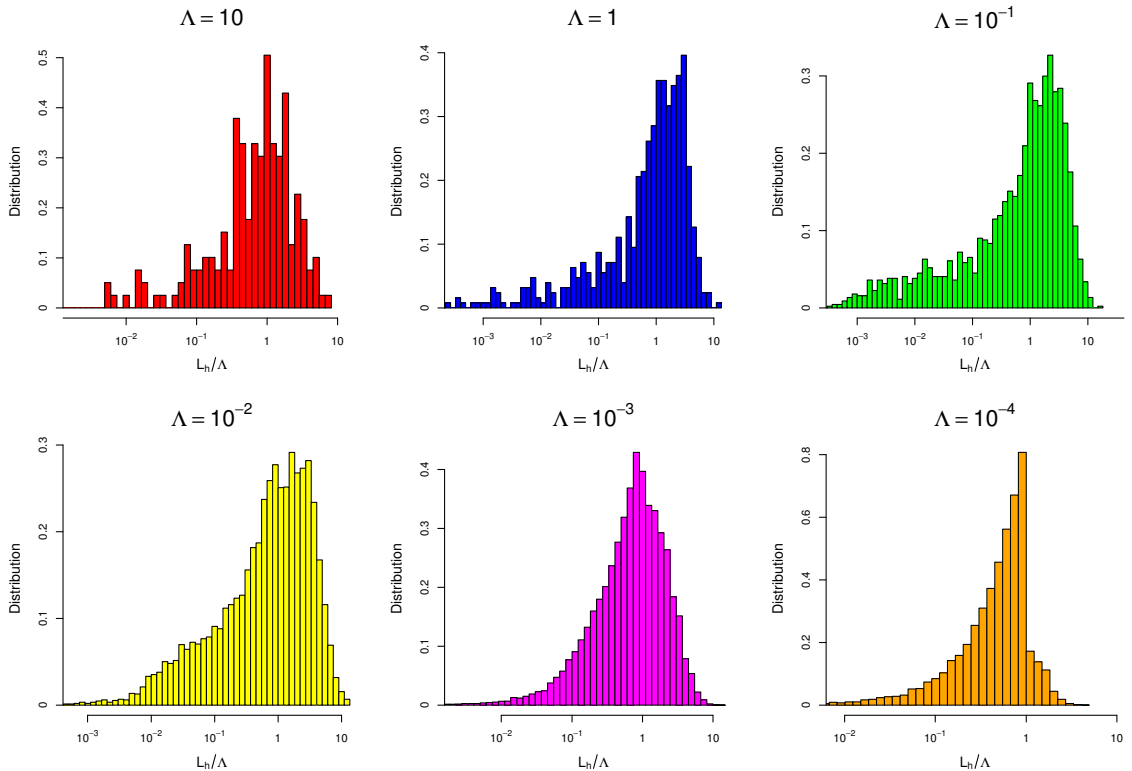


Figure 5.7: Distribution (normalized to unity) of the size  $L_h$  of the FoF-halos extracted from the simulation box for different values of the parameter  $\Lambda = \ell_{fov}/\ell$  in a semi-log representation. These results are for the case of an initial PS  $P_{init}(k) = k^4$  evolved at  $t_s = 22$ . The value of the parameter  $\Lambda$  decreases from left to right and from top to bottom. The red, blue, green, yellow, magenta and orange plots correspond respectively to a value of  $\Lambda = 10, 1, 10^{-1}, 10^{-2}, 10^{-3}$  and  $10^{-4}$ .

In Fig. 5.7 is shown the PDF of the size  $L_h$  of the FoF-halos, renormalized by the parameter  $\Lambda$ . For  $\ell_{fov}$  between  $\ell$  and  $10^{-2} \ell$  we observe a reasonably stable form with a peak somewhere between  $\Lambda$  and  $10\Lambda$ . As we go towards smaller  $\Lambda$  we see a sharper peak appear, which also shifts to smaller  $\Lambda$ . That this latter behaviour is indicative of the sparseness limit will become clearer below. We note that these plots also suggest that the properties of FoF-halos are not a very “clean” way to single out scale-invariant properties: the algorithm is not a simple coarse-graining which breaks the system into subsystems of a single size, but rather it selects out sub-systems with quite a broad range of sizes. Given that scale invariance applies in a limited range of scale (between 4 and 5 orders of magnitude in this case), this means in practice that even when the FoF-algorithm picks out mostly structures with a size in this range, it also includes some structures which fall outside the range. In Fig. 5.7 we see that at only  $\Lambda = 1$  does the full range of sizes fall within the range of scale invariance. At  $\Lambda = 0.1$  we already have a significant “pollution” by structures of size less than  $10^{-3} \ell = x_{min}$ .

Shown in Fig. 5.8 is the measured distribution of the density of the FoF-halos. The qualitative behaviours are quite similar to in the previous plots: in the range

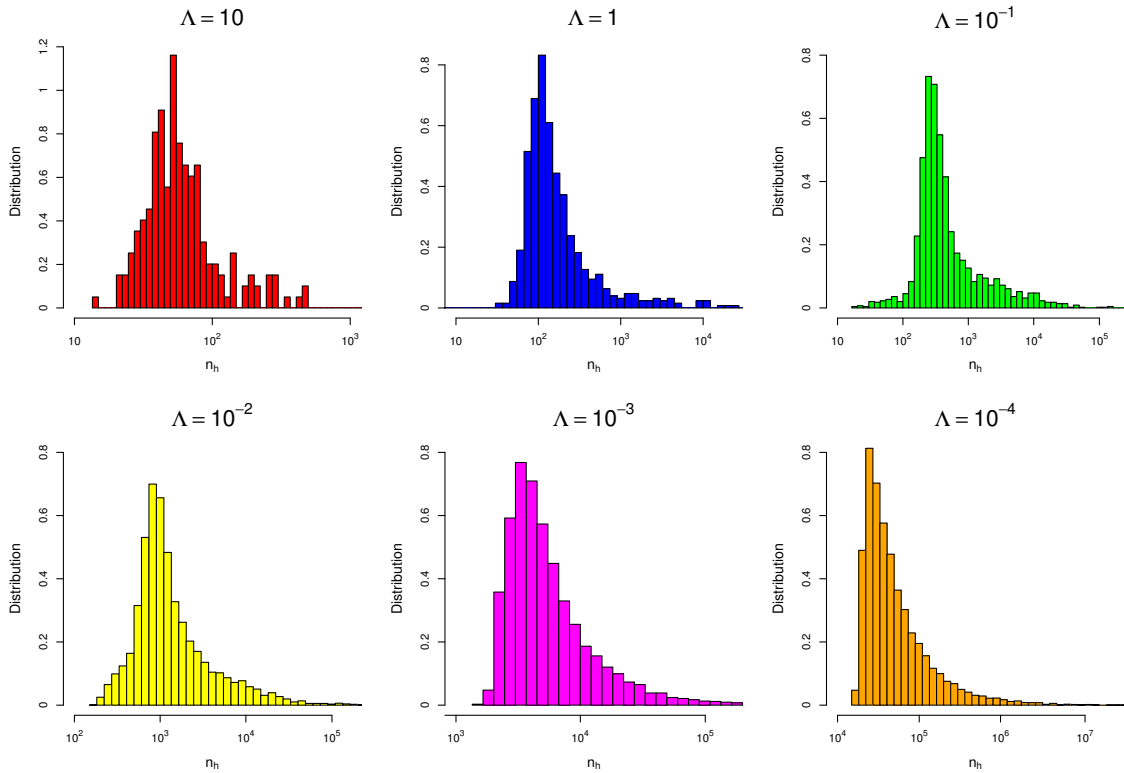


Figure 5.8: Distribution (normalized to unity) of the local density  $n_h = N_h/L_h$  of the FoF-halos extracted from the simulation box for different values of the parameter  $\Lambda$  in a semi-log representation. The color code is the same as in previous figure.

$\Lambda \in [10^{-2}, 10]$  there is a roughly stable form which becomes modified at the two smaller  $\Lambda$  (to an almost strictly monotonically decreasing form). As we noted above, the FoF-algorithm singles out regions in which the density is strictly larger than a threshold equal to  $2/\ell_{fof}$ . As can be seen in the plots this strict lower limit (imposed again by the sparseness) begins to play a role for  $\Lambda = 10^{-2}$ , and at  $\Lambda = 10^{-3}$  clearly defines the sharp cut-off which has appeared. The FoF-algorithm is then selecting out single structures with density around and slightly larger than  $n_{min} = 2/\ell_{fof}$ .

The histogram of the number  $N_c$  of particles in the FoF-halos is shown in Fig. 5.9. These plots show much more clearly how the effect of sparseness (*i.e.* the existence of a lower cut-off in the scale invariance) already “pollutes” the statistics of the FoF-halos when  $\ell_{fof} \gg x_{min}$ : we see already at  $\Lambda = 1$  a significant number of halo with only a few particles. For the two smallest values the 2 particles FoF-halos completely dominate, and clearly the properties we saw in the previous two figures at these values were indeed, as supposed, indicative of the sparseness limit. Indeed we can infer that the plot for  $\Lambda = 10^{-4}$  in Fig. 5.7 is essentially just the distribution of nearest-neighbours distances in the distribution with the sharp cut arising from the upper cut-off at  $L_h = \ell_{fof}$ .

In summary, the FoF-algorithm picks out FoF-halos of which the statistical properties carry information about the scale invariance in the distributions, but in a very limited range as the algorithm mixes quite strongly a range of scales.

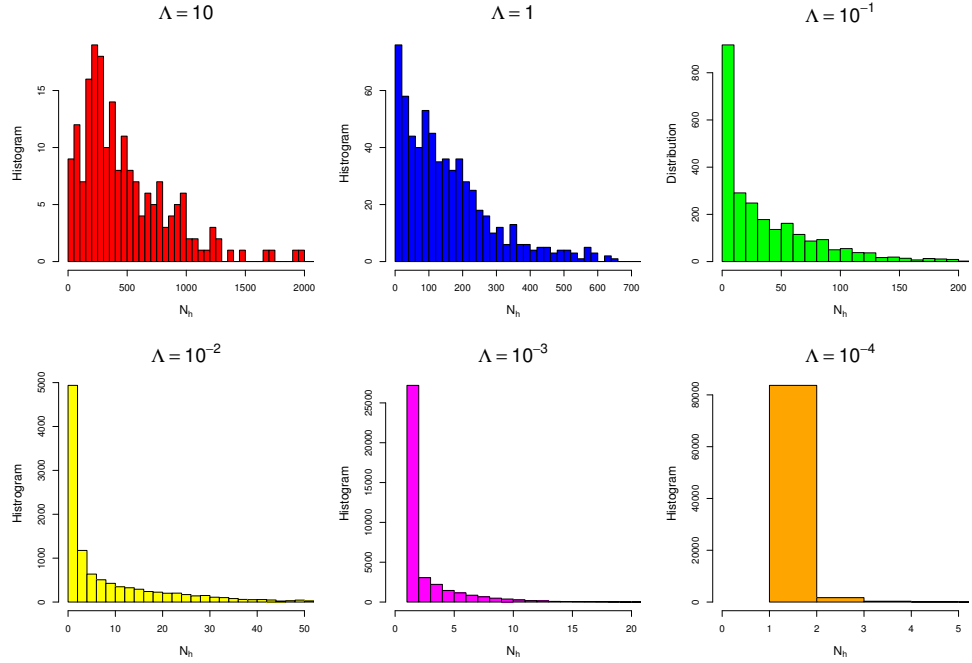


Figure 5.9: Histogram of the mass function, *i.e.* the histogram of the number of particles in the FoF-halos extracted from the simulation box, for different values of the parameter  $\Lambda$ . The color code is the same as in previous figures.

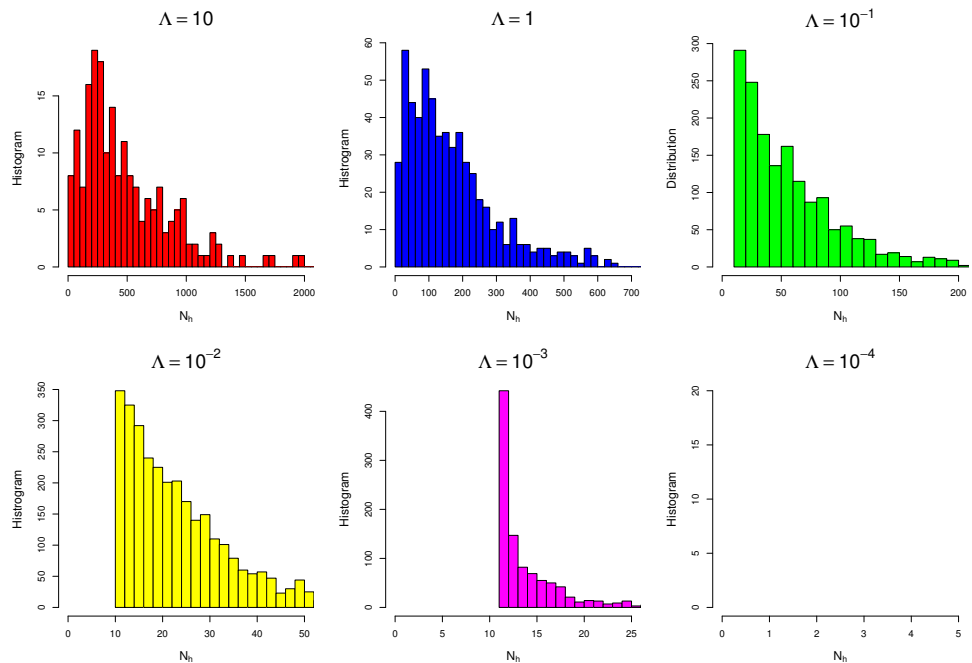


Figure 5.10: Histogram of the mass function as in Fig. 5.9 using an arbitrary cut on the minimal number of particles in the FoF-halos, *i.e.*  $N_h > 10$ .

### 3.2 Testing for virialization of halos

In this section, we consider whether the concept of virialization, which applies strictly to isolated finite systems, is of relevance to the “halos” selected out by the FoF-algorithm, whose basic characteristics we have just discussed. In particular we wish to see whether there is a particular value, or range of values, of  $\ell_{fov}$  for which the algorithm appears to pick out, typically, sub-systems which are virialized.

#### Virialization of isolated subsystems

The question we first answer is what virial relation applies to a finite isolated subsystem in our system. To do so we recall explicitly the equations of motion of such a subsystem. We recall that *isolated* means that particles in subsystem do not cross other particles outside it. We then have

$$\frac{d^2}{dt^2}(x_i - x_{CM}) + \Gamma \frac{d}{dt}(x_i - x_{CM}) = \frac{N_i^>(t) - N_i^<(t)}{2n_0} + (x_i - x_{CM}), \quad (5.12)$$

where  $x_{CM}$  represents in both cases the position of the center of mass of the subsystem.  $N_i^<(t)$  (respectively  $N_i^>(t)$ ) represents the number of particles on the left (respectively on the right) of the particle  $i$  at time  $t$ . We have seen that the rhs can be divided into two distinct contributions. The first one represents the finite gravitational force contribution from particles belonging to the subsystem,  $f_{grav}$ , and the second one stands for the background contribution  $f_{back}$ .

If such a finite isolated subsystem reaches a dynamical equilibrium on a timescale much shorter than the expansion timescale ( $\sim \Gamma^{-1}$ ), we expect it to be virialized. Following Chapter 2, the usual virial relation can be generalized in this case to include the contribution from the background, *i.e.* the term  $f_{back}$ , and becomes

$$2 \sum_{i=1}^{N_c} \frac{1}{2} v_i^2 + \sum_{i=1}^{N_c} x_i \cdot f_{grav}^i + \sum_{i=1}^{N_c} x_i \cdot f_{back}^i = 0, \quad (5.13)$$

where  $v_i$  and  $x_i$  are the velocity and the position of the  $i^{th}$  particle with respect to the velocity and position of the center of mass ( $v_{CM}$  and  $x_{CM}$ ) of the subsystem. This relation is strictly valid if the system is in a steady state, so that the second derivative of the moment of inertia  $I$  cancels, *i.e.*  $\frac{d^2I}{dt^2} = 0$ . Since  $\frac{f_{grav}}{f_{back}} \sim \frac{N_h}{n_0} \frac{1}{L_c}$  the background term is negligible in the virial relation if  $\frac{n_h}{n_0} \gg 1$ , *i.e.* if the mean density of the subsystem is much greater than the global mean density. As discussed in Chapter 4, this is precisely the same assumption in fact which allows one to neglect the damping term, and assume virialization.

Thus we can expect the “usual” virial relation for a finite isolated  $1-d$  self-gravitating system, *i.e.*

$$2K - U = 0, \quad (5.14)$$

to hold *if* the subsystem may be considered as isolated and is significantly overdense (*i.e.*  $n_h/n_0 \gg 1$ ). For the FoF-halos, we note that  $n_h/n_0 \geq \ell/\ell_{fov} = 1$  by construction (since  $L_h \geq N_h \ell_{fov}$ ). Thus for  $\Lambda \ll 1$  our FoF-halos are necessarily overdense, while for  $\Lambda > 1$  they are not. Then we will apply for  $\Lambda > 1$  a cut on our

candidate virialized FoF-halos to select only those with  $\frac{n_h}{n_0} > 1$ . Fig. 5.8 shows that this cut is of marginal relevance.

We note that the crucial assumption involved in deriving the scalar virial theorem is that the moment of inertia  $I$  is time-independent. However, in a system with a small number of particles, there are necessarily statistical fluctuations in  $I$  simply due to the finite-size, and Eqs. (5.13) and (5.14) could be expected to hold only for time-averaged values of  $K$  and  $U$ . Let us summarize the steps of our analysis:

- we find and extract the FoF-Halos in our simulation box for a given  $\ell_{fov}$ ,
- we discard FoF-halos with  $n_h < n_0$ ;
- we calculate the position and velocity of the center of mass of each FoF-halo;
- we measure the virial ratio  $V = 2K/U$  of each FoF-halo measuring velocities with respect to its center of mass.

As in the previous section we consider here results only for the case of the quintic model with an initial PS  $P_{init}(k) \propto k^4$  evolved to  $t_s = 22$ .

### Spatial distribution of the virial ratio

In Fig. 5.11 is plotted the virial ratio of each of the FoF-halos at the position of its center of mass for a given  $\Lambda = \ell_{fov}/\ell = 10^{-2}$  in two separate regions of the full system.

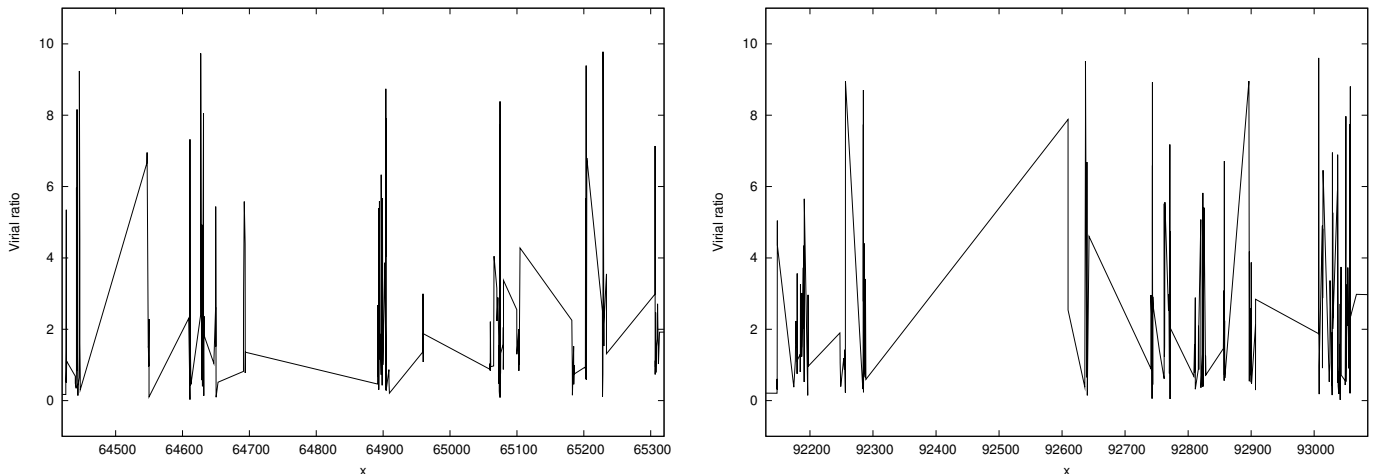


Figure 5.11: Measure of the virial ratio as a function of the center of mass of the FoF-halos for two different samples extracted from the simulation box at time  $t_s = 22$  and  $\Lambda = 10^{-2}$ .

The signal appears highly disorganized and unpredictable in its detailed behavior, and presents structures on all scales. These two different samples of about the same extend in space are taken around two different positions in the simulation box. We see that the general aspect is the same in the two samples but all the details are different and could not have been predicted from looking at a single sample.

We show in Fig. 5.12 the histogram of the virial ratio for these same regions.

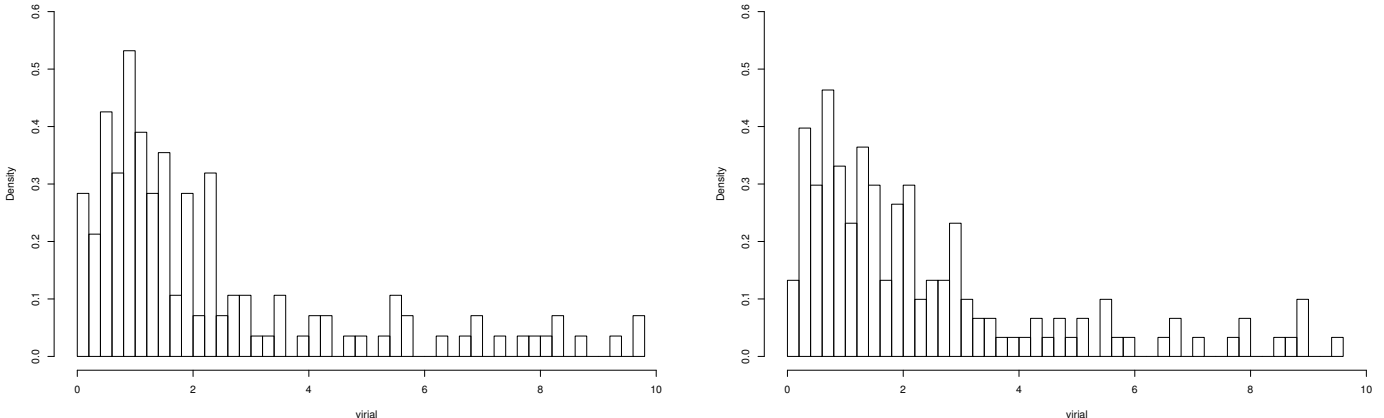


Figure 5.12: Distribution (normalized to unity) of the virial ratio of FoF-halos for the two regions shown in Fig. 5.11 measured for  $\Lambda = 10^{-2}$ .

The two histograms in Fig. 5.12 resemble one another very strongly. This provides clear evidence that, although the detailed properties of the signal appear not to be predictable, its statistical properties are self-averaging, *i.e.* the distribution of the virial ratio in samples of the size considered does appear to converge well to a sample-independent statistical quantity. This observation suggests that a probabilistic approach to the question of virialization of the halos can indeed be used. It is this approach which we now use.

### Probability distribution of the virial ratio

In the following we thus study the behaviour of the distribution of the virial ratios of the FoF-halos selected with the FoF-algorithm, as a function of  $\ell_{fov}$ .

In Fig. 5.13 is shown the measured distribution of the virial ratio for different values of the parameter  $\Lambda$ . The overall qualitative appearance of these plots is quite similar to Figs. 5.7 and 5.8 in the previous section: there appears to be a roughly stable shape in the range  $\Lambda \in [10^{-2}, 1]$  which is strongly modified at  $\Lambda = 10^{-3}$ . In this first range, the distribution presents a non-symmetric behaviour with a maximum virial ratio  $V_{max}$  in the range  $[0, 2]$ , and a tail on the right of the distribution at large virial ratio. This tail becomes more and more predominant as the value of  $\Lambda$  decreases. At smaller  $\Lambda$  we see that the main contribution to the distribution of the virial ratio comes from large values of it and that structures with virial ratio in the range  $[0, 2]$  are not present. We note further that the increasing importance of the contribution of virial ratios much larger than unity as  $\Lambda$  decreases is coherent physically with the hypothesis that, at the scale  $x_{min}$ , marking the lower cut-off to self-similarity, one has a transition to approximately smooth virialized clusters exactly as envisaged in the stable clustering hypothesis: subsystems of such clusters will simply, because of the super-extensivity of potential energy, be expected to have large virial ratios.

We thus posit that the existence of this apparently stable PDF roughly centered on unity means we can say that the halos in the range of scales corresponding to

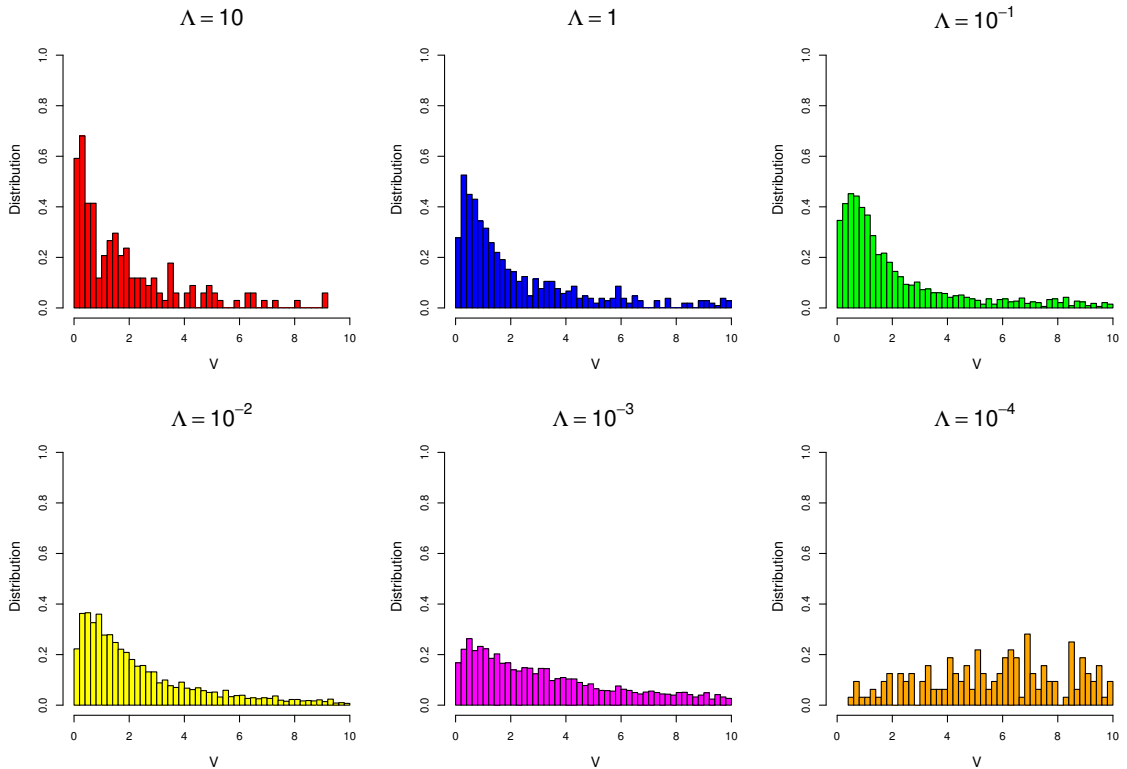


Figure 5.13: Distribution (normalized to unity) of the virial ratio  $V$  for different values of the parameter  $\Lambda$ . The color code is the same as in previous figures.

scale invariance are typically virialized. In other words we posit that the observed scale invariant clustering can, in a statistical sense, be associated to virialization in this range of scale.

To probe further whether this is a well justified interpretation, we examine now whether there are the physically expected correlations of virialization with parameters characterizing the halos. We consider in particular the size of the halos and the distance to the nearest halo, *i.e.* the distance between two particles at the extremities of two different halos.

We start with a qualitative inspection of Fig. 5.14 and 5.15, which show the dependence of the fraction of FoF-halos with a virial ratio  $V \leq 2$  (blue curve) and  $V > 2$  (red curve) as a function of the size  $L_h$  of these structures, and then as the nearest halo distance  $d_{nh}$  for different values of the parameter  $\Lambda$ .

The plots show more quantitatively than above that there is a clear *tendency to virialization* for a range of  $\ell_{fov}$  down to  $\Lambda = 10^{-2}$ : there is apparently a correlation between such virialization and the two chosen parameters, *i.e.* the size of the halos and the distance to the next halo. For what concerns the size, it is in each case the halos in a range around  $\ell_{fov}$  which most clearly show the tendency to virialization. The high values of the virial ratio do indeed appear to come from the extremes of halos much larger and much smaller than  $\ell_{fov}$ . This is consistent with the inter-

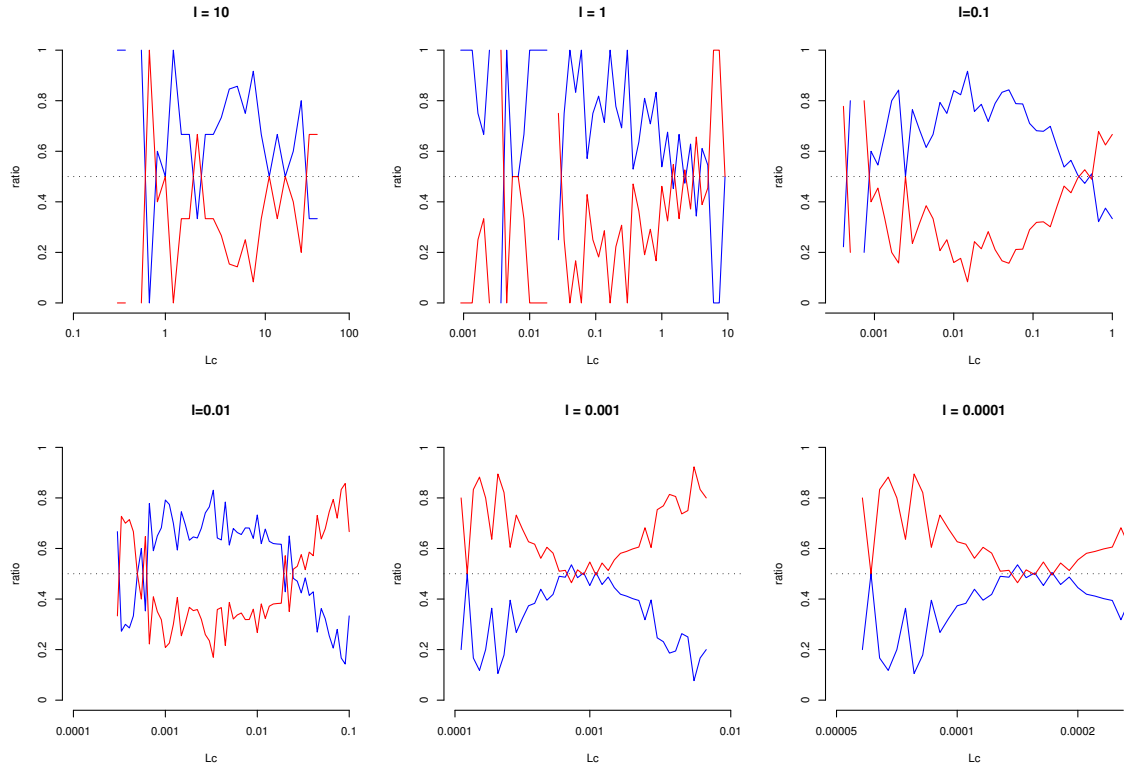


Figure 5.14: Fraction of FoF-halos with a virial ratio  $V \leq 2$  (blue curve) and  $V > 2$  (red curve) as a function of the size  $L_h$  of the FoF-halos for different values of  $\Lambda$ . The fraction is the number of halos with a given range of virial ratio ( $V \leq 2$  or  $V > 2$ ) divided by the total number of halos selected out by the FoF-algorithm at the given linking-length. The color code is the same as in previous figures.

pretation that these are, in both cases, in fact sub-structures of larger halos. For what concerns the nearest-halo distance we also observe the expected correlation. Roughly if a halo is separated spatially we would expect it to be isolated to a better approximation, *i.e.* that it has not interacted with the rest of the system for a longer time, and thus that it would be better virialized.

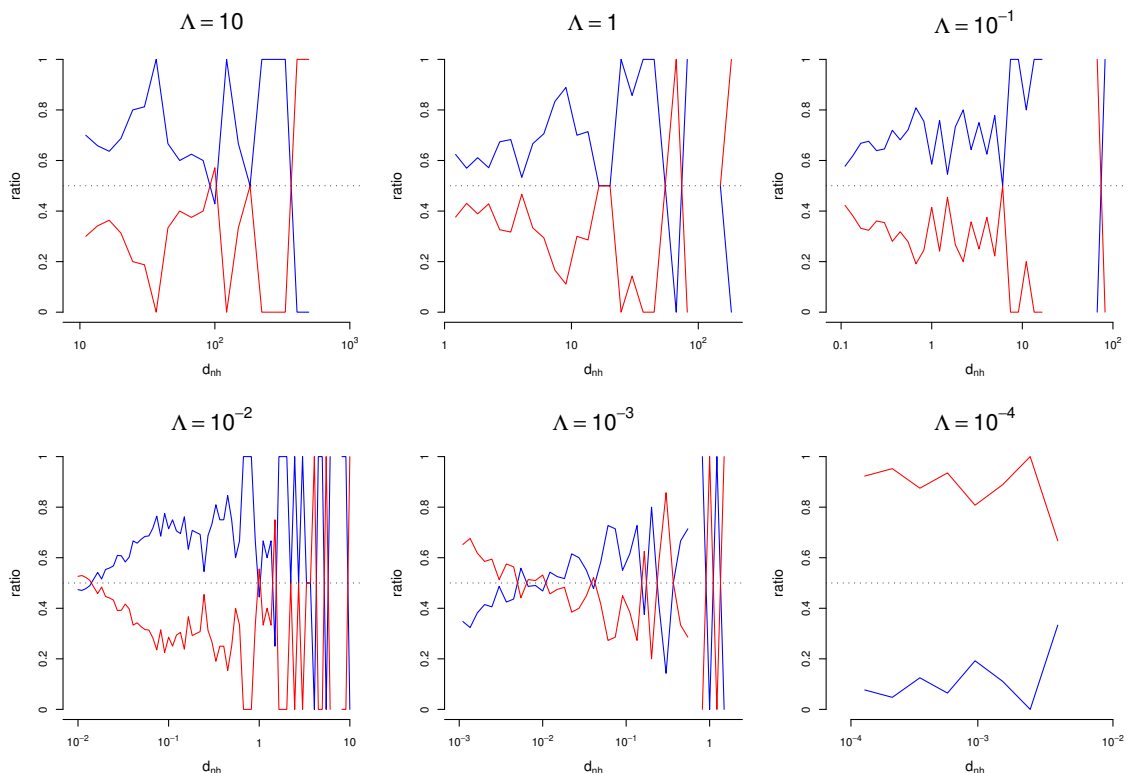


Figure 5.15: Fraction of FoF-halos with a virial ratio  $V \leq 2$  (blue curve) and  $V > 2$  (red curve) as a function of the nearest-halo distance  $d_{nh}$  for different values of  $\Lambda$ . The proportion is defined as the number of halos with a given range of virial ratio ( $V \leq 2$  or  $V > 2$ ) divided by the total number of halos selected out by the FoF-algorithm and at the given linking-length. The color code is the same as in previous figures.

To test more quantitatively these conclusions drawn from visual analysis of these plots we perform a statistical hypothesis test, Pearson’s chi-square test [40]. We divide our set of selected FoF-halos (for a given value of the parameter  $\Lambda$ ) into the two distinct populations, one with  $V \leq 2$  and the second one with  $V > 2$ . We then consider two distinct classes, one with size  $L_h > \Lambda$  and the second one with  $L_h \leq \Lambda$ . Likewise we consider two other distinct classes, one with nearest-halo separation  $d_{nc} > 2\Lambda$  and  $d_{nc} \leq 2\Lambda$ . Pearson’s chi-square test tests the null hypothesis stating that the occurrence of these two populations is statistically independent. An *observation*  $O_{ij}$  is the number of halos in the population “ $i$ ” and for class “ $j$ ”. Each observation is allocated to one cell of a two-dimensional array of cells (called a table). If there are  $r$  rows and  $c$  columns in the table, the *theoretical frequency* for a cell, given the hypothesis of independence is

$$E_{ij} = \frac{\sum_{k=1}^c O_{ik} \sum_{k=1}^r O_{kj}}{N_{tot}}, \quad (5.15)$$

where  $N_{tot}$  is the total number of FoF-halos in our *sample*, and fitting the model of *independence* reduces the number of degrees of freedom by  $q = r + c - 1$ . The value of the test-statistic is

$$X^2 = \sum_{i=1}^r \sum_{j=1}^c \frac{(O_{ij} - E_{ij})^2}{E_{ij}}. \quad (5.16)$$

The distribution of this statistic is a  $\chi^2$  distribution with  $(r - 1) \times (c - 1)$  degrees of freedom (*i.e.* the number of cells  $(r \times c)$  minus the reduction in degrees of freedom  $q$ ). To extract quantitative information, we report in Tables 5.3 and 5.4 the  $p$ -values of this test. In statistical hypothesis testing, the  $p$ -value is the probability of obtaining a test statistic at least as extreme as the one that was actually observed, assuming that the null hypothesis is “true”. In our particular case, the null hypothesis consists in assuming that the two distinct populations are independent, and that the deviation between the observation and the theoretical expectation is a coincidence. The lower the  $p$ -value, the less likely the result is if the null hypothesis is true, and consequently the more “significant” the result is, in the sense of statistical significance. One often accepts the alternative hypothesis (*i.e.* rejection of the null hypothesis) if the  $p$ -value is less than 0.05 corresponding to a 5% chance of rejecting the null hypothesis when it is true [40]. The  $p$ -value for the  $\chi^2$  test is  $\text{Prob}(\chi^2 \geq X^2)$ , the probability of observing a value at least as extreme as the test statistic for a  $\chi^2$  distribution with  $(r - 1) \times (c - 1)$  degrees of freedom.

| $\Lambda$  | 10    | 1         | 0.1        | 0.01       | 0.001 | 0.0001 |
|------------|-------|-----------|------------|------------|-------|--------|
| $p$ -value | 0.004 | $10^{-6}$ | $10^{-14}$ | $10^{-16}$ | 0.002 | 0.6    |

Table 5.3: Result of Pearson’s chi square test for the two distinct populations ( $V \leq 2$  and  $V > 2$ ) and with two distinct classes ( $L_c \leq l$  and  $L_c > l$ ). In the range of scale-invariant clustering, the  $p$ -value is small enough to reject the null hypothesis. However, for small values of  $\Lambda$ , this tendency disappears as we see that the  $p$ -value clearly excludes the rejection of the null hypothesis.

The results obtained in Tab. 5.3 show that, in the range of scale-invariant clustering, the  $p$ -value is small enough to reject the null hypothesis. This means that the fact that the FoF-halos with  $L_h \leq \Lambda$  mainly contribute to  $V \leq 2$  is not a coincidence. However, for small values of  $\Lambda$ , *i.e.* outside the range of scale-invariant clustering, represented here by  $\Lambda = 10^{-4}$ , this tendency disappears as we see that the  $p$ -value clearly excludes the rejection of the null hypothesis.

| $\Lambda$  | 10  | 1   | 0.1  | 0.01       | 0.001      | 0.0001 |
|------------|-----|-----|------|------------|------------|--------|
| $p$ -value | 0.5 | 0.2 | 0.01 | $10^{-16}$ | $10^{-16}$ | 0.6    |

Table 5.4: Result of Pearson's chi square test for the two distinct populations ( $V \leq 2$  and  $V > 2$ ) and with two distinct classes ( $d_{nh} \geq 2 \Lambda$  and  $d_{nc} < 2 l$ ). In the range of scale invariant clustering, the  $p$ -values show the tendency to reject the null hypothesis. However, this result is not clear for the values of the parameter  $\Lambda = 10$  and 1.

The results obtained in Tab. 5.4 show the tendency to reject the null hypothesis in the range of scale invariant clustering, *i.e.* the fact that the FoF-halos with nearest halo separation  $d_{nh} \geq 2 \times \Lambda$  mainly contribute to  $V \leq 2$  is not a coincidence. However, this result is not clear for the values of the parameter  $\Lambda = 10$  and 1. Analysing Fig. 5.15 we see that the departure from the expected result would be justified by the fact that structures with  $V > 2$  are too under-represented in the system. This result would be explained by the tendency of *spatially isolated structures* to dynamically evolve enough in time to reach statistically a virial equilibrium.

We show next in Fig. 5.16 the impact of making a cut on the size of the halos  $L_h$  and on the nearest-halo distance  $d_{nh}$ , *i.e.* we exclude from our halos at any  $\Lambda$  those with  $L_h > \Lambda$  and  $d_{nh} < 2\Lambda$ , on the distribution of the virial ratio. In comparaison with Fig. 5.13, we see that the contribution to the tail of the measured distribution has noticeably reduced, leading to a stronger reproducibility of the signal.

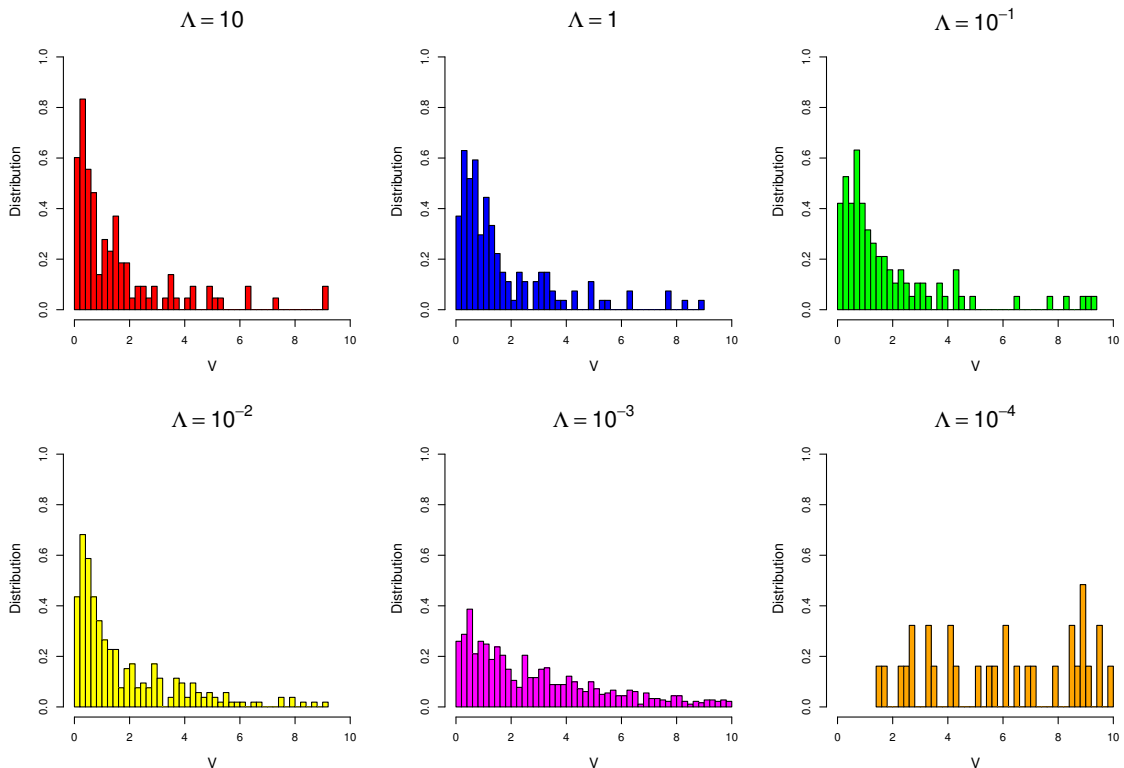


Figure 5.16: Distribution (normalized to unity) of the virial ratio for different values of the parameter  $\Lambda$ , *i.e.* as in Fig. 5.13, but now with two additional cuts applied: we exclude from our halos at any  $\Lambda$  those with  $L_h > \Lambda$  and  $d_{nh} < 2\Lambda$ . The color code is the same as in previous figures.

Information about the reproducibility of the signal can also be extracted from the cumulative distribution function (CDF) of the different distributions obtained for the different values of the linking-length.

We show in Figs. 5.17 and 5.18 the CDF of the virial ratio of the FoF-halos for decreasing values of the parameter  $\Lambda$  with and without the same cut used above. Above the scale  $x_{min}$  marking the lower cut-off to the self-similar regime, we see reproducibility of the statistical signal. This is illustrated by the red, blue and green CDF. Below the scale  $x_{min}$ , the shape of the CDF changes dramatically; this variation characterizes well the end of the self-similar regime. This qualitative inspection illustrates the improvement of the reproducibility of the signal when we consider these cuts on the size of the structures and the one on the nearest-halo separation.

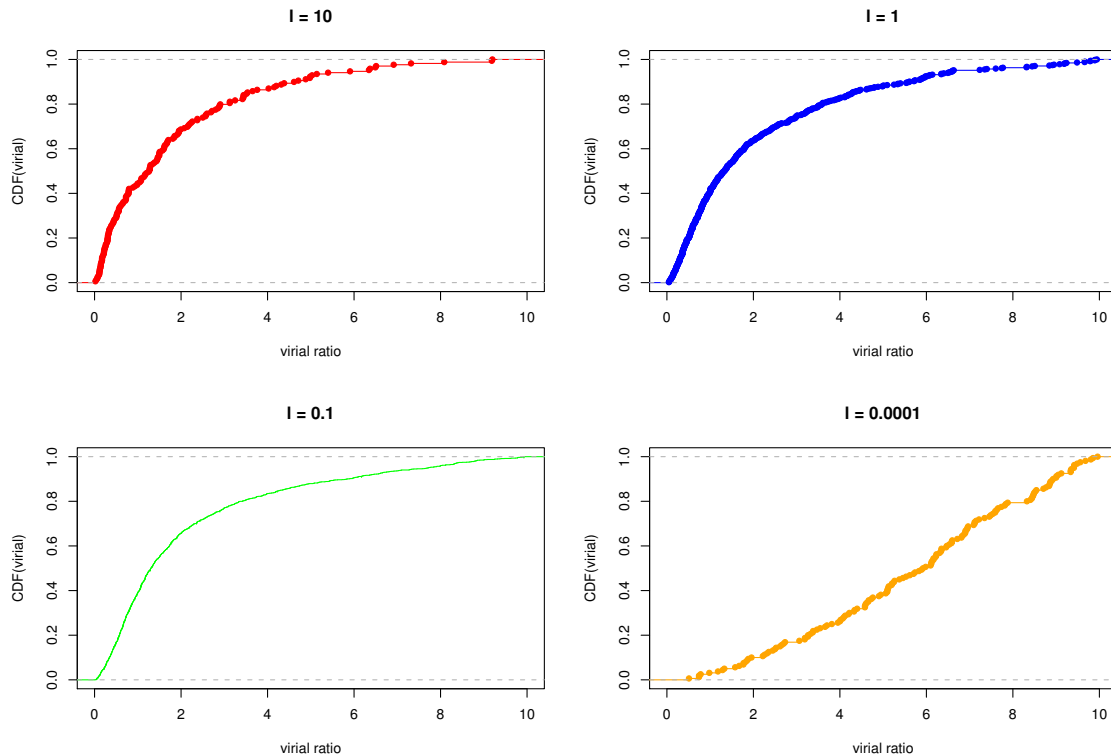


Figure 5.17: Cumulative distribution function of the virial ratio for different values of  $\Lambda$ . The color code is the same as in previous figures. We see a strongly reproducible signal. The orange curve shows that the behaviour of the CDF changes dramatically when  $\ell_{fov} < x_{min}$ .

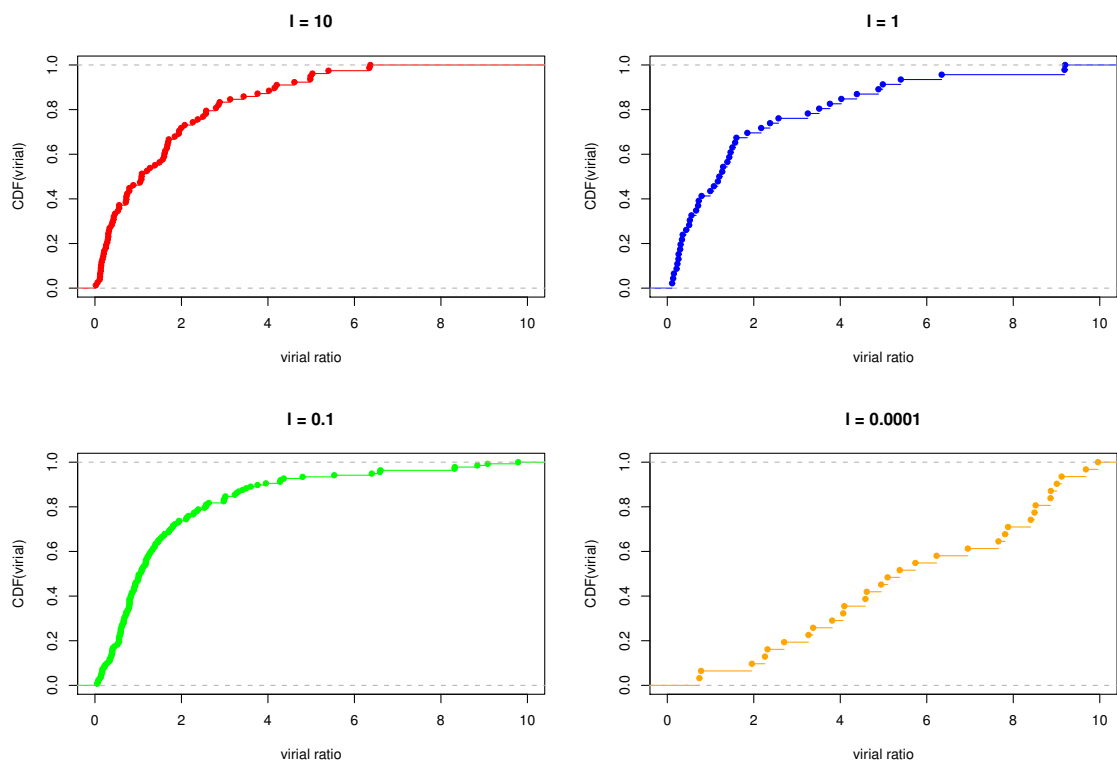


Figure 5.18: Cumulative distribution function of the virial ratio for different values of  $\Lambda$ . We consider the statistical cuts on the size of the halos and the nearest-halo separation discussed in the text. The color code is the same as in previous figures. We still see a strongly reproducible signal.

### 3.3 Statistical tests for stability of the probability distribution of the virial ratio in scale-invariant regime

#### The Kolmogorov-Smirnov test as a quantitative study of reproducibility

To more quantitatively characterize the reproducibility of the probability distribution of the virial ratio, we consider finally a statistical test of the different probability density function. We use the Kolmogorov-Smirnov (K-S) test that is a form of minimum distance estimation used as a nonparametric test to compare two samples. The K-S test is the one of the most useful and general nonparametric methods for comparing two samples, as it is sensitive to differences in both location and shape of the empirical cumulative distribution functions of the two samples [40]. The K-S statistic quantifies a distance between the empirical distribution functions of the two samples. The null distribution of this statistic is calculated under the null hypothesis that the samples are drawn from the same distribution.

To perform this test, we define the K-S statistic  $D_{n,m} = \sup_x |F_n(x) - F_m(x)|$  where  $n$  and  $m$  represent the number of data in the two samples, and where  $F_n(x)$  and  $F_m(x)$  are the cumulative distribution functions obtained with the 2 samples. The null hypothesis is rejected at level  $\alpha$  if

$$\sqrt{\frac{nm}{n+m}} D_{n,m} > D_\alpha, \quad (5.17)$$

where  $D_\alpha$  is a chosen critical value of the test statistic such that  $\text{Prob}(D_{n,m} < D_\alpha) = 1 - \alpha$ . This two-samples test checks whether the two data samples come from the same distribution. This *does not* specify what the common distribution is.

We then consider the  $p$ -value of this test to extract quantitative information about the reproducibility of the pdf of the virial ratio. Generally, one rejects the null hypothesis if the  $p$ -value is smaller than or equal to the significance level, often represented by the Greek letter  $\alpha$ . If the level is 0.05, then results that are only 5% likely or less, given that the null hypothesis is true, are deemed extraordinary.

| $\Lambda$ | 1    | 0.1  | 0.01      | 0.001      |
|-----------|------|------|-----------|------------|
| 10        | 0.26 | 0.23 | 0.04      | $10^{-10}$ |
| 1         |      | 0.70 | 0.03      | $10^{-16}$ |
| 0.1       |      |      | $10^{-6}$ | $10^{-16}$ |
| 0.01      |      |      |           | $10^{-16}$ |

Table 5.5: Result of the Kolmogorov-Smirnov-2-samples test between the different measured distribution of  $V$ . Each case in the table corresponds to the  $p$ -value of the KS-test between the two samples obtained with the values of the parameter  $\Lambda$  corresponding to the first raw and the first column.

We perform the K-S test for the different distribution functions and bring together the different  $p$ -values in Table 5.5. We see that the  $p$ -values in the fifth column, corresponding to the K-S test between samples obtained with  $\Lambda = 10^{-3}$  and the smaller ones, is extremely small; we can thus reject the null hypothesis with

more than 99% of confidence, *i.e.* the samples do not come from the same distribution. In the second and the third column, the  $p$ -value is very large, and do not allow us to reject the null hypothesis, *i.e.* we cannot conclude that the different samples obtained with  $\Lambda = 10, 1, \text{ and } 10^{-1}$  come from different distributions. The fourth column, corresponding to the KS-test between the sample obtained with  $\Lambda = 10^{-2}$  and the other ones, is a limit case where we cannot reject the null hypothesis or accept it with enough confidence. This result is in agreement with the fact that the end of the regime of scale invariant clustering is roughly located at a scale between  $10^{-6}$  and  $10^{-8}$ .

Furthermore, this quantitative inspection illustrates that the signal looks reproducible in the regime of scale-invariant clustering, but shows above all the end of this reproducibility at the end of the regime of scale invariant clustering. It is interesting to go a little further into detail and to study the impact of the cuts on size of the structures and on the nearest-halo separation discussed above on the K-S test and the  $p$ -values which follow.

### Condition on the size of the structures

We have qualitatively seen previously that the FoF-halos selected out from the simulation box with  $L_h \leq \Lambda$  mainly contributed to  $V \leq 2$ . We perform the K-S

| $\Lambda$ | 1    | 0.1  | 0.01      | 0.001      |
|-----------|------|------|-----------|------------|
| 10        | 0.27 | 0.23 | 0.04      | $10^{-10}$ |
| 1         |      | 0.70 | 0.03      | $10^{-16}$ |
| 0.1       |      |      | $10^{-5}$ | $10^{-16}$ |
| 0.01      |      |      |           | $10^{-16}$ |

Table 5.6: Result of the Kolmogorov-Smirnov-2-samples test between the different measured distribution of  $V$  obtained with the cut on the size of the halos. Each case in the table corresponds to the  $p$ -value of the KS-test between the two samples obtained with the values of the parameter  $\Lambda$  corresponding to the first raw and the first column.

test and bring together the different  $p$ -values in Tab. 3.3. Without changing the conclusion we made previously about the rejection of the null hypothesis, we see that the results presented in Tab. 3.3 do not present significant difference with the results referred in Tab. 5.5. The cut on the size  $L_h$  of the FoF-halos is thus not statistically relevant for this test.

### Condition on the nearest-halos separation

We have seen that, given a linking-length, we obtain that two different FoF-halos are inevitably separated with a distance  $\ell_{gap} > \ell_{fof}$ . Due to the arbitrary choice of  $\ell_{fof}$ , it is interesting to analyse the impact of the cut on the nearest-neighbours separation on the reproducibility of the measured distribution of the virial ratio.

We consider structures with a nearest-neighbour at distance  $d_{nh} \geq 2\Lambda$ . Following the same quantitative approach as previously, the  $p$ -values obtained with the K-S test are brought together in Table 3.3. We see that if we consider the fifth column,

| $\Lambda$ | 1    | 0.1  | 0.01 | 0.001     |
|-----------|------|------|------|-----------|
| 10        | 0.97 | 0.14 | 0.27 | $10^{-3}$ |
| 1         |      | 0.68 | 0.84 | $10^{-2}$ |
| 0.1       |      |      | 0.46 | $10^{-4}$ |
| 0.01      |      |      |      | $10^{-8}$ |

Table 5.7: Result of the Kolmogorov-Smirnov-2-samples test between the different measured distribution of  $V$  obtained with the cut on the nearest-halo distribution. Each case in the table corresponds to the  $p$ -value of the KS-test between the two samples obtained with the values of the parameter  $\Lambda$  corresponding to the first raw and the first column.

the  $p$ -value is always small and we can reject the null hypothesis. This simply means that the sample corresponding to  $\Lambda \leq 10^{-3}$  does not correspond to the same distribution than the ones corresponding to larger value of the linking-length. As far as the other columns are concerned, we clearly see a significant difference with the results presented in Tab. 5.5 and Tab. 3.3. The conclusion is still the same as the obtained  $p$ -values do not still allow us to reject the null hypothesis, *i.e.* we cannot conclude that the different samples obtained with  $\Lambda = 10, 1, 10^{-1}$ , and  $10^{-2}$  come from different distributions, but this statistical cut significantly improves the non-rejection of the null hypothesis.

This result shows that the nearest-halo separation has a significant impact on the reproducibility of the distribution of the virial ratio. Its effect is to reduce the contribution of the tail to the measured distribution of the virial ratio, and thus to improve the statistical reproducibility of the signal.

## 4 Conclusion

In the first section of this chapter we saw that there is indeed very clear evidence for scale-invariance in the non-linear clustering that develops in the class of toy models we have considered. We used a multi-fractal analysis to measure the spectrum of fractal exponents and studied their dependence on the model and initial conditions. In the static model the results are quite consistent with a simple homogeneous fractal, while in the expanding cases there is a significant multi-fractality.

In the second part of our analysis we explored the applicability of a description of the clustering like that used canonically in cosmological simulations, that in terms of “halos”. We used the simplest kind of “Friends of Friends” algorithm, which has one free parameter, the linking-length  $\ell_{fof}$ . We described some of the statistical properties of the selected halos as a function of  $\ell_{fof}$ , and then focussed on the question of whether these selected halos are, typically, virialized. Such virialization is an indicator of the degree to which they behave as independent sub-systems, whose elements interact essentially only with one another on a time scale sufficient to establish a kind of equilibrium. We found that there is indeed evidence that, when  $\ell_{fof}$  is in the range where it effectively picks out structures on length scales where the clustering is scale-invariant, the PDF of the halos virial ratio is peaked about

unity. We observed also that the tail of the distribution at large virial ratio could be associated with halos larger or smaller than the typical size, and thus result from the fact that the algorithm does not strictly pick out a single scale.

This leads us to conclude that in the regime of scale-invariant clustering the distribution can be described as a “virialized hierarchy”. By this we mean that the distribution in space, when appropriately analyzed at any scale, can be considered as a collection of approximately virialized sub-systems. These “halos”, however, are not smooth objects of a single characteristic size as assumed in the  $3-d$  cosmological setting. Only at the very small scale at which self-similarity and scale-invariance break down (*i.e.* the scale  $x_{min}$  defined in Chapter 4) is there evidence for roughly *smooth* virialized structures. Further, we have reported here only results for the case of an initial PS with  $n = 4$ , and it should be verified that the same conclusions apply to other cases, and also to the static limit. More specifically, it would be interesting to see whether it is possible to relate the evolution of the scale  $x_{min}$  and the associated correlation amplitude  $\xi_{max}$  in cases where stable clustering does not apply to “merging” of halo type structures.

This analysis could be developed on various points. For example we have analysed the distribution at just one time, while it could clearly be instructive to study the evolution of the “halos” in time to more directly probe the extent to which they can be considered to evolve as independent sub-systems. It would be interesting also to study alternative algorithms for halo selection analogous to ones other than the FOF-algorithm which have been developed in cosmology, and to verify that the conclusions we have come to here do not depend on the specific FoF-algorithm we have used.

# Chapter 6

## A dynamical classification of the range of pair interactions

In this chapter, we report results which generalize to any pair interaction decaying as a power-law at large separation the approach used in Chapter 3 to determine whether the  $1 - d$  gravitational force is defined in an infinite system. This is an interesting question as the Newtonian gravitation is clearly a particular long-range interaction, for which linear amplification emerges from linear fluid theory.

In so doing, we formalize and describe a simple classification of pair interactions which is different to the usual thermodynamic one, discussed in Chapter 1, applied to determine *equilibrium* properties (see e.g. [31, 42, 136]), and which we believe should be very relevant in understanding aspects of the out of equilibrium *dynamics* of these systems. Instead of considering the convergence properties of *potential energy* in the usual thermodynamic limit, we consider therefore those of the *force* in the same limit. Thus, while in the former case one considers (see e.g. [136]) the mathematical properties of essential functions describing systems at equilibrium in the limit  $N \rightarrow \infty$ ,  $V \rightarrow \infty$  at fixed particle density  $n_0 = N/V$ , we will consider the behavior of functions characterising the forces in this same limit. More specifically we consider, following an approach introduced by Chandrasekhar for the case of gravity [33, 71], the definedness of the probability distribution function (PDF) of the force field in statistically homogeneous infinite particle distributions. To avoid any confusion we will refer to the usual thermodynamic limit in this context simply as the *infinite system limit*. Indeed the existence or non-existence of the quantities we are studying in this limit has no direct relation here to the determination of properties at thermal equilibrium. Further, in the context of the literature on long-range interactions the term “thermodynamic limit” is now widely associated with the generalized such limit taken so that relevant macroscopic quantities become independent of  $N$  and  $V$  (for a discussion see e.g. [13]).

We also discuss a further (and different) classification which can be given of the range of pair interactions based on dynamical considerations. This arises when one addresses the question of whether dynamics under a given pair interaction may be defined in *infinite systems*, i.e., in a manner analogous to that in which it is defined for self-gravitating masses in an infinite universe.

In this chapter we consider the general analyticity properties of the PDF of the total force at an arbitrary spatial point in such a particle distribution. We show that, for any pair force which is bounded, this PDF in the infinite volume limit is

either well defined and rapidly decreasing, or else vanishes pointwise. This means that it suffices for almost all cases of interest to show that some chosen moment of the PDF converges to a finite value in this limit (or diverges) in order to establish that the whole PDF itself is well-defined (or ill defined). We then give a general and formal expression for the variance of the total force PDF in a generic infinite uniform stochastic process in terms of the pair force and the two-point correlation properties of the SPP. From this we then deduce our principal result that the force PDF exists strictly in the infinite system limit if and only if the pair force is absolutely integrable at large separations, while it can be defined only in a weaker sense, introducing a regularization, when the pair force is not absolutely integrable. We discuss the physical relevance of the use of such a regularization, which is just a generalization of the so-called “Jeans swindle” used to define the dynamics of (classical non-relativistic) self-gravitating particles in an infinite universe. By analyzing the evolution of density perturbations in an infinite system, we show that the physical relevance of such a regularization of the forces requires also a constraint on the behavior of the PDF of total *force differences* as a function of system size. The text of this chapter is taken from an article published in J. Stat. Phys. [68].

## 1 The force PDF in uniform stochastic point processes: general results

We first recall the definitions of some basic quantities used in the statistical characterization of a stochastic point process and define the total force PDF (see e.g. [71] for a detailed discussion). We then derive some results on the analyticity properties of the latter quantity which we will exploit in deriving our central results in the next section.

### 1.1 Stochastic point processes

In order to study the properties of the force field in the infinite system limit given by  $N \rightarrow \infty$ ,  $V \rightarrow \infty$  with fixed average density  $n_0 > 0$  for a large scale uniform and spatially homogeneous particle system, we generalize the approach introduced by Chandrasekhar in [33] for the total gravitational field in a homogeneous Poisson particle distribution to more general cases and spatial dimensions. To do so we need to characterize statistically point-particle distributions in this limit, and we do this using the language of stochastic point processes (SPP). The microscopic number density of a single realization of the process is

$$n(\mathbf{x}) = \sum_i \delta(\mathbf{x} - \mathbf{x}_i) \quad (6.1)$$

where  $\delta$  is the  $d$ -dimensional Dirac delta function,  $\mathbf{x}_i$  is the position of the  $i^{th}$  system particle and the sum runs over all the particles of the system. We will limit our discussion to particle distributions in a euclidean  $d$ -dimensional space which are (i) statistically translationally invariant (i.e. spatially homogeneous or stationary) and (ii) large scale uniform in the infinite volume limit. Property (i) means that the statistical properties around a given spatial point of the particle distribution do

not depend on the location of the point. In other words the statistical weights of two realizations of the point process, of which one is the rigidly translated version of the other, are the same and do not depend on the translation vector. In particular this implies that the ensemble average (i.e. average over the realizations of the SPP)  $\langle n(\mathbf{x}) \rangle$  of the microscopic number density takes a constant value  $n_0 > 0$  independent of  $\mathbf{x}$ . Moreover the two-point correlation function of the microscopic density  $\langle n(\mathbf{x})n(\mathbf{x}') \rangle$  depends only on the vector distance  $\mathbf{x} - \mathbf{x}'$ . Feature (ii) means that the average particle number fluctuation  $\delta N(R) = (\langle N^2(R) \rangle - \langle N(R) \rangle^2)^{1/2}$  in a sphere of radius  $R$  increases slower with  $R$  than the average number  $\langle N(R) \rangle_0 V(R)$  with  $R$ , where  $V(R) \propto R^d$  is the volume of the  $d$ -dimensional sphere.

Let us start by considering a generic realization of the particle distribution in a finite volume  $V$  and let the total number of particles of the given realization be  $N$ . The particle positions  $\mathbf{x}_i$  are fully characterized statistically by the joint probability density function (PDF)  $\mathcal{P}_N(\{\mathbf{x}_i\})$  conditional to having  $N$  particles in the realization ( $\{\mathbf{x}_i\}$  indicates the set of positions of all system particles in the given realization). As a simple, but paradigmatic example we can think of the homogeneous  $d$ -dimensional Poisson point process. In this case  $\mathcal{P}_N(\{\mathbf{x}_i\}) = V^{-N}$  simply and independently of the value of  $n_0$ . Given a function  $X(\{\mathbf{x}_i\})$  of the  $N$  particle positions in the volume  $V$  its average, conditional to the value of  $N$ , can be written as

$$\langle X \rangle_N \equiv \int_V \left[ \prod_{i=1}^N d^d x_i \right] \mathcal{P}_N(\{\mathbf{x}_i\}) X(\{\mathbf{x}_i\}),$$

where the position of each particle is integrated in the volume  $V$ . In order to evaluate the *unconditional* average of the property  $X$ , for which all possible outcomes of the value  $N$  are considered, one would need the probability  $q_N$  of having  $N$  particles in the volume  $V$ , which permits to write:

$$\langle X \rangle = \sum_{N=0}^{\infty} q_N \langle X \rangle_N, \quad (6.2)$$

in a strict analogy with the grand canonical ensemble average in equilibrium statistical mechanics. However, since we are restricting the discussion to large scale uniform particle distributions, for which  $\delta N(R)/\langle N(R) \rangle$  vanishes for asymptotically large  $R$ , we expect that the larger the volume  $V$  the narrower will be the peak around  $N = \langle N(V) \rangle = n_0 V$  in which the measure  $q_N$  will be concentrated (for simplicity we have indicated with  $V$  both the region and its size). Asymptotically we expect that only the term of index  $N_0 V$  will contribute to the sum in Eq. (6.2), i.e., for sufficiently large  $V$  we can write:

$$\langle X \rangle \simeq \langle X \rangle_{N_0 V}.$$

In other words we can consider that for sufficiently large  $V$  the conditional PDF  $\mathcal{P}_{n_0 V}(\{\mathbf{x}_i\})$  characterizes completely the statistical properties of the particle distribution in the finite volume  $V$  and use this to evaluate in the following subsection the statistical properties of the total force. This is exactly what has been done, for instance, by Chandrasekhar in [33] to calculate the total gravitational force PDF in the Poissonian case.

In Appendix A we recall some of the basic definitions and properties of the statistical characterizations of uniform SPP. We will use below notably two essential properties of  $S(\mathbf{k})$ , the *structure factor* (SF), which follow from its definition:

$$\lim_{k \rightarrow 0} k^d S(\mathbf{k}) = 0, \quad (6.3)$$

i.e, the SF is an integrable function of  $\mathbf{k}$  at  $k = 0$ , and

$$\lim_{k \rightarrow \infty} S(\mathbf{k}) = 1. \quad (6.4)$$

## 1.2 General expression for the force PDF

Let us consider now that the particles in any realization of the SPP interact through a pair force  $\mathbf{f}(\mathbf{x})$ , i.e.,  $\mathbf{f}(\mathbf{x})$  is the force exerted by a particle on another one at vectorial separation  $\mathbf{x}$ . Further we will assume that the pair force is *central*, i.e.,

$$\mathbf{f}(\mathbf{x}) = \hat{\mathbf{x}} f(x), \quad (6.5)$$

where  $\hat{\mathbf{x}} = \mathbf{x}/x$ , and *bounded*, i.e.,

$$\exists f_0 < \infty, |\mathbf{f}(\mathbf{x})| = f(x) \leq f_0 \quad \forall \mathbf{x} \quad (6.6)$$

These assumptions simplify our calculations considerably, but do not limit our aim which is to establish the relation solely between the statistical properties of the force field and *the behavior of the pair interaction at large distances*. Note that the second assumption means that, in cases such as the gravitational or the Coulomb interaction, the divergence at zero separation is assumed appropriately regularized. We will briefly describe in our conclusions below how our results could be generalized to include such singularities.

Let us assume for the moment that the system volume  $V$  is *finite*. As shown above, if  $V$  is sufficiently large, one can consider that the number of particles in this volume is deterministically  $N_0 V$ . We will deal with the important problem of the infinite volume limit defined by  $N, V \rightarrow \infty$  with  $N/V \rightarrow n_0 > 0$  in the next subsection, by studying directly the limit  $V \rightarrow \infty$  with fixed  $N_0 V$ . The total force field  $\mathbf{F}(\mathbf{x})$  at a point  $\mathbf{x}$ , i.e., the force on a test particle placed at a point  $\mathbf{x}$ , may thus be written

$$\mathbf{F}(\mathbf{x}) = \sum_{i=1}^N \mathbf{f}(\mathbf{x} - \mathbf{x}_i) = \sum_{i=1}^N \frac{\mathbf{x} - \mathbf{x}_i}{|\mathbf{x} - \mathbf{x}_i|} f(|\mathbf{x} - \mathbf{x}_i|). \quad (6.7)$$

The force field  $\mathbf{F}(\mathbf{x})$  may be considered as a stochastic variable with respect to the SPP. Choosing arbitrarily the origin as the point where the total force is evaluated, the PDF of this force is formally defined by<sup>1</sup>

$$P_N(\mathbf{F}) = \int_V \left[ \prod_{i=1}^N d^d x_i \right] \mathcal{P}_N(\{\mathbf{x}_i\}) \delta \left[ \mathbf{F} + \sum_i \mathbf{f}(\mathbf{x}_i) \right],$$

<sup>1</sup>We consider here the *unconditional* force PDF, i.e., the force is that at an arbitrary spatial point, rather than that on a point occupied by a particle which belongs to the particle distribution. It is the latter case, of the *conditional* force PDF, which is often considered in calculations of this kind (see e.g. [65, 66, 153]). The distinction is not important here as the constraints we derive, which depend on the *large scale* correlation properties of the particle distribution, would be expected to be the same in both cases.

where we have used, as assumed, that  $\mathbf{f}(-\mathbf{x}_i) = -\mathbf{f}(\mathbf{x}_i)$ . Using the identity

$$\delta(\mathbf{y}) = \frac{1}{(2\pi)^d} \int d^d q e^{i\mathbf{q}\cdot\mathbf{y}} \quad (6.8)$$

this can be rewritten as

$$P_N(\mathbf{F}) = \frac{1}{(2\pi)^d} \int d^d q e^{i\mathbf{q}\cdot\mathbf{F}} \int_V \left[ \prod_{i=1}^N d^d x_i e^{i\mathbf{q}\cdot\mathbf{f}(\mathbf{x}_i)} \right] \mathcal{P}_N(\{\mathbf{x}_i\}).$$

The integral over the spatial coordinates in the above equation defines the *characteristic function* of the total field  $\mathbf{F}$

$$\tilde{P}_N(\mathbf{q}) = \int_V \left[ \prod_{i=1}^N d^d x_i e^{i\mathbf{q}\cdot\mathbf{f}(\mathbf{x}_i)} \right] \mathcal{P}_N(\{\mathbf{x}_i\}), \quad (6.9)$$

so that

$$P_N(\mathbf{F}) = \frac{1}{(2\pi)^d} \int d^d q e^{i\mathbf{q}\cdot\mathbf{F}} \tilde{P}_N(\mathbf{q}).$$

The integral over spatial configurations in Eq. (6.9) can be conveniently rewritten as an integral over the possible values of the pair forces due to each of the  $i = 1, \dots, N$  particles:

$$\tilde{P}_N(\mathbf{q}) \equiv \int \left[ \prod_{i=1}^N d^d f_i e^{i\mathbf{q}\cdot\mathbf{f}_i} \right] \mathcal{Q}_N(\{\mathbf{f}_i\}), \quad (6.10)$$

where

$$\mathcal{Q}_N(\{\mathbf{f}_i\}) = \int_V \left[ \prod_{i=1}^N d^d x_i \right] \mathcal{P}_N(\{\mathbf{x}_i\}) \prod_{i=1}^N \delta[\mathbf{f}_i - \mathbf{f}(\mathbf{x}_i)] \quad (6.11)$$

is the joint PDF for the pair forces  $\mathbf{f}_i$ . Note that, since  $\mathbf{F}$  is the sum of the variables  $\{\mathbf{f}_i\}$  its characteristic function  $\tilde{P}_N(\mathbf{q})$  can be given as

$$\tilde{P}_N(\mathbf{q}) = \tilde{\mathcal{Q}}_N(\{\mathbf{q}_i = \mathbf{q}\}) \quad (6.12)$$

where  $\tilde{\mathcal{Q}}_N(\{\mathbf{q}_i\})$  is the  $Nd$ -dimensional FT of the joint pair forces PDF  $\mathcal{Q}_N(\{\mathbf{f}_i\})$ , i.e.,

$$\tilde{\mathcal{Q}}_N(\{\mathbf{q}_i\}) = \int \left[ \prod_{i=1}^N d^d f_i e^{i\mathbf{q}_i \cdot \mathbf{f}_i} \right] \mathcal{Q}_N(\{\mathbf{f}_i\}). \quad (6.13)$$

### 1.3 Analyticity properties of the force PDF

From the fact that the pair force is *bounded* it follows that  $\mathcal{Q}_N(\{\mathbf{f}_i\})$  has a compact support, and, since it is absolutely integrable (by definition), FT theory (see e.g. [98]) implies that its characteristic function  $\tilde{\mathcal{Q}}_N(\{\mathbf{q}_i\})$  is an analytic function of the variables  $\{\mathbf{q}_i\}$ . Consequently  $\tilde{P}_N(\mathbf{q})$  is an analytic function of  $\mathbf{q}$ . Again from FT theory one has therefore that  $P_N(\mathbf{F})$  is a rapidly decreasing function of  $\mathbf{F}$ :

$$\lim_{F \rightarrow \infty} F^\alpha P_N(\mathbf{F}) = 0, \quad \forall \alpha > 0.$$

Thus  $P_N(\mathbf{F})$  is a well-defined function of which all moments finite, i.e.,  $0 < \langle |\mathbf{F}|^n \rangle < +\infty$  for any  $n \geq 0$ .

Let us now consider what happens when we take the limit  $V \rightarrow \infty$  with  $N_0 V$ . On one hand the joint PDF  $\mathcal{Q}_N(\{\mathbf{f}_i\})$  remains non-negative and absolutely integrable at all increasing  $V$ . On the other hand the support of this function remains compact with a diameter unaffected by the values of  $V$ , but fixed only by  $f_0$ . Therefore we expect that the FT theorem keeps its validity also in the infinite system limit resulting in an analytical

$$\tilde{P}(\mathbf{q}) \equiv \lim_{\substack{V \rightarrow \infty \\ N/V_0}} P_N(\mathbf{F}).$$

Therefore we will have that

$$P(\mathbf{F}) \equiv \lim_{\substack{V \rightarrow \infty \\ N_0 V}} P_N(\mathbf{F})$$

satisfies

$$\lim_{F \rightarrow \infty} F^\alpha P(\mathbf{F}) = 0, \quad \forall \alpha > 0.$$

There are then only two possibilities for the behavior of  $\tilde{P}_N(\mathbf{q})$  in the infinite system limit:

1. It converges to an absolutely integrable function which is *not identically zero* everywhere, giving a  $P(\mathbf{F})$  which is normalizable and non-negative on its support. Further all the integer moments of  $|\mathbf{F}|$  are positive and finite.
2. It converges to zero everywhere, giving  $P(\mathbf{F}) \equiv 0$ . More specifically  $P_N(\mathbf{F})$  with  $N_0 V$  converges point-wise to the null function: it becomes broader and broader with increasing  $N$  (and  $V$ ), but with an amplitude which decreases correspondingly and eventually goes to zero in the limit.

This latter case is analogous to the case of the sum of identically distributed uncorrelated random variables: if this sum is not normalized with the appropriate power of the number  $N$  of such variables, the PDF of the sum vanishes point-wise in a similar way in the limit  $N \rightarrow \infty$ .

In summary it follows from these considerations of the analyticity properties of  $\tilde{P}_N(\mathbf{q})$  at increasing  $V$  that the case of a well defined, but fat tailed  $P(\mathbf{F})$ , can be excluded: in the infinite system limit the force PDF, if defined, is expected to be a normalizable and rapidly decreasing function.

## 2 Large distance behavior of pair interactions and the force PDF

In this section we use the result derived in the previous section to infer the main result of this paper: the relation between the large scale behavior of the pair interaction and the force PDF in the infinite system limit. We thus consider, as above, a central and bounded pair force such that

$$f(x) \simeq \frac{g}{x^{\gamma+1}} \quad \text{for } x \rightarrow \infty, \quad (6.14)$$

or, equivalently, a pair interaction corresponding to a two-body potential  $V(x) \simeq g/(\gamma x^\gamma)$  at large  $x$  for  $\gamma \neq 0$  (and from  $V(x) \simeq -g \ln x$  for  $\gamma = 0$ ). Since the pair force is bounded, we have  $\gamma > -1$ .

Given the final result derived in the previous section, it follows that, to determine whether the force PDF exists, it is sufficient to analyze a single *even* moment of this PDF: because the PDF, when it exists, is rapidly decreasing, any such moment is necessarily finite and non-zero in this case, and diverges instead when the PDF does not exist. We choose to analyze the behavior of the second moment,  $\langle F^2 \rangle$ , which is equal to the variance of the PDF since the first moment  $\langle F \rangle$  is zero (see below). We choose this moment because, as we will now see, it can be expressed solely in terms of the FT of  $f(\mathbf{x})$  and of the SF of the microscopic density of the particle distribution. From these expressions we can then infer easily our result.

## 2.1 Variance of the force in infinite system limit

The formal expression of the total force acting on a test particle (i.e. the force field) at  $\mathbf{x}$  in the infinite system limit may be written

$$\mathbf{F}(\mathbf{x}) = \int d^d x' \frac{\mathbf{x} - \mathbf{x}'}{|\mathbf{x} - \mathbf{x}'|} f(|\mathbf{x} - \mathbf{x}'|) n(\mathbf{x}') \quad (6.15)$$

where the integral is over the infinite space and  $n(\mathbf{x})$ , given in Eq. (6.1), is the density field in a realization of the general class of *uniform* SPP we have discussed with positive mean density  $n_0$ .

It is simple to show, using Eq. (6.15) and the definition of the SF that formally

$$\langle \mathbf{F}^2 \rangle = \frac{1}{(2\pi)^d} \int d^d k |\tilde{\mathbf{f}}(\mathbf{k})|^2 S(k) \quad (6.16)$$

where  $\tilde{\mathbf{f}}(\mathbf{k})$  is the ( $d$ -dimensional) FT of  $\hat{\mathbf{x}}f(x)$ . It is straightforward to show that  $\tilde{\mathbf{f}}(\mathbf{k}) = \hat{\mathbf{k}}\tilde{f}(k)$ , where the explicit expression for  $\tilde{f}(k)$  is given in the appendix<sup>2</sup>. We can thus write

$$\begin{aligned} \langle \mathbf{F}^2 \rangle &= \frac{1}{(2\pi)^d} \int d^d k |\tilde{f}(k)|^2 S(k) \\ &= \frac{1}{2^{d-1}\pi^{d/2}\Gamma(d/2)} \int_0^\infty dk k^{d-1} |\tilde{f}(k)|^2 S(k), \end{aligned} \quad (6.17)$$

where  $\Gamma(x)$  is the usual Euler Gamma function.

## 2.2 Force PDF for an integrable pair force

Let us now consider the integrability of the integrand in Eq. (6.17). We start with the case in which  $f(x)$  is not only bounded but integrable in  $\mathbb{R}^d$ , i.e., with  $\gamma > d - 1$ . Given these properties, it is straightforward to verify, using the conditions (6.3) and (6.4) on  $S(k)$  and standard FT theorems, that the function  $|\tilde{f}(k)|^2 S(k)$  is also integrable in  $\mathbb{R}^d$ . The variance is therefore finite, from which it follows that the PDF exists, and furthermore that all its moments are finite.

---

<sup>2</sup>Note that only in  $d = 1$  does  $\tilde{f}(k)$  coincide with the direct FT of  $f(x)$ .

## 2.3 Force PDF for a non-integrable pair forces

For a pair force which is absolutely non-integrable, i.e.,  $\gamma < d - 1$ , the FT  $\tilde{\mathbf{f}}(\mathbf{k})$  of  $\mathbf{f}(\mathbf{x})$  in Eq. (6.17) is defined only in the sense of distributions, i.e., the integrals over all space of  $f(x)$  must be defined by a symmetric limiting procedure. Physically this means that the expression Eq. (6.15) for the force on a particle in infinite space must be calculated as

$$\mathbf{F}(\mathbf{x}) = \lim_{\mu \rightarrow 0^+} \lim_{V \rightarrow \infty} \int_V \frac{\mathbf{x} - \mathbf{x}'}{|\mathbf{x} - \mathbf{x}'|} f(|\mathbf{x} - \mathbf{x}'|) e^{-\mu|\mathbf{x} - \mathbf{x}'|} n(\mathbf{x}') d^d x', \quad (6.18)$$

where the two limits do not commute. In other words,  $\mathbf{F}(\mathbf{x})$  is defined as the zero screening limit of a screened version of the simple power law interaction in an infinite system. The expression Eq. (6.17) is then meaningful when  $\tilde{f}(k)$  is taken to be defined in the analogous manner with the two limits  $\mu \rightarrow 0^+$  of the screening and  $V \rightarrow \infty$  (i.e. with the minimal non-zero mode  $k \sim 1/V \rightarrow 0^+$ ) taken in the same order as indicated in Eq. (6.18).

Let us consider then again, for the case  $\gamma < d - 1$ , the integrability of the integrand in Eq. (6.17). To do so we need to examine in detail the small  $k$  behavior of  $\tilde{f}(k)$ . It is shown in the appendix that, as one would expect from a simple dimensional analysis, for  $f(r \rightarrow \infty) \sim 1/r^{\gamma+1}$  we have  $f(k \rightarrow 0) \sim k^{-d+\gamma+1}$  in any  $d$ , for the case of a pair force which is not absolutely integrable, and bounded, i.e.,  $-1 < \gamma < d - 1$ . It follows then from Eq. (6.17) that the variance is finite for a given  $\gamma$  only for a sub-class of uniform point processes, specifically those which satisfy

$$\lim_{k \rightarrow 0} k^{-d+2\gamma+2} S(k) = 0, \quad (6.19)$$

i.e., for  $S(k \rightarrow 0) \sim k^n$  with

$$n > d - 2\gamma - 2 = -d + 2(d - 1 - \gamma). \quad (6.20)$$

For uniform point processes violating this condition, i.e., with  $S(k \rightarrow 0) \sim k^n$  and  $-d < n \leq -d + 2(d - \gamma - 1)$ , the variance diverges. It follows from the results on the PDF of  $\mathbf{F}$  presented in the previous section that the total force itself  $\mathbf{F}(\mathbf{x})$  is then badly defined in the infinite system limit.

These results of Sec. 2.2 and Sec. 2.3 combined are the central ones in this paper, anticipated in the introduction.

*Firstly*, when pair forces are absolutely integrable at large separations, the total force PDF is well defined in the infinite system limit, while for pair forces which are not absolutely integrable this quantity is ill defined. This has the simple physical meaning anticipated in the introduction: when this PDF is well defined, the force on a typical particle takes its dominant contribution from particles in a finite region around it; when instead the PDF is ill defined far-away contributions to the total force dominate, diverging with the size of the system. Thus absolutely integrable pair forces with  $\gamma > d - 1$  are, in this precise sense, “short-range”, while they are “long-range” when  $\gamma \leq d - 1$ . To avoid confusion with the usual classification of the range of interactions based on the integrability properties of the interaction potential, we will adopt the nomenclature that interactions in the case  $\gamma > d - 1$  are *dynamically short-range*, while for  $\gamma \leq d - 1$  they are *dynamically long-range*. Thus

an interaction with  $d - 1 < \gamma \leq d$  can be described as *thermodynamically long-range but dynamically short-range*.

Secondly the results in Sec. 2.3 detail how, for  $\gamma \leq d - 1$ , the force PDF in the infinite system limit may be defined provided an additional prescription is given for the calculation of the force. In the next section we explain the physical meaning and relevance of this result.

### 3 Definedness of dynamics in an infinite uniform system

The regularization Eq. (6.18) is simply the generalization to a generic pair force with  $\gamma \leq d - 1$  of one which is used for the case of Newtonian gravity, often referred to as the “Jeans swindle” (see e.g. [25]). It was indeed originally introduced by Jeans [86] in his treatment of self-gravitating matter in an infinite universe. However, as explained by Kiessling in [95], its denomination as a “swindle” is very misleading, as it can be formulated in a mathematically rigorous and physically meaningful manner, precisely as in Eq. (6.18).

The prescription Eq. (6.18) simply makes the force on a particle defined by setting to zero the ill defined contribution due to the non-zero mean density:

$$\langle \mathbf{F}(\mathbf{x}) \rangle = \lim_{\mu \rightarrow 0^+} n_0 \int \frac{\mathbf{x} - \mathbf{x}'}{|\mathbf{x} - \mathbf{x}'|} f(|\mathbf{x} - \mathbf{x}'|) e^{-\mu|\mathbf{x} - \mathbf{x}'|} d^d x' = 0, \quad (6.21)$$

The force on a particle can thus be written as

$$\mathbf{F}(\mathbf{x}) = \lim_{\mu \rightarrow 0^+} \int \frac{\mathbf{x} - \mathbf{x}'}{|\mathbf{x} - \mathbf{x}'|} f(|\mathbf{x} - \mathbf{x}'|) e^{-\mu|\mathbf{x} - \mathbf{x}'|} \delta n(\mathbf{x}') d^d x', \quad (6.22)$$

where  $\delta n(\mathbf{x}') = n(\mathbf{x}') - n_0$  is the density fluctuation field. It is straightforward to show that the derived constraint (6.20) corresponds simply to that which can be anticipated by a naive analysis of the convergence of the integral Eq. (6.22): treating  $\delta n(\mathbf{x}')$  as a deterministic function (rather than a stochastic field) one can require it to decay at large  $|\mathbf{x}'|$  with a sufficiently large exponent in order to give integrability; taking the FT to infer the behavior of  $|\tilde{\delta n}(\mathbf{k})|^2$  one obtains the condition (6.20).

The relevance of the results we have derived for the force PDF in the infinite system limit using this regularization arises thus, as it does in the case of Newtonian gravity, when one addresses the following question: is it possible to define consistently *dynamics* under a given pair interaction in an infinite system which is uniform at large scales? As we now discuss, generalizing considerations given in [3] for the specific case of gravity in  $d = 1$ , the answer to this question is in fact phrased in terms of the definedness of the PDF of *force differences* rather than that of forces. This leads then to our second classification of pair interactions.

#### 3.1 Evolution of fluctuations and definedness of PDF

Let us consider first an infinite particle distribution which is such that the total force PDF is defined *at some given time*, i.e., for  $\gamma > d - 1$  we may consider any uniform SSP, while for  $\gamma < d - 1$  we may consider (employing the regularization discussed)

only the class of SSP with fluctuations at large scales obeying the condition (6.20) *at this time*. The forces on particles at this initial time are then well defined. This will only remain true, however, after a finite time interval, if the evolved distribution continues to obey the same condition (6.20). Let us determine when this is the case or not.

In order to do so, it suffices to consider the evolution of the density fluctuations, and specifically of the SF at small  $k$ , due to the action of this force field. Given that we are interested in the long-wavelength modes of the density field, we can apply the differential form of the continuity equation for the mass (and thus number) density between an initial time  $t = 0$  and a time  $t = \delta t$ :

$$n(\mathbf{x}, \delta t) - n(\mathbf{x}, 0) = \vec{\nabla}[n(\mathbf{x}, 0)\mathbf{u}(\mathbf{x}, 0)] \quad (6.23)$$

where  $\mathbf{u}(\mathbf{x}, 0)$  is the infinitesimal displacement field. Subtracting the mean density  $n_0$  from both sides, and linearizing in  $\delta n(\mathbf{x}, \delta t) = [n(\mathbf{x}, \delta t) - n_0]$  and  $\mathbf{u}(\mathbf{x}, 0)$ , we obtain, on taking the FT,

$$\tilde{\delta n}(\mathbf{k}, \delta t) = \tilde{\delta n}(\mathbf{k}, 0) + i n_0 \mathbf{k} \cdot \tilde{\mathbf{u}}(\mathbf{k}, 0). \quad (6.24)$$

Taking the square modulus of both sides, in the same approximation we get

$$\begin{aligned} |\tilde{\delta n}(\mathbf{k}, \delta t)|^2 &- |\tilde{\delta n}(\mathbf{k}, 0)|^2 = \\ n_0^2 k^2 |\tilde{\mathbf{u}}(\mathbf{k})|^2 + 2k n_0 \text{Im}[\tilde{\delta n}(\mathbf{k}, 0)\tilde{\mathbf{u}}^*(\mathbf{k}, 0)]. \end{aligned} \quad (6.25)$$

If the displacements are generated solely by the forces acting (i.e. assuming velocities are initially zero), we have that

$$\mathbf{u}(\mathbf{x}, 0) = \frac{1}{2}\mathbf{F}(\mathbf{x}, 0)\delta t^2 \quad (6.26)$$

and thus, that  $|\tilde{\mathbf{u}}(\mathbf{k})|^2 \propto |\mathbf{F}(\mathbf{k})|^2$ . The latter quantity is given, using Eq. (6.16), by

$$|\mathbf{F}(\mathbf{k})|^2 = |\tilde{f}(k)|^2 S(k). \quad (6.27)$$

In the analysis in the previous section we used the result that at small  $k$ ,  $\tilde{f}(k) \sim k^{-d+\gamma+1}$ . Thus  $|\tilde{\mathbf{u}}(\mathbf{k})|^2 \sim k^{2m+n}$ , where  $m = -d + \gamma + 1$ , if  $S(k) \sim k^n$ . It then follows, from Eq. (6.25), that the small  $k$  behavior of the time-evolved SF is given by

$$S_{\delta t}(k \rightarrow 0) \sim k^n + k^{1+m+n} + k^{2+2m+n}. \quad (6.28)$$

It can be inferred that the leading small  $k$  behavior of the SF is unchanged if and only if  $m + 1 \geq 0$ , i.e.,  $\gamma \geq d - 2$ . Gravity ( $\gamma = d - 2$ ) in the marginal case is which the long wavelength contribution to the SF generated by the evolution has the same exponent as the initial SF: this is the well known phenomenon of *linear amplification* of initial density perturbations (see e.g. [25, 126]) which applies<sup>3</sup> in infinite self-gravitating systems (derived originally by Jeans).

---

<sup>3</sup>The result does not apply, however, when  $n > 4$  [126]; the reason is that fluctuations with  $S(k \rightarrow 0) \sim k^4$  arise generically from any rearrangement of matter due to dynamics which conserves mass and momentum locally. These effects are neglected implicitly above when we use the continuum approximation to the density fluctuation field.

If, on the other hand,  $\gamma < d - 2$  (i.e. the interaction is “more long-range” than gravity in  $d$  dimensions) the exponent of the small  $k$  behavior is reduced from  $n$  to  $n - 2(d - 2 - \gamma)$ . Given that our result is for an infinitesimal time  $\delta t$ , this indicates in fact a pathological behavior: in any finite time interval the exponent  $n$  should become, apparently, arbitrarily large and negative, while, as shown in Sect. 1, the constraint  $n > -d$  is imposed by the assumed large scale uniformity of the SPP. In other words this result means that, in the infinite system limit, when  $\gamma < d - 2$ , the condition of large scale uniformity is violated immediately by the dynamical evolution. The reason is simply that in this case the *rate of growth of a perturbation at a given scale increases with the scale*. Indeed this is the essential content of the analysis given just above: through the continuity equation, the perturbation to the density field is proportional to the *gradient of the displacement field*, which in turn is simply proportional to the *gradient of the force*. As we now detail more explicitly, when  $\gamma < d - 2$ , this quantity diverges with the size of the system.

### 3.2 PDF of force differences

Let us consider now the behavior of the PDF of the difference of the forces between two spatial points separated by a fixed vector distance  $\mathbf{a}$ :

$$\Delta\mathbf{F}(\mathbf{x}; \mathbf{x} + \mathbf{a}) \equiv \mathbf{F}(\mathbf{x}) - \mathbf{F}(\mathbf{x} + \mathbf{a}). \quad (6.29)$$

If this quantity is well defined in the infinite system limit, its PDF  $\mathcal{P}(\Delta\mathbf{F}; a)$  will be independent of  $\mathbf{x}$  and will have a parametric dependence only on  $a = |\mathbf{a}|$  because of the assumed statistical translational and rotational invariance of the particle distribution.

The analysis of the properties of  $\mathcal{P}(\Delta\mathbf{F}; a)$  in the infinite volume limit is formally exactly the same as that given above for the total force  $\mathbf{F}$ , with the only replacement of the pair force in Eq. (6.14) by the *pair force difference*:

$$\Delta\mathbf{f}(\mathbf{x}, \mathbf{x} + \mathbf{a}) = \mathbf{f}(\mathbf{x}) - \mathbf{f}(\mathbf{x} + \mathbf{a}), \quad (6.30)$$

i.e., the difference of the pair forces on two points located at  $\mathbf{x}$  and  $\mathbf{x} + \mathbf{a}$  due to a point at the origin. Assuming again the possible small scale singularities in this pair force difference to be suitably regulated, our previous analysis carries through, the only significant change being that, as  $x \rightarrow \infty$ ,

$$\Delta\mathbf{f}(\mathbf{x}, \mathbf{x} + \mathbf{a}) \sim a\hat{\mathbf{x}}/x^{\gamma+2}. \quad (6.31)$$

Proceeding in exactly the same manner to analyse  $\mathcal{P}(\Delta\mathbf{F}; a)$ , we find that

- For  $\gamma > d - 2$ , i.e., if the *gradient of the pair force at fixed  $a$  is an absolutely integrable function* of  $\mathbf{x}$  at large separations, the PDF  $\mathcal{P}(\Delta\mathbf{F}; a)$  is well defined in the infinite system limit, and is a rapidly decreasing function of its argument for any SPP. This is true without any regularization.
- For  $\gamma \leq d - 2$ , on the other hand, a well defined PDF may be obtained only by using the regularization like that introduced above in Eq. (6.18). Therefore the PDF of the force differences then remains well defined, i.e., the force difference

$\Delta\mathbf{F}(\mathbf{x}; \mathbf{a})$  remains finite at all  $\mathbf{x}$ , only in a sub-class of SPP defined by the constraint

$$n > d - 2\gamma - 4 = -d + 2(d - 2 - \gamma). \quad (6.32)$$

For the case of gravity  $\gamma = d - 2$  this coincides with the full class of uniform SPP, while for any smaller  $\gamma$ , it restricts to a sub-class of the latter.

### 3.3 Conditions for definedness of dynamics in an infinite system

Our analysis in Sec. 3.1 of the evolution of density perturbations under the effect of the mutual pair forces gave the sufficient condition  $\gamma \geq d - 2$  for the consistency of the dynamics in the infinite system limit, but with the assumption that the total force PDF was itself defined. This means that, in the range  $d - 2 \leq \gamma < d - 1$ , the result derived applies only to the sub-class of infinite uniform particle distributions in which the large scale fluctuations obey the condition (6.20). It is straightforward to verify, however, that the analysis and conclusions of Sec. 3.1 can be generalized to cover all uniform SPP for  $\gamma \geq d - 2$ . In line with the discussion given above, the analysis requires in fact only assumptions about the behavior of the gradient of the forces, rather the forces themselves. More specifically, the only equation which explicitly contains the force, Eq. (6.26), is a purely formal step which can be modified to include the possibility that the force diverges with system size. Indeed if the force — at a given point — includes such a divergence it is sufficient that this divergence cancels out when we calculate the difference between this force and that at a neighboring point. Physically this means simply that, as discussed above, when we consider the relative motions of particles, it is sufficient to consider relative forces. Further, as we are considering the limit of an infinite system in which there is no preferred point (i.e. statistical homogeneity holds), only relative motions of points has physical significance, and therefore only the spatial variation of the forces can have physical meaning. These latter statements can be viewed as a kind of corollary to Mach's principle: if the mass distribution of the universe is, as it is in the case we consider, such that there is no preferred point in space (and, specifically, no center of mass) inertial frames which give absolute meaning to forces (rather than tidal forces) cannot be defined.

In summary our conclusion is that the necessary and sufficient condition for dynamics to be defined in the infinite system limit — in analogy to how it is defined for Newtonian self-gravitating particles in a infinite universe of constant density — is that the gradient of the pair force be absolutely integrable at large separations. Gravity is the marginal (logarithmically divergent) case in which such a dynamics can be defined, but only by using a prescription such as Eq. (6.18). Further these conditions on the range of pair forces can be expressed simply as one on the existence of the PDF of force differences of points as finite separations in the infinite system limit.

## 4 Discussion and conclusions

In conclusion we make some brief remarks on how the results derived here relate to previous work in the literature on force PDFs. In this context we also discuss the important assumption we made throughout the article, that the pair force considered was *bounded*. Finally we return briefly to the question of the relevance of the classification dividing interactions according to the integrability properties of the pair force, concerning which we have reported initial results elsewhere [67].

The first and most known calculation of the force PDF is that of Chandrasekhar [33], who evaluated it for the gravitational pair interaction in an infinite homogeneous Poisson particle distribution (in  $d = 3$ ). This results in the so-called *Holtzman* distribution, a probability distribution belonging to the Levy class (i.e. power law tailed with a diverging second moment) with  $P(\mathbf{F}) \sim F^{-9/2}$  at large  $F$ . According to our results here, a well defined PDF may be obtained for such a force law, which is *not* absolutely integrable at large separations, only by using a prescription for the calculation of the force in the infinite system limit. In his calculation Chandrasekhar indeed obtains the force on a point by summing the contributions from mass in *spheres* of radius  $R$  centered on the point considered, and then taking  $R \rightarrow \infty$  (with  $n_0$  fixed). This prescription is a slight variant of the one we have employed (following Kiessling [95]): instead of the smooth exponential screening of the interaction, it uses a “spherical top-hat” screening so that the force may be written formally as in Eq. (6.18) with the replacement of  $e^{-\mu|\mathbf{x}-\mathbf{x}'|}$  by a Heaviside function  $\Theta(\mu^{-1} - |\mathbf{x} - \mathbf{x}'|)$ . It is straightforward to verify that the result of Chandrasekhar is unchanged if the smooth prescription Eq. (6.18) is used instead. As the Poisson distribution corresponds to an SF  $S(k \rightarrow 0) \sim k^n$  with  $n = 0$ , the general condition (6.20) for the existence of the PDF we have derived, which gives  $n > -1$  for gravity in  $d = 3$ , is indeed satisfied. The fact that the PDF is power-law tailed (and thus *not* rapidly decreasing) arises from the fact that the calculation of Chandrasekhar does not, as done here, assume that the singularity in the gravitational interaction is regularized. Indeed it is simple to show explicitly [71] that this power law tail arises from the divergence in the pair force at zero separation. This can be done by considering the contribution to the total force on a system particle due to its nearest neighbor particle, which turns out to have a power law tail identical, both in exponent and amplitude, to that of the full  $P(\mathbf{F})$ .

Our analysis shows that it is true in general that well defined, but power-law tailed force PDFs, can arise only when there are singularities in the pair force: for a bounded force we have seen that the PDF is necessarily rapidly decreasing when it exists. More specifically, returning to the analysis of Sec. 1.3, it is straightforward to see that the crucial property we used of  $\mathcal{Q}_N(\{\mathbf{f}_i\})$ , that it have *compact support*, is no longer valid when the pair force has singularities. The analyticity properties which lead to a rapidly decreasing PDF may then not be inferred. We note that this is true at finite  $N$ , and has nothing to do with the infinite volume limit, i.e., the appearance of the associated power-law tail arises from the possibility of having a single particle which give an unbounded contribution rather than from the combination of the contribution of many particles which then diverges in the infinite system limit. The exponent in such a power-law tail will depend on the nature of the divergence at small separation. More specifically, for a central pair force as considered above and now with a singularity  $f(x \rightarrow 0) \sim 1/x^a$ , a simple generalization of the analysis

for the case of gravity (see [?]) of the leading contribution to the total force coming from the nearest neighbor particle leads to the conclusion that  $P(F \rightarrow \infty) \sim F^{-d-\frac{d}{a}}$  (where  $F = |\mathbf{F}|$ ). This implies that the variance diverges (i.e. the PDF becomes fat-tailed) for  $a > d/2$ .

Force PDFs have been calculated in various other specific cases. Wesenberg and Molmer [153] derived that of forces exerted by randomly distributed dipoles in  $d = 3$ , corresponding to a pair force with  $\gamma = 2$ . According to our results this is the marginal case in which a summation prescription is required for the force, and indeed a prescription using spheres, like that used by Chandrasekhar for gravity, is employed. We note that [153] focusses on the power-law tails associated with the singularity at zero separation of the force, which lead in this case (as can be inferred from the result summarized above) to the divergence of the first moment of the force PDF. One of us (AG) has given results previously [65] for the PDF for a generic power-law interaction in  $d = 1$  for  $\gamma > -1$  in our notation above. The conditional force PDF is then derived for the case of an infinite “shuffled lattice” of particles, i.e., particles initially on an infinite lattice and then subjected to *uncorrelated* displacements of finite variance, and using again, as Chandrasekhar, a “spherical top-hat” prescription for the force summation (for  $\gamma \leq 0$ , when the pair force is not absolutely integrable). It is simple to show [71] that such a distribution has an SF with  $n = 2$  at small  $k$ , and thus the existence of the force PDF in these cases is again in line with the constraint (6.20) derived. Power-law tails are again observed in these cases, and their exponents related explicitly to the singularity in the assumed power-law force at zero separation.

The calculation of Chandrasekhar has been generalized in [66] to the case of particles on an infinite shuffled lattice. This leads again, in line with condition (6.20), to a well defined PDF, again with or without power-law tails according to whether the singularities in the pair force are included or not. Chavanis [35] considers, on the other hand, the generalization of Chandrasekhar calculation (for the PDF of gravitational forces in a Poisson distribution) to  $d = 2$  and  $d = 1$ . The condition (6.20 for gravity ( $\gamma = d - 2$ ) gives  $n > -d + 2$ , which implies that the force PDF is not defined in the infinite system limit we have considered for  $d \leq 2$ , and indeed in [35] well defined PDFs are obtained in  $d = 2$  and  $d = 1$  by using a different limiting procedure involving in each case an appropriate rescaling of the coupling with  $N$ . The physical meaning of such a procedure is discussed in [?], which considers in detail the calculation of the force PDF for gravity in  $d = 1$  in a Poisson distribution (as in [35]). An exact calculation of the force PDF of the *screened* gravitational force in the infinite system limit is given, which allows one to see in this case exactly how the general result given here is verified in this specific case: all moments of the PDF diverge simultaneously as the screening length is taken to infinity, giving a PDF which converges point-wise to zero. The force PDF for gravity in  $d = 1$  for a class of infinite particle distributions generated by perturbing a lattice has been derived recently in [70]. It is straightforward to show that one of the conditions imposed on the perturbations to obtain the PDF, that the variance of the perturbations be finite, corresponds in fact to the condition  $n > 1$  which coincides precisely with the more general condition (6.20) derived here. Unlike in the other specific cases just discussed, it turns out that in this case (gravity in  $d = 1$ ) it is in fact necessary to use the smooth prescription Eq. (6.18). As explained in

detail in [70], the top-hat prescription does not give a well defined result in this case, because surface contributions to the force which do not decay with distance in this case are not regulated by it. We underline that the general result given in the present article are for this specific prescription Eq. (6.18). Further analysis would be required to derive the general conditions in which a top-hat prescription also gives the same (and well-defined) PDF.

Finally let us comment on why we anticipate the classification of pair interactions according to their “dynamical range”, formalized here using the force PDF, should be a useful and relevant one physically in the study of systems with long-range interactions. The reason is that this classification reflects, as we have explained, the relative importance of the mean field contribution to the force on a particle, due to the bulk, compared with that due to nearby particles. Now it is precisely the domination by the former which is understood to give the regime of *collisionless* dynamics which is expected to lead to the formation of QSS states, which are usually interpreted to be stationary states of the Vlasov equations describing such a regime of the dynamics (see e.g. [13]). In a recent article [67] a numerical and analytical study has been reported which provides strong evidence for the following result, very much in line with this naive expectation: systems of particles interacting by attractive power law pair interactions like those considered here can always give rise to QSS; however when the pair force is *dynamically short-range* their existence requires the presence of a sufficiently large soft core, while in the *dynamically long-range* case QSS can occur independently of the core, whether hard or soft, provided it is sufficiently small. In other words only in the case of a pair force which is “dynamically long-range” can the occurrence of QSS be considered to be the result only of the long distance behavior of the interaction alone. This finding is very consistent with what could be anticipated from the preceding (naive) argument: the effect of a “soft core” is precisely to reduce the contribution to the force due to nearby particles, which would otherwise dominate over the mean field force in the case of a pair force which is absolutely integrable at large distances. Indeed the meaning of “sufficiently large” specified in [67] is that the size of the soft core must increase in an appropriate manner with the size of the system as the limit  $N \rightarrow \infty$  is taken, while we have always implicitly assumed it to be fixed in units of the interparticle distance here.



# Conclusion and perspectives

In Chapters 3, 4 and 5 of this thesis, we have presented a simplified  $1 - d$  toy model to study the temporal evolution of *infinite* self-gravitating systems, considering a class of initial conditions analogous to those canonically studied in cosmology. In so doing, we have revisited a basic question concerning the definition of the gravitational force in  $1 - d$  infinite point distributions. We then have discussed different dynamical toy models which incorporate this definition of the force — the simple conservative Newtonian dynamics and one which incorporates a damping term mimicking the effect of  $3 - d$  expansion.

We then have presented in Chapter 4 the results of numerical investigations of the dynamical evolution of  $1 - d$  self-gravitating toy models, starting with a class of initial conditions analogous to those studied in cosmology: lattices perturbed to produce an initial power spectrum in a simple power-law form, *i.e.*  $P_{init}(k) \propto k^n$  at small  $k$ . We have observed very strong qualitative similarities between the evolution of  $1 - d$  and  $3 - d$  systems when the exponent of the initial power spectrum was equal to 0 and 2. We have observed specifically the hierarchical nature of the clustering, and brought to light the mechanism of linear amplification determining the growth of non-linearity scale. Moreover, we have shown that “self-similarity” is indeed observed in  $1 - d$  system in both the static and expanding cases just as in  $3 - d$ . We have shown, however, that qualitative differences can be identified between the static and expanding cases. The shape of the correlation function has appeared to be a function of the exponent  $n$  of the initial power spectrum and of the damping term  $\Gamma$  in the expanding case, and to be independent of this exponent in the static limit ( $\Gamma = 0$ ). This result again coincides with  $3 - d$  numerical simulation.

The  $1 - d$  self-gravitating model has also given us the opportunity to investigate easily structure formation in the limit of “causal fluctuations”, *i.e.*  $P(k) \propto k^4$  at small  $k$ . We have shown that, differently to the case where  $P(k) \propto k^0$  or  $k^2$  at small  $k$ , the evolution of the PS at small  $k$  is not, as expected, the one predicted from linear theory. However, despite the non-validity of the linear amplification of the small  $k$  PS, the non-linear structure formation does show asymptotically a self-similar evolution.

Due to the absence of smoothing at small scale (which is impossible in  $3 - d$   $N$ -body simulations), our  $1 - d$  model allowed us to identify the lower cut-off marking the end of the self-similar regime at small-scale,  $x_{min}$  say. We have shown that this cut-off was explained naturally by a “stable-clustering” hypothesis, a result which allowed us to determine the exponent in the self-similar regime in terms of the exponent  $n$  of the initial power spectrum and the damping term  $\Gamma$ . The stable clustering hypothesis we have described, however, is actually subtly different from the original

one introduced by Peebles in  $3 - d$  in an EdS universe [126]: we assumed only the stable clustering applies below the scale  $x_{min}$  marking the lower cut-off, and not necessarily to the strongly non-linear regime as a whole. Thus we assumed, in our derivation of the exponent characterizing the self-similar regime, only that stable clustering applies at an ultraviolet scale fixed by the resolution of the simulation (or, physically, by the scale at which the very first structures form).

We have then explored and characterized further in Chapter 5 the scale-invariant properties of the particle distributions produced in these  $1 - d$  self-gravitating models. We used a multifractal analysis to measure the spectrum of fractal exponents and studied their dependence on the model and initial conditions. We concluded that, in the static model the results are quite consistent with a simple homogeneous fractal, while in the expanding cases there is significant multi-fractality. Furthermore, we have explored the applicability of a description of the clustering like that used canonically in cosmological simulations, that in terms of “halos”. We used the simplest kind of “Friend-of-Friend” algorithm and focussed on the question whether these selected halos are, typically, virialized. The study of the virial ratios we have presented indicated that such halos can be considered as entities with a dynamical relevance, as they show a clear tendency to have a virial ratio of order unity (which is the behaviour of an isolated structure). It emerged from this analysis that one can effectively decompose the distribution of particles into a collection of structures which are, statistically, virialized. The “statistical virialization” we have observed using the halo analysis applies across the range of the scale-invariant clustering. Thus the strongly non-linear clustering in these models is accurately described as a virialized fractal structure, very much in line with the “clustering hierarchy” which Peebles originally envisaged qualitatively as associated with stable clustering [126]. If transposed to  $3 - d$  these results would imply, notably, that cold-dark matter halos (or even subhalos) are 1) not well modeled as smooth objects, and 2) that the supposed “universality” of their profiles is, like apparent smoothness, an artefact of poor numerical resolution. There are, however, clearly two possible conclusions one can draw from this analysis:

- A) These  $1 - d$  models produce non-linear clustering which is qualitatively different in its nature to that in  $3 - d$ , or
- B) The spatial resolution in  $3 - d$  simulations up to now has been too limited to reveal the nature of clustering in cold dark matter cosmologies, which is correctly reflected (qualitatively) in the  $1 - d$  simulations.

We believe that, despite the impressive computational size and sophistication of  $3 - d$  cosmological simulations, conclusion B may well be the correct one. The very largest modern studies in a cosmological volume acces roughly two decades in scale in the non-linear regime while reference studies in the literature of power law initial conditions in EdS cosmology [51, 139] measure the crucial power-law behaviour in the correlation function over at most one decade. If we were to perform our  $1 - d$  simulations at comparable resolution to large cosmological simulations like Smith et al. [139], we would certainly have a great difficulty in establishing the scale invariant nature of the strongly non-linear clustering arising from power law initial conditions. Although halos defined exactly as in three dimensions might look clumpy, an

approximately smooth profile could be determined for them if they were averaged (as they can be in three dimensions when spherical symmetry is assumed). Higher resolution 3D simulations of smaller regions have shown over the last decade that there is in fact much more substructure inside halos than was originally anticipated (see, e.g., [45, 76, 115]), and some very recent work [161] even comes to the conclusion that halos are indeed, intrinsically grainy rather than smooth. Previous analyses by other authors (see, e.g., [72, 149]) have also argued for similar conclusions based on the analysis of 3D simulations.

Let us consider nevertheless one possible consideration in favour of (the more conservative) conclusion A. In the expanding (i.e. damped) 1D models, the stable clustering prediction fits the measured exponents extremely well. Early 3D studies for EdS cosmologies (e.g. [51]) measured exponents roughly consistent with the stable clustering prediction, but later studies (e.g. [139]) have found significant disagreement. This disagreement is attributed to physical mechanisms which cause the fundamental assumption of stability to be violated — by the evident fact that *there are* interactions between “halos”, which can even lead to their merging into single structures. We have noted that in one dimension tidal forces vanish, and structures can interact only when they actually physically cross one another. While merging may occur, it may be that it is a less efficient process than in three dimensions. Thus the excellent agreement in the 1D models compared to EdS may perhaps be attributed to the fact that these models probably represent poorly the role of such physical effects. The essential question, however, is not whether these effects play a role and can lead to deviations from stable clustering, but whether such effects can *qualitatively* change the nature of clustering, destroying scale invariance by smoothing out the distribution *on a scale related to the upper cut-off* to scale invariance. Our study of the case  $\Gamma = 0$  suggests that the answer is negative. The prediction of stable clustering does not work in this case, and like in three dimensions, one obtains a small value of the exponent which does not sensibly depend on  $n$ . The physical reasons why the exponent is close to, but different to, the stable clustering prediction are a priori the ones just cited. Further, as we have mentioned, the lower cut-off  $x_{min}$  remains constant as in the stable clustering hypothesis, of order the initial lattice spacing (and unrelated to the upper cut-off).

These results on 1D models suggest directions for 3D investigations which might establish definitively the correctness of conclusion B. We note, for example, that the 1D models lead one to expect that the exponents derived phenomenologically to characterize the highly non-linear density field inside smoothed halos (i.e. the “inner slope” of halos) should be closely related to the exponent  $\gamma$  determined from the correlation function. Indeed — in the approximation of a simple fractal behavior in the strongly non-linear regime, which the spectrum of multi-fractal exponents measured in [114] suggests should be quite good — the mean density about the centre of such halos will decrease just as about any random point, i.e., with the *same* exponent  $\gamma$ . Despite the contradiction with the widely claimed “universality” of such exponents in halos profiles, such a hypothesis cannot currently be ruled out, as the determination of such exponents is beset by numerical difficulties (arising again from the limited resolution of numerical simulations). In a study of halo profiles obtained from power law initial conditions Knollmann et al. [97] show explicitly that the results for the halo exponents depend greatly on what numerical fitting procedure

## CONCLUSION AND PERSPECTIVES

---

is adopted. While one procedure gives “universality” (i.e. exponents independent of  $n$ ), a different one favors clearly steepening inner profiles for larger  $n$ . Indeed we note that the numerical values for the inner slopes obtained by Knollman et al. [97] are, for the larger  $n$  investigated, in quite good agreement with the exponent predicted by stable clustering.

Our considerations here are strictly relevant only to dissipationless *cold* dark matter simulations. If the initial conditions are “warm” or “hot”, or if other non-gravitational interactions are turned on, the associated physical effects will tend to smooth out the matter distribution up to some scale (and thus destroy the scale invariance up to this scale). Nevertheless, if the conclusion B is correct even for this idealized case, it is likely to have very important observational implications relevant to testing standard cosmological models — intrinsically clumpy or grainy halos lead, for example, to very different predictions for dark matter annihilation (see, e.g. [4, 76]). At larger scales the possible link to the striking power-law behavior which characterizes galaxy correlations over several decades (see, e.g., [99, 106, 125]) — which was the motivation for original work on stable clustering [125] and is naturally interpreted as indicative of underlying scale invariance in the matter distribution (see, e.g. [72, 99]) — is intriguing.

In the last Chapter 6 of this thesis, we have reported results which generalize to any pair interaction decaying as a power-law at large separation the approach used in Chapter 3 to determine whether the  $1 - d$  gravitational force is defined in an infinite system. This is an interesting question as the gravitational force is clearly a particular long-range interaction, for which linear amplification emerges from linear fluid theory. We have formalized and described a simple classification of pair interactions which is different to the usual thermodynamic one applied to determine equilibrium properties, and which we believe should be very relevant in understanding aspects of the out of equilibrium dynamics of these systems. Instead of considering the convergence properties of *potential energy* in the usual thermodynamic limit, we have considered therefore those of the *force* in the same limit. Thus, while in the former case one considers (see e.g. [136]) the mathematical properties of essential functions describing systems at equilibrium in the limit  $N \rightarrow \infty$ ,  $V \rightarrow \infty$  at fixed particle density  $n_0 = N/V$ , we have considered the behavior of functions characterising the forces in this same limit. More specifically we have considered the definedness of the probability distribution function (PDF) of the force field in statistically homogeneous infinite particle distributions. We have also discussed a further (and different) classification which can be given of the range of pair interactions based on dynamical considerations. This arises when one addresses the question of whether dynamics under a given pair interaction may be defined in *infinite systems*, i.e., in a manner analogous to that in which it is defined for self-gravitating masses in an infinite universe. We have then deduced our principal result that the force PDF exists strictly in the infinite system limit if and only if the pair force is absolutely integrable at large separations, while it can be defined only in a weaker sense, introducing a regularization, when the pair force is not absolutely integrable. We have discussed the physical relevance of the use of such a regularization, which is just a generalization of the so-called “Jeans swindle” used to define the dynamics of (classical non-relativistic) self-gravitating particles in an infinite universe. By ana-

lyzing the evolution of density perturbations in an infinite system, we have shown that the physical relevance of such a regularization of the forces requires also a constraint on the behavior of the PDF of total *force differences* as a function of system size. We expect that this classification reflects, as we have explained, the relative importance of the mean field contribution to the force on a particle, due to the bulk, compared with that due to nearby particles. Now it is precisely the domination by the former which is understood to give the regime of *collisionless* dynamics which is expected to lead to the formation of QSS states, which are usually interpreted to be stationary states of the Vlasov equations describing such a regime of the dynamics (see e.g. [13]).

Work in progress will use the power of  $1 - d$  models, which is their simple implementation in numerical studies, to study the impact of the range of the interaction and of the presence of a regularization (hard or soft core) at small scale on the dynamics which is expected to lead to the formation of QSS states. We will use an exact  $N$ -particles code, optimized to run using *Graphical Processing units* (GPU) programming. This simplified approach will give us the opportunity to follow the dynamical evolution of the systems directly in the one-particle phase-space, analysis which is impossible in three dimensions.

## CONCLUSION AND PERSPECTIVES

# Appendix A

## One and two point properties of uniform SPP

In this appendix we give the general one and two-point statistical characterization of a SPP which is uniform on large scales.

The description of the correlation properties of a generic uniform SPP is given by the  $n$ -point correlation functions of the density field. For our considerations it will turn out to be sufficient to consider only the two-point properties, and more specifically it will be most convenient to characterize them in reciprocal space through the *structure factor* (SF) (or power spectrum). This is defined by

$$S(\mathbf{k}) = \lim_{V \rightarrow \infty} \frac{\langle |\tilde{n}(\mathbf{k}; V)|^2 \rangle}{n_0 V} \quad (\text{A.1})$$

where

$$\tilde{n}(\mathbf{k}; V) = \int_V d^d x e^{-i\mathbf{k}\cdot\mathbf{x}} [n(\mathbf{x}) - n_0]. \quad (\text{A.2})$$

With these normalisations the SF of an uncorrelated Poisson process is  $S(\mathbf{k}) = 1$ . For a statistically isotropic point process  $S(\mathbf{k}) \equiv S(k)$ , where  $k = |\mathbf{k}|$ . We recall here that  $S(\mathbf{k})$  is the Fourier transform (FT) of the connected two point density correlation function:

$$S(\mathbf{k}) = \int d^d x e^{-i\mathbf{k}\cdot\mathbf{x}} C(\mathbf{x})$$

where

$$C(\mathbf{x}) = \frac{\langle n(\mathbf{x}_0 + \mathbf{x}) n(\mathbf{x}_0) \rangle - n_0^2}{n_0} = \delta(\mathbf{x}) + n_0 h(\mathbf{x}).$$

In the last expression we have explicitly separated in the correlation function  $C(\mathbf{x})$  the shot noise term  $\delta(\mathbf{x})$ , present in all SPP and due to the “granularity” of the particle distribution, from the “off-diagonal” term  $n_0 h(\mathbf{x})$  which gives the actual spatial correlations between different particles.

In the paper we study the convergence properties of forces at large distances and are thus mainly interested in the properties of the SF at small  $k$ . In this respect we will use the following limit on the SF which follows from the assumed uniformity of the SPP:

$$\lim_{k \rightarrow 0} k^d S(\mathbf{k}) = 0,$$

i.e, the SF is an integrable function of  $\mathbf{k}$  at  $k = 0$ . This constraint simply translates in reciprocal space the requirement from uniformity on the decay of relative fluctuations of the number of particles contained in a volume  $V$  about the mean at large  $V$ :

$$\lim_{V \rightarrow \infty} \frac{\langle N(V)^2 \rangle - \langle N(V) \rangle^2}{\langle N(V) \rangle^2} = 0.$$

Given that  $\langle N(V) \rangle \propto V$ , the root mean square fluctuation of particle number  $N$  in a volume  $V$  must diverge slower than the volume  $V$  itself in order that this condition be fulfilled. (This is equivalent to saying that  $C(\mathbf{x})$  must vanish at large  $x$ ).

We use likewise in the paper only one constraint on the large  $k$  behavior of the SF, which is valid for any uniform SPP (see e.g. [?]) and coincides with the shot noise term in the correlation function  $C(\mathbf{x})$ :

$$\lim_{k \rightarrow \infty} S(\mathbf{k}) = 1.$$

## Appendix B

### Small $k$ behavior of $\tilde{\mathbf{f}}(\mathbf{k})$

We are interested in the small  $k$  behavior of the Fourier transform  $\tilde{\mathbf{f}}(\mathbf{k})$  of the pair force in  $d$  dimensions in the case where the pair force  $\mathbf{f}(\mathbf{x}) = \hat{\mathbf{x}}f(x)$ , where  $\hat{\mathbf{x}} = \frac{\mathbf{x}}{|\mathbf{x}|}$ , is non-integrable but converges to zero at  $x \rightarrow \infty$ , i.e.,  $f(r) \sim r^{-(\gamma+1)}$  at large  $x$  with  $-1 < \gamma \leq d - 1$ .

We first show that for a function  $\mathbf{f}(\mathbf{x}) = \hat{\mathbf{x}}f(x)$ , its Fourier transform,  $\tilde{\mathbf{f}}(\mathbf{k}) = \text{FT}[\mathbf{f}(\mathbf{x})](\mathbf{k})$ , can be written  $\tilde{\mathbf{f}}(\mathbf{k}) = \hat{\mathbf{k}} \psi(k)$  where  $\psi(k)$  is a function depending only on the modulus of  $\mathbf{k}$  and  $\hat{\mathbf{k}} = \frac{\mathbf{k}}{|\mathbf{k}|}$ . In order to obtain this result, we start by writing

$$\tilde{\mathbf{f}}(\mathbf{k}) = \int d^d x \mathbf{f}(\mathbf{x}) e^{-i\mathbf{k}\cdot\mathbf{x}} = \int d^d x \hat{\mathbf{x}} f(x) e^{-i\mathbf{k}\cdot\mathbf{x}},$$

where this integral is defined in the sense of functions or distributions according to the integrability of  $f(x)$ .

In the following we denote by  $(\hat{\mathbf{e}}_1, \hat{\mathbf{e}}_2, \dots, \hat{\mathbf{e}}_n)$  the cartesian vector basis in  $d$ -dimension and we define  $(r, \theta_1, \theta_2, \dots, \theta_{d-1})$  the hyper-spherical coordinates of  $\mathbf{x}$ . Considering  $\mathbf{k} = k \hat{\mathbf{e}}_1$  and denoting for simplicity  $\theta = \theta_1$ , we can write

$$\tilde{\mathbf{f}}(\mathbf{k}) = \int d^d x \hat{\mathbf{x}} f(x) e^{-ikx \cos \theta},$$

where

$$d^d x = \left( \prod_{j=0}^{d-1} \sin^j(\theta_{d-j}) d\theta_{d-j} \right) x^{d-1} dx.$$

Projecting  $\tilde{\mathbf{f}}(\mathbf{k})$  on the cartesian basis, it is easy to see that the only non-vanishing term is  $\hat{\mathbf{e}}_1 \cdot \tilde{\mathbf{f}}(\mathbf{k})$  which gives

$$\begin{aligned} \hat{\mathbf{e}}_1 \cdot \tilde{\mathbf{f}}(\mathbf{k}) &= C_{\theta_i \neq 1} \int_0^\infty dx x^{d-1} \\ &\times \int_0^\pi d\theta \sin^{n-2}(\theta) \cos \theta f(x) e^{-ikx \cos \theta}, \end{aligned}$$

where  $C_{\theta_i \neq 1}$  is a constant term coming from the integration over all the hyper-spherical coordinates  $\theta_i$  with  $i \neq 1$ . We thus can write  $\tilde{\mathbf{f}}(\mathbf{k}) = \hat{\mathbf{k}} \psi(k)$  where  $\psi(k)$  is a function depending only on the modulus of  $\mathbf{k}$ .

We now focus our attention on the small  $k$  behavior of the term

$$\int_0^\infty dx x^{d-1} f(r) e^{-ikx \cos \theta}, \quad (\text{B.1})$$

where the function  $f(x)$  is non-integrable but converges to zero at  $x \rightarrow \infty$ , i.e.,  $f(x) \sim x^{-(\gamma+1)}$  at large  $x$  with  $-1 < \gamma \leq d-1$ , and thus can be written  $f(x) = x^{-(\gamma+1)} + h(x)$  with  $h(x)$  a smooth function, integrable at  $x = 0$  and such that  $x^{\gamma+1} h(x) \rightarrow 0$  for  $x \rightarrow \infty$ .

Defining explicitly eq.(B.1) in the sense of distributions, the small  $k$  behavior is determined by this leading divergence at  $x \rightarrow \infty$ ,

$$\lim_{\mu \rightarrow 0} \int_0^\infty dx x^{d-1} \frac{e^{-\mu x}}{x^{\gamma+1}} e^{-ikx \cos \theta}, \quad (\text{B.2})$$

where the parameter  $\mu > 0$ . We define  $\alpha = d - \gamma - 2$  which satisfies  $-1 \leq \alpha < d-1$  and rewrite eq. (B.2)

$$\lim_{\mu \rightarrow 0} \int_0^\infty dx x^\alpha e^{-(ik \cos \theta + \mu)x}.$$

This can be easily calculated with Laplace's transform and gives

$$\int_0^\infty dx x^\alpha e^{-(ik \cos \theta + \mu)x} = \frac{\Gamma(\alpha + 1)}{(\mu + ik \cos \theta)^{\alpha+1}}.$$

We can conclude that

$$\begin{aligned} & \lim_{\mu \rightarrow 0} \int_0^\infty dx x^{d-1} \frac{e^{-\mu x}}{x^{\gamma+1}} e^{-ikx \cos \theta} \\ &= i^{-(\alpha+1)} \cos^{-(\alpha+1)}(\theta) \Gamma(\alpha + 1) k^{-(\alpha+1)} \sim k^{\gamma-d+1}. \end{aligned}$$

# Bibliography

- [1] <http://www.amara.com/papers/nbody.html>.
- [2] Gabrielli A. and Joyce M. Two-point correlation properties of stochastic "cloud processes". *PRE*, 77:031139, 2008.
- [3] Gabrielli A. and Joyce M. Gravitational force in an infinite one-dimensional poisson distribution. *PRE*, 81:021102, 2010.
- [4] N. Afshordi, R. Mohayaee, and E. Bertschinger. *Phys. Rev. D*, 81:101301, 2010.
- [5] M. Antoni and S. Ruffo. Clustering and relaxation in long-range hamiltonian dynamics. *Phys. Rev.*, E(52):2361, 1995.
- [6] V. A. Antonov. *Vest. Leningr. Gos. Univ.*, 7:135, 1962.
- [7] E. Aurell and D. Fanelli. *Astron. Astrophys.*, (395):399, 2002.
- [8] E. Aurell and D. Fanelli. Self-gravitating systems in a three dimensional expanding universe. 2002.
- [9] E. Aurell, D. Fanelli, S. N. Gurbatov, and A. Yu. Moshkov. The inner structure of zeldovich pancakes. *Physica D*, 186:171–184, 2003.
- [10] E. Aurell, D. Fanelli, and P. Muratore-Ginanneschi. *Physica*, D(148):272, 2001.
- [11] T. Baertschiger, M. Joyce, A. Gabrielli, and F. Sylos Labini. Gravitational dynamics of an infinite shuffled lattice of particles. *Phys. Rev.*, E(75):021113, 2007.
- [12] J. Bagla. *Curr. Sci.*, (88):1088, 2005.
- [13] R. Balescu. *Equilibrium and nonequilibrium statistical mechanics*. Wiley, new york edition, 1975.
- [14] J. M. Bardeen, J. R. Bond, N. Kaiser, and A. S. Szalay. *Astrophys. J.*, 304:15, 1986.
- [15] J. Barré. *Mécanique statistique et dynamique hors équilibre de systèmes avec interactions à longue portée*. PhD thesis, 2003.

## BIBLIOGRAPHY

---

- [16] J. Barré, F. Bouchet, T. Dauxois, and S. Ruffo. Birth and long-time stabilization of out-of-equilibrium coherent structures. *Europhys. J.*, B(29):577, 2002.
- [17] J. Barré, F. Bouchet, T. Dauxois, and S. Ruffo. Out-of-equilibrium states as statistical equilibria of an effective dynamics. *Phys. Rev. Lett.*, 89:110601, 2002.
- [18] J. Barré, D. Mukamel, and S. Ruffo. Inequivalence of ensembles in a system with long range interactions. *Phys. Rev. Lett.*, 87:030601, 2001.
- [19] M. Baus and J.-P. Hansen. *Physics Reports*, (59):1, 1980.
- [20] M. Le Bellac. *Des phénomènes critiques aux champs de jauge*. Cnrs edition.
- [21] A. J. Benson, C. S. Frenck, C. M. Baugh, S. Cole, and C. G. Lacey. *Mon. Not. R. Astron. Soc.*, 327:1041, 2001.
- [22] F. Bernardeau. Large-scale structure formation in the quasi-linear regime. *Proc. XXXIth Moriond meeting*, 1996.
- [23] E. Bertschinger. Self-similar secondary infall and accretion in an einstein de sitter universe. *Astrophys. J. Supp.*, 58:39–66, 1985.
- [24] E. Bertschinger. Simulations of structure formation in the universe. *Annu. Rev. Astron. Astrophys.*, 36:599–654, 1998.
- [25] J. Binney and S. Tremaine. *Galactic dynamics*. Princeton University Press, 1994.
- [26] M. Blume, V. J. Emery, and R. B. Griffiths. Ising model for  $\lambda$ -transition and phase separation in  $he^3-he^4$  mixtures. *Phys. Rev.*, A(4):1071, 1971.
- [27] S. Borgani. The multifractal behaviour of hierarchical density distributions. *Mon. Not. R. Astron. Soc.*, 260:537–549, 1993.
- [28] W. Braun and K. Hepp. The vlasov dynamics and its fluctuations in the  $1/n$  limit of interacting particles. *Comm. Math. Phys.*, 56:101, 1977.
- [29] T. Buchert. *Mon. Not. R. Astron. Soc.*, (254):729, 1992.
- [30] A. Campa, T. Dauxois, and S. Ruffo. Statistical mechanics and dynamics of solvable models with long-range interactions. *Physics Reports*, 480:57, 2009.
- [31] A. Campa, A. Giansanti, G. Morigi, and F. Sylos Labini. *Dynamics and Thermodynamics of Systems with Long Range Interactions: Theory and Experiments*. American institute of physics edition, 2007.
- [32] S. Chandrasekhar. *Principles of Stellar Dynamics*. University of chicago press edition, 1942.
- [33] S. Chandrasekhar. *Rev. Mod. Phys.*, 15:1, 1943.

- [34] P. H. Chavanis. *Statistical mechanics of two-dimensional vortices and stellar systems*, volume 602 of *Lecture Notes in Physics*. Springer edition, 2002.
- [35] P. H. Chavanis. *European Physical Journal*, B(70):413, 2009.
- [36] P. H. Chavanis, J. Sommeria, and R. Robert. Statistical mechanics of two dimensional vortices and collisionless stellar systems. *Astrophys. J.*, 471:385, 1996.
- [37] J. Colberg, S. D. M. White, A. Pearce, and F. R. Yoshida. *Mon. Not. R. Astron. Soc.*, 308:593, 1999.
- [38] J. M. Colberg, S. D. M. White, and N. Yoshida. *Mon. Not. R. Astron. Soc.*, 319:209, 2000.
- [39] S. Colombi, F.R. Bouchet, and L. Hernquist. Self-similarity and scaling behavior of scale-free gravitational clustering. *Astrophys. J.*, 465:14, 1996.
- [40] W. J. Conover. *Practical Nonparametric Statistics, Third Edition*. John wiley and sons, new york edition, 1999.
- [41] R. Courant and D. Hilbert. *Methods of Mathematical Physics, Volume II*. Wiley-interscience edition, 1962.
- [42] T. Dauxois, S. Ruffo, E. Arimondo, and M. Wilkens. *Dynamics and Thermodynamics of Systems with Long Range Interactions*. Springer, berlin edition, 2002.
- [43] T. Dauxois, S. Ruffo, and L. F. Cugliandolo. *Long-Range Interacting Systems*. Oxford university press edition, 2009.
- [44] A. Dembo and O. Zeitouni. *Large deviations techniques and their applications*. Springer-verlag, new-york edition, 1998.
- [45] J. Diemand, J. Moore, and J. Stadel. *Nature*, 433:389, 2005.
- [46] K. Dolag, S. Borgani, S. Schindler, A. Diaferio, and A. M. Bykov. Simulation techniques for cosmological simulations. *Space science reviews*, 134:229–268, 2008.
- [47] J. R. Dorfman. *An introduction to chaos in nonequilibrium statistical mechanics*. Cambride univ. press edition, 2001.
- [48] B. Dubrulle and M. Lachièze-Rey. On the multifractal analysis of galaxy catalogs with box-counting methods. *Astron. Astrophys.*, 289:667–672, 1994.
- [49] G. Efstathiou, M. Davis, and C.S. Frenk. *Astrophys. J. Supp*, 57:241, 1985.
- [50] G. Efstathiou, M. Davis, S. D. M. White, and C.S. Frenk. Numerical techniques for large cosmological  $n$ -body simulations. *Astrophys. J. Supp*, 57:241–260, 1985.

## BIBLIOGRAPHY

---

- [51] G. Efstathiou, C.S. Frenk, White S., and M. Davis. *Mon. Not. R. Astron. Soc.*, 235:715, 1988.
- [52] R. S. Ellis. *Large deviations and statistical mechanics*. Springer-verlag, new-york edition, 1985.
- [53] Y. Elskens and D. Escande. *Microscopic dynamics of Plasmas and Chaos*. Iop publishing, bristol edition, 2002.
- [54] R. Emden. *Gaskugeln, Teubner, Leipzig*, 1907.
- [55] C. L. Bennett et al. et al. Cosmic temperature fluctuations from two years of cobe differential microwave radiometers observations. *Astrophys. J. Supp*, 436:423–442, 1994.
- [56] D. W. Hogg et al. et al. Cosmic homogeneity demonstrated with luminous red galaxies. *Astrophys. J.*, 624:54–58, 2005.
- [57] E. Komatsu et al. et al. Five-year wilkinson microwave anisotropy probe (wmap) observations: Cosmological interpretation. *Astrophys. J. Supp*, 180:330–376, 2009.
- [58] V. E. Eke et al. et al. Galaxy groups in the 2dfgrs: the group-finding algorithm and the 2pigg catalogue. *Mon. Not. R. Astron. Soc.*, 348:866, 2004.
- [59] W. H. Press et al. et al. *Numerical Recipes 3rd Edition: The Art of Scientific Computing*. Cambridge University Press, 2007.
- [60] S. et al. Perlmutter. Measurements of omega and lambda from 42 high-redshift supernovae. *Astrophys. J.*, 517:565–586, 1999.
- [61] A. et al. Riess. Observational evidence from supernovae for an accelerating universe and a cosmological constant. *Astronomical Journal*, 116:1009–1038, 1998.
- [62] P. Ewald. Die berechnung optischer und elektrostatischer gitterpotentiale. *Ann. Phys.*, 369:253–287, 1921.
- [63] G. L. Eyink and H. Spohn. Negative-temperature states and large scale, long-lived vortices in two-dimensional turbulence. *J. Stat. Phys*, 70:833, 1993.
- [64] J. Filmore and P. Goldreich. *Astrophys. J.*, 281:9, 1984.
- [65] A. Gabrielli. *Phys. Rev.*, E(72):066113, 2005.
- [66] A. Gabrielli, T. Baertschiger, M. Joyce, B. Marcos, and F. Sylos Labini. *Phys. Rev.*, E(74):021110, 2006.
- [67] A. Gabrielli, M. Joyce, and B. Marcos. Quasi-stationary states and the range of pair interactions. *Phys. Rev. Lett.*, (to appear):arXiv:cond-mat/1004.5119, 2010.

- [68] A. Gabrielli, M. Joyce, B. Marcos, and F. Sicard. A dynamical classification of the range of pair interactions. *J. Stat. Phys.*, 141:970–989, 2010. to appear.
- [69] A. Gabrielli, M. Joyce, B. Marcos, and P. Viot. Causality constraints on fluctuations in cosmology: a study with exactly solvable one dimensional models. *Europhys. Lett.*, 66:171, 2004.
- [70] A. Gabrielli, M. Joyce, and F. Sicard. One dimensional gravity in infinite point distributions. *Phys. Rev. E*, 80:041108, 2009.
- [71] A. Gabrielli, F. Sylos Labini, M. Joyce, and L. Pietronero. *Statistical Physics for Cosmic Structures*. Springer, 2004.
- [72] J. Gaite. Halos and voids in a multifractal model of cosmic structure. *Astrophys. J.*, 658:11.
- [73] G. Gallavotti. *The elements of mechanics*. Springer-Verlag, 1983.
- [74] M. J. Geller and J. P. Huchra. Groups of galaxies. iii - the cfa survey. *Astrophys. J. Supp.*, 52:61, 1983.
- [75] B. Gnedenko. *The theory of probability*. Mir Publishers, Moscow, 1975.
- [76] T. Goerdt, O.Y. Gnedin, B. Moore, J. Diemand, and J. Stadel. *Mon. Not. R. Astron. Soc.*, 375:191, 2007.
- [77] P. Grassberger and I. Procaccia. Measuring the strangeness of strange attractors. *Physica D*, 9:189, 1983.
- [78] D. H. E. Gross. Microcanonical thermodynamics: phase transitions in small systems. *Lecture Note in Physics*, 66, 2001.
- [79] J. E. Gunn and J. R. Gott. *Astrophys. J.*, 176:1, 1972.
- [80] T. C. Halsey, M. H. Jensen, L. P. Kadanoff, I. Procaccia, and B. Shraiman. *Physical Review A*, (33):1141, 1986.
- [81] P. Hertel and W. Thirring. Soluble model for a system with negative specific heat. *Ann. Phys.*, 63:520, 1971.
- [82] F. Hohl and M. Feix. *Astrophys. J.*, 147:147, 1967.
- [83] D. D. Holm, J. E. Marsden, T. Ratiu, and A. Weinstein. Nonlinear stability of fluid and plasma equilibria. *Phys. Rep.*, 123:1–116, 1985.
- [84] B. Jain and E. Bertschinger. *Astrophys. J.*, 456:43, 1996.
- [85] B. Jain and E. Bertschinger. *Astrophys. J.*, 509:517, 1998.
- [86] J. H. Jeans. *Phil. Trans. Roy. Soc.*, 199:1, 1902.
- [87] A. Jenkins, C.S. Frenk, S. D. M. White, J. M. Colberg, S. Cole, A. Evrard, H. M. P. Couchman, and N. Yoshida. *Mon. Not. R. Astron. Soc.*, 321:372, 2001.

## BIBLIOGRAPHY

---

- [88] M. Joyce and B. Marcos. *Phys. Rev.*, D(75):063519, 2007.
- [89] M. Joyce, B. Marcos, A. Gabrielli, T. Baertschiger, and F. Sylos Labini. *Phys. Rev. Lett.*, (95):011304, 2005.
- [90] M. Joyce and T. Worrakitpoonpon. Relaxation to thermal equilibrium in the self-gravitating sheet model. *J. Stat. Phys.*, 10:10012, 2010.
- [91] H. E. Kandrup. Geometric approach to secular and nonlinear stability for spherical star clusters. *Astrophys. J.*, 351:104–113, 1990.
- [92] G. Kauffmann, J. M. Colberg, A. Diaferio, and S. D. M. White. *Mon. Not. R. Astron. Soc.*, 303:188, 1999.
- [93] M. K. H. Kiessling. Statistical mechanics of classical particles with logarithmic interactions. *Comm. Pure App. Math.*, 46:27, 1993.
- [94] M. K. H. Kiessling and J. K. Percus. Nonuniform van-derwaals theory. *J. Stat. Phys.*, 78:1337, 1995.
- [95] M.K.-H Kiessling. *Adv. Appl. Math.*, (31):132, 2003.
- [96] A. Knebe. How to simulate the universe in a computer. *Astronomical Society of Australia*, 22(3):184–189, 2004.
- [97] S. R. Knollmann, C. Power, and A. Knebe. *Mon. Not. R. Astron. Soc.*, 385:545, 2008.
- [98] A. Kolmogorov and S. Fomin. *Elements of the Theory of Functions and Functional Analysis*. Dover publication, new york edition, 1999.
- [99] F. Sylos Labini, M. Montuori, and L. Pietronero. *Phys. Rep.*, 293:61, 1998.
- [100] M. Lax. Relation between canonical and microcanonical ensembles. *Phys. Rev.*, 97:1419, 1955.
- [101] I. H. Li and H. K. C. Yee. Finding galaxy groups in photometric-redshift space: the probability friends-of-friends algorithm. *Astronomical Journal*, 135:809, 2008.
- [102] H. B. Liu, B. C. Hsieh, P. T. P. Ho, L. Lin, and R. Yan. A new galaxy group finding algorithm: Probability friends-of-friends. *Astrophys. J.*, 681:1046–1057, 2008.
- [103] D. Lynden-Bell and R. Wood. The gravothermal catastrophe in isothermal spheres and the onset of red-giant structure for stellar system. *Mon. Not. R. Astron. Soc.*, 138:495, 1968.
- [104] B. Mandelbrot. *The fractal geometry of Nature*. Freeman edition, 1982.
- [105] B. Marcos, T. Baertschiger, M. Joyce, A. Gabrielli, and F. Sylos Labini. *Phys. Rev.*, D(73):103507, 2006.
- [106] M. Masjedi et al. *Astrophys. J.*, 644:54, 2006.

- [107] J. L. McCauley. *Physica*, A(309):183, 2002.
- [108] M. E. Merchan and A. Zandivarez. Galaxy groups in the third data release of the Sloan Digital Sky Survey. *Astrophys. J.*, 630:759, 2005.
- [109] J. Messer and H. Spohn. Statistical mechanics of the isothermal lane-emden equation. *J. Stat. Phys.*, 29:561, 1982.
- [110] B.N. Miller. *Trans. Th. Stat. Phys.*, (34):367, 2005.
- [111] B.N. Miller and J.L. Rouet. *Phys. Rev.*, E(65):056121, 2002.
- [112] B.N. Miller and J.L. Rouet. Development of fractal geometry in a one-dimensional gravitational system. *C. R. Phys.*, (7):383, 2006.
- [113] B.N. Miller, J.L. Rouet, and E. Le Guiriec. Development of fractal geometry in a 1+1 dimensional universe. *Phys. Rev.*, E(76):036705, 2007.
- [114] Bruce N. Miller and Jean-Louis Rouet. Cosmology in one dimension: fractal geometry, power spectra and correlation.
- [115] B. Moore, T. Quinn, F. Governato, J. Stadel, and G. Lake. *Mon. Not. R. Astron. Soc.*, 310:1147, 1999.
- [116] J. Navarro, C. Frenk, and S. D. M. White. *Astrophys. J.*, 462:563, 1996.
- [117] J. F. Navarro, C. S. Frenck, and S. D. M. White. *Astrophys. J.*, 490:493, 1997.
- [118] J. F. Navarro, A. Ludlow, V. Springel, J. Wang, M. Vogelsberger, S. D. M. White, A. Jenkins, C.S. Frenk, and A. Helmi. The diversity and similarity of simulated cold dark matter halos. *Mon. Not. R. Astron. Soc.*, 402(1):21–34, 2010.
- [119] J. Neyman and E.L. Scott. *Astrophys. J.*, 116:144.
- [120] Alain Noullez, Duccio Fanelli, and Erik Aurell. A heap-based algorithm for the study of one-dimensional particle systems. *Journal of Computational Physics*, 186:697–703, 2003.
- [121] A. Nusser and R. K. Sheth. *Mon. Not. R. Astron. Soc.*, 303:685, 1999.
- [122] L. Onsager. Statistical hydrodynamics. *Nuovo Cimento Suppl.*, 6:279, 1949.
- [123] E. Ott. *Chaos in Dynamical Systems*. Cambridge Univ. Press edition, 2002.
- [124] T. Padmanabhan. Statistical mechanics of gravitating systems. *Phys. Rep.*, 188:285–362, 1990.
- [125] P.J.E. Peebles. *Astrophys. J.*, 189:51, 1974.
- [126] P.J.E. Peebles. *The Large-Scale Structure of the Universe*. Princeton University Press, 1980.

## BIBLIOGRAPHY

---

- [127] A. A. Penzias and R. W. Wilson. A measurement of excess antenna temperature at 4080 mc/s. *Astrophys. J.*, 142:419–421, 1965.
- [128] A. Del Popolo. The cups/core problem and the secondary infall model. *Astrophys. J.*, 698:2093, 2009.
- [129] C. Power, J. F. Navarro, A. Jenkins, C. S. Frenck, S. D. M. White, V. Springel, J. Stadel, and T. Quinn. The inner structure of  $\Lambda$ CDM halos i: A numerical convergence study. *Mon. Not. R. Astron. Soc.*, 338(1):14–34, 2003.
- [130] W. H. Press and P. Schechter. *Astrophys. J.*, 187:425, 1974.
- [131] J. R. Primack and M. A. K. Gross. *Hot dark matter in cosmology: current aspects of neutrino physics*. Springer, Berlin, caldwell edition, 2001.
- [132] T. Quinn, N. Katz, J. Stadel, and G. Lake. Time stepping n-body simulations. *astro-ph/9710043v1*, 1997.
- [133] C. Reidl and B. Miller. *Astrophys. J.*, 371:371, 1991.
- [134] J.L. Rouet and M.R. Feix. *Phys. Rev.*, E(59):73, 1999.
- [135] J.L. Rouet, M.R. Feix, and M. Navet. *Vistas Astron.*, (33):357, 1990.
- [136] D. Ruelle. *Statistical mechanics: rigorous results*. Benjamin, new-york edition, 1969.
- [137] White S. volume Lecture given at les houches, 1993.
- [138] G. Severne and M. Luwel. *Astrophys. Sp. Sci.*, 122:299, 1986.
- [139] R. E. Smith, J. A. Peacock, A. Jenkins, White S., C.S. Frenk, F. R. Pearce, P. A. Thomas, G. Efstathiou, and H. M. P. Couchman. Stable clustering, the halo model and nonlinear cosmological spectra. *Mon. Not. R. Astron. Soc.*, 341:1311, 2003.
- [140] R. S. Somerville and J. R. Primack. *Mon. Not. R. Astron. Soc.*, 310:1087, 1999.
- [141] V. Springel. The cosmological simulation code gadget-2. *Mon. Not. R. Astron. Soc.*, 364:1105–1134, 2005.
- [142] V. Springel, N. Yoshida, and S. D. M. White. Gadget: a code for collisionless and gasdynamical cosmological simulations. *New Astronomy*, 6:79–117, 2001.
- [143] J. Stadel et al. Quantifying the heart of darkness with ghalo - a multi-billion particle simulation of our galactic halo. *Mon. Not. R. Astron. Soc. Let.*, 398(1):21–25, 2009.
- [144] B. Stahl, M. K. H. Kiessling, and K. Schindler. Phase-transitions in gravitating systems and the formation of condensed objects. *Planet. Space Sci.*, 43:271, 1995.
- [145] T. Tatekawa and K. Maeda. *Astrophys. J.*, (547):531, 2001.

- [146] R. A. Treumann and W. Baumjohann. *Advanced space plasma physics*. Imperial College Press, London, 1997.
- [147] C. Tsallis. Possible generalization of boltzmann-gibbs statistics. *J. Stat. Phys.*, 52:479, 1988.
- [148] T. Tsuchiya and N. Gouda. *Phys. Rev.*, E(61):948, 2000.
- [149] P. Valageas. *Astron. Astrophys.*, 347:757, 1999.
- [150] P. Valageas. *Astron. Astrophys.*, (450):450, 2006.
- [151] P. Valageas. *Phys. Rev.*, E(74):016606, 2006.
- [152] R. H. Wechsler, J. S. Bullock, J. R. Primack, A. V. Kravtsov, and A. Dekel. *Astrophys. J.*, 568:52, 2002.
- [153] J. H. Wesenberg and K. Molmer. *Phys. Rev. Lett.*, 93:143903, 2004.
- [154] S. D. M. White, C. S. Frenck, and M. Davis. Clustering in a neutrino-dominated universe. *Astrophys. J.*, 274, 1983.
- [155] S. D. M. White and M. Rees. *Mon. Not. R. Astron. Soc.*, 183:341, 1978.
- [156] Y. Yamaguchi, F. Bouchet, J. Barré, T. Dauxois, and S. Ruffo. Stability criteria of the vlasov equation and quasi-stationary states of the hmf model. *Physica A*, 337(1-2):36, 2004.
- [157] T. Yano and N. Gouda. *Astrophys. J. Supp.*, (118):267, 1998.
- [158] K. R. Yawn and Bruce N. Miller. Incomplete relaxation in a twomass one-dimensional self-gravitating system. *Phys. Rev. E*, 68(5):056120, 2003.
- [159] D. H. Zanette and M. A. Montemurro. Dynamics and nonequilibrium states in the hamiltonian mean-field model: A closer look. *Phys. Rev. E*, 67:031105, 2003.
- [160] Y. Zeldovich. *Adv. Astron. Ap.*, 3:241, 1965.
- [161] M. Zemp, J. Diemand, J. Kuhlen, P. Madau, B. Moore, D. Potter, J. Stadel, and L. Widrow. *Mon. Not. R. Astron. Soc.*, 394:641, 2009.

## BIBLIOGRAPHY

---



---

## RÉSUMÉ

La formation des structures dans l'univers demeure une des interrogations majeures en cosmologie. La croissance des structures dans le régime linéaire, où l'amplitude des fluctuations est faible, est bien comprise analytiquement, mais les simulations numériques à  $N$ -corps restent l'outil principal pour sonder le régime “non-linéaire” où ces fluctuations sont grandes. Nous abordons cette question d'un point de vue différent de ceux utilisés couramment en cosmologie, celui de la physique statistique et plus particulièrement celui de la dynamique hors-équilibre des systèmes avec *interaction à longue portée*. Nous étudions une classe particulière de modèles  $1 - d$  qui présentent une évolution similaire à celle rencontrée dans les modèles  $3 - d$ . Nous montrons que le clustering spatial qui se développe présente des propriétés (fractales) d'invariance d'échelles, et que des propriétés d'auto-similarité apparaissent lors de l'évolution temporelle. D'autre part, les exposants caractérisant cette invariance d'échelle peuvent être expliqués par l'hypothèse du “stable-clustering”. En suivant une analyse de type halos sélectionnés par un algorithme “friend-of-friend”, nous montrons que le clustering non-linéaire de ces modèles  $1 - d$  correspond au développement d'une “hiérarchie fractale statistiquement virielisée”. Nous terminons par une étude formalisant une classification des interactions basée sur des propriétés de convergence de la force agissant sur une particule en fonction de la taille du système, plutôt que sur les propriétés de convergence de l'énergie potentielle, habituellement considérée en physique statistique des systèmes avec interaction à longue portée.

---

## MOT-CLEFS

Formation de structures, Interactions longue portée, Simulations  $N$ -corps

---

## ABSTRACT

The formation of structures in the universe is one of the major questions in cosmology. The growth of structure in the linear regime of low amplitude fluctuations is well understood analytically, but  $N$ -body simulations remain the main tool to probe the “non-linear” regime where fluctuations are large. We study this question approaching the problem from the more general perspective to the usual one in cosmology, that of statistical physics. Indeed, this question can be seen as a well posed problem of out-of-equilibrium dynamics of systems with *long-range interaction*. In this context, it is natural to develop simplified models to improve our understanding of this system, reducing the question to fundamental aspects. We define a class of infinite  $1 - d$  self-gravitating systems relevant to cosmology, and we observe strong qualitative similarities with the evolution of the analogous  $3 - d$  systems. We highlight that the spatial clustering which develops may have scale invariant (fractal) properties, and that they display “self-similar” properties in their temporal evolution. We show that the measured exponents characterizing the scale-invariant clustering can be very well accounted for using an appropriately generalized “stable-clustering” hypothesis. Further by means of an analysis in terms of halo selected using a friend-of-friend algorithm we show that, in the corresponding spatial range, structures are, statistically virialized. Thus the non-linear clustering in these  $1 - d$  models corresponds to the development of a “virialized fractal hierarchy”. We conclude with a separate study which formalizes a classification of pair-interactions based on the convergence properties of the forces acting on particles as a function of system size, rather than the convergence of the potential energy, as it is usual in statistical physics of long-range-interacting systems.

---

## KEYWORDS

Cosmological structure formation, Long range interactions,  $N$ -body simulations

---